Studies of Supported Pt-Sn Alloy Catalysts for the Catalytic Dehydrogenation of Alkanes

Lidan Deng

2014

Preface

For a long time it has been known that an alloy (bimetallic) surface can exhibit chemical and catalytic properties that are quite different from those of the surfaces of the individual metal and another element. Research on alloy catalysts was firstly done by G. M Schwab, A. Couper and D.A. Dowden in the late 1940s with the purpose of establishing links between the structural and catalytic properties of a surface. However, due to the lack of adequate techniques for the preparation and characterization of the surface of alloys, no real progress was made at an experimental level. In the 1960s and 1970s the development of alloy catalysts for hydrocarbon reforming in the petrochemical industry increased the need for a fundamental understanding of the behavior of alloy surfaces, and renewed the interest in catalysis by alloys. This effort provided the basis for the concepts of "ensemble" and "ligand or electronic" effects, which are commonly used to rationalize the superior activity or selectivity of alloy catalysts. In the last two decades, the development of new and reliable techniques for surface characterization has made feasible a systematic study of the properties of alloy surfaces. It is now possible to explore relationships between the structural, electronic and chemical properties of a bimetallic surface in detail. Experiments performed using the modern techniques of surface science have given exciting insights into phenomena responsible for the behavior of bimetallic surfaces.

In this thesis, the author chose Pt-Sn alloy catalysts as the object of study, which is one of the effective catalysts for dehydrogenation of alkanes such as isobutane, propane, and ethylbenzene. The detailed structural properties of Pt-Sn alloy catalysts as well as the structure-activity relationship in the dehydrogenation of alkanes were expected to be clarified. From this point of view, a series of Pt-Sn alloy catalysts with the different structural properties were papered by controlling the preparation conditions. On the another hand, many techniques including X-ray diffraction (XRD), Transmission electron microscope(TEM), High angle annular dark field-scanning transmission

electron microscope (HADDF-STEM) and EDX spectra, CO adsorption, X-ray photoelectron spectroscopy (XPS), X-ray absorption fine structure (XAFS) and so on were utilized to reveal the structure of Pt-Sn alloy catalysts comprehensively and carefully. Based on this information, the synthesis-structure-activity relationship over Pt-Sn alloy catalysts was discussed in detail.

It was found that the different synthesis conditions resulted into the different interaction between Pt and Sn, and this interaction plays an important role in the catalytic activity in the dehydrogenation of alkanes. Pt and SnO_x ($0<x<2$) oxides can form the strong interaction like strong-metal-support-interaction (SMSI) under the pretreatment in N_2 at high temperature (1073 K), and worked as the active sites for the dehydrogenation reactions. Much stronger interaction between Pt and Sn can be introduced with the pretreatment in H_2. The ordered Pt-Sn solid solutions (Pt-Sn alloys) such as Pt_xSn_y($x/y>3$), Pt_3Sn, PtSn were formed, and their compositions were affected by the reduction methods, reduction temperature and Sn/Pt ratios. Pt_3Sn showed the highest activity, while PtSn showed no or low activity. As for Pt_3Sn active species, its behavior during the reaction and regeneration were also interested and inspired. Its surface restructure including changes in the surface fraction of Pt-Sn alloys (during the reaction), phase separation and re-alloy between Pt and Sn were indicated by XPS, XAFS and catalytic tests. Furthermore, the interaction between Pt and Sn was also influenced by the support. Using SBA-15 that was characterized with its high surface area and special textural structure as the support, Pt-Sn alloy particles were more stable during the dehydrogenation of ethylbenzene than SiO_2, thus Pt-Sn/SBA-15 exhibited higher stability than Pt-Sn/SiO_2. Moreover, this thesis also accidentally discovered the strong interaction between Pt and SiO_2 under the high reduction temperature (>1073 K). This interaction introduced the high activity over Pt/SiO_2 for the dehydrogenation of propane. This new finding explored the present cognition about strong metal and support interaction (SMSI), which is important phenomenon in the heterogeneous catalysis. It also gave another viewpoint to understand the nature of alloy catalyst because SMSI, SMOI (strong metal and oxides interaction) and alloying between two metals or one

metal and metal oxide explain one thing: the interaction between two parts in one system.

Under the supervision of Professor Tsunehiro Tanaka and Professor Tetsuya Shishido, the studies presented in this thesis were performed at Department of Molecular Engineering, Graduate School of Engineering, Kyoto University and Department of Applied Chemistry, Graduate School of Urban Environmental Sciences, Tokyo Metropolitan University from 2011 to 2014 with the financial supports from the program of Element Strategy Initiative for Catalysts & Batteries (ESICB) and China Scholarship Council (CSC). The author wishes to make her sincere and great acknowledgements to Professor Tsunehiro Tanaka and Professor Tetsuya Shishido for their exact guidance, consistent helps and supports during the experiments, insightful discussion and patient modification during the paper writing and submitting. Moreover, the studies in the present thesis cannot be well finished without the great helps from Professor Kentaro Teramura, Dr. Saburo Hosokawa, Dr. Hiroki Miura, Professor Kenji Wada, Mr. Eichi Watanabe of Tokyo Metropolitan University and some seniors from the laboratory of Professor Tsunehiro Tanaka including Mr. Hiroaki Nasu, Mr. Yoshihisa Takayama, Dr. Tomoyuki Kitano, Dr. Shinya Furukawa, Mr. Hiroyuki Asakura. They taught the author to do experiments, and gave the valuable suggestions about this research.

A lot of thanks should be also dedicated to Mr. Akira Yamamoto, Mr. Zheng Wang, Mr. Shoji Iguchi for their helpful discussions and a lot of aids in experiments. The author also had a pleasure work with Mr. Shoji Tanaka of Kyoto University, Mr. Takuto Arakawa of Tokyo Metropolitan University on the studies of ethylbenzene dehydrogenation over Pt-Sn catalysts. Thank them very much for their special thinking and abilities, giving the author much supports through the studies. Thank all students in the lab of Professor Tsunehiro Tanaka and the lab of Professor Tetsuya Shishido. The days being together became the best memories of the author. Special thanks are conveyed to Secretary Ms. Ayako Tanaka, Ms. Mami Nishio and Ms. Yoshiko Amemiya for her kind official supports. Thank all the members of the group of catalysis research and everyone the author met in

Japan. Best wishes for everyone!

Finally, the author expresses the great appreciation to her parents, every family member for their enduing supports and loves. The author also thanks sincerely to her good friends in Japan and China for their sincere friendships.

Lidan Deng

Kyoto, Tokyo
June, 2014

CONTENTS

General Introduction

Propylene and Styrene

Propylene (prepene) is the key building block in the chemical industry. It broad spectrum of derivatives results in a very diverse end market ranging from packing materials and synthetic textiles to antifreezing agents, solvents, and coatings. In 2010[1], more than 55% of propylene consumption was for the production of polypropylene in the Western European countries. Approximately 13% of the propylene was used in the production of propylene oxide, which is a chemical precursor for the synthesis of propylene glycol and polyols. The rest of the production was used in the synthesis of cumene (about 8%), acrylonitrile, isopropyl alcohol, and many other industrially relevant chemicals. The market for propylene as a basic intermediate petrochemical continues to grow at average rates of 4-5% per year[2].

By the early 1990s [3], the propylene production profile was 70% steam cracking (SC), 23% fluid-catalytic-cracking (FCC), and 7% catalytic propane dehydrogenation. In SC of various hydrocarbons, the main product is ethylene. Propylene was co-produced as the by-product. Propylene growth rate has been lagged behind with ethylene growth rate because that ethylene is the largest-volume petrochemical produced worldwide. For instance, the yield of ethylene and propylene varies between 24-55% and 1.5-18%, respectively depending greatly on the feedstock type and operating conditions [4]. As a result, the production of propylene via dehydrogenation of propane has grown in view of the availability of low-cost propane and the potential to make up the shortfall of propylene supply left by conventional crackers.

Styrene (vinyl benzene) is another important monomer in modem petrochemical

industry. It is mainly used for the production of many different polymeric material, in which the most important ones are polystyrene, styrene-acrylonitrile, acylonitorile-buadiene-styrene (ABS) and styrene-butadiene latex[5]. Recently styrene is produced by two processes[6]: (i) dehydrogenation of ethylbenzene (eq) and (ii) as a by-product in the epoxidation of propene with ethylbenzene hydroperoxide over Mo complex-based catalysts. The former process accounts for more than 90% of the worldwide capacity which is approximately $13x10^6$ tones per year. The latter process is commercialized by ARCO Chemical (formerly Oxirane) and Shell, currently producing approximately l.2 x 10^6 tons of styrene per year.

Catalytic Dehydrogenation of alkanes

As shown above, the catalytic dehydrogenation of alkanes has a considerable industrial impact. Catalytic dehydrogenation of propane represents another promising route to obtain propylene. Recent studies on propane dehydrogenation mainly focus on two aspects: catalytic oxidative dehydrogenation (OHP) and catalytic dehydrogenation (DHP). In OHP, oxygen is used as the oxidant, and water is formed as a by-product instead of hydrogen. Therefore, the reaction becomes exothermic and avoids the thermodynamic constraints of DHP. Previous studies [7-12] have shown that V_2O_5 or supported vanadia such as V_2O_5/SiO_2, V_2O_5/Al_2O_3, V_2O_5/TiO_2 is the most active and selective metal oxide for the oxidative dehydrogenation of alkanes including propane. Its reducible nature leads to the rapid redox cycles required for a catalytic turnover. For instance[13], Vanadium-magnesium oxides were found to show a selectivity of up to 65% at 10% conversion in the oxidative dehydrogenation of propane to propylene.

Besides OHP, DHP seems more admiring because the valuable H_2 for our society can also be produced with C-H cleavage in propane together with propylene. Typically,

Pt- or Cr-based catalysts are used in commercial dehydrogenation plants. The selectivity towards propylene ranged from 80 to 100%. However, these catalyst systems often showed low stability due to the coke formation, and need frequent regeneration. For example, De Rossi, S et al[14, 15] reported that $CrOx/ZrO_2$ is highly active and selective in the dehydrogenation of propane at 723-823 K, but is not stable. The conversion to propylene decreases from 54 to 19 % after 100 mins of reaction. Moreover, Cr-based catalysts often brought severe pollution to environment. Consequently, much research has been devoted to develop platinum or modified platinum catalysts[16-26] dehydrogenation catalysts to increase DHP activity, while diminishing undesired side reactions such as cracking, thus prolonging the life time.

The admirable performance of platinum or modified platinum catalysts in the catalytic dehydrogenations of alkanes such as ethane, propane, isobutane and n-butane also implied the potentiality of these catalysts in the catalytic dehydrogenation of ethylbenzene to styrene. Unfortunately recently there is few related research. In the catalytic dehydrogenation of ethylbenzene, a commercial Fe-K oxide catalyst was typically used in the presence of the superheated steam at 600-700℃[6]. Nonetheless, this catalyst has some disadvantages: unstable active Fe^{3+} sites[27], loss and redistribution of the potassium promoter[27] and a rapid deactivation due to the coke deposition[5]. Moreover, steam used is in a large excess molar amount with respect to ethylbenzene (6-12:1)[28], leads to a huge amount of energy consumption. Therefore, the application of platinum or modified platinum catalysts in the catalytic dehydrogenation of ethylbenzene is promising.

Pt-Sn Alloy Catalysts

Pt-Sn alloy catalyst is one kind of the effective catalysts for the catalytic

dehydrogenation of alkanes [17-19, 21, 24]. The addition of Sn to Pt/support catalyst systems has been found to effectively alter the product distribution through the inhibition of hydrogenolysis, isomerization, cracking and coke formation, thereby enhancing the catalyst selectivity and stability.

Initially, it is necessary to make clear the definition of alloy catalysts. Vladimir Ponec[29] once explained this term to the following conclusion: conveniently, alloy is a metallic system containing two or more components, irrespective of their intimacy of mixing or, precise manner of mixing. Actually, catalysis on alloy catalysts has seen many advances over the past few decades[30, 31]. Alloy catalysts, which often show electronic and chemical properties that are distinct from those of their parent metals, present as the new catalysts with enhanced selectivity, activity and stability. Currently, they are widely utilized in the electrocatalysts for fuel cells[32-37] and many catalytic applications such as dehydrogenation[38, 39], CO oxidation[40, 41] and so on. The wonderful catalytic behaviors of these alloy catalysts triggered much interests and widely studies on alloy catalysts including their detailed structures as well as mechanisms of their promotional roles on the catalytic behaviors over relevant reactions, as summarized in several reviews[29-31, 42, 43]. However, the mechanism by which the promoter metal modifies the catalytic behavior of individual metal remains a matter of debate due to the complicated nature of alloy system such as Pt-Sn.

First of all, the synthesis of alloy catalysts with the designated particle size, particle shape, metal compositions and so on from a materials science perspective is one interesting point. Xiaodong Wang et al. [44] synthesized different Pt-Sn bimetallic nanoparticles (particle size, shape and metal composition) with organic capping agents by colloidal chemistry method. The short Pt-Sn bimetallic nanowires having an average

width of 2.3 nm and lengths ranging from 5 to 20 nm were synthesized by a seed-mediated growth with amine-capped bimetallic particles as precursors. Boualleg, Malika et al. [45, 46] found unexpected, spontaneous and selective formation of colloidal Pt_3Sn nanoparticles using organometallic Pt and Sn complexes. Secondly, a considerable amount of interest is also focused on the research on structural properties of alloy catalysts, since is related to the origins of their novel catalytic properties. What is difficulty is that the details about the structure of alloy catalyst system should be shown or characterized. The studies on this aspect are also our main work. Thus, it will be discussed in detail in the following section "Characterization of Alloy Catalysts". Finally, many researchers pointed out that alloy catalyst structures would most likely change during reactions, it is critical to identify the atomic arrangement of alloy catalysts under temperatures, pressures, and reaction media relevant to catalytic reactions. Therefore, the studies on alloy catalysts under the *in-situ* reaction conditions are paid much attention. Feng Tao et al.[41] found that alloy (bimetallic nanoparticles) underwent segregation of the metals, driven by oxidizing and reducing environments. The behaviors in restructuring and chemical response of $Rh_{0.5}Pd_{0.5}$ and $Pt_{0.5}Pd_{0.5}$ nanoparticle catalysts under the reaction conditions illustrate the flexibility and tenability of the structure of bimetallic nanoparticle catalysts during catalytic reactions. The similar phenomena were also pointed out by Uemura, Yohei et al[47, 48] in the case of Pt-Sn alloys.

Characterization of Alloy Catalysts

As mentioned above, many special properties that alloy catalysts display, the tunable electronic properties, material-specific ensemble effects, directly affect their activity and/or selectivity. Therefore, the precise, atomistic characterization of alloy

catalysts is important for the studies on alloy catalysts, also one of the main challenges. X-ray diffraction (XRD) is the one technique for the characterization of alloy catalyst systems. When compared with the diffraction patterns of monometallic system, the alloy (bimetallic) ones often show distinct shifts of the Bragg reflections to lower or higher degrees, which is often regards as the clear proof of the alloying of two metals, meaning that the systems are not only a physical mixture of two metal nanoparticles[44, 49]. Moreover, Virnovskaia, Anastasia et al. [50] studied Pt-Sn/Mg(Al)O catalyst with Fourier transform infrared spectroscopy (FT-IR), using CO as a probe molecule, pointed out simultaneously a geometric and a chemical effect of Sn on the surface properties of the exposed Pt atoms. Different from the obscure results from the FT-IR spectrogram, the elemental mapping using transmission electron microscopy (TEM) can detect the elemental maps of selected PtSn particles[49], thus illustrate the interaction between them even though this technique only depicts the local information (a few of alloy particle). Vu, Bao Khanh et al. [51] used high-resolution transmission electron microscopy (HRTEM) to observe the different types of Pt-Sn alloys, such as Pt_3Sn, PtSn based on their special lattice parameters.

Besides the techniques listed above, X-ray absorption spectroscopy (XAS), which often contains two main branches: X-ray Absorption Near Edge Structure (XANES) and Extended X-ray Absorption Fine Structure (EXAFS), is another powerful technique for the studies on alloy catalysts. A critical feature in the XANES region is the “white line”, caused by a rapid increase in X-ray absorption of the target element in the catalyst material, which is closely related to the excitation of electrons in the target element atoms from the low energy-orbitals into the higher energy, for example, unoccupied d-states. Therefore, the main utility of the white line in XANES region is the

characterization of the electronic states of the designated element in the catalyst. In the EXAFS region, the ejected photoelectron has sufficient energy to scatter from the absorbing atom to the surrounding atoms and then backscatter to the absorbing atom. Due to the wave-particle duality, the outgoing and backscattered electrons can constructively or destructively interfere with each other, making it possible to extract some information about the local coordination environment of the target atoms.

Due to these properties of XAS, its application in the studies of the alloy (bimetallic) catalysts has widely reported[52]. One interesting point about it is for determining the detailed electronic states of the atoms, which is closely related to their catalytic behaviors[53, 54]. As early as 1984, Mansour, AN [55, 56] started the research on X-ray absorption threshold resonances (white lines) on metal catalysts and extracted some information about the electronic states of the metals. Another power about XAS is that Extended X-ray absorption fine structure (EXAFS) spectroscopy can provide quantitative information about the nanocatalysts's size, shape, details of core-shell architecture, as well as static and dynamic disorder in metal-metal bond lengths. This technique became the powerful tool for the details of alloy catalysts' structure.

Outline of the Present Thesis

This thesis focuses on the elucidation of the structure of Pt-Sn alloy catalyst, which is the famous catalyst in catalytic dehydrogenation of alkanes. Based on the characterization results from XRD, XPS, XAFS, TEM, CO-adsorption combined with the catalytic testes in propane dehydrogenation, the active structure of Pt-Sn alloy catalyst for C-H bond activation was pointed out.

This thesis consists of six chapters. Chapter 1 describes the effect of pretreatment atmosphere (the oxidized (O_2), inert (N_2) and reductive (H_2) pretreatment

atmosphere) on the structure and activity of Pt-Sn/SiO_2 for dehydrogenation of propane. It was found that Pt-Sn alloy (Pt_3Sn) formed in the reductive atmosphere, which showed the best catalytic activity in the dehydrogenation of propane.

Chapter 2 further found that different from Direct reduction (DR) reduction method, calcination-reduction (CR) method led to the formation of another kind of alloy, PtSn, while is not active for propane dehydrogenation.

In Chapter 3, DR method was used to prepare a series of Pt-Sn/SiO_2 catalysts. The effects of Sn/Pt ratio and reduction temperature on the detailed catalyst structure and catalytic behaviors were investigated. It was found that 1Pt1Sn/SiO_2_1073K (Sn/Pt ratio=1, reduced at 1073 K), composed of highly dispersed Pt_3Sn alloy particles decorated with SnO_2 exhibited the highest activity.

Chapter 4 deals with the behavior of active species on Pt-Sn/SiO_2 catalyst during the dehydrogenation of propane to propylene and regenerations. It was found that besides coke formation, the surface Sn(Ⅳ)/Sn(0) obviously increased after the reaction. H_2 in the feeding gas increased the stability of Pt-Sn/SiO_2. The regeneration (firstly calcination in air followed reduction in H_2) effectively recovered the activity of the deactivated catalyst trough the re-alloy between Pt and SnO_2.

Chapter 5 compared the catalytic behaviors of Pt-Sn/SiO_2 and Pt-Sn/SBA-15 in the dehydrogenation of ethylbenzene. It was found that the higher surface area and special textural properties of SBA-15 improved catalytic activity, selectivity and stability. Pt-Sn alloy particles were highly dispersed and stable over SBA-15 during the reaction time.

Chapter 6 reported that the strong interaction between Pt and SiO_2 originated from the reduction pretreatment at high temperature (1073 K), which led to high activity

of Pt/SiO_2 in the dehydrogenation of propane.

References

[1] H.M.T. Galvis and K.P. de Jong, ACS Catalysis, 3 (2013) 2130.

[2] A. Farshi, F. Shaiyegh, S.H. Burogerdi and A. Dehgan, Petroleum Science and Technology, 29 (2011) 875.

[3] R. Buyanov and N. Pakhomov, Kinetics and Catalysis, 42 (2001) 64.

[4] Rahimi, Nazi Karimzadeh and Ramin, Applied Catalysis A: General, 398 (2011) 1.

[5] G. Meima and P. Menon, Applied Catalysis A: General, 212 (2001) 239.

[6] F. Cavani and F. Trifiro, Applied Catalysis A: General, 133 (1995) 219.

[7] M. Argyle, K. Chen, A. Bell and E. Iglesia, Journal of Catalysis, 208 (2002) 139.

[8] H. Kung and M. Kung, Applied Catalysis A: General, 157 (1997) 105.

[9] E. Mamedov and V. Corberan, Applied Catalysis A: General, 127 (1995) 1.

[10] T. Blasco and J. Nieto, Applied Catalysis A: General, 157 (1997) 117.

[11] A. Khodakov, B. Olthof, A. Bell and E. Iglesia, Journal of Catalysis, 181 (1999) 205.

[12] A. Khodakov, J. Yang, S. Su, E. Iglesia and A.T. Bell, Journal of Catalysis, 177 (1998) 343.

[13] M. Chaar, D. Patel and H. Kung, Journal of Catalysis, 109 (1988) 463.

[14] S. De Rossi, G. Ferraris, S. Fremiotti, E. Garrone, G. Ghiotti, M. Campa and V. Indovina, Journal of Catalysis, 148 (1994) 36.

[15] S. Derossi, G. Ferraris, S. Fremiotti, A. Cimino and V. Indovina, Applied Catalysis A: General, 81 (1992) 113.

[16] P. Sun, G. Siddiqi, M. Chi and A.T. Bell, Journal of Catalysis, 274 (2010) 192.

[17] G. Aguilar-Rios, P. Salas, M. Valenzuela, H. Armendariz, J. Wang and J. Salmones, Catalysis Letters, 60 (1999) 21.

[18] O. Barias, A. Holmen and E. Blekkan, Journal of Catalysis, 158 (1996) 1.

[19] R. Cortright and J. Dumesic, Journal of Catalysis, 148 (1994) 771.

[20] S. Kogan, H. Schramm and M. Herskowitz, Applied Catalysis A: General, 208 (2001) 185.

[21] M.S. Kumar, D. Chen, A. Holmen and J.C. Walmsley, Catalysis Today, 142 (2009) 17.

[22] M.S. Kumar, D. Chen, J.C. Walmsley and A. Holmen, Catalysis Communications, 9 (2008) 747.

[23] A. Sault, A. Martino, J. Kawola and B. Elaine, Journal of Catalysis, 191 (2000) 474.

[24] S. Stagg, C. Querini, W. Alvarez and D. Resasco, Journal of Catalysis, 168 (1997) 75.

[25] P. Sun, G. Siddiqi, W.C. Vining, M. Chi and A.T. Bell, Journal of Catalysis, 282 (2011) 165.

[26] I. Yarusov, E. Zatolokina, N. Shitova, A. Belyi and N. Ostrovskii, Catalysis Today, 13 (1992) 655.

[27] B. Herzog and H. Rase, Ind. Eng. Chem. Prod. Res. Dev., 23 (1984) 187.

[28] N. Mimura, I. Takahara, M. Saito, T. Hattori, K. Ohkuma and M. Ando, Catalysis Today, 45 (1998) 61.

[29] V. Ponec, Applied Catalysis A: General, 222 (2001) 31.

[30] M. Sankar, N. Dimitratos, P.J. Miedziak, P.P. Wells, C.J. Kiely and G.J.

Hutching, Chem. Soc. ReV., 41 (2012) 8099.

[31] A.K. Singh and Q. Xu, chemcatchem, 5 (2012) 652.

[32] H. Gasteiger, S. Kocha, B. Sompalli and F. Wagner, Applied Catalysis B: Environmental 56 (2005) 9.

[33] M. Min, J. Cho, K. Cho and H. Kim, Electrochimica Acta, 45 (2000) 4211.

[34] J. Greeley and M. Mavrikakis, Nature Materials, 3 (2004) 810.

[35] J.H. Kim, S.M. Choi, S.H. Nam, M.H. Seo, S.H. Choi and W.B. Kim, Applied Catalysis B: Environmental, 82 (2008) 89.

[36] V. Stamenkovic, B.S. Mun, K.J.J. Mayrhofer, P.N. Ross, N.M. Markovic, J. Rossmeisl, J. Greeley and J.K. Norskov, Angewandte Chemie-International Edition, 45 (2006) 2897.

[37] M.E. Tague, J.M. Gregoire, A. Legard, E. Smith, D. Dale, R. Henning, F.J. Disalvo, R.B.v. Dover and H.D. Abruna, Journal of The Electrochemical Society, 159 (2012) F880.

[38] F. Besenbacher, I. Chorkendorff, B. Clausen, B. Hammer, A.N. Molenbroek, JK and I. Stensgaard, Science, 279 (1998) 1913.

[39] D. Rouabah and J. Fraissard, Journal of Catalysis, 144 (1993) 30.

[40] R. Mu, X. Guo, Q. Fu and X. Bao, The Journal of Physical Chemistry, 115 (2011) 20590.

[41] F. Tao, M.E. Grass, Y. Zhang, D.R. Butcher, J.R. Renzas, Z. Liu, J.Y. Chung, B.S. Mun, M. Salmeron and G.A. Somorjai, Science, 322 (2008) 932.

[42] S. Zafeiratos, S. Piccinin and D. Teschner, Catalysis Science & Technology, 2 (2012) 1787.

[43] W. Yu, M.D. Porosoff and J.G. Chen, Chemical Reviews, 112 (2012) 5780.

[44] X. Wang, J. Stoever, V. Zielasek, L. Altmann, K. Thiel, K. Al-Shamery, M. Baumer, H. Borchert, J. Parisi and J. Kolny-Olesiak, Langmuir, 27 (2011) 11052.

[45] M. Boualleg, D. Baudouin, J.-M. Basset, F. Bayard, J.-P. Candy, J.-C. Jumas, L. Veyre and C. Thieuleux, Chemical Communications, 46 (2010) 4722.

[46] M. Boualleg, J.-M. Basset, J.-P. Candy, V. Caps, J.-C. Jumas, S. Norsic, E.A. Quadrelli, L. Veyre and C. Thieuleux, Chemcatchem, 4 (2012) 1729.

[47] Y. Uemura, Y. Inada, K.K. Bando, T. Sasaki, N. Kamiuchi, K. Eguchi, A. Yagishita, M. Nomura, M. Tada and Y. Iwasawa, The Journal of Physical Chemistry, 115 (2011) 5823.

[48] Y. Uemura, Y. Inada, K.K. Bando, T. Sasaki, N. Kamiuchi, K. Eguchi, A. Yagishita, M. Nomura, M. Tada and Y. Iwasawa, Phys. Chem. Chem. Phys., 13 (2011) 15833.

[49] Z. Paal, A. Wootsch, D. Teschner, K. Lazar, I.E. Sajo, N. Gyorffy, G. Weinberg, A. Knop-Gericke and R. Schlogl, Applied Catalysis A: General, 391 (2011) 377.

[50] A. Virnovskaia, S. Morandi, E. Rytter, G. Ghiotti and U. Olsbye, J. Phys. Chem. C, 111 (2007) 14732.

[51] B.K. Vu, M.B. Song, I.Y. Ahn, Y.-W. Suh, D.J. Suh, W.-l. Kim, H.-L. Koh, Y.G. Choi and E.W. Shin, Applied Catalysis A: General, 400 (2011) 25.

[52] A.I. Frenkel, Chem. Soc. ReV., 41 (2012) 8163.

[53] F. Garin, Catalysis Today, 89 (2004) 255.

[54] B. Hammer and J. Norskov, Surface Science, 343 (1995) 211.

[55] A. Mansour, D. Sayers, J. Cook, Jr, D. Short, R. Shannon and J. Katzer, J. Phys. Chem. , 88 (1984) 1778.

[56] A. Mansour, J. Cook and D. Sayers, J. Phys. Chem., 88 (1984) 2330.

Chapter 1

Effect of pretreatment atmosphere on the activity of Pt-Sn/SiO_2 for propane dehydrogenation

Abstract

The structure of Pt-Sn/SiO_2 and its activity for propane dehydrogenation differed with the pretreatment atmosphere. Large Pt metal particles formed together with amorphous SnO_2 on Pt-Sn/SiO_2 treated with oxidized pretreatment atmosphere (O_2), which showed no catalytic activity. After the pretreatment in the inert atmosphere (N_2), Pt metal was highly dispersed with a strong Pt-SnO_x ($x<2$) interaction. This interaction became stronger with the treatment temperature and introduced high catalytic activity in propane dehydrogenation. The highest catalytic activity of Pt-Sn/SiO_2 was observed when the catalyst precursor was pretreated in the reductive atmosphere (H_2) which leads to the alloy formation between Pt and Sn. The Pt_3Sn phase was dominant over Pt-Sn/SiO_2 reduced in H_2 atmosphere at 1073 K. Different electronic states of Pt were detected in Pt-Sn/SiO_2 catalysts treated with the different atmosphere, which influenced C-H bond activation and propylene desorption in the dehydrogenation of propane. Therefore, these catalysts showed the different catalytic behaviors.

Introduction

Propylene is an important raw material for many petrochemicals such as polypropene, acrolein, polyacrylonitrile and acrylic acid. It is conventionally produced as a byproduct of steam cracking of naphtha for ethylene production [1, 2] or recovered from refinery processes, especially from fluid catalytic cracking (FCC)[3]. In recent years, the production of propene via thermal catalytic dehydrogenation of propane has grown in view of the availability of low-priced propane in shale gas[4, 5]. Compared with the conventional process, the catalytic dehydrogenation of propane is an attractive alternative because it is more energy-conserving and minimizes the formation of methane and coke byproducts. With a suitable catalyst system, higher activity and selectivity towards propylene are expected to be achieved under more environmentally-benign conditions.

Platinum-tin (Pt-Sn) catalyst [6-10], in the form of supported nanoparticles, is one of the most suitable catalysts for the thermal dehydrogenation of light alkanes. This bimetallic catalyst often exhibits better activity, selectivity and stability than supported Pt monometallic catalysts. However the accurate nature of the Pt-Sn systems is still unclear. Many characterization techniques have been used to study the detailed structures of Pt-Sn systems. Fourier transform infrared spectroscopy (FT-IR) of adsorbed CO was once used to characterize Pt-Sn/Mg(Al)O catalyst[11]. A simultaneous geometric and a chemical effect of Sn on the surface properties of the exposed Pt atoms were found based on the different CO adsorption behaviors over Pt/Mg(Al)O and Pt-Sn/Mg(Al)O catalyst. In contrast, another study [12] reported that the singleton vibration frequencies of CO on both Pt/Al_2O_3 and $Pt\text{-}Sn/Al_2O_3$ bimetallic samples lay within the range 2041 ± 6 cm-1, suggesting the small electronic effect of Sn

on Pt in their catalysts. Different from the obscure results from the FT-IR spectrogram [11-13], High resolution transmission electron microscopy (HRTEM) with a connected energy dispersive X-ray (EDX) technique directly observed Pt-Sn alloys which present different lattice parameters and element compositions[9, 14]. However this technique did not cover the complete information of Pt-Sn systems and only depicts the local information (a few of alloy particles). X-ray diffraction (XRD), which reflects the bulk properties of catalysts and can confirm the presence of different Pt-Sn alloys based on their different lattice parameters [15-18], whereas it requires the large crystalline size and well-ordered part to overcome the detection limit. XAFS (X-ray absorption fine structure) which is often applied as X-ray absorption near edge structure (XANES) and Extended X-ray absorption fine structure (EXAFS) well remedy the defects of XRD [7, 14, 19-21]. It can detect the target element in both crystals and the amorphous/microcrystalline structure of the catalysts. XANES [22], due to its sensitivity to the charge states of metals, adsorbates, and support materials, is a premier tool to study electronic structure of catalytic materials. EXAFS [23], due to its local structure sensitivity and excellent spatial resolution, is a preferred technique for investigating geometric properties of bimetallic catalysts in the nano size.

As discussed above, the catalytic behaviors of Pt-Sn catalysts were closely related to their detailed structures. The elucidation of the structure of Pt-Sn catalyst, especially the strong interaction between Pt and Sn, is necessary to understand the active site for the catalytic reactions and the reaction mechanism. Herein, in the present work, Pt/SiO_2 precursor (as the references) and $Pt\text{-}Sn/SiO_2$ precursor were first prepared with $H_2PtCl_6 \cdot 6H_2O$ and $SnCl_2 \cdot 2H_2O$ as the starting materials by impregnation method. XAFS analysis in our previous study [24, 25] showed that the states of Pt and Sn

species on Pt-Sn/SiO_2 precursor were similar with $PtCl_2$ and SnO_2 respectively, indicating no interaction between Pt and Sn on Pt-Sn/SiO_2 precursor. Pt-Sn/SiO_2 precursor was then pretreated under different pretreatment atmospheres: oxidative atmosphere, inert atmosphere and reduction atmosphere at low (773 K) or high (1073 K) temperature. The effects of pretreatment conditions (atmosphere, temperature) on the structures of the final Pt-Sn catalysts as well as their catalytic performances were investigated with the catalytic tests in propane dehydrogenation reactions and combined techniques including X-ray diffraction (XRD), Transmission electron microscopy (TEM), X-ray absorption fine structure analysis (XAFS), CO adsorption, and X-ray photoelectron spectroscopy (XPS). Based on the results, the structure-catalytic activity relationship, especially the interaction between Pt and Sn in the Pt-Sn/SiO_2 catalysts, was discussed.

Experimental

Catalyst Preparation

Silica (JRC-SIO-9, 334 m^2 g^{-1}) was used as the support for the preparation the Pt-Sn catalysts. Prior to impregnation, the SiO_2 support was treated at 773 K for 3h in air. Pt/SiO_2 precursor was prepared by impregnating the SiO_2 support with an adequate volume of aqueous $H_2PtCl_6 \cdot 6H_2O$ (3 wt% Pt), stirring at 353 K for 3 h, and then drying at 353 K for 20 h. The precipitate was noted as Pt/SiO_2 precursor. A bimetallic Pt-Sn/SiO_2 precursor was prepared by the sequential impregnation. Pt/SiO_2 precursor was added to acetone solutions of $SnCl_2 \cdot 2H_2O$ (Wako, 97%), stirred at 353 K for 3 h, and dried at 353 K for 20 h. The Pt content was 3wt. %. The molar ration of Pt to Sn was 1.

Prior to the reaction, the catalyst precursors were pretreated in three kinds of

atmospheres: 1) Oxidative atmosphere: the catalyst precursor was *in situ* treated in 20 vol% O_2 diluted with N_2 (total flow rate 50ml min^{-1}) at 773 K or 1073 K for 1 h, and then cooled to 773 K in N_2 (100ml min^{-1}). 2) Inert atmosphere: the catalyst precursor was *in situ* treated with N_2 (total flow rate 50ml min^{-1}) at 773 K or 1073 K for 1 h, and then cooled to 773 K in N_2 (100ml min^{-1}). 3) Reduction atmosphere: the catalyst precursor was *in situ* reduced in 20 vol% H_2 diluted with N_2 (total flow rate 50ml min^{-1}) at 773 K or 1073 K for 1 h. Finally, the catalyst was cooled to 773 K in N_2 (100ml min^{-1}). The obtained catalysts were denoted as Pt-Sn/SiO_2_x K O_2/N_2/H_2, x indicates the pretreatment temperature.

Propane dehydrogenation

Propane dehydrogenation was carried out in a quartz reactor (i.d. 10 mm) with a bed catalyst at atmospheric pressure with 20 vol.% of propane diluted with N_2 at 773 K. The total flow rate was 100 mL min^{-1}. The catalyst precursor (50 mg) was placed between quarts wool. The gas hourly space velocity (GHSV) was 24 L $h^{-1}g^{-1}$. The composition of gas was analyzed by using an on-line gas chromatograph (Shimadzu GC-8A, Japan) equipped with TCD (5A Molecular Sieve column) and methanizer FID (Porapak-Q column) detectors.

Characterization

All characterization was carried out on catalysts after *in situ* pretreatment. Brunauer–Emmett–Teller (BET) specific surface areas were estimated from N_2 isotherms obtained using a BELSORP 28SA (BEL Japan, Osaka, Japan) at 77 K. The analyzed samples were evacuated at 573 K for 3 h prior to the measurements.

The amount of CO adsorbed on the catalysts at room temperature was determined by the CO pulse method by using an Okura BP-2 instrument (Okura Riken,

Japan) interfaced with a TCD. Prior to CO adsorption, the catalyst precursor was *in situ* pretreated in oxidative/inert/reductive atmosphere at 773 K or 1073 K for 1 h.

X-ray diffraction (XRD) patterns were obtained using a MultiFlex DR powder X-ray diffractometer (Rigaku, Tokyo, Japan) with Cu Kα radiation (λ = 1.5405 Å). The samples were scanned from 2θ = 38° to 46° at a scanning resolution of 0.01°.

Transmission electron microscope (TEM) images were obtained using a JEOL JEM–2100F. The samples were prepared by depositing drops of methanol suspensions containing small amounts of the powders onto carbon-coated copper grids (Okenshoji Co. Ltd.), followed by evaporation of the methanol in air.

X-ray absorption experiments were carried out at BL01B1 of SPring-8 (Hyogo, Japan). The ring energy was 8 GeV, and the stored current was 99.5 mA. Pt L_3 and L_2-edge (11.56 and 13.27 keV) X-ray absorption spectra were recorded in air at room temperature using a Si (111) monochromator in transmission mode. Sn K-edge (29.19 keV) X-ray absorption spectra were recorded in air at room temperature using a Si (311) monochromator in fluorescence mode. The data processing was performed using the REX2000 Ver.2.5.9 (Rigaku) and FEFF8.40 programs.

X-ray photoelectron spectra (XPS) were acquired by using an ULVAC PHI 5500MT. The spectra were measured using Mg Kα radiation (15 kV, 400 W) in a chamber at a base pressure of ~ 10^{-7} Pa. All spectra were calibrated using C1s (284.80 eV) as a reference. Peak fitting was performed for Sn $3d_{5/2}$ using XPSPeak 4.1 software (UK Surface Analysis Forum). The Shirley function was used for background subtraction.

Results

Catalytic activities of Pt-Sn/SiO_2 catalysts

The initial conversions of propane over Pt/SiO_2 and $Pt\text{-}Sn/SiO_2$ catalysts are present in Fig.1 (A) and (B), respectively. It shows the different activities over Pt/SiO_2 and $Pt\text{-}Sn/SiO_2$ catalysts treated in the different pretreatment atmospheres. In the oxidative atmosphere, except for $Pt\text{-}Sn/SiO_2$_773 K O_2 which showed quite low activity, the other catalysts totally presented no activity. In the inert atmosphere, supported Pt monometallic catalysts were inactive, while Pt-Sn bimetallic catalysts showed activity towards propane dehydrogenation, suggesting the promotional role of Sn. The increase in treatment temperature from 773 K to 1073 K further improved the catalyst activity. The most interesting phenomenon took place in the case of the reduction atmosphere: the propane conversion was only 5% over Pt/SiO_2_773 K. However, it increased into 21.3 % on Pt/SiO_2_1073 K. It was implied that the high reduction temperature improved the catalytic activity over supported Pt monometallic catalyst. The promotional role of Sn was also obvious in the catalysts treated in reductive atmosphere. The conversion of propane reached 22.5% on $Pt\text{-}Sn/SiO_2$_773 K and 26.5% on $Pt\text{-}Sn/SiO_2$_1073 K. The selectivity towards propylene over Pt/SiO_2_1073 K and Pt/SiO_2_1073 K was respectively 94% or 99% (data no shown here). A trace amount of methane and ethane were detected as by-products when Pt/SiO_2_1073 K was used. It was suggested that the addition of Sn not only improved activity, but also increased in the selectivity towards propylene.

XRD patterns and TEM images

Fig. 2 compared XRD patterns of Pt/SiO_2 (spectrum a) and $Pt\text{-}Sn/SiO_2$ (spectrum b) catalysts under the different pretreatment conditions. The formation of Pt metal over Pt/SiO_2 catalyst was confirmed by the Pt (111) reflection peak at 2θ=39.8° and Pt (200) reflection peak at 2θ=46.2° (ICSD 41525), indicating that the precursor of

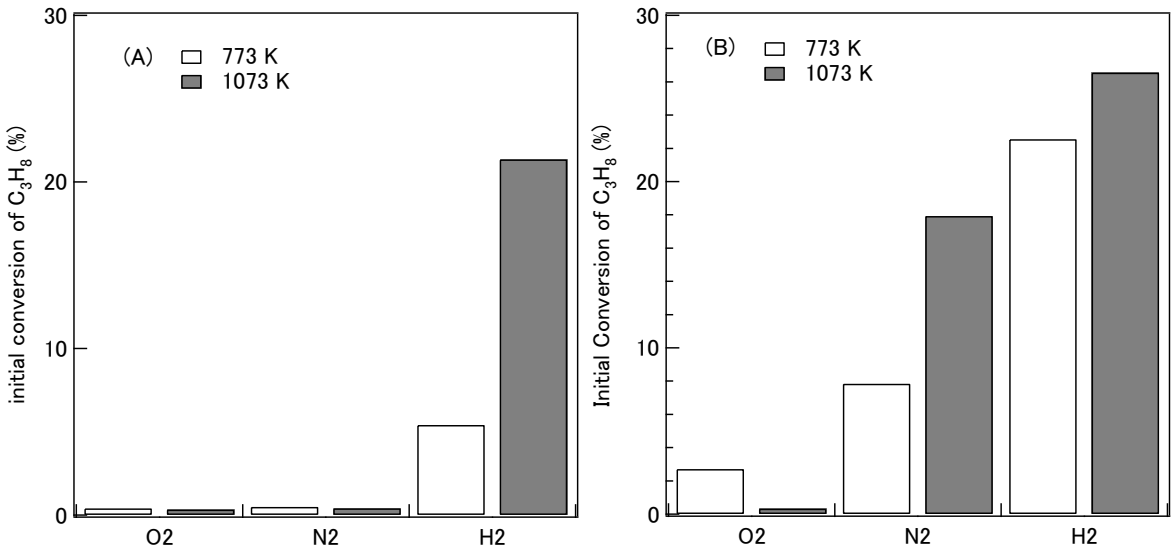

Figure 1 Initial conversion of propane over Pt/SiO_2 (A) and $Pt\text{-}Sn/SiO_2$ (B) pretreated in different atmosphere and temperature (773 K or 1073 K).

Pt ($H_2PtCl_6 \cdot 6H_2O$) finally decomposed into Pt metal regardless the treatment atmosphere (the oxidative, inert or reduction) and temperature (773 K,1073 K). However, the different full-width at half maximum (FWHM) of these diffraction peaks in XRD patterns suggested that pretreatment atmosphere greatly influenced the particle size of Pt formed (Pt dispersion) even though it did not affect the phase of Pt formed. This result is compatible with the TEM observations over Pt/SiO_2 catalysts. The average particle size of Pt is about 25~26 nm after the oxidative pretreatment, 8~11 nm after the inert pretreatment, 2~3 nm after the reduction pretreatment (Table 1). Reduction atmosphere favors the formation of small nano-size Pt particles. Even after the reduction at very high temperature (1073 K) Pt particles retained small size (ca. 2nm).

In the case of bimetallic $Pt\text{-}Sn/SiO_2$ catalysts, the situation is totally different. Under the oxidative pretreatment atmosphere, seen in Fig. 2(1) and (2), $Pt\text{-}Sn/SiO_2$_773 K O_2 displayed no diffraction peaks due to Pt metal or other species. However, Pt metal with fcc structure was present on $Pt\text{-}Sn/SiO_2$_1073 K O_2. Its average particle size from

TEM observation (Fig. 3(A')) is ca. 8.7 nm. In contrast, the average particle size of Pt-Sn/SiO_2_773 K O_2 is as small as 3.3 nm, shown in Fig. 3(A). The pretreatment at high temperature (1073 K) in oxidative atmosphere resulted into the formation of large Pt particles over Pt-Sn/SiO_2_1073 K O_2. Under the inert pretreatment atmosphere, seen in Fig. 2(3) and (4), no obvious diffraction peaks due to Pt metal or other species were found on Pt-Sn/SiO_2_773 K N_2 and Pt-Sn/SiO_2_1073 K N_2. Their TEM images in Fig. 3(B and B') also showed much smaller Pt species when Sn was added to the monometallic system. In the case of the reduction pretreatment atmosphere, as suggested from XRD patterns in Fig. 2(5) and (6), Pt-Sn alloys formed on Pt-Sn bimetallic catalysts with the clear diffraction peak located around 2θ=39° for the Pt_3Sn alloy phase (111) (ICSD 105796) and two peaks around 42° and 44° for the PtSn alloy phase (ICSD 42593). The average sizes of Pt species over Pt-Sn/SiO_2_773 K H_2 and Pt-Sn/SiO_2_1073 K H_2 were small. They are 1.9 nm and 2.6 nm, respectively (Table 1).

XAFS analysis

Pt XAFS analysis

X-ray absorption fine structure (XAFS) measurements have been carried out on Pt-Sn/SiO_2_1073 K O_2, Pt-Sn/SiO_2_1073 K N_2 and Pt-Sn/SiO_2_1073 K H_2. Their X-ray absorption near edge structure (XANES) spectra at Pt L_3 and L_2-edge were shown in Fig.4. Since the Pt L_3 and L_2-edge X-ray absorption white lines correspond to electronic transitions from $2p_{3/2}$ and $2p_{1/2}$ core level states and directly reflect the electronic states of the vacant *d* orbitals of platinum, the L_3 edge reflects the final vacant *d* states of both $5d_{3/2}$ and $5d_{5/2}$ levels, while the L_2 edge reflects that of only the $5d_{3/2}$ level[22]. The white lines of Pt L_3 and L_2-edge over Pt-Sn/SiO_2_1073 K O_2 (spectrum (a)) exhibited the similar position and intensity with those of Pt foil (spectrum (d)), suggesting Pt

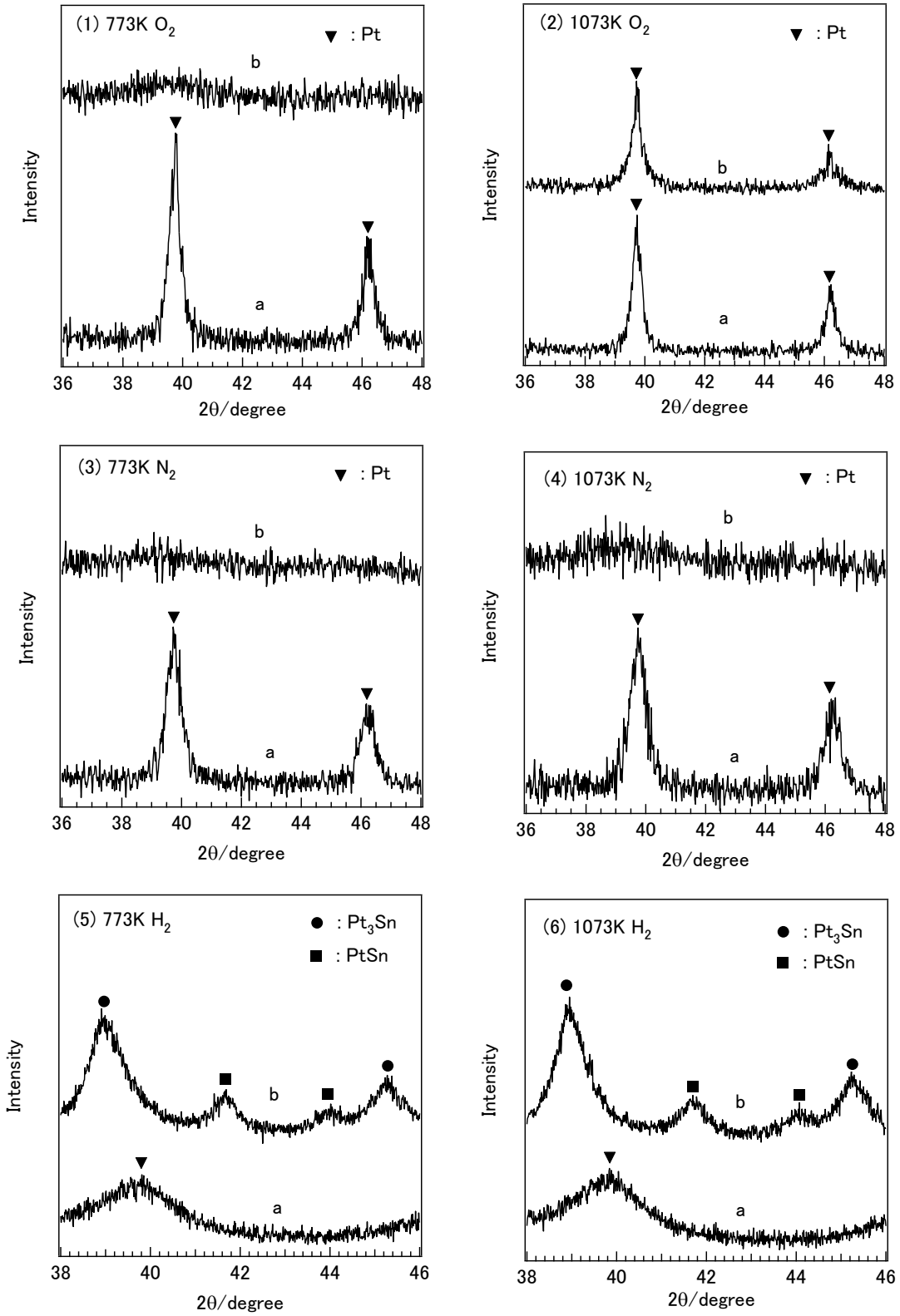

Figure 2 XRD patterns of Pt/SiO_2 (a) and $Pt\text{-}Sn/SiO_2$ (b) pretreated in different conditions

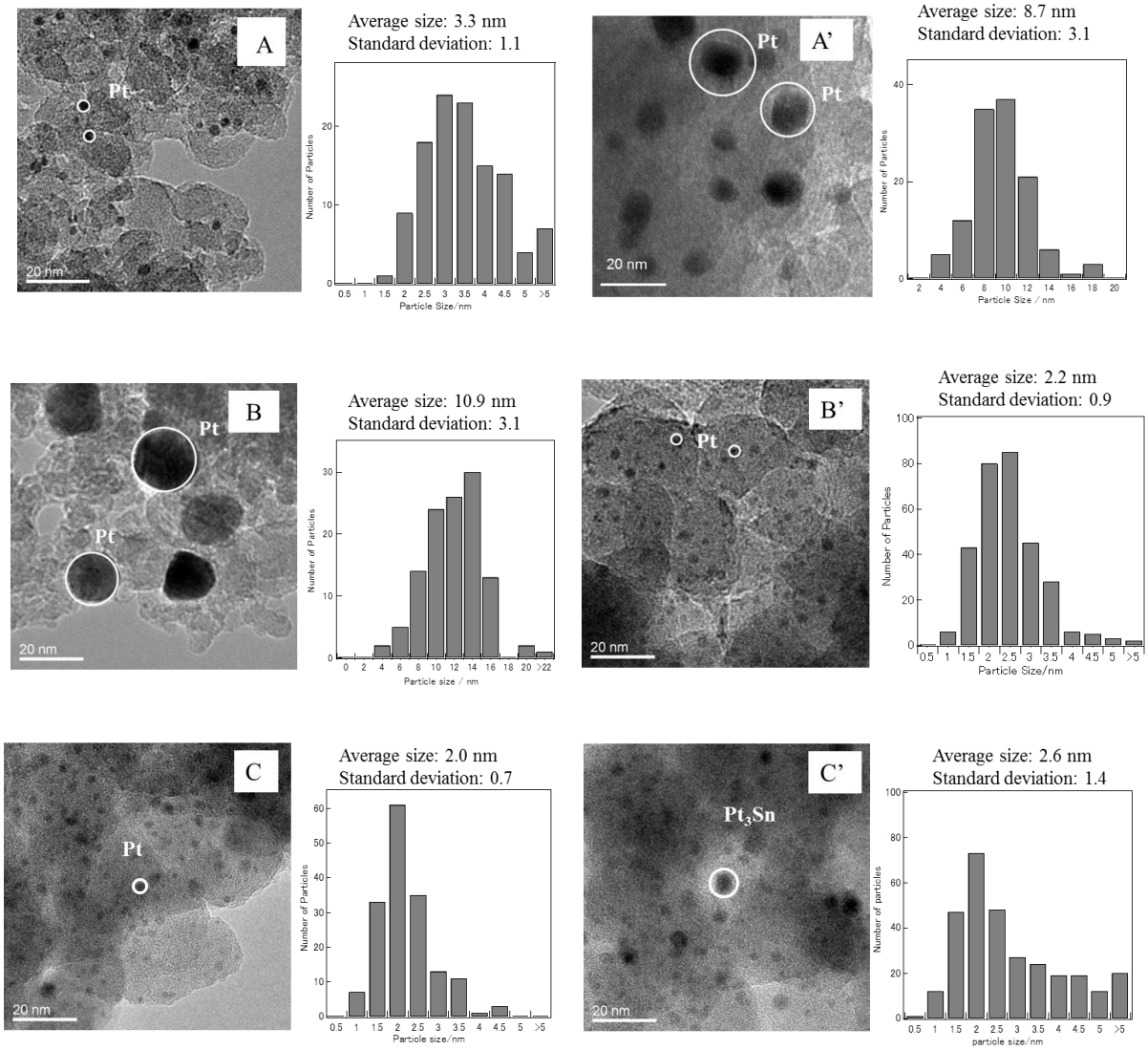

Figure 3 TEM images and the histograms of (A) Pt-Sn/SiO_2_773K O_2, (A') Pt-Sn/SiO_2_1073K O_2, (B) Pt/SiO_2_1073K N_2, (B') Pt-Sn/SiO_2_1073K N_2, (C) Pt/SiO_2_1073K H_2, (C') Pt-Sn/SiO_2_1073K H_2.

metal phase on Pt-Sn/SiO_2_1073K O_2, being compatible with XRD result. Compared with Pt-Sn/SiO_2_1073 K O_2, the white line intensities of Pt L_3 and L_2-edge over Pt-Sn/SiO_2_1073 K N_2 (spectrum (b)) increased, while those over Pt-Sn/SiO_2_1073 K H_2 (spectrum (c)) decreased. In Pt-Sn/SiO_2_1073 K O_2, the electronic state of Pt is similar with that of Pt metal nanoparticles. The increased white line intensity over

Pt-Sn/SiO_2_1073 K N_2 than Pt-Sn/SiO_2_1073 K O_2 indicated that the electron flowing from Pt to the surrounding atoms. In contrast, there is the opposite electron transfer in the case of Pt-Sn/SiO_2_1073 K H_2 because its white line intensity decreased and smaller than that of Pt-Sn/SiO_2_1073 K O_2.

Figure 5(A) shows the k^3-weighted EXAFS oscillations at the Pt L_3-edge of Pt-Sn/SiO_2 catalysts reduced at O_2, N_2 and O_2, and Pt foil as the reference sample. The EXAFS oscillations of Pt-Sn/SiO_2_1073 K O_2 exhibited essentially similar features to those of Pt foil. In its Fourier transforms (FTs) of the EXAFS spectrum shown in Figure 5(B), Pt-Pt linkage (around 0.26 nm) was observed, indicating that the supported Pt species on the Pt-Sn precursor was reduced to the metallic state even after the pretreatment in the oxidized atmosphere at 1073 K. The EXAFS oscillation of Pt-Sn/SiO_2_1073 K N_2 was also similar to that of Pt foil, although the intensity of the oscillations was much weaker. The peak around 0.26 nm in the FTs of the EXAFS spectra of the Pt-Sn/SiO_2_1073K N_2 is assignable to Pt–Pt linkage. A smaller Pt–Pt contribution than that observed for the Pt-Sn/SiO_2_1073 K O_2 indicates that small Pt nanoparticles (ca. 2.2 nm) formed on Pt-Sn/SiO_2_1073 K N_2. Furthermore, a weak and split feature around 0.21–0.28 nm appeared in the EXAFS FTs of Pt-Sn/SiO_2_1073 K H_2, implying the interference of scattered electrons by Sn and Pt as reported by Uemura[14, 21] and Ramallo-Lopez[20]. We have previously reported the results of curve-fitting analysis of the EXAFS data for Pt-Sn/SiO_2_1073 K H_2[24]. By assuming two shells (Pt–Pt and Pt–Sn linkages), the EXAFS data for Pt-Sn/SiO_2_1073 K H_2 was fitted, and the bond distances of Pt–Pt and Pt–Sn were calculated to be slightly shorter than the crystallographic values (Pt–Pt = 0.283 nm and Pt–Sn = 0.283 nm) observed in the Pt_3Sn crystal. This is due to the formation of small particles of Pt_3Sn alloy. Both the

coexistence of a small fraction of PtSn phase and the interference of Pt and Sn scattering resulted in relatively larger R-factors.

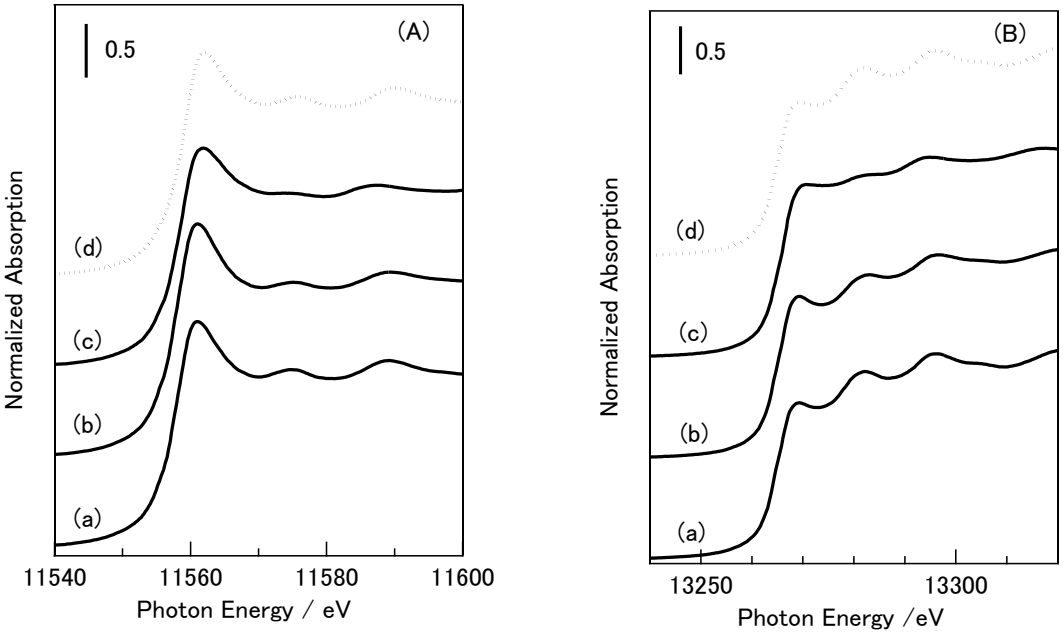

Figure 4 Pt L_3-edge(A) and L_2-edge(B) XANES spectra of Pt-Sn/SiO_2 and Pt foil reference: (a) Pt-Sn/SiO_2_1073K O_2, (b) Pt-Sn/SiO_2_1073K N_2, (c) Pt-Sn/SiO_2_1073K H_2, (d) Pt foil.

Sn XAFS analysis

Figure 6 shows Sn K-edge XANES spectra of Pt-Sn/SiO_2 catalysts pretreated in the different atmospheres, and those of reference samples (Sn foil and SnO_2). The intensity of the absorption band of Pt-Sn/SiO_2_1073 K O_2 is almost same with that of SnO_2. It is evident that Sn species in Pt-Sn/SiO_2_1073 K O_2 was transformed to 4+ valence from $SnCl_2 \cdot 2H_2O$ after the impregnation-calcination process. The white line intensity of Pt-Sn/SiO_2_1073 K N_2 was slightly lower than that of Pt-Sn/SiO_2_1073 K O_2. The white line intensity of Pt-Sn/SiO_2_1073 K H_2 was lowest. The position was higher than that of Sn foil, but lower than that of SnO_2.

There were clear Sn-O bondings in the range of 0.15-0.2 nm for all Pt-Sn/SiO_2

catalysts as shown in the EXAFS Fourier transforms (Fig. 7(B)), which confirms the oxidized state of Sn in all catalysts regardless of pretreatment atmosphere. The weak peaks around 0.2–0.3 nm in the FTs of the EXAFS oscillations of Pt-Sn/SiO_2_1073 K N_2 and Pt-Sn/SiO_2_1073 K H_2 suggests the contribution of Sn–Pt linkage as a result of the close location of Pt and SnO_2 or the formation of Pt-Sn alloy phase. Indeed, the EXAFS data for Pt-Sn/SiO_2_1073 K H_2 was well fitted by assuming two shells (Sn–O and Sn–Pt linkages)[24]. The Sn–O bond distance (0.203 nm) estimated by curve-fitting analysis was similar to the crystallographic value for SnO_2 ($r_{Sn–O}$ = 0.2052 nm) and smaller than that of SnO ($r_{Sn–O}$ = 0.2153 nm). The number of O atoms surrounding Sn atoms in Pt-Sn/SiO_2_1073 K H_2 was 4.1, which is smaller than that of SnO_2 (N_O = 6), probably owing to amorphous SnO_2 phases and nanoparticles different from bulk SnO_2. These results indicate that Pt-Sn alloy particles were present alongside highly dispersed SnO_2 on the Pt-Sn/SiO_2_1073 K H_2.

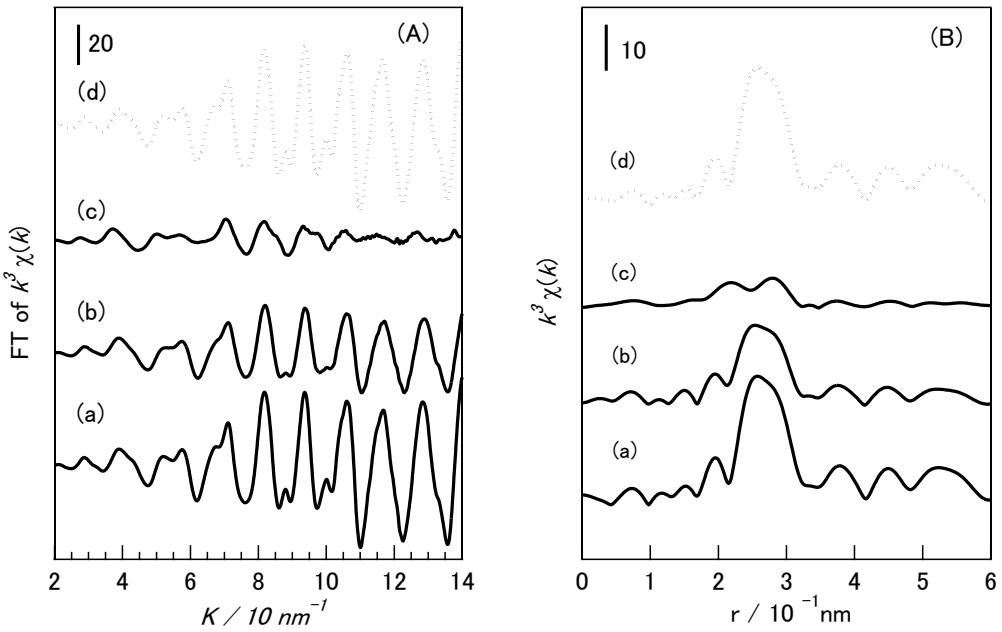

Figure 5 k^3-weighted EXAFS oscillation at Pt L_3-edge (A) and their Fourier transforms (B): (a) Pt-Sn/SiO_2_1073K O_2, (b) Pt-Sn/SiO_2_1073K N_2, (c) Pt-Sn/SiO_2_1073K H_2, (d) Pt foil.

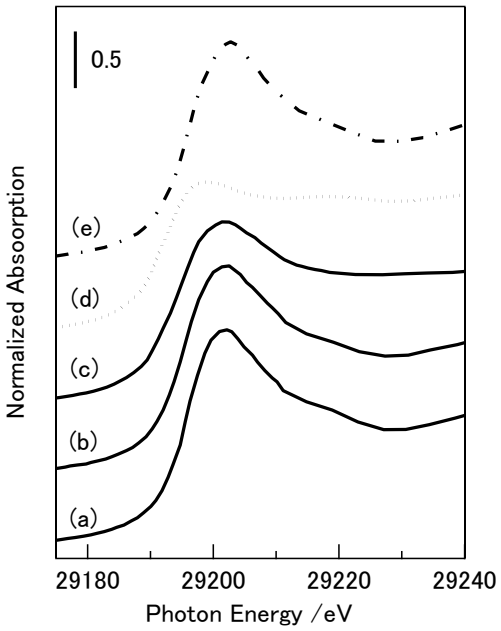

Figure 6 Sn K-edge XANES spectra of Pt-Sn/SiO_2 and references: (a) Pt-Sn/SiO_2_1073K O_2, (b) Pt-Sn/SiO_2_1073K N_2, (c) Pt-Sn/SiO_2_1073K H_2, (d) Sn foil, (e) SnO_2.

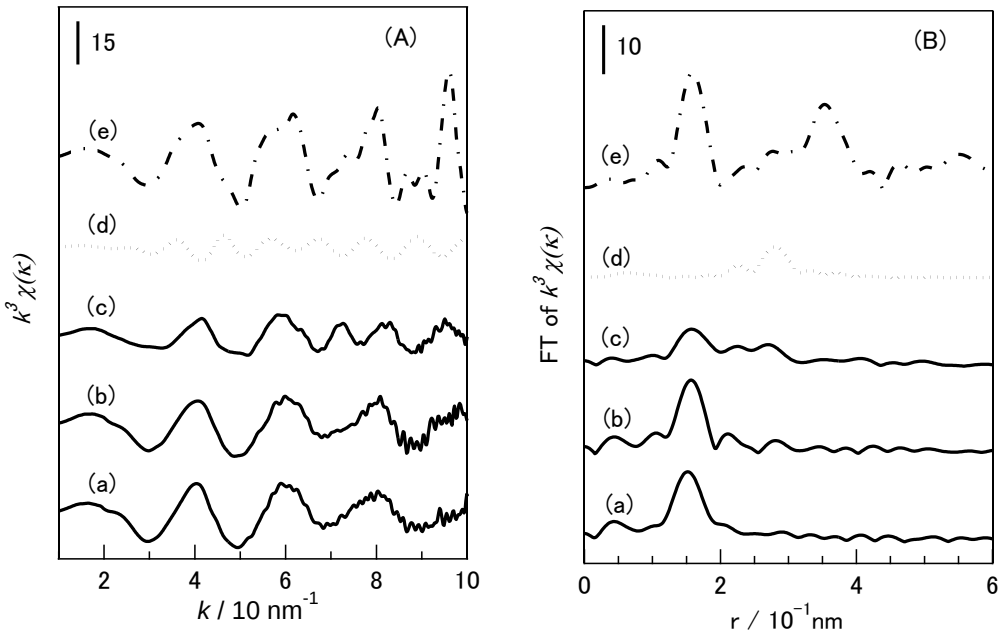

Figure 7 k^3-weighted EXAFS oscillation at Sn K-edge (A) and their Fourier transforms (B): (a) Pt-Sn/SiO_2_1073K O_2, (b) Pt-Sn/SiO_2_1073K N_2, (c) Pt-Sn/SiO_2_1073K H_2, (d) Sn foil, (e) SnO_2.

CO adsorption behaviors and XPS surface analysis

Table 1 summarized the amount of CO adsorbed on different Pt-Sn/SiO_2 catalysts at room temperature. The amount of CO adsorbed on Pt/SiO_2 catalysts were also listed as the references. CO adsorption is a method used very frequently for the characterization of Pt-based catalysts. It can be used to quantify the active surface area of supported Pt catalysts, determine the metal dispersion[26], and study the interaction between Pt and the support or other promoters[27]. Small Pt particles (high dispersion) provided more accessible surface Pt atoms for CO adsorption, while larger Pt particles (low dispersion) generally resulted into the small amount of CO adsorption. In our studies, about 54.9 μmol g^{-1} CO adsorbed on Pt/SiO_2_773 K H_2 on which the average Pt metal particle size is about 2.0 nm. Large Pt metal particles (ca. 25-26 nm) were present on Pt/SiO_2 monometallic catalysts after pretreatment in the oxidized atmosphere, and no CO adsorbed on them. Small amount of CO adsorbed on Pt/SiO_2 catalysts after pretreatment in the inert atmosphere. The addition of Sn into Pt/SiO_2 system effectively improved Pt dispersion in the both oxidized and inert atmosphere. The average Pt particle sizes are in the range of 2.2-3.3 nm over these Pt-Sn/SiO2 catalysts. CO adsorptions on them slightly increased compared with the corresponding Pt/SiO_2 catalysts, and were still smaller than the CO adsorption over Pt/SiO_2_773 K H_2 which presents the similar particle size (2.0 nm) with them. This result suggested that Sn addition increased the dispersion of Pt metal and CO adsorption on them, whereas it also probably led to the deposition of Sn species on the surface Pt metal particles and decreased the CO adsorption on them. After the pretreatment in the reductive atmosphere, CO adsorption on Pt-Sn bimetallic catalysts drastically decreased even the high dispersion of Pt species on them. Only 18.1 μmol g^{-1} CO adsorbed on

Pt-Sn/SiO_2_773 K H_2 and 6.5 μmol g^{-1} CO on Pt-Sn/SiO_2_1073 K H_2. The XRD data

Table 1 Physical and chemical properties of Pt/SiO_2 and Pt-Sn/SiO_2 catalysts.

Catalysts[a]	BET surface area[b](m^2g^{-1})	Average Particle Size[c](nm)	CO adsorption[d] (μmol g^{-1})
Pt/SiO_2_773K O_2	355	25.6 ± 9.7	1.1
Pt/SiO_2_1073K O_2	332	26.0 ± 20.1	0.0
Pt-Sn/SiO_2_773K O_2	311	3.3 ± 1.1	9.4
Pt-Sn/SiO_2_1073K O_2	300	8.7 ± 3.1	2.3
Pt/SiO_2_773 K N_2	311	9.3 ± 7.2	3.8
Pt/SiO_2_1073 K N_2	303	10.9 ± 3.1	0.9
Pt-Sn/SiO_2_773K N_2	298	3.1 ± 1.1	10.8
Pt-Sn/SiO_2_1073K N_2	330	2.2 ± 0.9	10.6
Pt/SiO_2_773K H_2	340	2.0 ± 0.7	54.9
Pt/SiO_2_1073K H_2	320	2.6 ± 1.2	40.3
Pt-Sn/SiO_2_773K H_2	282	2.0 ± 1.2	18.1
Pt-Sn/SiO_2_1073K H_2	300	2.6 ± 1.4	6.5

a: The molar ratio of Pt to Sn was fixed as 1:1. The loading amout of Pt is 3wt%.

b: The surface area of SiO_2 (JRC-SIO-9) is 325 m^2 g^{-1}.

c: Average particle size was calculated by counting up over 300 black dots from TEM observation.

displayed that Pt-Sn alloy formed on H_2-pretreated catalysts. Alloy formation may contribute to the small CO adsorption on Pt- Sn/SiO_2_773 K H_2 and Pt-Sn/SiO_2_1073 K H_2. Indeed, various Pt based alloys, such as PtRu, PtMo or PtSn, presented a better CO

tolerance (lower CO adsorption) than pure platinum[28]. Alloying with these second metals probably modified the electronic and geometric state of Pt and thus inhibited CO adsorption on alloy catalysts.

Figure 8 shows the Pt 4f (A) and Sn 3d (B) XPS spectra of Pt-Sn/SiO_2 catalysts pretreated in the different atmospheres. The binding energies of the Pt $4f_{7/2}$ and $4f_{5/2}$ peaks were 71.6 and 74.8 eV, respectively on Pt-Sn/SiO_2_1073 K N_2, and Pt-Sn/SiO_2_1073 K H_2. Based on these binding energies, the valence of platinum in the Pt-Sn/SiO_2 catalysts was assigned to Pt^0. As for Pt-Sn/SiO_2_1073 K O_2, Pt $4f_{7/2}$ and $4f_{5/2}$ peaks shifted towards lower binding energy, located at 71.1 and 74.4 eV, respectively. This sift may be due to the larger Pt metal particles on Pt-Sn/SiO_2_1073 K O_2 than those on Pt/SiO_2_773 K H_2, Pt-Sn/SiO_2_1073 K N_2, and Pt-Sn/SiO_2_1073 K H_2. In the case of the Sn 3d region, the binding energy of the Sn $3d_{5/2}$ peaks on Pt-Sn/SiO_2_1073 K H_2 was located at 486.5 eV, higher than the values usually reported for metallic Sn (484.9 eV) and lower than those typically reported for Sn oxides (487.1 eV). This suggests the coexistence of metallic Sn and Sn oxides on Pt-Sn/SiO_2_1073 K H_2. It is also obvious that the binding energies of Sn $3d_{5/2}$ peak shifted to higher energy when pretreatment atmosphere transformed from reductive one to inert and oxidized ones, indicating a decrease in the surface Sn^0/Sn^{IV} ratio. The surface ratio of Sn^0/Sn^{IV} on Pt-Sn/SiO_2_1073 K H_2, Pt-Sn/SiO_2_1073K N_2 and Pt-Sn/SiO_2_1073 K O_2 was determined to be 32/68, 35/65, and 44/56, respectively, from the deconvolution results. This observation is consistent with the Sn K-edge XAFS results discussed above: on Pt-Sn/SiO_2_1073 K H_2, one part of the Sn formed Pt-Sn alloy and the left was present as small, highly dispersed SnO_2 particles.

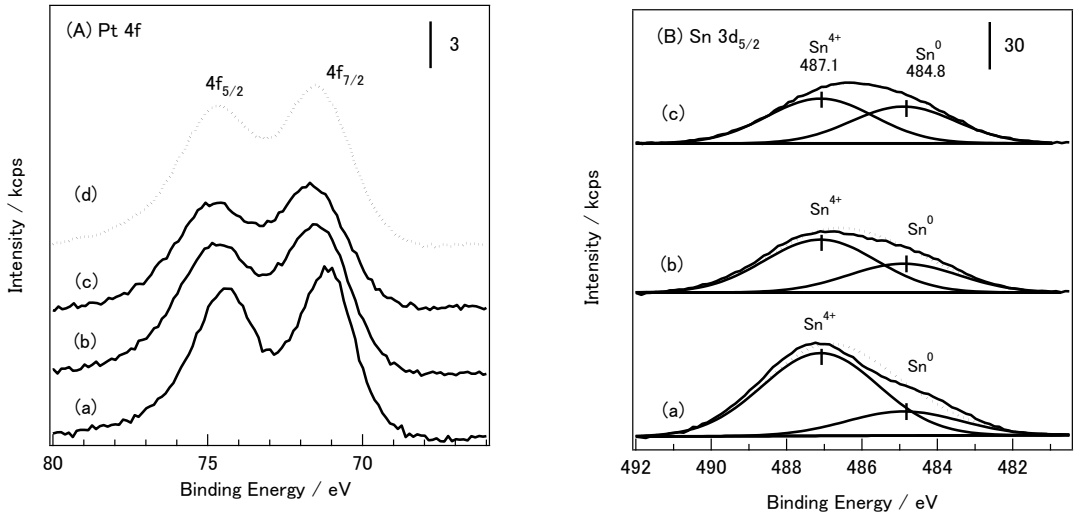

Figure 8 XPS spectra of Pt level and Sn level for (a) Pt-Sn/SiO_2_1073 K O_2, (b) Pt-Sn/SiO_2_1073 K N_2, (c) Pt-Sn/SiO_2_1073 K H_2, (d) Pt/SiO_2_773 K H_2 (reference sample).

Discussion

D. Radivojevic et al. [29] once prepared Pt/SiO_2 precursor with impregnating SiO_2 with aqueous solutions of H_2PtCl_6 •$6H_2O$, and studied its behaviors in the calcination (air atmosphere) or reduction treatment. It was found that the reduction of SiO_2 supported platinum precursor removes chlorine species efficiently at very low temperatures (around 373 K) and results in well-dispersed catalysts. In the present paper, it was further shown that the pretreatment atmosphere has a great influence on the Pt dispersion over Pt/SiO_2 catalysts and the structure of Pt-Sn/SiO_2 catalyst. The order of Pt dispersion over Pt/SiO_2 catalysts was Pt/SiO_2_O_2 < Pt/SiO_2_N_2 < Pt/SiO_2_H_2. The effect of pretreatment atmosphere on the structure of the Pt-Sn/SiO_2 catalysts is represented in Scheme 1. The pretreatment in the oxidative atmosphere led to the week interaction between large Pt metal particles and small SnO_2. Pt-Sn/SiO_2_1073 K O_2 shows no activity for propane dehydrogenation. The strong interaction between small Pt

metal particles and SnO_2 (Pt-SnO_x(x<2) interaction) was introduced with the inert pretreatment atmosphere at 1073 K. Pt-Sn/SiO_2_1073 K N_2 shows high activity in the dehydrogenation of propane. Pt-Sn alloys formed after pretreat Pt-Sn/SiO_2 precursor in the reductive atmosphere. Pt-Sn/SiO_2_1073 K H2 mainly possessed small Pt_3Sn alloy particles (ca. 2.6 nm) decorated with a highly dispersed SnO_2. And it showed the best catalytic behaviors in the dehydrogenation of propane.

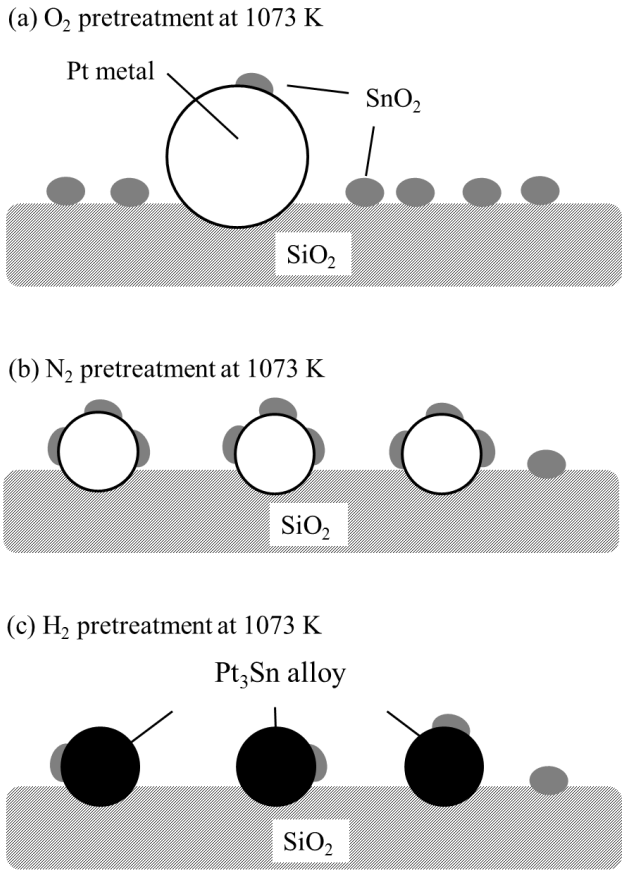

Scheme 1 The effects of pretreatment atmosphere on the structure of Pt-Sn/SiO_2 catalysts.

XANES analysis of Pt in these catalysts (Fig. 4) show that the electronic state of Pt in Pt-Sn/SiO_2_1073 K O_2 was similar with that of Pt atoms in Pt foil, while it is more electron-deficient in Pt-Sn/SiO_2_1073 K N_2. It is probably originated from the

electronic modification of highly dispersed SnO_2 decorated on the surface of Pt metal particles. A partially reduced oxide species (SnO_x (x<2)) is probably formed in the interface between Pt and SnO_2 during high-temperature pretreatment in the inert atmosphere. This phenomenon is similar with the strong metal-support interactions (SMSI) for metal (Rh, Pt, Pd, etc.) catalysts supported on SMSI oxides (TiO_2, Nb_2O_5,V_2O_3, MnO) and metal/non-SMSI oxide (SiO_2) catalysts promoted with SMSI oxides[30-34]. The unique properties of reduced SnO_x/Pt(111) surfaces were also found in CO oxidation[35, 36], electro-oxidation of methanol[37], cellulose conversion [38].

In contrast, the electronic state of Pt in Pt-Sn/SiO_2_1073 K H_2 is more electron-rich compared with both Pt-Sn/SiO_2_1073 K O_2 and Pt-Sn/SiO_2_1073 K N_2. Pt_3Sn alloy was detected on it by XRD and XAFS. Indeed, when Pt alloyed with Sn which has a lower electronegativity than Pt (Pt 2.2, Sn 1.8), the electrons donated form Sn to Pt and led to the electronic modification of Pt. Pt being more electron-rich in Pt-Sn alloys was also found in the previous reports[14, 21, 39]. Furthermore, S. Pick [40] pointed out that when Pt alloyed with Sn, Pt d- and Sn p-electrons hybridized, leads to a lowering of the local density of electronic states at the Fermi lever and to a downward shift of the Pt local d-band. Stamenkovic, V. et al [41] studied Pt alloys involving 3d metals for the oxygen reduction reaction. It was found that the activity versus d-band center position of Pt in these Pt-M alloys exhibits a classical volcano-shaped dependence.

During the dehydrogenation of propane, the first step is the absorption of saturated hydrocarbon (propane) on the catalyst surface. The theory calculation with density functional theory method done by Nykanen L. and Honkala K.[42] shows that propane adsorption on Pt (111) and Pt_3Sn alloy surfaces is week and mediated by van

der Walls interactions. Yang Minglei et al. [43] also reported that propane is physisorbed on the Pt and PtSn surfaces with First Principles calculations. The TPD spectra of propane adsorbed on Pt-Sn/SiO_2_1073 K O_2, Pt-Sn/SiO_2_1073 K N_2 and Pt-Sn/SiO_2_1073 K H_2 involved in the present work (Fig. 9(A)) also show the week propane adsorption on them without significant site preference on any of the studied surfaces. All these results support the interpretation that saturated propane only physisorbs on the surfaces. The second step in the reaction, the activation of the first C–H bond of propane molecule, is often regards as the rate-determining step[44, 45]. Supported platinum nanoparticle due to its high density of electronic states close to the Fermi level, a characteristic that contributes to C-H bond activation, is one of the most suitable catalysts for the thermal dehydrogenation of light alkanes even it suffers from low alkene selectivity and the rapid deactivation due to coking. As mentioned above, the electronic states of Pt were modified in the cases Pt-Sn/SiO_2_1073 K N_2 and Pt-Sn/SiO_2_1073 K H_2. The unique states of Pt atoms in Pt-SnO_x ($x<2$) interface and Pt_3Sn alloy probably enhanced C-H bond activation. Furthermore, they also modified the behaviors of propylene desorption (the third step of the reaction) and propylene dehydrogenation on them. The related theory calculations [42, 43, 46] show that the introduction of Sn lowers the energy barrier for propylene desorption and simultaneously increases the activation energy for propylene dehydrogenation (being a positive effect on the selectivity toward propylene production). The TPD spectra of propylene adsorbed on Pt-Sn/SiO_2_1073 K O_2, Pt-Sn/SiO_2_1073 K N_2 and Pt-Sn/SiO_2_1073 K H_2 involved in the present work (Fig. 9(B)) were not present large difference between Pt-Sn/SiO_2_1073 K O_2 and Pt-Sn/SiO_2_1073 K H_2. However, less adsorption of propylene over Pt-Sn/SiO_2_1073 K H_2 than Pt-Sn/SiO_2_1073 K N_2 was

observed, which may explain the slight higher activity over the former one.

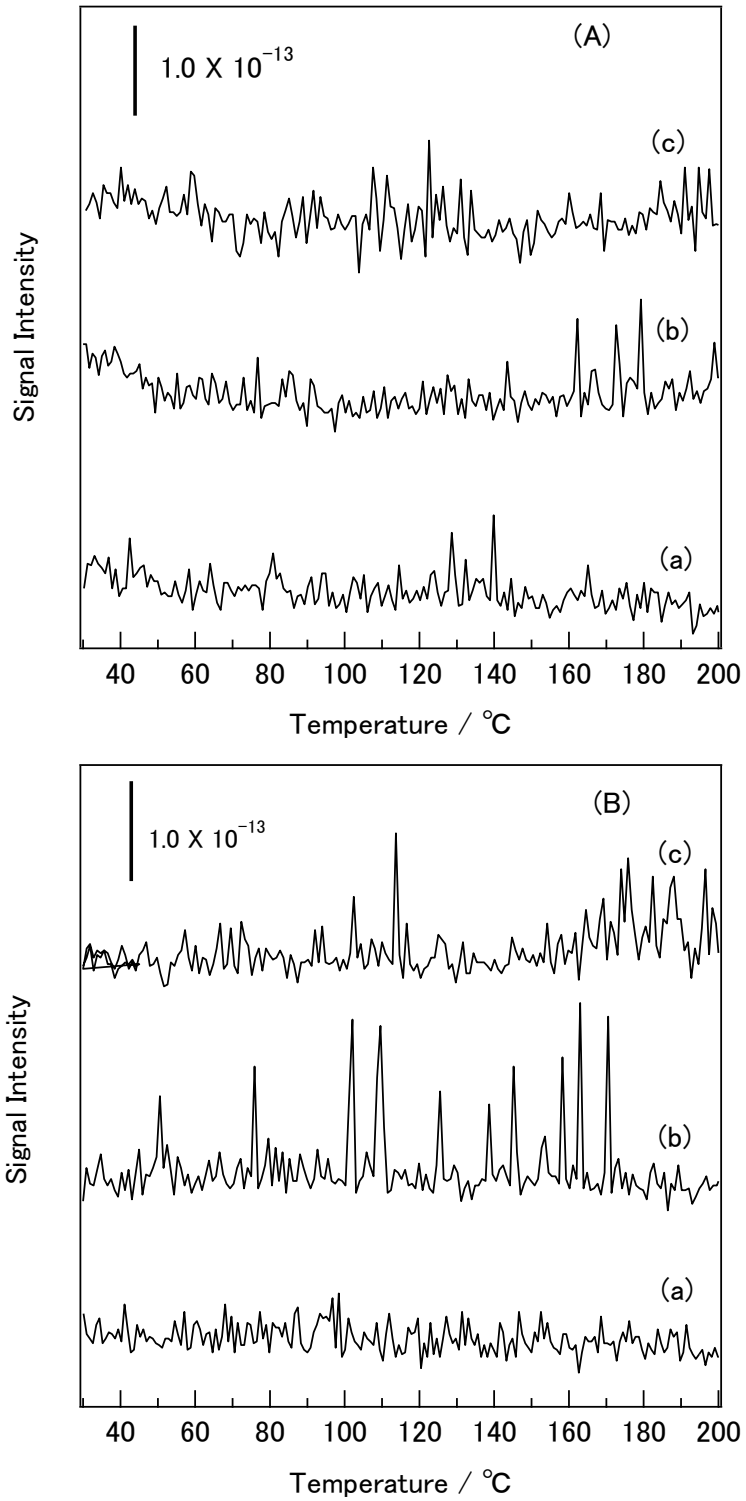

Figure 9 TPD profiles of propane (A) and propylene (B) adsorption on (a) Pt-Sn/SiO_2_1073 K O_2, (b) Pt-Sn/SiO_2_1073 K N_2, (c) Pt-Sn/SiO_2_1073 K H_2.

Conclusion

Pt-Sn/SiO_2 catalysts with the different structure can be obtained with varying the pretreatment atmosphere over Pt-Sn/SiO_2 precursor. The inert atmosphere (N_2) led to strong interaction between Pt and SnO_2 at high pretreatment temperature (1073 K), thus Pt metal was highly dispersed on SiO_2. This interaction is probably responsible for the high activity of the catalyst in propane dehydrogenation. The reductive atmosphere (H_2) introduced the alloy formation between Pt and Sn. The Pt_3Sn phase was dominant over Pt-Sn/SiO_2 reduced in H_2 atmosphere at 1073 K, which exhibited the best catalytic behaviors.

References

[1] N. Rahimi and R. Karimzadeh, Appl. Catal. A, 398 (2011) 1.

[2] Y. Yoshimura, N. Kijima, T. Hayakawa, K. Murata, K. Suzuki, F. Mizukami, K. Matano, T. Konishi, T. Oikawa, M. Saito, T. Shiojima, K. Shiozawa, K. Wakui, G. Sawada, K. Sato, S. Matsuo and N. Yamaoka, Catalysis Surveys from Japan, 4 (2000) 57.

[3] A. Farshi, F. Shaiyegh, S.H. Burogerdi and A. Dehgan, Petroleum Science and Technology, 29 (2011) 875.

[4] H.M.T. Galvis and K.P. de Jong, ACS Catalysis, 3 (2013) 2130.

[5] S. Derossi, G. Ferraris, S. Fremiotti, E. Garrone, G. Ghiotti, M.C. Campa and V. Indovina, Journal of Catalysis, 148 (1994) 36.

[6] R. Cortright and J. Dumesic, Journal of Catalysis, 148 (1994) 771.

[7] A. Iglesias-Juez, A.M. Beale, K. Maaijen, T.C. Weng, P. Glatzel and B.M. Weckhuysen, Journal of Catalysis, 276 (2010) 268.

[8] S. Stagg, C. Querini, W. Alvarez and D. Resasco, Journal of Catalysis, 168 (1997) 75.

[9] B.K. Vu, M.B. Song, I.Y. Ahn, Y.-W. Suh, D.J. Suh, W.-l. Kim, H.-L. Koh, Y.G. Choi and E.W. Shin, Appl. Catal. A, 400 (2011) 25.

[10] O. Barias, A. Holmen and E. Blekkan, Journal of Catalysis, 158 (1996) 1.

[11] A. Virnovskaia, S. Morandi, E. Rytter, G. Ghiotti and U. Olsbye, J. Phys. Chem. C, 111 (2007) 14732.

[12] K. Balakrishnan and J. Schwank, Journal of Catalysis, 138 (1992) 491.

[13] S. deMiguel, A. Castro and O. Scelza, Catalysis Letters, 36 (1996) 201.

[14] Y. Uemura, Y. Inada, K.K. Bando, T. Sasaki, N. Kamiuchi, K. Eguchi, A. Yagishita, M. Nomura, M. Tada and Y. Iwasawa, The Journal of Physical Chemistry, 115 (2011) 5823.

[15] M. Ellner, Journal of the Less-Common Metals, 78 (1981) 21.

[16] P. Durussel, R. Massara and P. Feschotte, Journal of Alloys and Compounds, 215 (1994) 175.

[17] I.R. Harris, M. Norman and A. Bryant, Journal of the Less-Common Metals, 16 (1968) 427.

[18] Z. Paal, A. Wootsch, D. Teschner, K. Lazar, I.E. Sajo, N. Gyorffy, G. Weinberg, A. Knop-Gericke and R. Schlogl, Appl. Catal. A, 391 (2011) 377.

[19] A.I. Frenkel, Chem. Soc. Rev., 41 (2012) 8163.

[20] J. Ramallo-Lopez, G. Santori, L. Giovanetti, M. Casella, O. Ferretti and F. Requejo, J. Phys. Chem. B, 107 (2003) 11441.

[21] Y. Uemura, Y. Inada, K.K. Bando, T. Sasaki, N. Kamiuchi, K. Eguchi, A. Yagishita, M. Nomura, M. Tada and Y. Iwasawa, Phys. Chem. Chem. Phys., 13 (2011)

15833.

[22] A.N. Mansour, J.W. Cook and D.E. Sayers, Journal of Physical Chemistry, 88 (1984) 2330.

[23] J.-D. Grunwaldt and B.S. Clausen, Topics in Catalysis, 18 (2002) 37.

[24] L. Deng, T. Shishido, K. Teramura and T. Tanaka, Catalysis Today, 232 (2014) 33.

[25] L. Deng, H. Miura, T. Shishido, S. Hosokawa, K. Teramura and T. Tanaka, ChemCatChem, in press (2014).

[26] T. Tanabe, Y. Nagai, T. Hirabayashi, N. Takagi, K. Dohmaea, N. Takahashi, S.i. Matsumoto, H. Shinjoh, J.N. Kondo, J.C. Schouten and H.H. Brongersma, Applied Catalysis A: General, 370 (2009) 108.

[27] C. Ocal and S. Ferrer, The Journal of Chemical Physics, 84 (1986) 6474.

[28] Z. Liu, G.S. Jackson and B.W. Eichhorn, Angewandte Chemie-International Edition, 49 (2010) 3173.

[29] D. Radivojevic, K. Seshan and L. Lefferts, Appl. Catal. A, 301 (2006) 51.

[30] S.-I. Ito, T. Fujimori, K. Nagashima, K. Yuzaki and K. Kunimori, Catalysis Today, 57 (2000) 247.

[31] S.-I. Ito, C. Chibana, K. Nagashima, S. Kameoka, K. Tomishige and K. Kunimori, Applied Catalysis A: General, 236 (2002) 113.

[32] S. M.S., Journal of Catalysis, 93 (1985) 216.

[33] M.A. Vannice and C.C. Twu, Journal of Catalysis, 82 (1983) 213.

[34] S.J. Tauster, S.C. Fung and R.L. Garten, Journal of the American Chemical Society, 100 (1978) 170.

[35] S. Axnanda, W.-P. Zhou and M.G. White, Phys. Chem. Chem. Phys., 14 (2012)

10207.

[36] S.D. Gardner, G.B. Hoflund, B.T. Upchurch, D.R. Schryer, E.J. Kielin and J. Schryer, Journal of Catalysis, 129 (1991) 114.

[37] W.-P. Zhou, W. An, D. Su, R. Palomino, P. Liu, M.G. White and R.R. Adzic, The Journal of Physical Chemistry letters, 3 (2012) 3286.

[38] T. Deng and H. Liu, Green Chemistry, 15 (2013) 116.

[39] J.H. Kim, S.M. Choi, S.H. Nam, M.H. Seo, S.H. Choi and W.B. Kim, Applied Catalysis B: Environmental, 82 (2008) 89.

[40] S. Pick, Surface Science, 436 (1999) 220.

[41] V. Stamenkovic, B.S. Mun, K.J.J. Mayrhofer, P.N. Ross, N. Markovic, J. Rossmeisl, J. Greeley and J.K. Nørskov, Angewandte Chemie-International Edition, 45 (2006) 2897.

[42] L. Nykanen and K. Honkala, The Journal of Physical Chemistry, 115 (2011) 9578.

[43] M.-L. Yang, Y.-A. Zhu, X.-G. Zhou and D. Chen, ACS Catalysis, 2 (2012) 1247.

[44] A.W. Hauser, J. Gomes, M. Bajdich, M. Head-Gordon and A.T. Bell, Phys. Chem. Chem. Phys., 15 (2013) 20727.

[45] J.-M.M. Millet, Topics in Catalysis, 38 (2006) 83.

[46] L. Nykanen and K. Honkala, ACS Catalysis, 3 (2013) 3026.

Chapter 2
Effect of reduction method on the activity of Pt-Sn/SiO_2 for dehydrogenation of propane

Abstract

The effect of reduction method (direct reduction (*DR*), decomposition in inert gas (*DI*) and calcination-reduction (*CR*)) on the catalytic performances of Pt-Sn/SiO_2 catalyst in the dehydrogenation of propane was investigated. The Pt-Sn/SiO_2 (*DR*) showed the highest activity among the catalysts tested. The order of activities of Pt/SiO_2 and Pt-Sn/SiO_2 catalysts was Pt/SiO_2 (*DR*) $\leqq$ Pt-Sn/SiO_2 (*CR*) < Pt-Sn/SiO_2 (*DI*) < Pt-Sn/SiO_2 (*DR*). The results of structural characterization by X-ray diffraction (XRD), CO pulse, transmission electron microscopy (TEM), and Pt L_{III} and Sn K-edges X-ray absorption fine structure (XAFS) spectroscopy indicated that Pt_3Sn alloy nanoparticle was mainly formed on the Pt-Sn/SiO_2 (*DR*). In the case of the Pt-Sn/SiO_2 (*CR*) catalyst, PtSn alloy particle was mainly dispersed on SiO_2. On the other hand, Pt metal particles and highly dispersed SnO_2 were present on the Pt-Sn/SiO_2 (*DI*). The relationship between activity and structure of platinum-tin catalysts suggested that Pt_3Sn alloy acts as active site for dehydrogenation of propane, whereas PtSn alloy shows low or no activity.

Introduction

The catalytic dehydrogenation of light alkanes such as propane and butane is of great interest due to growing demands of alkenes as an important raw chemical intermediate to produce rubber, plastics and many other products [1,2]. The conventional way of light alkenes in the petrochemical industry is steam cracking of alkanes, naphtha, and gas oil. The steam cracking is typically carried out above 1000 K. Thus, this reaction is energetically-unfavorable and shows low selectivity to alkenes. For example, in the case of steam cracking of naphtha, the yields of ethane and propylene are ca. 30 and 20 %, with substantial amounts of by-products including methane and coke. On the other hand, catalytic dehydrogenation of light alkanes provides an alternative for producing light alkenes as well as hydrogen.

Supported platinum-tin alloy catalysts have been widely studied in catalytic dehydrogenation of propane (DHP) [3-6]. The addition of Sn to Pt/support catalyst system has been found to favor selective lower alkane dehydrogenation, suppress the coke formation and increase the lifetime of the catalyst. These positive effects of Sn on the catalytic performance of supported Pt catalysts have been interpreted from both a geometrical (ensemble) and an electronic point of view [3-12]. Despite extensive studies, the role of Sn in a Pt-Sn catalyst remains elusive and the accurate nature of Pt-Sn system is complicated for many years. It has been well known that the properties of Pt-Sn alloy catalyst have been found to depend on the several factors such as support, metallic precursor, and preparation procedure [8, 13, 14]. Moreover, the active alloy phases often collapse into each metal oxide under ambient oxygen, resulting in deactivation of catalyst. Uemura et al. reported the reductive formation and oxidative phase separation of Pt_3Sn alloy nanoparticle in the reduction and oxidation processes by

the *in situ* time resolved XAFS techniques [15,16]. This indicates that the stability of supported alloy catalyst is affected by the reaction and regeneration conditions [6, 15, 16]. As a consequence, there has been considerable interest in developing means to control the interactions between platinum and tin by appropriate catalyst preparation, pretreatment, and regeneration procedure.

In the present study, three different reduction procedures (direct reduction (*DR*), decomposition in inert gas (*DI*) and calcination-reduction (*CR*)) were applied to prepare a series of Pt-Sn/SiO_2 catalysts with different interactions between platinum and tin. The structure of platinum and tin was investigated by using X-ray absorption fine structure (XAFS) at Pt L_{III}- and Sn K-edges, TEM, CO-pulse, XRD techniques, and the catalytic test in propane dehydrogenation. The effect of reduction procedures on the nature of the Pt-Sn systems was investigated. The relationship between the structure of Pt-Sn nanoparticles and activity for propane dehydrogenation was discussed.

Experimental

Catalyst preparation

A silica (JRC-SIO-9, 334 m^2 g^{-1}) was used as support to prepare Pt and Pt-Sn catalysts. Prior to impregnation, the SiO_2 support was treated at 773 K for 3h in air. Silica-supported Pt catalyst (Pt/SiO_2) was prepared by impregnation of SiO_2 with the adequate volume of an aqueous solution of $H_2PtCl_6 \cdot 6H_2O$ (Wako, 99.9%), followed by the stirring at 353 K for 3h and dried at 353 K for 20h. A bimetallic Pt-Sn/SiO_2 was prepared by sequential impregnation method. The SiO_2 support was firstly impregnated with an aqueous solution of $H_2PtCl_6 \cdot 6H_2O$, and then stirred at 353K for 3h, and dried at 353 K for 20h. Then the precipitate was added to an acetone solution of $SnCl_2 \cdot 2H_2O$

(Wako, 97%), stirred at 353 K for 3h and dried at 353 K for 20h to yield the catalyst precursor. The Pt content was 3wt.%. The molar ration of Pt to Sn was 1.0. Prior to the reaction, the catalyst precursor was reduced by following three methods (Scheme 1): (1) Direct reduction (*DR*) The catalyst precursor was *in situ* reduced in 20 vol% H_2 diluted with N_2 (total flow rate 50ml min^{-1}) at 1073 K for 1h, and then cooled to 773 K in N_2 (100ml min^{-1}). (2) Decomposition in inert gas (*DI*) The catalyst precursor was treated with N_2 (total flow rate 50ml min^{-1}) at 1073 K for 1h, and then cooled to 773 K in N_2 (100ml min^{-1}). (3) Calcination-Reduction (*CR*) The catalyst precursor was firstly calcined in 20vol % O_2 diluted with N_2 (total flow rate 50ml min^{-1}) at 773 K for 1 h, and then reduced in 20 vol% H_2 diluted with N_2 (total flow rate 50ml min^{-1}) at 1073 K for 1h. Finally, the catalyst was cooled to 773 K in N_2 (100ml min^{-1}).

Propane dehydrogenation

Propane dehydrogenation was carried out by using a quartz reactor at atmospheric pressure with C_3H_8/N_2 (20/80) mixed gas at 773 K. Total flow rate was 100 ml min^{-1}. The catalyst precursor (50 mg) was placed between quarts-wool. The gas composition was analyzed with an on-line gas chromatographs (Shimadzu GC-8A, Japan) equipped with a TCD (Molecular Sives-5A column) and a methanizer FID (Porapak-Q column) detectors.

Characterization

The Brunauer—Emmett—Teller (BET) specific surface area was estimated from N_2 isotherm at 77 K. The N_2 adsorption isotherm measurements were carried out by using a BELSORP 28SA (BEL Japan, Osaka, Japan) at 77 K. Prior to the measurement, each sample was evacuated at 573 K for 3 h. The amount of adsorbed CO was

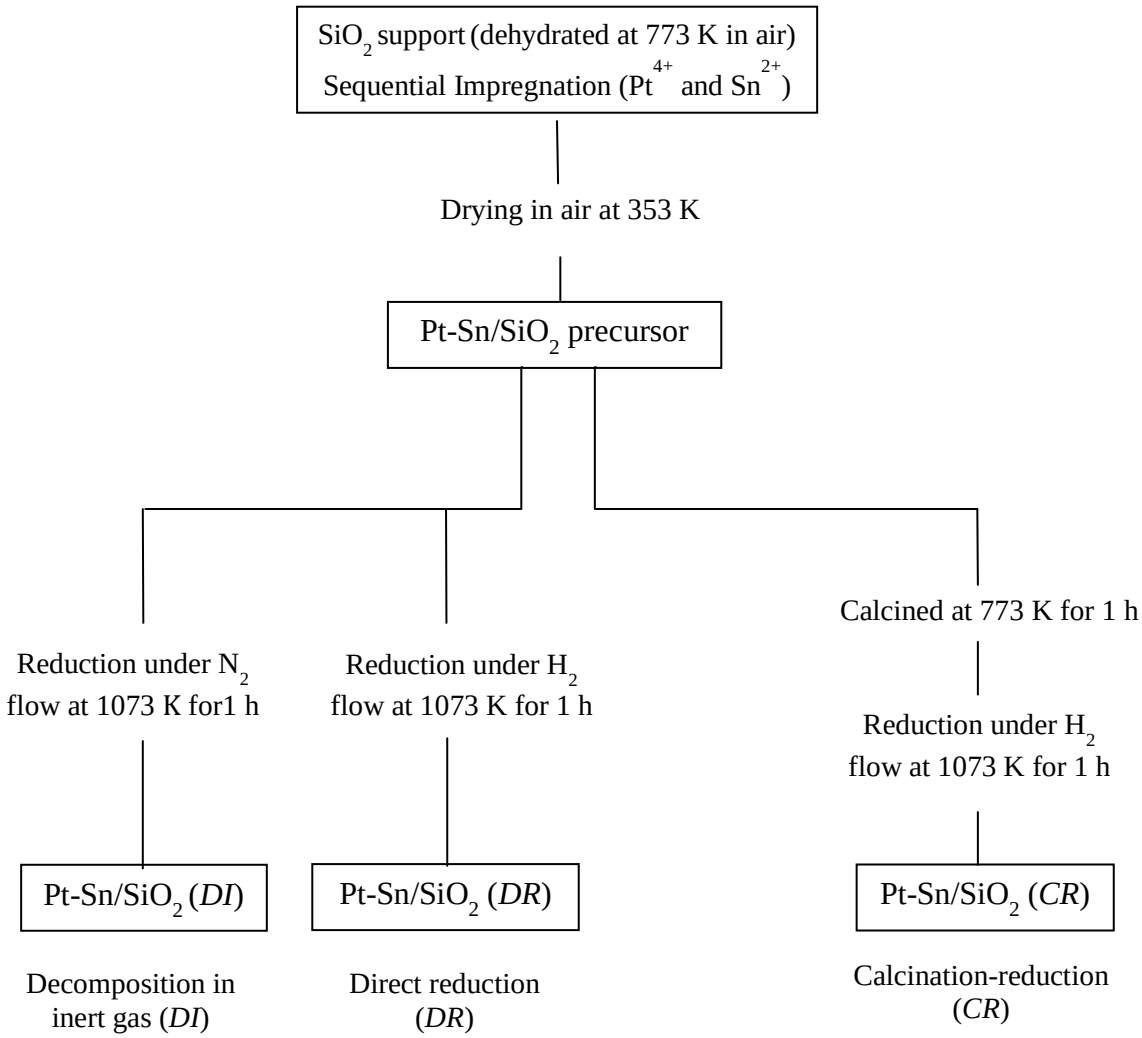

Scheme 1. Scheme of catalyst preparation and reduction.

determined by CO pulse method with an Okura BP-2 instrument (Okura Riken, Japan) interfaced with a TCD. X-ray diffraction (XRD) patterns were obtained by means of a MultiFlex DR powder X-ray diffractometer (Rigaku, Tokyo, Japan) with Cu Kα radiation (χ = 1.5405 Å). The samples were scanned from 2θ=38° to 46° at the scanning rate of 0.067 s^{-1} and the resolution of 0.01°. TEM images were obtained by a JEOL JEM–2100F transmission electron microscope operating at an accelerating voltage of 200 kV. TEM samples were prepared by depositing drops of a methanol suspension containing small amounts of the powders onto a carbon-coated copper grid (Okenshoji

Co. Ltd.) following the evaporation of methanol in air. X-ray absorption experiments were carried out at the BL01B1 at SPring-8 (Hyogo, Japan). The ring energy was 8 GeV, and the stored current was 99.5 mA. The Pt L_{III}-edge (11.56 keV) X-ray absorption spectra were recorded by using a Si (111) monochromator in transmission mode in air at room temperature. The Sn K-edge (29.19 keV) X-ray absorption spectra were recorded by using a Si (311) monochromator in fluorescence mode in air at room temperature. The data reduction was performed by using the REX2000 Ver.2.5.9 (Rigaku) and FEFF8.40 programs [91].

Results

Propane dehydrogenation

Figure 1 shows the time course of propane conversion on Pt/SiO_2 and Pt-Sn/SiO_2 catalysts. The propane conversion on Pt/SiO_2 (*DR*) was quite low (ca. 5 %) and sharply declined, indicating that monometallic Pt catalyst showed a low activity and stability. The Pt-Sn/SiO_2 (*DR*) catalyst showed the highest activity and selectivity towards propylene (> 99%). A trace amount of methane and ethane were detected as by-products. Up to now, many researchers have reported the positive effect of Sn on the catalytic property of supported Pt catalyst for dehydrogenation of propane [6, 12, 18, 19], butane [7, 20], isobutane [4, 21], and hexane [8]. Generally, the selectivity to alkene improved by the addition of Sn because of the suppression of hydrogeolysis property, but the activity decreased. In contrast, in the case of the Pt-Sn/SiO_2 (*DR*) catalyst, the addition of Sn improved not only the catalytic performance (activity and selectivity to propylene) but also the stability. On the other hand, the Pt-Sn/SiO_2 (*CR*) catalyst showed a low activity and the selectivity to propylene on Pt-Sn/SiO_2 (*CR*) was slightly lower (ca. 95 %) than Pt-Sn/SiO_2 (*DR*), regardless of the coexistence of Sn with

Pt. The conversion of propane on Pt-Sn/SiO_2 (*DI*) was higher than Pt-Sn/SiO_2 (*CR*), but lower than Pt-Sn/SiO_2 (*DR*). The selectivity to propylene on Pt-Sn/SiO_2 (*DI*) was about 99%. The activity gradually decreased with time on stream.

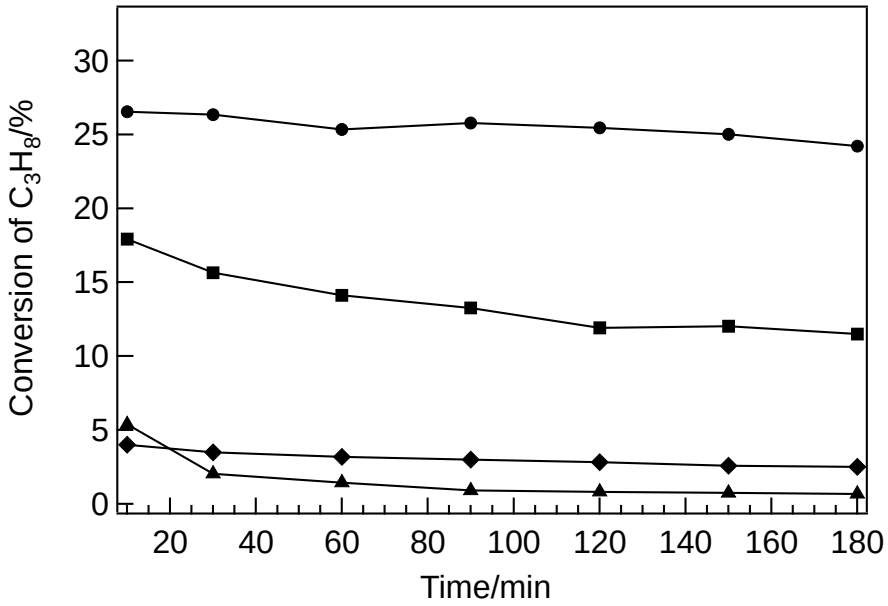

Figure 1 Time course of conversion of propane. (●) Pt-Sn/SiO_2 (*DR*), (■) Pt-Sn/SiO_2 (*DI*), (◆) Pt-Sn/SiO_2 (*CR*)(▲) Pt/SiO_2 (*DR*) (773 K)

Physical and chemical properties of Pt/SiO_2 and Pt-Sn/SiO_2

Table 1 summarizes the BET specific surface area and the amount of adsorbed CO. Figure 2 shows TEM images of Pt/SiO_2 and Pt-Sn/SiO_2, and the particle size histograms of black spot observed in TEM images. Black spots were assigned to Pt or Pt-Sn alloy particle on SiO_2. The BET surface area of Pt/SiO_2 (*DR*) was slightly larger than bare SiO_2. On the Pt/SiO_2 (*DR*), small Pt particles whose mean particle size was about 2.0 nm were observed. When Sn was added into monometallic Pt catalyst system, the BET surface area slightly decreased compared with that of Pt/SiO_2 (*DR*). The particle size on Pt-Sn/SiO_2 catalysts (2.2−3.3 nm) was slightly larger than that on Pt/SiO_2 catalyst regardless of the reduction method. However, the amount of adsorbed CO remarkably decreased by the addition of Sn. These results suggest the formation of

Pt-Sn alloy and/or the deposition of Sn species on the surface of Pt metal particle. Meriaudeau et al. reported that the addition of Sn to Pt reduced the strength of Pt-CO bond by the preferential blocking of higher binding sites of Pt by Sn [19]. The reduction of strength of Pt-CO bond was interpreted as this geometric effect. Recently, Wang et al. synthesized Pt-Sn intermetallic, core/shell, and alloy nanoparticles by using colloidal technique, and investigated the CO adsorption properties of prepared Pt-Sn compounds [22]. The intensity of linearly adsorbed CO clearly decreased with increasing the surface Sn/Pt ratio, that is, the increasing of Sn surface coverage. On the other hand, Liu et al reported that the PtSn@Pt core-shell nanoparticle electrocatalysts prepared by potential cycling of PtSn intermetallic nanoparticles in CO-saturated H_2SO_4 solutions exhibited a substantially higher CO-tolerance property to Pt, PtRu alloy, and PtSn alloy catalysts [23]. They proposed that the superior CO-tolerance of the PtSn@Pt catalyst was mainly due to the electronic effect of the PtSn core on the Pt shell. In our cases, the catalysts prepared by the different reduction methods exhibited different catalytic activities, which were not proportional to the amount of adsorbed CO, in other words, the number of accessible Pt sites on Pt-Sn/SiO_2 catalyst. Therefore, the change in local structure and electronic state of Pt and Sn should be considered.

Table 1 Physical and chemical properties of Pt/SiO_2 and Pt-Sn/SiO_2.

Catalysts	Pt content (wt%)	Sn content[a] (wt%)	BET surface area[b] ($m^2 g^{-1}$)	CO adsorption[c] ($\mu mol\ g^{-1}$)
Pt/SiO_2 (*DR*)	3.0	-	334	54.9
Pt-Sn/SiO_2 precursor	3.0	1.8	242	-
Pt-Sn/SiO_2 (*DI*)	3.0	1.8	326	10.6
Pt-Sn/SiO_2 (*DR*)	3.0	1.8	296	6.5
Pt-Sn/SiO_2 (*CR*)	3.0	1.8	290	7.3

a: The molar ratio of Pt to Sn was fixed as 1:1.
b: The surface area of SiO_2(JRC-SIO-9) is 325 $m^2 g^{-1}$.
c: The amount of CO adsorption was estimated from the CO-pulse experiments.

XRD patterns of Pt/SiO_2 and $Pt\text{-}Sn/SiO_2$

Figure 3 shows the XRD patterns of Pt/SiO_2 and $Pt\text{-}Sn/SiO_2$ catalysts. The XRD patterns of Pt/SiO_2 (*DR*) and $Pt\text{-}Sn/SiO_2$ (*DI*) exhibit a peak at 2θ=39.8°, which is assigned to Pt (111). The full-width at half maximum (FWHM) of this diffraction line of $Pt\text{-}Sn/SiO_2$ (*DI*) was slightly narrower than that of Pt/SiO_2 (*DR*), indicating that the crystalline size of Pt metal on $Pt\text{-}Sn/SiO_2$ (*DI*) was slightly larger than that on Pt/SiO_2 (*DR*). This result was consistent with TEM observation. However, as mentioned above, the amount of adsorbed CO on $Pt\text{-}Sn/SiO_2$ (*DI*) was much smaller than that on Pt/SiO_2 (*DR*). Moreover, no diffraction line due to Sn compounds including SnO and SnO_2 appeared in XRD patterns of $Pt\text{-}Sn/SiO_2$ catalysts regardless of reduction method. This indicates that Sn species was separated from Pt metal, and was highly dispersed on the

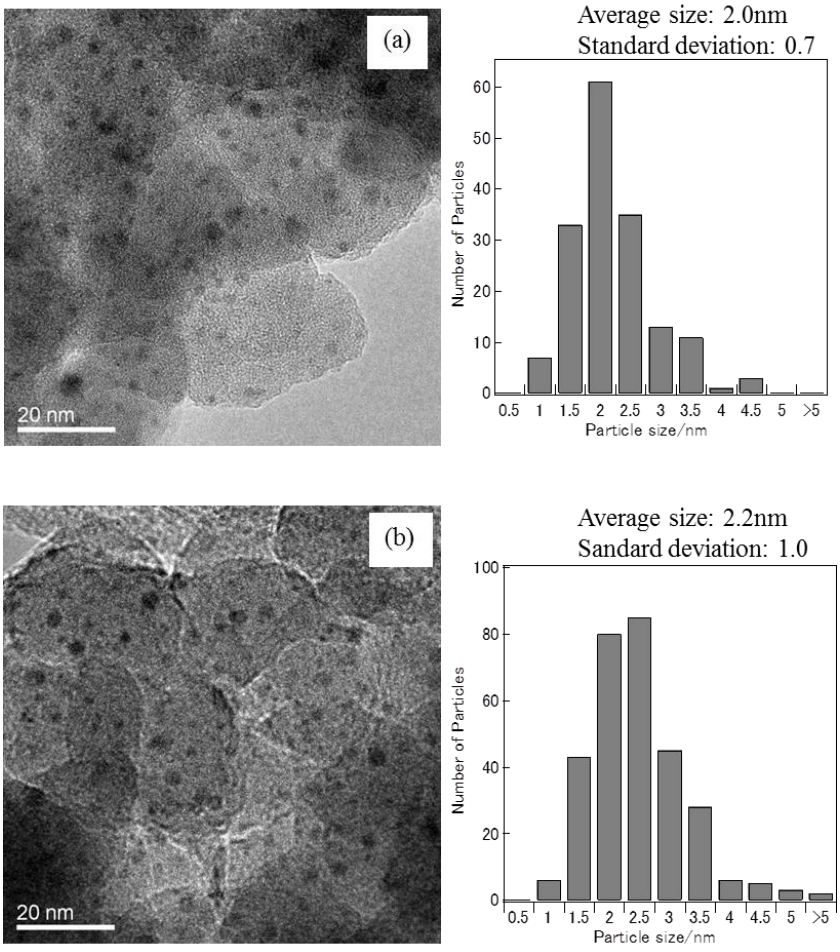

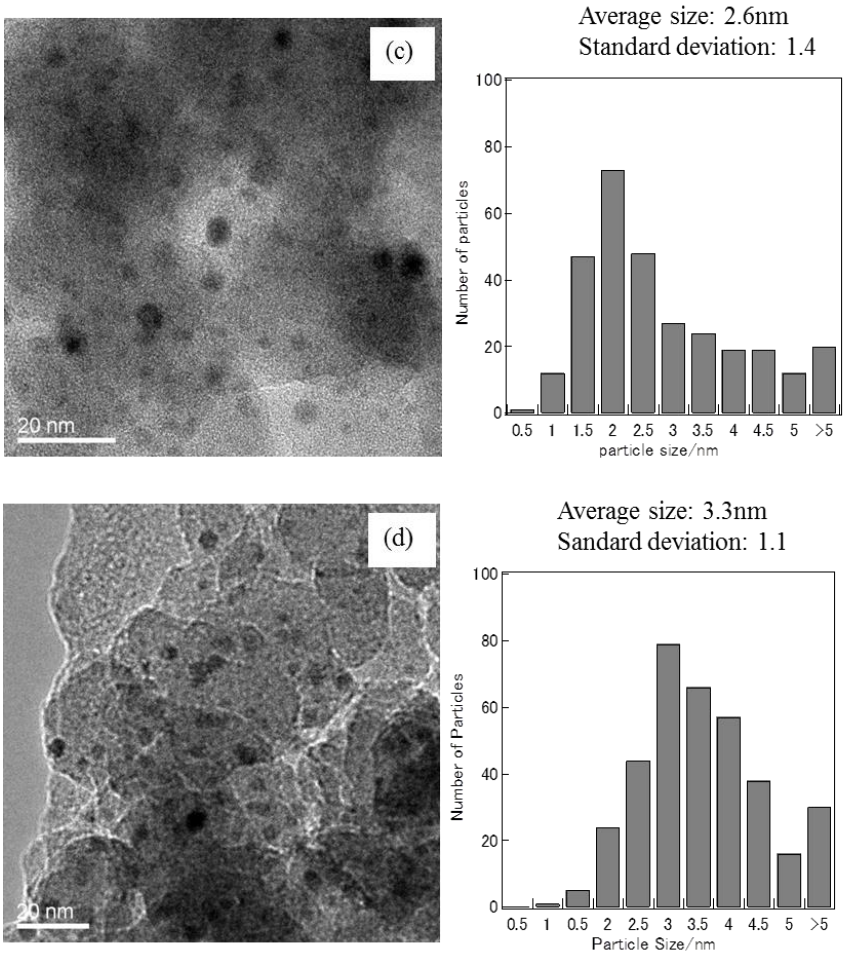

Figure 2　TEM images and particle size distributions of (a) Pt/SiO_2 (*DR*) (773 K), (b) $Pt\text{-}Sn/SiO_2$ (*DI*), (c) $Pt\text{-}Sn/SiO_2$ (*DR*), and (d) $Pt\text{-}Sn/SiO_2$ (*CR*).

$Pt\text{-}Sn/SiO_2$ (*DI*) catalyst. Considering a small amount of adsorbed CO, it is likely that the surface of Pt metal on $Pt\text{-}Sn/SiO_2$ (*DI*) was partially covered with highly dispersed SnO and/or SnO_2. The XRD pattern of $Pt\text{-}Sn/SiO_2$ (*DR*) shows two diffraction lines around 2θ=39° and 45° for the Pt_3Sn alloy phase (ICSD 105796) together with diffraction lines around 42° and 44° for the PtSn alloy phase (ICSD 42593). These lines are assignable to Pt_3Sn (111) (2θ=38.93°), Pt_3Sn (200) (2θ=45.26°), PtSn(102) (2θ =41.81°), and PtSn(110) (2θ=44.10°), respectively. The intensities of diffraction lines for Pt_3Sn alloy phase are much stronger than those for PtSn alloy phase, suggesting that

the major part of Pt-Sn/SiO_2 (*DR*) catalyst possesses the Pt_3Sn alloy structure in the fcc arrangement. In the case of Pt-Sn/SiO_2 (*CR*), diffraction lines for the PtSn alloy phase was mainly observed in addition to weak diffraction lines for the Pt_3Sn alloy phase. This suggests that PtSn alloy, which is the same structure as NiAs, is mainly formed on Pt-Sn/SiO_2 (*CR*).

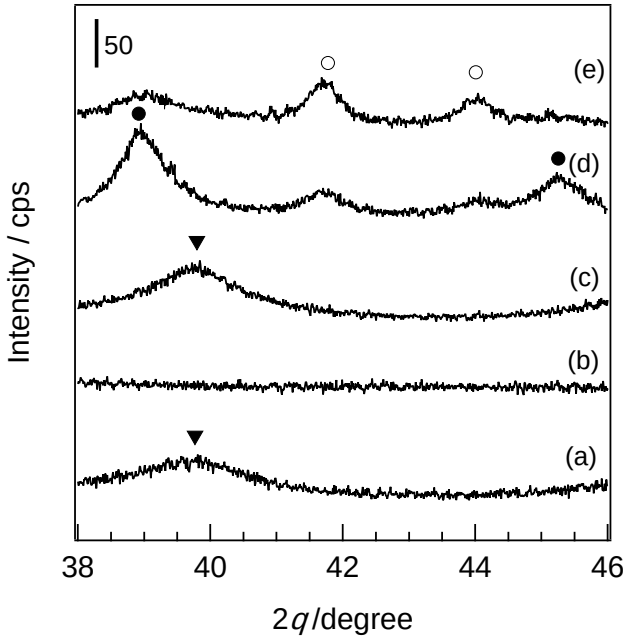

Figure 3 XRD patterns of (a) Pt/SiO_2 (*DR*) (773 K), (b) Pt-Sn/SiO_2 catalyst precursor, (c) Pt-Sn/SiO_2 (*DI*), (d) Pt-Sn/SiO_2 (*DR*), and (e) Pt-Sn/SiO_2 (*CR*). (●) Pt_3Sn, (○) PtSn, (▼) Pt

XAFS analysis of Pt/SiO_2 and Pt-Sn/SiO_2

Pt L_{III}-edge XAFS

Figure 4 shows Pt L_{III}-edge XANES spectra of Pt/SiO_2, Pt-Sn/SiO_2 catalysts, and reference samples (Pt foil, $PtCl_2$, and PtO_2). XANES spectrum of Pt-Sn/SiO_2 catalyst precursor exhibited essentially the same features as that of $PtCl_2$. This suggests that Pt^{2+} species having Pt-Cl bond such as $[PtCl_4]^{2-}$ adsorbed on SiO_2 surface. After reduction, platinum in all catalysts possessed the similar feature as that of Pt metal. The

white line intensities of Pt/SiO_2 (*DR*) and $Pt\text{-}Sn/SiO_2$ (*DI*) were similar each other, and slightly higher than that of Pt foil. As for $Pt\text{-}Sn/SiO_2$ (*DR*) and $Pt\text{-}Sn/SiO_2$ (*CR*), their spectra were close and the white line intensities were slightly less than that of Pt foil. Since the intensity of the white line reflects the vacancy population of the 5d orbital of Pt [24, 25], the intensity of white line decreases when Pt receives electrons from the surrounding atoms. From this viewpoint, the decrease of white lines of $Pt\text{-}Sn/SiO_2$ (*DR*) and $Pt\text{-}Sn/SiO_2$ (*CR*) strongly suggests an electron donation from Sn to Pt and alloy formation between Pt and Sn. A similar result has previously observed in Pt-Sn bimetallic catalysts by Uemura et al. [15, 16]. They assigned this small decrease in the white line intensity to the formation of a Pt-Sn alloy since the d-electron density of platinum atoms will increase with alloying with Sn that shows lower electronegativity than Pt.

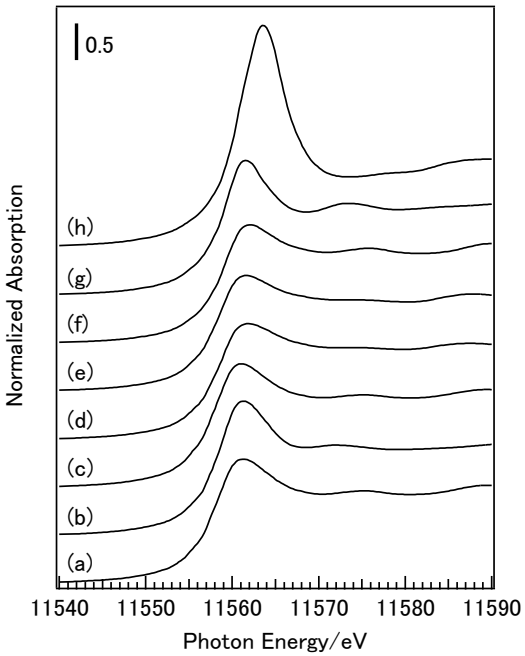

Figure 4 Pt L_{III}-edge XANES spectra of Pt/SiO_2, $Pt\text{-}Sn/SiO_2$ and references: (a) Pt/SiO_2 (*DR*) (773 K), (b) $Pt\text{-}Sn/SiO_2$ catalyst precursor,, (c) $Pt\text{-}Sn/SiO_2$ (*DI*), (d) $Pt\text{-}Sn/SiO_2$ (*DR*), (e) $Pt\text{-}Sn/SiO_2$ (*CR*), (f) Pt foil, (g) $PtCl_2$, (h) PtO_2.

Figure 5(A) shows k^3-weighted EXAFS oscillation at Pt L_{III}-edge. The EXAFS oscillation of Pt-Sn/SiO_2 catalyst precursor exhibited essentially the same features as that of $PtCl_2$. In the radial structure function (RSF) of Pt-Sn/SiO_2 catalyst precursor shown in Figure 5(B), the peak around 0.19 nm assigned to Pt–Cl linkage appeared. This peak disappeared after the reduction. Combined with the XANES spectrum of Pt-Sn/SiO_2 catalyst precursor, these results suggest that during impregnation and dryness, $[PtCl_6]^{2-}$ species in $H_2PtCl_6 \cdot 6H_2O$ precursor was transformed to $[PtCl_4]^{2-}$ and adsorbed on SiO_2. After the following reduction treatment, $[PtCl_4]^{2-}$ was decomposed and reduced to Pt metal or Pt–Sn alloy. The EXAFS oscillation of Pt-Sn/SiO_2 (*DI*) catalyst is similar to that of Pt foil, although the intensity of oscillation is weaker than that of Pt foil. The peak around 0.25 nm in the RSF of Pt-Sn/SiO_2 (*DI*) catalyst is assignable to Pt–Pt linkage. A smaller Pt–Pt contribution than that in Pt foil indicates that small Pt nanoparticle (ca. 2.2 nm) was formed on Pt-Sn/SiO_2 (*DI*).

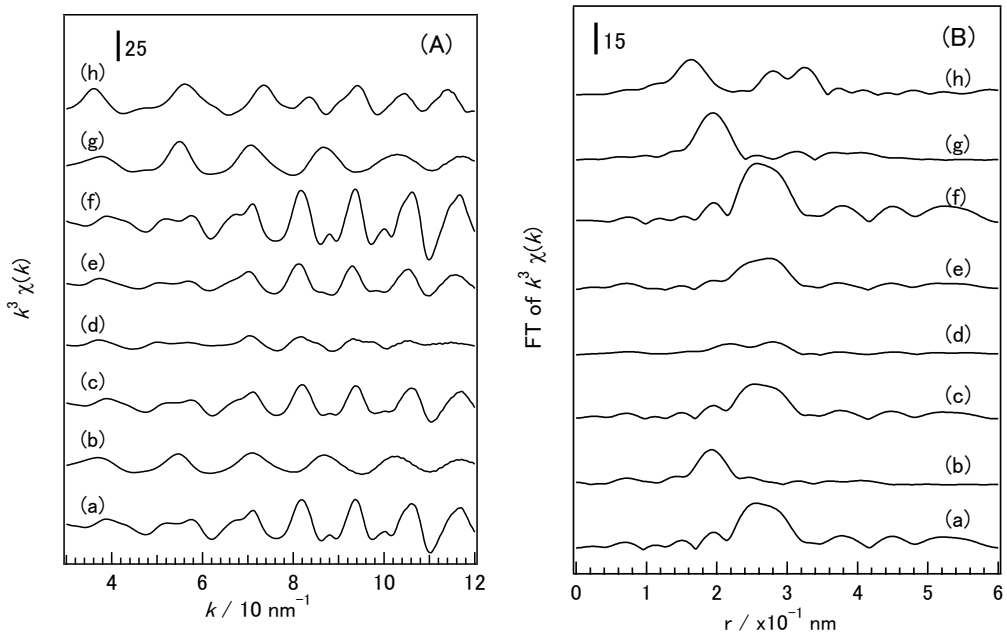

Figure 5 (A) k^3-weighted EXAFS oscillation at Pt L_{III}-edge and (B) their Fourier transforms: (a) Pt/SiO_2 (*DR*) (773 K), (b) Pt-Sn/SiO_2 catalyst precursor, (c) Pt-Sn/SiO_2

(*DI*), (d) Pt-Sn/SiO_2 (*DR*), (e) Pt-Sn/SiO_2 (*CR*), (f) Pt foil, (g) $PtCl_2$, (h) PtO_2.

In contrast, the EXAFS oscillation of Pt-Sn/SiO_2 (*DR*) is significantly different from and much weaker than that of Pt foil. This suggests the interference of scattered electrons by Sn and Pt, in other words, the contribution of Pt–Sn linkage in addition to Pt–Pt linkage in the Pt-Sn alloy phase as reported by Uemura et al. Table 2 and Figure 6 show the curve-fitting analysis of Pt-Sn/SiO_2 (*DR*) catalyst. The EXAFS data for Pt-Sn/SiO_2 (*DR*) catalyst were well fitted by assuming two shells (Pt–Pt and Pt–Sn linkages). No Pt–O linkage was observed, indicating that the all of supported Pt species was completely reduced to metallic state after the treatment with H_2 diluted with N_2 at 1073 K. The bond distances of Pt–Pt and Pt–Sn of Pt-Sn/SiO_2 (*DR*) catalyst were shorter than the crystallographic values (Pt–Pt = 0.283 nm and Pt–Sn = 0.283 nm) in the Pt_3Sn crystal [26]. The ratio of the coordination numbers, $N_{Pt\text{-}Sn}/N_{Pt\text{-}Pt}$, was 0.49 which is compatible with 0.50 expected for Pt_3Sn. The coexistence of a small fraction of PtSn phase (Fig. 2) and the interference of Pt and Sn scattering in the Pt-Sn/SiO_2 (*DR*) catalyst result in relatively larger *R*-factors. In the case of Pt-Sn/SiO_2 (*CR*), the EXAFS

Table 2 The curve-fitting results of the Pt L_{III}-edge EXAFS data for Pt-Sn/SiO_2 (*DR*)

	N	$r/10^{-1}$nm	ΔE/eV	$\sigma^2/10^{-2}$nm^2
Pt-Sn	1.8(5)	2.73(1)	3(2)	0.006(4)
Pt-Pt	3.7(6)	2.78(1)	7(2)	0.006(1)
Pt-Sn*	4	2.83		*(Pt_3Sn_1)
Pt-Pt*	8	2.83		*(Pt_3Sn_1)

N: Coordination number; ΔE: threshold energy difference; *r*: bond distance; σ: Debye-Waller factor, *k* range / 10 nm^{-1} 3.5 < *k* < 13.0, *r* range / 10^{-1} nm 0.18 < *r* < 0.32, *R*-factor: 4.4 % * Crystallographic data

oscillation is different from that of Pt-Sn/SiO_2 (*DR*). Moreover, the oscillation period was slightly different from that of Pt foil. These results and XRD pattern suggest the formation of PtSn alloy phase on Pt-Sn/SiO_2 (*CR*).

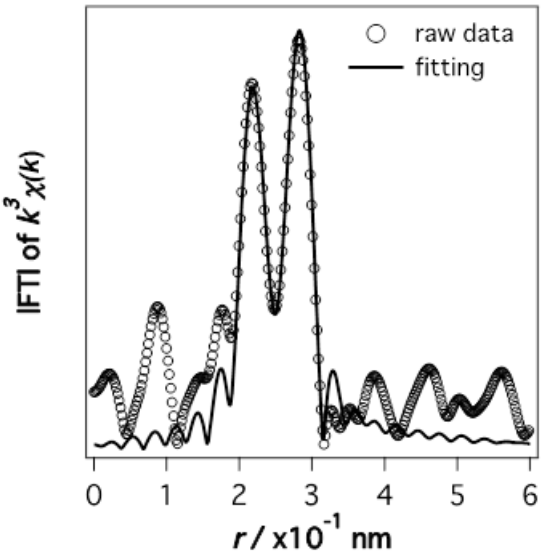

Figure 6 The curve-fitting analysis of the Pt L_{III}-edge EXAFS data for Pt-Sn/SiO_2 (*DR*) catalyst.

Sn K-edge XAFS

Figure 7 shows Sn K-edge XANES spectra of Pt-Sn/SiO_2 catalysts, and reference samples (Sn(II)O and Sn(IV)O_2). The white line intensity of Pt-Sn/SiO_2 catalyst precursor was much higher than that of SnO, and slightly lower than that of SnO_2. This suggests that Sn^{2+} was oxidized to Sn^{4+} during the impregnation in air. In the case of Pt-Sn/SiO_2 (*DI*), the white line intensity was slightly lower than that of SnO_2, and the peak assignable to Sn–O linkage around 0.16 nm was observed in the RSF (Figure 7). Moreover, no X-ray diffraction peaks due to SnO_2 appeared (Figure 2) and the amount of adsorbed CO was much smaller than that on Pt/SiO_2 (*DR*). Based on these results, we proposed that highly dispersed SnO_2 was formed and a part of Pt surface on Pt-Sn/SiO_2 (*DI*) was covered with SnO_2 (SnO_2 decorated the surface of Pt metal).

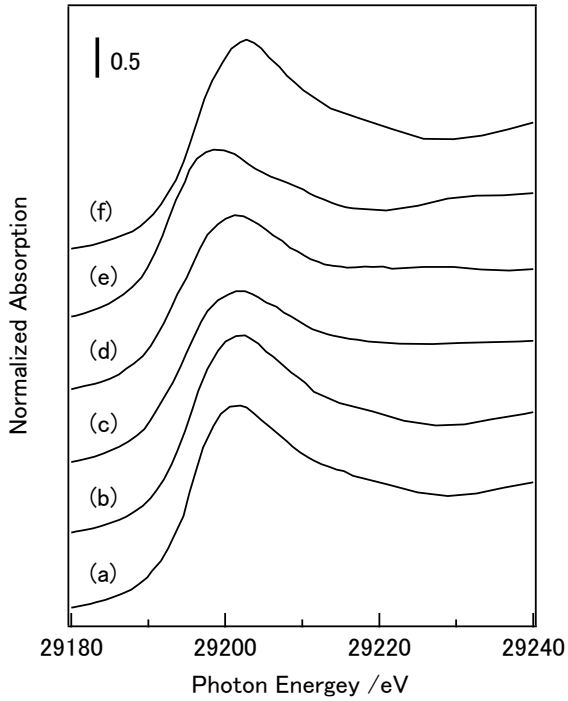

Figure 7 Sn K-edge XANES spectra of Pt-Sn/SiO_2 and references: (a) Pt-Sn/SiO_2 catalyst precursor, (b) Pt-Sn/SiO_2 (*DI*), (c) Pt-Sn/SiO_2 (*DR*), (d) Pt-Sn/SiO_2 (*CR*), (e) SnO, (f) SnO_2.

The white line intensity of Pt-Sn/SiO_2 (*DR*) was slightly higher than that of SnO, whereas much lower than that of SnO_2. The intensity of peak assignable to Sn–O linkage around 0.16 nm was less than that of Pt-Sn/SiO_2 (*DI*). Appreciable oscillation appeared around 0.75 nm^{-1} (Figure 8(A)). These results suggest that the EXAFS oscillation includes the contribution of Sn–Pt linkage as a result of the formation of Pt-Sn alloy phase. Table 3 and Fig. 9 show the curve-fitting analysis of Pt-Sn/SiO_2 (*DR*) catalyst. The EXAFS data for Pt-Sn/SiO_2 (*DR*) catalyst were well fitted by assuming two shells (Sn–Pt and Sn–O linkages). The RSF of the Pt-Sn/SiO_2 (*DR*) catalyst gave three weak peaks, at 0.15, 0.21, and 0.26 nm (Figure 8(B)). The first peak corresponds to a Sn–O linkage. The second and third peaks correspond to Sn–Pt linkage. The bond distances of Sn–Pt (0.274 nm) agrees with that of Pt–Sn (0.273 nm) shown in Table 2.

In the Pt_3Sn phase, a Pt atom is surrounded by 4 Sn atoms and 8 Pt atoms, while a Sn atom is surrounded by 6 Pt atoms (Figure 10). Thus, the ratio of the coordination numbers, $N_{Pt\text{-}Sn}/N_{Sn\text{-}Pt}$ is estimated to be 0.67 for Pt_3Sn. This value is almost compatible with 0.46 for Pt-Sn/SiO_2 (*DR*), considering a large uncertainty in the coordination number due to the coexistence of small fraction of PtSn alloy and the interference of Pt and Sn scattering (Tables 2 and 3). The coordination number of O surrounding Sn atoms in Pt-Sn/SiO_2 (*DR*) was ca. 4, which is smaller than that for bulk SnO_2. This is probably due to the formation of amorphous SnO_2 phase and small SnO_2 nanoparticles. Based on these results, we concluded that Pt_3Sn alloy particles were present together with highly dispersed SnO_2 on Pt-Sn/SiO_2 (*DR*).

Similarly, the white line intensity of Pt-Sn/SiO_2 (*CR*) was slightly higher than that of SnO, whereas much lower than that of SnO_2. Moreover, appreciable oscillation was also observed, even the position is slightly different from that of Pt-Sn/SiO_2 (*DR*). The RSF of the Pt-Sn/SiO_2 (*CR*) catalyst gave three weak peaks, at 0.15, 0.22, and 0.27 nm. The first peak corresponds to a Sn–O linkage similar with Pt-Sn/SiO_2 (*DR*). Although the positions of second and third peaks are slightly different from those of Pt-Sn/SiO_2 (*DR*), these peaks seem to correspond to Sn–Pt linkage. All of these structural analyses strongly suggest the coexistence of highly dispersed SnO_2 and Pt-Sn alloy whose local structure is different from that of Pt_3Sn alloy phase. Considering XRD pattern, we concluded that PtSn alloy particle was regarded as the main species on Pt-Sn/SiO_2 (*CR*) catalyst.

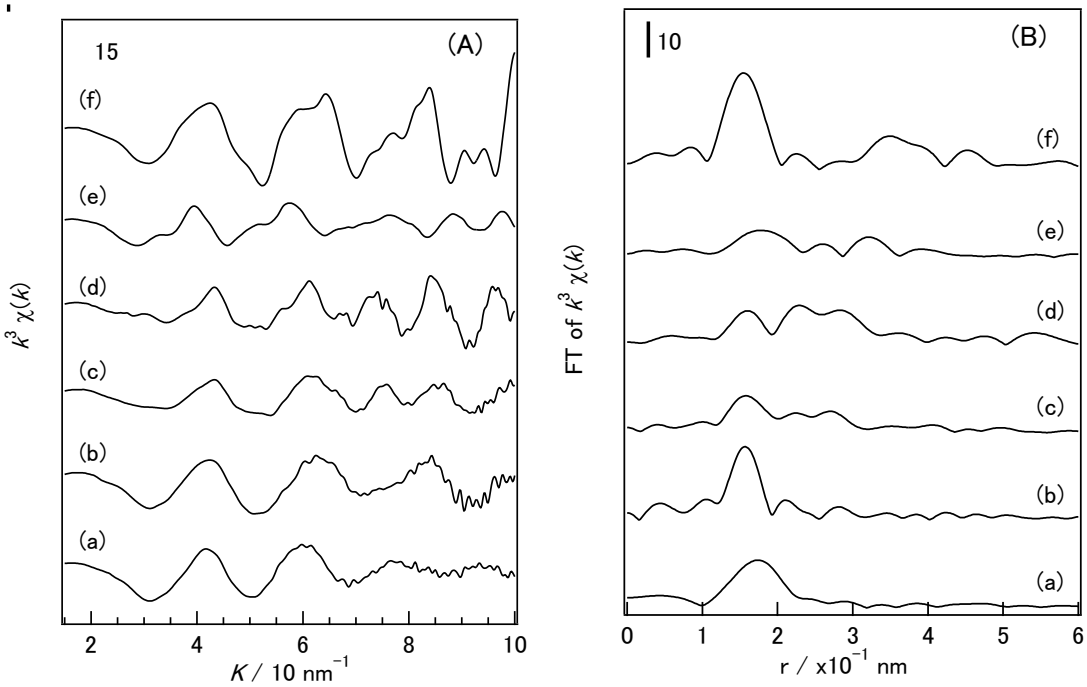

Figure 8 (A) k^3-weighted EXAFS oscillation at Sn K-edge and (B) their Fourier transforms: (a) Pt-Sn/SiO_2 catalyst precursor, (b) Pt-Sn/SiO_2 (*DI*), (c) Pt-Sn/SiO_2 (*DR*), (d) Pt-Sn/SiO_2 (*CR*), (e) SnO, (f) SnO_2.

Table 3 The curve-fitting results of the Sn K-edge EXAFS data for Pt-Sn/SiO_2 (*DR*)

	N	r /10^{-1}nm	ΔE/eV	$\sigma^2/10^{-2}$nm^2
Sn-Pt	3.9(6)	2.74(1)	-1(2)	0.008(1)
Sn-O	4.1(9)	2.03(1)	-1(3)	0.009(1)
Sn-Pt*	6	2.83		*(Pt_3Sn_1)
Sn-O*	6	2.05		*(SnO_2)

N: Coordination number; ΔE: threshold energy difference; *r*: bond distance; σ: Debye-Waller factor, *k* range / 10 nm^{-1} 3.5 nm < *k* < 13.0, *r* range / 10^{-1} nm 1.8 < *r* < 3.2, *R*-factor: 3.6 %

* Crystallographic data

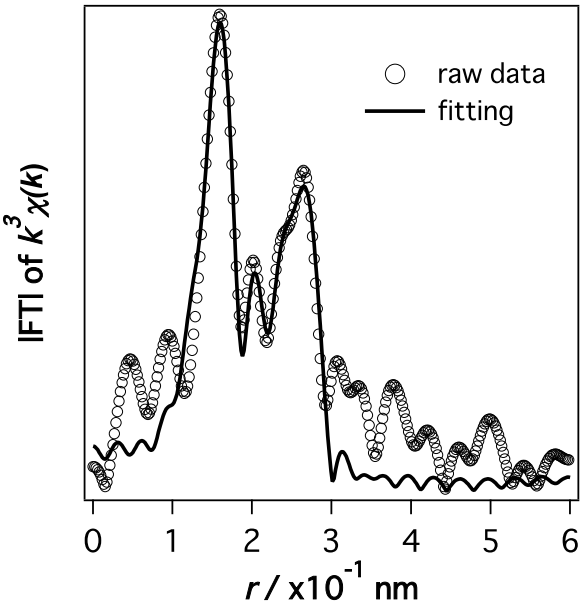

Figure 9 The curve-fitting analysis of Sn K-edge EXAFS data for Pt-Sn/SiO_2 (*DR*) catalyst.

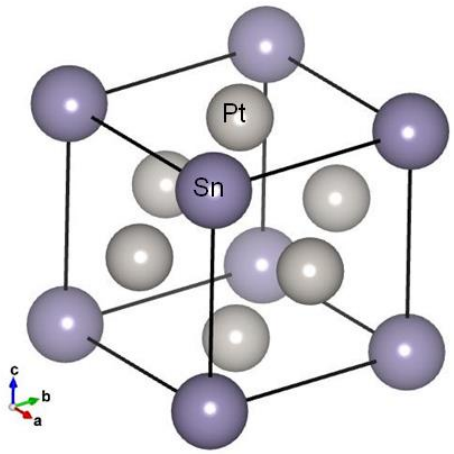

Figure 10 The atomic structure of Pt_3Sn alloy.

Discussion

The results of propane dehydrogenation over Pt/SiO_2 and Pt-Sn/SiO_2 catalysts show that the addition of tin to platinum improves the catalytic performance. Structural analyses by XRD, TEM, and XAFS techniques clearly indicate that the geometric and electronic states of platinum remarkably changed with the addition of tin followed by

different reduction method. It appears that the activity for propane dehydrogenation strongly depends on the structure and electronic state of platinum and tin.

The Pt/SiO_2 (*DR*) catalyst showed a low activity and stability. This clearly indicates that monometallic platinum is not active and is unstable. On the other hand, the $Pt\text{-}Sn/SiO_2$ (*DR*) catalyst, on which small Pt_3Sn alloy nanoparticles were present as the main phase, showed much higher activity than that of Pt/SiO_2 (*DR*). These results strongly suggest that Pt_3Sn alloy acts as active site for dehydrogenation of propane. Among the Pt-Sn alloy phases ($PtSn_4$, $PtSn_2$, Pt_2Sn_3, PtSn, and Pt_3Sn [27, 28]), a superior catalytic performance was often assigned to Pt_3Sn ally phase [7, 29-31]. The present work also showed that PtSn alloy was mainly formed on the $Pt\text{-}Sn/SiO_2$ (*CR*) catalyst, which showed a low activity, although the conversion of propane was stable. Thus, it would appear that PtSn alloy is not active for propane dehydrogenation despite the coexistence of platinum and tin. Likewise, Llorca et al reported that PtSn alloy showed high stability and selectivity in *n*-hexane dehydrogenation while the selectivity to benzene and hydrogenolysis products were low [8]. Recently, Yang et al. investigated the effect of Sn on the activity and selectivity of Pt catalyst in propane dehydrogenation by using density functional calculation (DFT) method [32]. They reported that the introduction of Sn lowers the energy barrier for propylene desorption and simultaneously increases the activation energy for propylene dehydrogenation, which has a positive effect on the selectivity toward propylene production, and proposed that the Pt_3Sn bulk alloy is the most suitable for propane dehydrogenation by considering the compromise between the catalytic activity and selectivity.

In the case of the $Pt\text{-}Sn/SiO_2$ (*DI*) catalyst, XRD, CO pulse, TEM, and XAFS results implied that monometallic platinum particle decorated with small SnO_2. When

Sn was absent (Pt /SiO_2 (*DI*) catalyst), the dispersion of Pt was quite low (data not shown), indicating that the introduction of Sn suppressed the aggregation of Pt. This implies the intimate contact of Sn with Pt. Although Pt_3Sn alloy phase was not detected by XRD and XAFS techniques, the conversion of propane on the Pt-Sn/SiO_2 (*DI*) catalyst was ca. 60 % of that on the Pt-Sn/SiO_2 (*DR*) catalyst having Pt_3Sn alloy phase. This relatively high activity is probably caused by the strong interaction between the platinum metal particle and highly dispersed SnO_2 such as electron transfer between SnO_2 and Pt, or the formation of Pt_3Sn alloy phase at the interface of platinum metal particle and highly dispersed SnO_2. The low ratio of surface to bulk would make the detection of formation of Pt_3Sn alloy at the interface of platinum metal particle and highly dispersed SnO_2 by XAFS difficult, since XAFS analysis yields the average information of surface and bulk. Therefore, further investigation is necessary to verify these hypotheses.

Conclusion

The Pt-Sn/SiO_2 catalysts were reduced by three methods (direct reduction (*DR*), decomposition in inert gas (*DI*) and calcination-reduction (*CR*)), and were examined for propane dehydrogenation. The activities of the Pt-Sn/SiO_2 catalysts were strongly influenced by the reduction method. Decomposition in inert gas (*DI*) method resulted in the coexistence of Pt metal and highly dispersed SnO_2 on SiO_2, which showed the medium activity among the catalysts tested. Direct reduction (*DR*) caused that Pt_3Sn alloy nanoparticle was mainly formed on Pt-Sn/SiO_2 (*DR*) catalyst, which showed the highest activity. Calcination-reduction (*CR*) method also led to PtSn alloy formation. PtSn alloy nanoparticles were present as the main phase. However, this catalyst was not active in propane dehydrogenation. The relationship between activity and structure of

platinum-tin alloy suggested that Pt_3Sn alloy acts as active site for dehydrogenation of propane, whereas PtSn alloy shows low or no activity.

References

[1] D. Akporiaye, S.F. Jensen, U. Olsbye, F. Rohr, E. Rytter, M. Ronnekleiv and A.I. Spjelkavik, Ind. Eng. Chem. Res., 40 (2001) 4741.

[2] D. Sanpilippo, Cattech, 4 (2000) 56.

[3] O.A. Barias, A. Holmen and E.A. Blekkan, J. Catal., 158 (1996) 1.

[4] R.D. Cortright and J.A. Dumesic, J. Catal., 148 (1994) 771.

[5] V. Galvita, G. Siddiqi, P.P. Sun and A.T. Bell, J. Catal., 271 (2010) 209.

[6] A. Iglesias-Juez, A.M. Beale, K. Maaijen, T.C. Weng, P. Glatzel and B.M. Weckhuysen, J. Catal., 276 (2010) 268.

[7] I. Kikuchi, M.A. Ohshima, H. Kurokawa and H. Miura, J. Jpn. Pet. Inst, 55 (2012) 206.

[8] J. Llorca, N. Homs, J.L.G. Fierro, J. Sales and P.R. delaPiscina, J. Catal., 166 (1997) 44.

[9] F. Somodi, Z.M. Peng, A. Getsoian and A.T. Bell, J. Phys. Chem. C, 115 (2011) 19084.

[10] R. Srinivasan, R.J. Deangelis and B.H. Davis, J. Catal., 106 (1987) 449.

[11] A. Virnovskaia, S. Morandi, E. Rytter, G. Ghiotti and U. Olsbye, J. Phys. Chem. C, 111 (2007) 14732.

[12] B.K. Vu, M.B. Song, I.Y. Ahn, Y.W. Suh, D.J. Suh, W.I. Kim, H.L. Koh, Y.G. Choi and E.W. Shin, Appl. Catal. A-Gen., 400 (2011) 25.

[13] I. Kikuchi, Y. Haibara, M. Ohshima, H. Kurokawa and H. Miura, J. Jpn. Pet. Inst, 55 (2012) 33.

[14] J. Salmones, J.A. Wang, J.A. Galicia and G. Aguilar-Rios, J. Mol. Catal. A-Chem., 184 (2002) 203.

[15] Y. Uemura, Y. Inada, K.K. Bando, T. Sasaki, N. Kamiuchi, K. Eguchi, A. Yagishita, M. Nomura, M. Tada and Y. Iwasawa, Physical Chemistry Chemical Physics, 13 (2011) 15833.

[16] Y. Uemura, Y. Inada, K.K. Bando, T. Sasaki, N. Kamiuchi, K. Eguchi, A. Yagishita, M. Nomura, M. Tada and Y. Iwasawa, J. Phys. Chem. C, 115 (2011) 5823.

[17] A.L. Ankudinov, B. Ravel, J.J. Rehr and S.D. Conradson, Phys. Rev. B, 58 (1998) 7565.

[18] M.S. Kumar, D. Chen, A. Holmen and J.C. Walmsley, Catal. Today, 142 (2009) 17.

[19] P. Meriaudeau, A. Thangaraj, J.F. Dutel and C. Naccache, J. Catal., 167 (1997) 180.

[20] T. Komatsu and H. Ikenaga, J. Catal., 241 (2006) 426.

[21] G.J. Siri, J.M. Ramallo-Lopez, M.L. Casella, J.L.G. Fierro, F.G. Requejo and O.A. Ferretti, Appl. Catal. A-Gen., 278 (2005) 239.

[22] X.D. Wang, L. Altmann, J. Stover, V. Zielasek, M. Baumer, K. Al-Shamery, H. Borchert, J. Parisi and J. Kolny-Olesiak, Chem. Mat., 25 (2013) 1400.

[23] Z.F. Liu, G.S. Jackson and B.W. Eichhorn, Angew. Chem.-Int. Edit., 49 (2010) 3173.

[24] A.N. Mansour, J.W. Cook and D.E. Sayers, J. Phys. Chem., 88 (1984) 2330.

[25] F.W. Lytle, J. Catal., 43 (1976) 376.

[26] J.S. Charlton, Cordeyha.M and I.R. Harris, Journal of the Less-Common Metals, 20 (1970) 105.

[27] P. Durussel, R. Massara and P. Feschotte, J. Alloy. Compd., 215 (1994) 175.

[28] P. Anres, M. Gaune-Escard, J.P. Bros and E. Hayer, J. Alloy. Compd., 280 (1998) 158.

[29] Z. Paal, A. Wootsch, D. Teschner, K. Lazar, I.E. Sajo, N. Gyorffy, G. Weinberg, A. Knop-Gericke and R. Schlogl, Appl. Catal. A-Gen., 391 (2011) 377.

[30] M.M. Schubert, M.J. Kahlich, G. Feldmeyer, M. Huttner, S. Hackenberg, H.A. Gasteiger and R.J. Behm, Physical Chemistry Chemical Physics, 3 (2001) 1123.

[31] C. Kappenstein, M. Guerin, K. Lazar, K. Matusek and Z. Paal, J. Chem. Soc.-Faraday Trans., 94 (1998) 2463.

[32] M.L. Yang, Y.A. Zhu, X.G. Zhou, Z.J. Sui and D. Chen, ACS Catal., 2 (2012)

Chapter 3

Dehydrogenation of propane over Pt-Sn/SiO_2 catalysts prepared by direct reduction method: Effects of Sn/Pt ratio and reduction temperature

Abstract

A series of Pt-Sn/SiO_2 catalysts with different Sn/Pt atomic ratios (1/3–3) were prepared by direct reduction method and tested for the dehydrogenation of propane to propylene. Structural characterization by X-ray diffraction (XRD), Transmission electron microscope (TEM), CO adsorption, X-ray photoelectron spectroscopy (XPS) and X-ray absorption fine structure (XAFS) analysis revealed that the Pt-Sn/SiO_2 catalysts possessed a highly dispersed Pt-Sn alloy core with a Sn-rich surface regardless of Sn/Pt ratio or reduction temperature. Highly dispersed SnO_2 coexisted with the Pt-Sn alloy particles, and part of the Pt-Sn alloy surface was covered with SnO_2. Among the catalysts prepared, 1Pt1Sn/SiO_2_1073K (Sn/Pt ratio=1, reduced at 1073 K), composed of Pt_3Sn alloy with a small fraction of PtSn alloy, exhibited the highest activity. In contrast, when the Sn/Pt ratio was larger than 1 and/or the reduction temperature was 1273 K, PtSn alloy was mainly observed, and the Pt-Sn/SiO_2 catalysts showed low activity.

Introduction

Propylene is an important raw material for a wide array of specialty chemicals such as polypropene, acrolein, polyacrylonitrile and acrylic acid. The conventional way of synthesizing propylene is steam cracking of alkanes, naphtha, or gas oil above 1000 K [1]. However, the steam cracking of naphtha produces a propylene yield of only ca. 20 % with substantial quantities of methane and cokes as byproducts. The production of propylene via thermal dehydrogenation of propane is an attractive alternative because it is more energy-conserving and minimizes the formation of methane and coke byproducts [2]. With a suitable catalyst system, higher yields and selectivity towards propylene are expected to be achieved under more environmentally-benign conditions.

Platinum-tin (Pt-Sn) catalyst, in the form of supported nanoparticles, is one of the most suitable catalysts for the thermal dehydrogenation of light alkanes [3]. This bimetallic catalyst often exhibits better activity, selectivity and stability than supported Pt monometallic catalysts, even though the details of the catalyst structure are still unclear. The properties of Pt-Sn catalysts have been found to strongly depend on the composition of the Pt and Sn precursors and the catalyst preparation procedure. The conventional preparation [4], co-impregnation or sequential impregnation of the support material with metal precursors followed by high-temperature calcination and reduction, and colloidal synthesis[5] have been generally applied to the preparation of supported Pt-Sn bimetallic catalysts. Colloidal synthesis [6] often exhibits better performance owing to control of the structural properties of the obtained PtSn bimetallic nanoparticles. However, the many more factors during preparation and the lack of systematic data on the effects of synthesis conditions mean that colloidal synthesis is not facile or comparable.

In our previous work [7], the conventional impregnation method was used to synthesize SiO_2 supported Pt-Sn bimetallic catalysts. Three different treatments (direct reduction (*DR*), decomposition in inert gas (*DI*) and calcination-reduction (*CR*)) were compared in detail. The Pt-Sn/SiO_2 prepared by the *DR* method (the impregnated precursor was directly reduced with H_2) showed the highest activity for the dehydrogenation of propane. It was found that Pt_3Sn alloy formed on the Pt-Sn/SiO_2 catalyst prepared by *DR* when the initial Pt/Sn ratio was 1.

Herein, the effects of reduction temperature and Sn/Pt ratio on the structure of Pt-Sn alloy nanoparticles on Pt-Sn/SiO_2 catalysts prepared by *DR* were further investigated in detail. Transmission electron microscopy (TEM), X-ray diffraction (XRD), X-ray absorption fine structure analysis (XAFS), CO adsorption, and X-ray photoelectron spectroscopy (XPS) were used to characterize the bulk and surface states of the Pt-Sn bimetallic catalysts. Furthermore, combined with catalytic propane dehydrogenation tests, the structure-catalytic activity relationship, especially the states of Pt in the Pt-Sn/SiO_2 catalysts, was discussed.

Experimental

Preparation: Silica (JRC-SIO-9, 334 $m^2\ g^{-1}$) was used as the support for the preparation of the Pt-Sn catalysts. Prior to impregnation, the SiO_2 support was treated at 773 K for 3 h in air. Pt/SiO_2 was prepared by impregnating the SiO_2 support with an adequate volume of aqueous $H_2PtCl_6 \cdot 6H_2O$ (3 wt% Pt), stirring at 353 K for 3 h, and then drying at 353 K for 20 h. The precipitate was noted as Pt/SiO_2 precursor. A bimetallic Pt-Sn/SiO_2 precursor was prepared by sequential impregnation. The precursors were added to acetone solutions of $SnCl_2 \cdot 2H_2O$ (Wako, 97%), stirred at 353 K for 3 h, and dried at 353 K for 20 h. The molar ratios of Sn to Pt used were 1/3, 1/2,

1/1, 2/1, and 3/1. Prior to catalytic experiments, the catalyst precursor was reduced *in situ* in 20 vol% H_2 diluted with N_2 (total flow rate 50 mL min^{-1}) at the designated temperature in the range of 773 K to 1273 K for 1 h. Finally, the catalyst was cooled to 773 K in N_2 (100 mL min^{-1}). The obtained catalysts were denoted xPtySn/SiO_2_zK, where x and y indicate the molar ratio of Pt to Sn and z is the reduction temperature.

Reaction: Propane dehydrogenation was carried out in a quartz reactor (i.d. 10 mm) at atmospheric pressure with 20 vol.% of propane diluted with N_2 at 773 K. The total flow rate was 100 mL min^{-1}. The catalyst precursor (50 mg) was placed between quartz wool. The gas hourly space velocity (GHSV) is about 21741 h^{-1}. The composition of gas was analyzed with an on-line gas chromatograph (Shimadzu GC-8A, Japan) equipped with TCD (5A Molecular Sieve column) and methanizer FID (Porapak-Q column) detectors.

Characterization: All characterization was carried out on catalysts after *in situ* reduction in H_2 atmosphere. Brunauer–Emmett–Teller (BET) specific surface areas were estimated from N_2 isotherms obtained using a BELSORP 28SA (BEL Japan, Osaka, Japan) at 77 K. The analyzed samples were evacuated at 573 K for 3 h prior to the measurements.

CO adsorption is a very frequently used method for the characterization of Pt-based catalysts. It can be used to quantify the active surface area of supported Pt catalysts, determine the metal dispersion[8], and also study the interaction between Pt and the support or other promoters[9]. The amount of CO adsorbed on the catalysts at room temperature was determined by the CO pulse method with an Okura BP-2 instrument (Okura Riken, Japan) interfaced with a TCD. Prior to the CO adsorption, the catalyst precursor was reduced *in situ* in 20 vol% H_2 diluted with N_2 (total flow rate 50

ml min^{-1}) at the designated temperature in the range of 773 K to 1273 K for 1 h. 1:1 stoichiometry ratio of Pt:CO was assumed for the calculation of accessible surface Pt atoms on the catalysts.

X-ray diffraction (XRD) patterns were obtained using a MultiFlex DR powder X-ray diffractometer (Rigaku, Tokyo, Japan) with Cu Kα radiation (λ=1.5405 Å). The samples were scanned from 2θ=38° to 46° at a scanning resolution of 0.01°.

High angle annular dark field-scanning transmission electron microscope (HADDF-STEM) images were obtained using a JEOL JEM-3200FS transmission electron microscope. The samples were prepared by depositing drops of ethanol suspensions containing small amounts of the powders onto carbon-coated copper grids (Okenshoji Co. Ltd.), followed by evaporation of the ethanol in air.

X-ray absorption experiments were carried out at BL01B1 of SPring-8 (Hyogo, Japan). The ring energy was 8 GeV, and the stored current was 99.5 mA. Pt L_3 and L_2-edge (11.56 and 13.27 keV) X-ray absorption spectra were recorded in air at room temperature using a Si (111) monochromator in transmission mode. Sn K-edge (29.19 keV) X-ray absorption spectra were recorded in air at room temperature using a Si (311) monochromator in fluorescence mode. The data processing was performed using the REX2000 Ver.2.5.9 (Rigaku) and FEFF8.40 programs.

X-ray photoelectron spectra (XPS) were acquired using an ULVAC PHI 5500MT. The spectra were measured using Mg Kα radiation (15 kV, 400 W) in a chamber at a base pressure of ~ 10^{-7} Pa. All spectra were calibrated using C1s(284.80 eV) as a reference. Peak fitting was performed for Sn $3d_{5/2}$ using XPSPeak software (UK Surface Analysis Forum). Shirley function was used for background subtraction.

Results

Propane dehydrogenation

The effect of Sn/Pt ratio on the activities of Pt-Sn/SiO_2 catalysts prepared by *DR* is shown in Figure 1. In our previous paper[7], we reported that Pt-Sn/SiO_2 (*DR*) showed a higher activity for dehydrogenation of propane than Pt/SiO_2 (*DR*), indicating that Sn improved the catalytic performance of the supported Pt catalyst. The promoting effect of Sn in the dehydrogenation of propane[3b], butane[3e], isobutane[3a], and hexane[3f] has previously been reported. In the case of the Pt-Sn/SiO_2 catalysts reduced at 773 K, the conversion of propane initially increased with the Sn/Pt ratio, and 1Pt1Sn/SiO_2_773 K and 1Pt2Sn/SiO_2_773 K showed high activity. However, the activity was drastically reduced at a Sn/Pt ratio of 3.0. The conversion of propane by the catalysts reduced at 1073 K also strongly depended on the Sn/Pt ratio, increasing approximately linearly with Sn/Pt ratio up to 1.0. Further increase in the Sn/Pt ratio caused significant decreases in activity. Reducing the catalysts at 1273 K resulted in quite low activities on Pt-Sn/SiO_2 catalysts except for 1Pt1Sn/SiO_2_1273 K. 1Pt1Sn/SiO_2_1273 K showed 11.8 % propane conversion. Overall, 1Pt1Sn/SiO_2_1073 K showed the highest activity among the catalysts tested, exhibiting a propane conversion of 26.5% and selectivity toward propylene of 99.4%. A trace amount of methane and ethane were detected as by-products. Moreover, 1Pt1Sn/SiO_2_1073 K is almost stable during the reaction time (3h). The remarkable decrease of propane conversion on it was not observed.

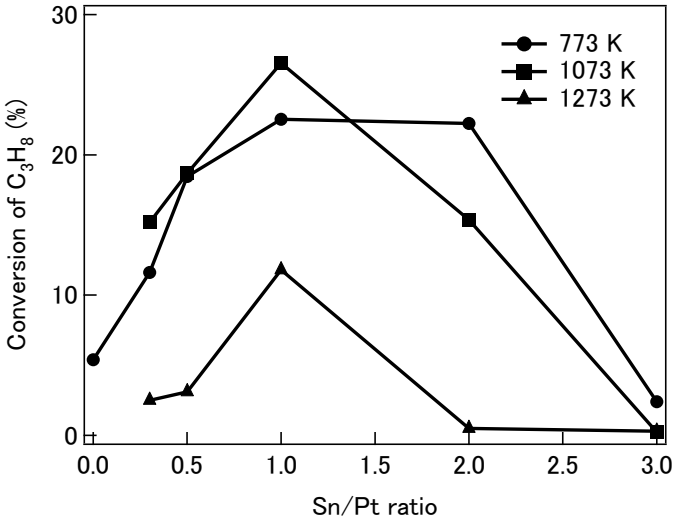

Figure 1 Effect of Sn/Pt ratio on the initial conversion of propane over Pt-Sn/SiO_2 catalysts reduced at 773 K, 1073 K and 1273 K.

The change in activity of the 1Pt1Sn/SiO_2 catalyst with reduction temperature is shown in Figure 2. The activity was found to slightly improve with increased reduction temperature up to 1073 K, and then remarkably decreased.

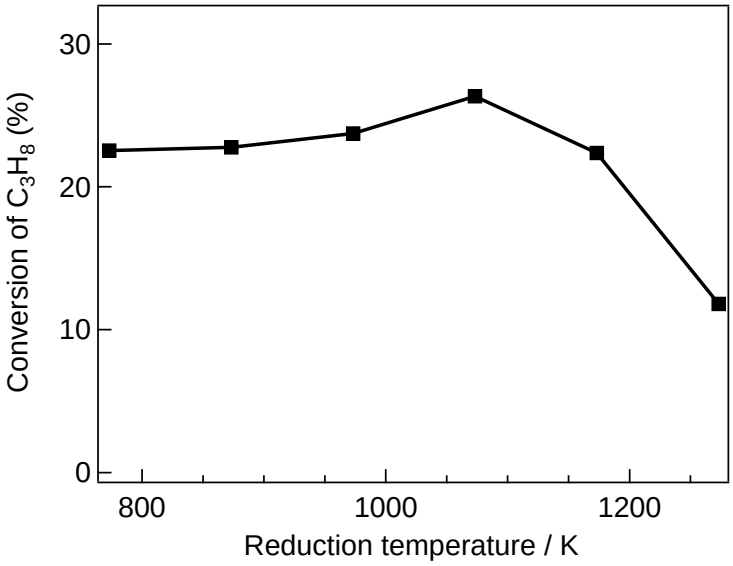

Figure 2 Effect of reduction temperature on the initial conversion of propane over 1Pt1Sn/SiO_2 catalysts.

Physical and chemical properties of Pt-Sn/SiO_2

Table 1 summarizes the BET specific surface area, amount of adsorbed CO, and average particle size estimated from HADDF-STEM images (Figure 3) of Pt-Sn/SiO_2 catalysts with various Sn/Pt ratios reduced at 773, 1073, and 1273 K. The BET surface area of Pt/SiO_2_773K (340 m^2 g^{-1}) was slightly larger than that of the Pt-Sn bimetallic catalysts (e.g., 297 m^2 g^{-1} for 3Pt1Sn/SiO_2_773 K). The BET surface areas of the Pt-Sn/SiO_2 catalysts reduced at 773 and 1073 K were found to be ca. 300 m^2 g^{-1} regardless of the Sn/Pt ratio. In contrast, BET surface area was decreased by reduction at 1273 K (ca. 210 m^2 g^{-1}).

The amount of adsorbed CO and average Pt particle size of Pt/SiO_2_773K were 54.9 μmol g^{-1} and ca. 1.1 nm, respectively. This result indicated that Pt was well dispersed on Pt/SiO_2 prepared by direct reduction. The addition of Sn to Pt/SiO_2 (Sn/Pt ratio=1/3, 1/2, 1, 2) caused a significant decrease in the amount of adsorbed CO and a modest increase in average particle size regardless of the reduction temperature. However, the average particle size was remarkably increased (ca. 5–6 nm) when the Sn/Pt ratio was 3.0 (1Pt3Sn/SiO_2), as shown in Figure 3. Meanwhile, a very low amount of adsorbed CO was detected on this catalyst.

The modification of the CO chemisorption properties of Pt by the addition of Sn has been reported by many researchers. Meriaudeau et al.[10] reported that Sn addition reduced the strength of Pt-CO bonds by preferential blocking higher binding sites of Pt. They interpreted this reduction of Pt-CO bond strength as being caused by a geometric effect. Recently, Wang et al.[11] synthesized Pt, PtSn (random alloy), and Pt@Sn (core/shell) catalysts using a colloidal synthesis method. They found a clear decrease in the intensity of linearly adsorbed CO on Pt sites in the order Pt > PtSn (random alloy) >

Table 1. Physical and chemical properties of Pt-Sn/SiO_2.

Catalyst[a]	Sn content (wt%) [b]	Surface area / $m^2\ g^{-1}$[c]	CO adsorption / $\mu mol\ g^{-1}$[d]	Average particle size / nm[e]
Pt/SiO_2 precursor	-	243	-	-
Pt/SiO_2_773K	-	340	54.9	1.1±0.7
3Pt1Sn/SiO_2_773K	0.6	297	19.1	1.7±0.8
2Pt1Sn/SiO_2_773K	0.9	305	21.5	1.5±0.6
1Pt1Sn/SiO_2_773K	1.8	282	18.1	1.8±0.9
1Pt2Sn/SiO_2_773K	3.5	288	9.6	1.9±0.7
1Pt3Sn/SiO_2_773K	5.2	270	n.d	6.3±2.4
3Pt1Sn/SiO_2_1073K	0.6	281	26.3	1.4±0.6
2Pt1Sn/SiO_2_1073K	0.9	316	26.0	1.4±0.6
1Pt1Sn/SiO_2_1073K	1.8	300	6.5	1.7±0.7
1Pt2Sn/SiO_2_1073K	3.5	300	9.7	2.3±1.3
1Pt3Sn/SiO_2_1073K	5.2	274	2.6	5.8±2.1
3Pt1Sn/SiO_2_1273K	0.6	206	1.9	2.0±0.7
2Pt1Sn/SiO_2_1273K	0.9	211	1.5	1.7±0.6
1Pt1Sn/SiO_2_1273K	1.8	200	1.4	1.8±1.2
1Pt2Sn/SiO_2_1273K	3.5	217	n.d	2.0±0.9
1Pt3Sn/SiO_2_1273K	5.2	227	n.d	3.2±2.4

[a] The loading amount of Pt was 3 wt%. [b] The molar ratio of Sn to Pt was1/3 1/2, 1/1, 2/1 or 3/1.
[c] The surface area of SiO2(JRC-SIO-9) is 325 m2 g−1.
[d] CO adsorption was measured with CO-pulse experiments.
[e] Average particle size was determined from the histogram of ca. 200 bright dots from HAADF-STEM images.

Pt@Sn (core/shell). The low amount of CO adsorbed on the Pt@Sn catalyst was attributed to the Sn surface covering and the absence of accessible surface Pt sites (geometric effects). In addition to the geometric effect, the change in electronic state of Pt on alloying with other metals has also been considered important in controlling CO chemisorption. Liu et al.[12] reported that PtSn@Pt core-shell nanoparticle electrocatalysts prepared by potential cycling of PtSn intermetallic nanoparticles in

CO-saturated H_2SO_4 solutions exhibited substantially higher CO-tolerance to Pt, PtRu alloy and PtSn alloy catalysts. They proposed that this superior CO-tolerance of the PtSn@Pt catalyst was mainly due to the electronic effects of the PtSn core on the Pt shell.

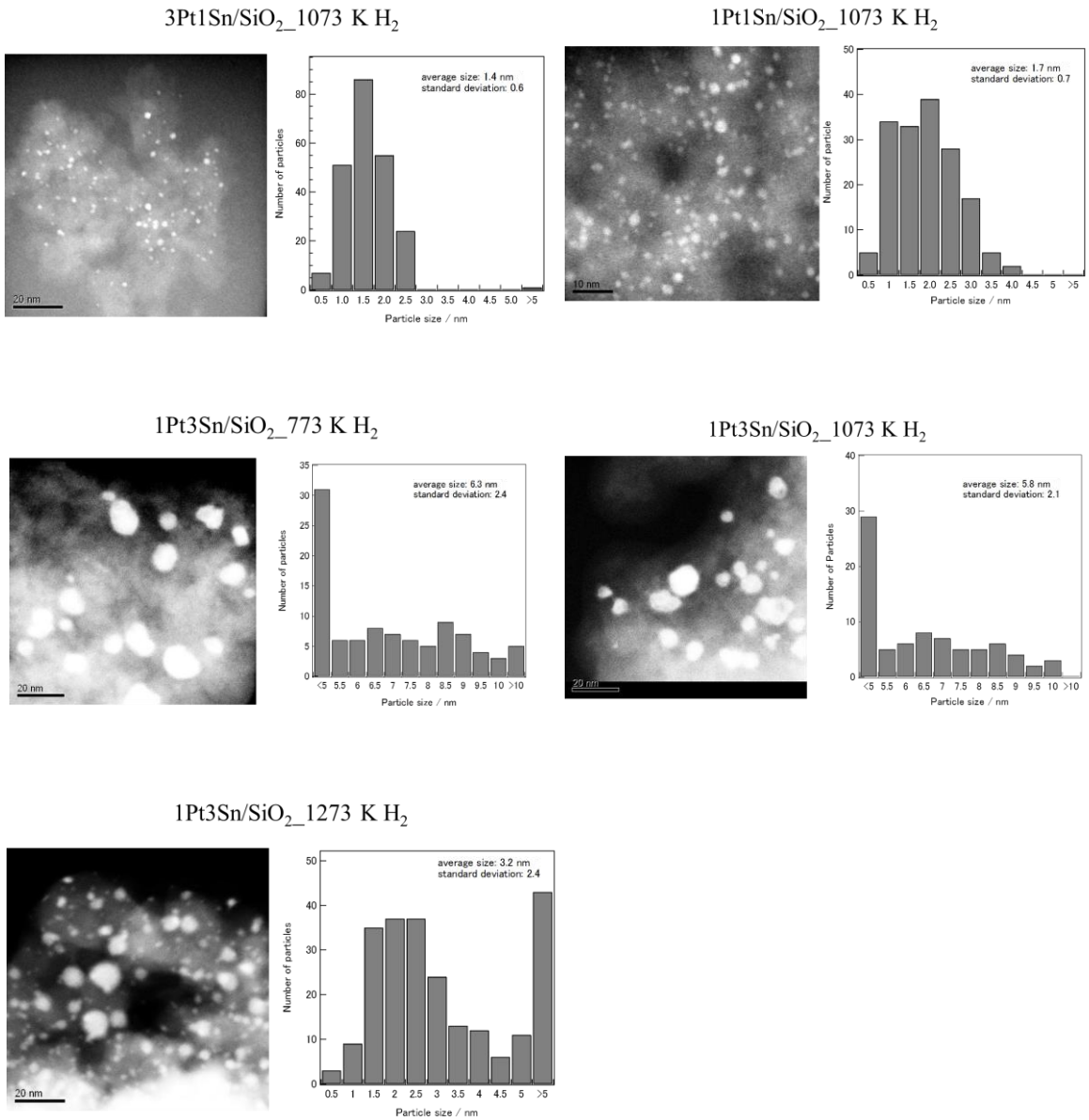

Figure 3 HAADF-STEM images of Pt-Sn/SiO_2 catalysts.

Table 2. TOF values over the catalysts.			
Catalyst	Propane conversion [a]	CO adsorption / μmol g^{-1} [b]	TOF / min^{-1} [c]
Pt/SiO_2_773K	5.4	54.9	16.1
3Pt1Sn/SiO_2_773K	11.6	19.1	99.4
2Pt1Sn/SiO_2_773K	18.5	21.5	140.8
1Pt1Sn/SiO_2_773K	22.5	18.1	203.4
1Pt2Sn/SiO_2_773K	22.2	9.6	378.3
1Pt3Sn/SiO_2_773K	2.4	0	-
3Pt1Sn/SiO_2_1073K	15.2	26.3	94.5
2Pt1Sn/SiO_2_1073K	18.7	26	117.7
1Pt1Sn/SiO_2_1073K	26.5	6.5	666.9
1Pt2Sn/SiO_2_1073K	15.4	9.7	259.7
1Pt3Sn/SiO_2_1073K	0.2	2.6	12.6
3Pt1Sn/SiO_2_1273K	2.5	1.9	215.3
2Pt1Sn/SiO_2_1273K	3.1	1.5	338.1
1Pt1Sn/SiO_2_1273K	11.8	1.4	1378.8
1Pt2Sn/SiO_2_1273K	0.5	0	-
1Pt3Sn/SiO_2_1273K	0.3	0	-

[a] The initial conversion of propane.
[b] CO adsorption was measured with CO-pulse experiments.
[c] TOF values were calculated based on CO adsorption.

Therefore, the results in this work suggest formation of Pt-Sn alloy such as Pt_3Sn, PtSn, $PtSn_2$, and/or deposition of Sn species on the surface of the Pt metal particles in the series of Pt-Sn/SiO_2 catalysts. Furthermore, the activities of these catalysts (Figure 1) were not proportional to the number of accessible Pt sites on their surfaces estimated from the amount of adsorbed CO (see Table 2). Thus, the effects of Sn/Pt ratio and reduction temperature on the local structure and electronic state of Pt and Sn should be considered to explain both the CO adsorption and catalytic behaviors of the Pt-Sn/SiO_2 catalysts.

XRD patterns of Pt-Sn/SiO_2

Figure 5 shows the XRD patterns of the catalysts with different Sn/Pt ratios and reduced at different temperatures. The XRD pattern of 3Pt1Sn/SiO_2_773K exhibited a broad peak at 2Θ = 39.3°. This position is lower than the peak of Pt metal (111) (2Θ = 39.8°) (ICSD 41525) and higher than the peak of Pt_3Sn alloy (111) (2Θ = 39.0°) (ICSD 105796). A similar shift of the characteristic peak of the (111) plane has previously been reported for various Pt-Sn alloys such as $Pt_{0.94}Sn_{0.06}$[13], $Pt_{0.93}Sn_{0.07}$[14], $Pt_{0.90}Sn_{0.10}$[15], and $Pt_{0.75}Sn_{0.25}$(Pt_3Sn)[13], accompanying lattice parameter expansion. Their XRD patterns are shown in Figure 4. The crystal structure of Pt_xSn_y alloys (x/y > 3) is face-centered cubic (fcc), similar to Pt metal. Based on Vegard's law, the broad peak observed for 3Pt1Sn/SiO_2_773K (2Θ = 39.3°) can be assigned to $Pt_{0.84}Sn_{0.16}$ alloy. The broad full-width at half maximum (FWHM) of this diffraction peak also implies the coexistence of various Pt_xSn_y alloys (x/y > 3).

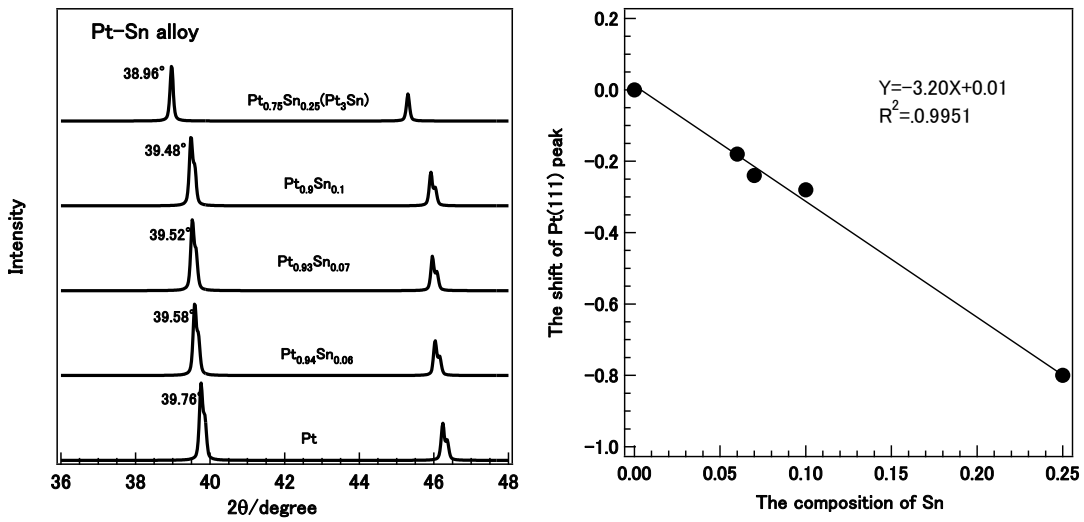

Figure 4 XRD patterns for Pt-Sn alloys from the previous reports [13, 14, 15] and Vegard's Law.

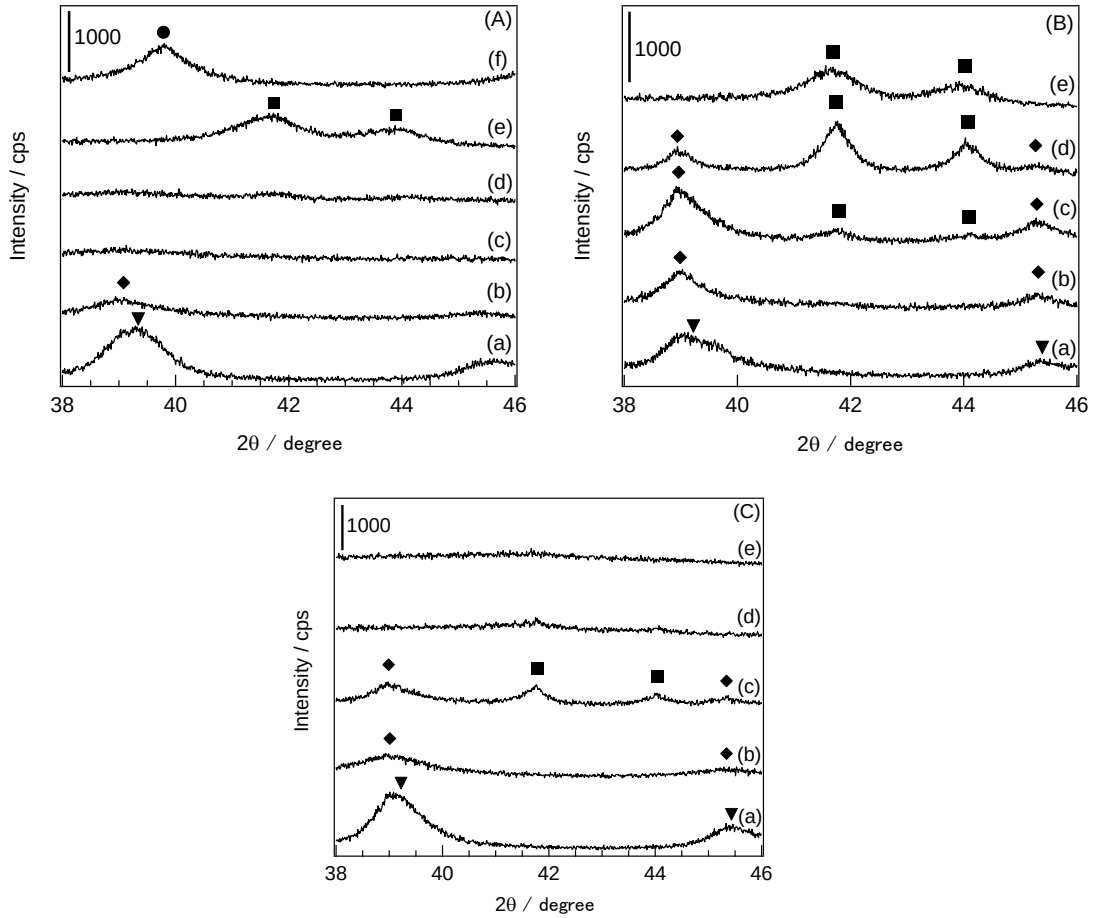

Figure 5　XRD patterns of Pt/SiO_2 and $Pt\text{-}Sn/SiO_2$ catalysts (A) reduced at 773 K, (B) reduced at 1073 K, and (C) reduced at 1273 K: (a) $3Pt1Sn/SiO_2$, (b) $2Pt1Sn/SiO_2$, (c) $1Pt1Sn/SiO_2$, (d) $1Pt2Sn/SiO_2$, (e) $1Pt3Sn/SiO_2$. (f) Pt/SiO_2,●: Pt ▼Pt_xSn_y (x/y > 3) ◆ Pt_3Sn ■ PtSn.

When the Sn content was further increased, a small diffraction peak at $2\Theta = 39°$ assignable to Pt_3Sn alloy (111) (ICSD 105796) was observed. No diffraction peaks were observed for $1Pt1Sn/SiO_2$_773K or $1Pt2Sn/SiO_2$_773K. Two diffraction peaks around 42° and 44° attributed to the PtSn alloy phase (ICSD 42593) were observed for $1Pt3Sn/SiO_2$_773K. Additionally, there were no obvious diffraction peaks due to Sn

compounds such as Sn metal and Sn oxides (SnO and SnO_2) even for 1Pt3Sn/SiO_2, which had a Sn content of 5.2 wt%.

When the reduction temperature was increased to 1073 K, the diffraction peaks of Pt_3Sn alloy appeared in the XRD patterns of 3Pt1Sn/SiO_2 and 2Pt1Sn/SiO_2. In the case of 3Pt1Sn/SiO_2, a shoulder peak assignable to Pt_xSn_y alloy ($x/y > 3$) was also observed. The XRD pattern of 1Pt1Sn/SiO_2 showed weak diffraction peaks of PtSn alloy alongside those of the Pt_3Sn alloy. Further increase in Sn content resulted in a decrease in intensity of the Pt_3Sn alloy diffraction peaks and an increase in those of the PtSn alloy. In the case of 1Pt3Sn/SiO_2, the diffraction peaks of Pt_3Sn alloy had vanished and those of PtSn alloy were weakened.

The XRD pattern of 3Pt1Sn/SiO_2_1273K showed an asymmetric diffraction peak at around $2\Theta = 39.2°$, similar to that observed for 3Pt1Sn/SiO_2_1073K, suggesting the coexistence of Pt_3Sn and Pt_xSn_y ($x/y > 3$) alloys. Weak diffraction peaks due to Pt_3Sn alloy appeared on the XRD patterns of 2Pt1Sn/SiO_2_1273K and 1Pt1Sn/SiO_2_1273K, but their intensities were weaker than those observed for the Pt-Sn/SiO_2 catalysts reduced at 1073 K. In the case of 1Pt1Sn/SiO_2_1273K, the diffraction peaks of PtSn alloy were also observed. These PtSn alloy peaks became quite weak for 1Pt2Sn/SiO_2_1073K, while the XRD pattern of 1Pt3Sn/SiO_2_1273K showed no diffraction peaks caused by Pt-Sn alloy.

XAFS analysis of Pt-Sn/SiO_2

Figure 6 shows the Pt L_3 and L_2-edge XANES spectra of 1Pt1Sn/SiO_2 catalysts reduced at 773 K, 1073 K and 1273 K, and those of reference samples (Pt/SiO_2 reduced at 773 K and Pt foil). The white line intensity at Pt L_3 and L_2-edges of 1Pt1Sn/SiO_2_773K was almost equal to that of Pt foil and lower than that of Pt/SiO_2

reduced at 773 K. In contrast, the white line intensity of 1Pt1Sn/SiO_2 reduced at 1073 K was slightly less than that of Pt foil. The intensity observed for 1Pt1Sn/SiO_2_1273K was lower than those for 1Pt1Sn/SiO_2_773K and 1Pt1Sn/SiO_2_1073K,

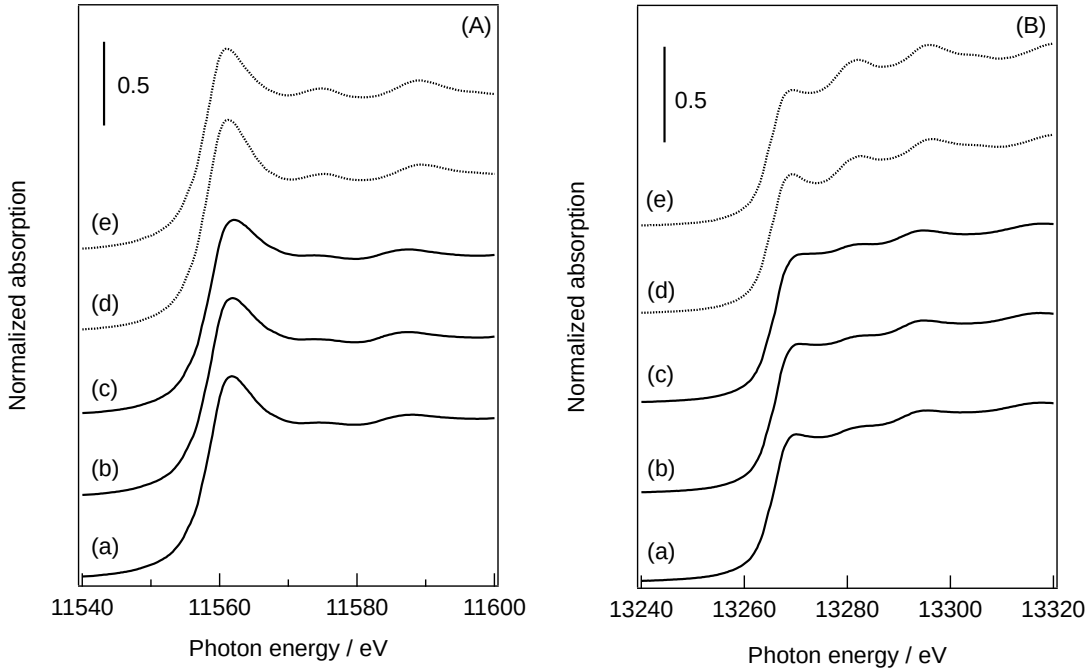

Figure 6 Pt L_3 and L_2 -edge XANES spectra of 1Pt1Sn/SiO_2 and references: (A) L_3-egde, (B) L_2-edge, (a) reduced at 773 K, (b) reduced at 1073 K, (c) reduced at 1273 K, (d) Pt/SiO_2 reduced at 773 K, (e) Pt foil.

and the width of the absorption band at the Pt L_3-edge was slightly broader, implying a different electronic state and local environment of platinum on 1Pt1Sn/SiO_2_1273K from those on the other catalysts.

The Pt L_3 and L_2-edge X-ray absorption white lines correspond to electronic transitions from $2p_{3/2}$ and $2p_{1/2}$ core level states and directly reflect the electronic states of the vacant *d* orbitals of platinum. The L_3 edge reflects the final vacant *d* states of both $5d_{3/2}$ and $5d_{5/2}$ levels, while the L_2 edge reflects that of only the $5d_{3/2}$ level. Lytle et al.[16] reported that the intensity of Pt L_3 X-ray absorption spectra is related to the

d-electron valences and the chemical environment. The lower intensity of the white lines observed for the 1Pt1Sn/SiO_2 catalysts than those for the Pt foil and Pt/SiO_2 suggests electron donation from Sn to Pt and alloy formation between Pt and Sn in this catalyst. Uemura et al.[17] also reported a lower white line intensity of Pt-Sn/Al_2O_3 catalyst (reduced at 573 K) than that of Pt foil, and assigned the small decrease to the formation of a Pt-Sn alloy because the *d*-electron density of platinum atoms is increased by alloying with Sn, which has a lower electronegativity than Pt (Pt 2.2, Sn 1.8)[18]. J H. Kim et al.[19] reported that the intensity of the white line was lower for Pt-Sn/C catalysts than that of Pt/C catalyst, which was attributed to partial filling of the unoccupied Pt 5d orbitals by electron donation from Sn. However, on the basis of Pt L_3-edge XANES spectra and quantum chemical density functional theory calculations, Linic and co-workers[20] proposed that the formation of Pt-Sn alloys does not lead to significant charge transfer such as electron donation between the constituent metal elements. Instead, they reported that the formation of Pt-Sn alloys results in a change in the width of the *d*-band localized on Pt by hybridization between the local *d*-orbital and the valence orbitals of neighboring atoms (Sn).

Figure 7(A) shows the k^3-weighted EXAFS oscillations at the Pt L_3-edge of 1Pt1Sn/SiO_2 catalysts reduced at 773 K, 1073 K and 1273 K, and reference samples (Pt/SiO_2 reduced at 773 K, and Pt foil). The EXAFS oscillations of the 1Pt1Sn/SiO_2 catalysts were significantly different and much weaker than those of the Pt foil and Pt/SiO_2 reduced at 773 K. The EXAFS oscillations of 1P1Sn/SiO_2_773K exhibited essentially similar features to those of 1P1Sn/SiO_2_1073K. In the Fourier transforms

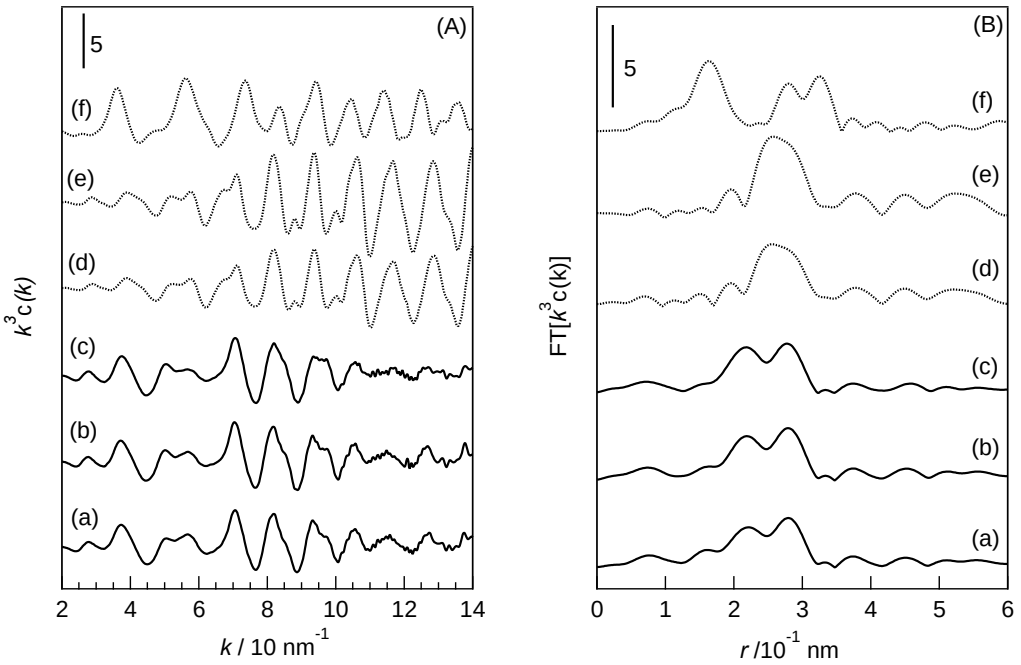

Figure 7 k^3-weighted EXAFS oscillation at Pt L_3-edge (A) and their Fourier transforms (B) of 1Pt1Sn/SiO_2 (a) reduced at 773 K, (b) reduced at 1073 K, (c) reduced at 1273 K, (d) Pt/SiO_2 reduced at 773 K (x 1/3), (e) Pt foil (x 1/3), (f) PtO_2 (x 1/2).

(FTs) of the EXAFS spectra of 1Pt1Sn/SiO_2 catalysts shown in Figure 7(B), no Pt–O linkage (around 0.17 nm) was observed, indicating that the supported Pt species was reduced to the metallic state after reduction at 773 K. Furthermore, a weak and split feature around 0.21–0.28 nm in the EXAFS FTs of the reduced catalysts suggests the interference of scattered electrons by Sn and Pt as reported by Uemura[17] and Ramallo-Lopez[21]. We have previously reported the results of curve-fitting analysis of the EXAFS data for 1Pt1Sn/SiO_2_1073 K[7]. By assuming two shells (Pt–Pt and Pt–Sn linkages), the EXAFS data for 1Pt1Sn/SiO_2_1073K was fitted, and the bond distances of Pt–Pt and Pt–Sn were calculated to be slightly shorter than the crystallographic values (Pt–Pt = 0.283 nm and Pt–Sn = 0.283 nm) observed in the Pt_3Sn crystal[22]. This is due to the formation of small particles of Pt_3Sn alloy. Both the coexistence of a small

fraction of PtSn phase and the interference of Pt and Sn scattering resulted in relatively larger *R*-factors.

The EXAFS oscillations of 1P1Sn/SiO_2_1273K were slightly different from those of 1P1Sn/SiO_2_773K and 1P1Sn/SiO_2_1073K. This indicates that the local structure of Pt in 1P1Sn/SiO_2_1273K was different from those of 1P1Sn/SiO_2_773K and 1P1Sn/SiO_2_1073K. Considering the XRD patterns of the 1P1Sn/SiO_2 catalysts, this is probably due to the increase in the fraction of PtSn phase.

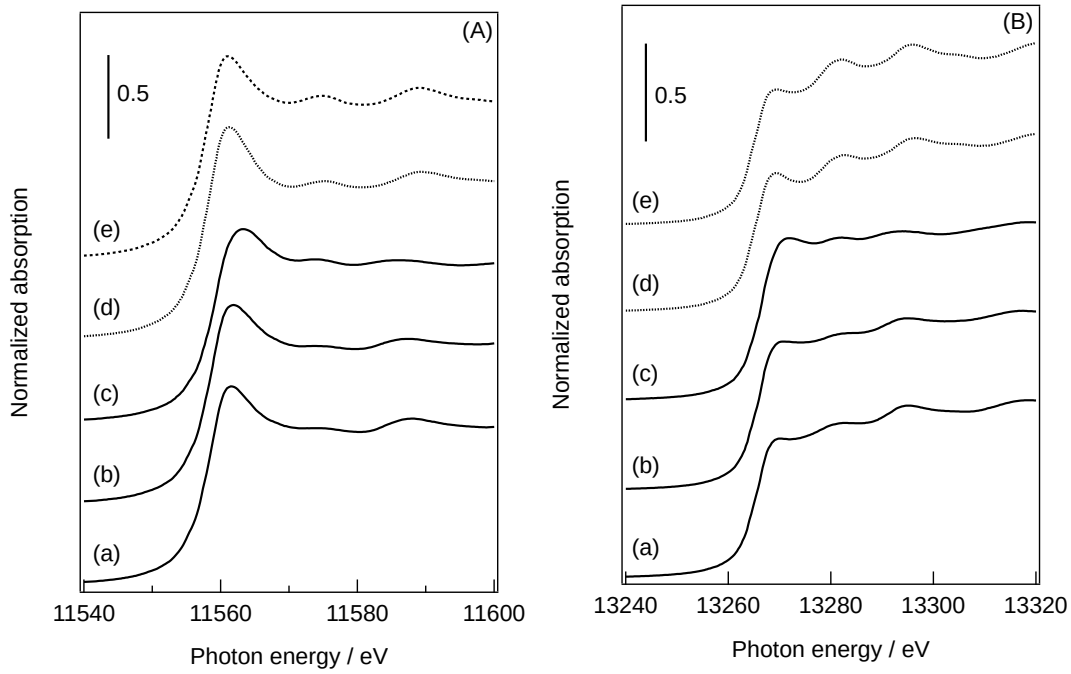

Figure 8 Pt L_3 and L_2 -edge XANES spectra of Pt-Sn/SiO_2 reduced at 1073 K, Pt/SiO_2 and Pt foil: (A) L_3-egde, (B) L_2-edge, (a) 3Pt1Sn/SiO_2, (b) 1Pt1Sn/SiO_2, (c) 1Pt3Sn/SiO_2, (d) Pt/SiO_2 reduced at 773 K, (e) Pt foil.

Figure 8 shows Pt L_3 and L_2-edge XANES spectra of Pt-Sn/SiO_2 catalysts with various Sn/Pt ratios reduced at 1073 K. The white line intensities at the Pt L_3 and L_2-edges of the 3Pt1Sn/SiO_2 and 1Pt1Sn/SiO_2 catalysts were lower than those of Pt foil and Pt/SiO_2. This result suggests electron donation from Sn to Pt and alloy formation

between Pt and Sn. In the case of 1Pt3Sn/SiO_2, the absorption band at the Pt L_3-edge was slightly shifted to a higher energy and the white line intensity at the Pt L_2-edge was higher than those observed for 3Pt1Sn/SiO_2, 1Pt1Sn/SiO_2 and Pt foil, indicating that the electronic state and local environment of platinum on 1Pt3Sn/SiO_2 is different from those on 3Pt1Sn/SiO_2, 1Pt1Sn/SiO_2, Pt/SiO_2 and Pt foil.

Figure 9(A) shows k^3-weighted EXAFS spectra at the Pt L_3-edge. The EXAFS oscillations of the 3Pt1Sn/SiO_2 catalyst were similar to those of Pt foil, although the intensity of the oscillations was much weaker. The peak around 0.25 nm in the FTs of the EXAFS spectra of the 3Pt1Sn/SiO_2 catalyst is assignable to Pt–Pt linkage. A smaller Pt–Pt contribution than that observed for the Pt foil indicates that small Pt nanoparticles (ca. 1.7 nm) had been formed on 3Pt1Sn/SiO_2.The EXAFS oscillations of the 1Pt3Sn/SiO_2 catalyst were significantly different from those of 3Pt1Sn/SiO_2, Pt/SiO_2 and Pt foil, and the oscillation period was slightly different from that observed for 1Pt1Sn/SiO_2. The two peaks at around 0.21 nm and 0.27 nm in the FTs of its EXAFS spectra (Figure 9(B)) are attributed to a conjunction of Pt–Sn and Pt–Pt bonds in Pt-Sn alloy phase. These results indicated that the contents of Pt-Sn alloys on 1Pt1Sn/SiO_2_1073K and 1Pt3Sn/SiO_2_1073K were larger than that on 3Pt1Sn/SiO_2_1073K. The different types of Pt-Sn alloy as well as their proportions led to the slight different spectra on 1Pt1Sn/SiO_2_1073K and 1Pt3Sn/SiO_2_1073K, consistent with the XRD results.

Figure 10 shows Sn K-edge XANES spectra of 1Pt1Sn/SiO_2 catalysts reduced at 773 K, 1073 K and 1273 K, and those of reference samples (Sn foil and SnO_2). The intensities of the absorption band of the 1Pt1Sn/SiO_2 catalysts were higher than that of

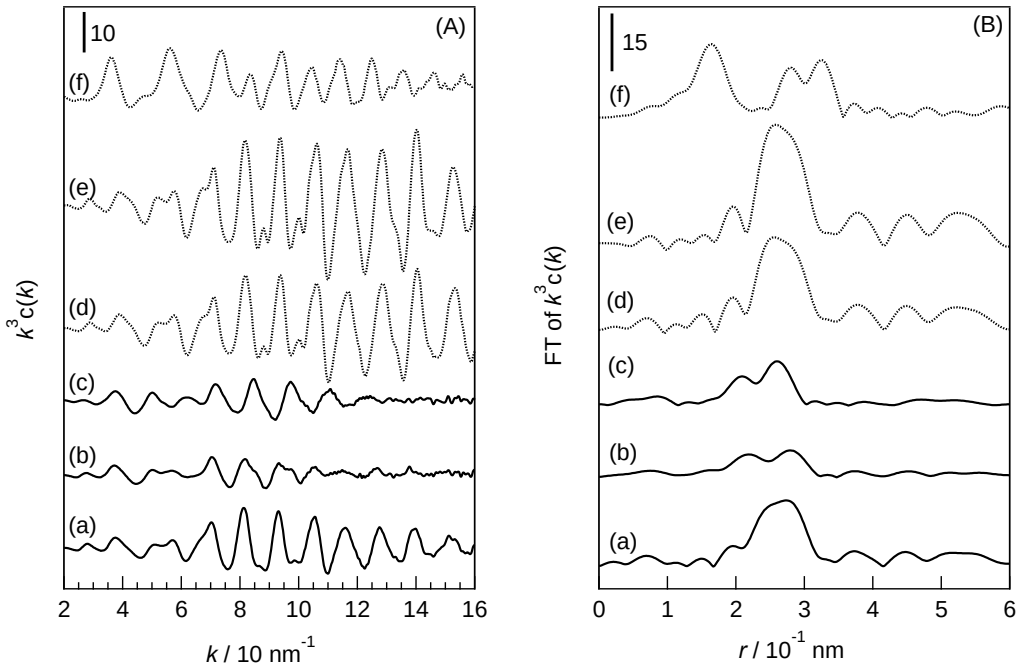

Figure 9 k^3-weighted EXAFS oscillation at Pt L_3-edge (A) and their Fourier transforms (B) of Pt-Sn/SiO_2 reduced at 1073 K, Pt/SiO_2, and Pt foil: (a) 3Pt1Sn/SiO_2, (b) 1Pt1Sn/SiO_2, (c) 1Pt3Sn/SiO_2, (d) Pt/SiO_2 reduced at 773 K, (e) Pt foil, (f) PtO_2.

Sn foil, but lower than that of SnO_2. The absorption edge position of the 1Pt1Sn/SiO_2 catalysts was higher than that of Sn foil, and slightly lower than that of SnO_2. Moreover, the intensity decreased with increasing reduction temperature. These results suggest that a mixture of Sn and Sn cations (Sn^{II} and Sn^{IV}) was present on the 1Pt1Sn/SiO_2 catalysts, and that the ratio of Sn^0/(Sn^{II} and Sn^{IV}) increased with the reduction temperature.

Figure 11(A) shows k^3-weighted EXAFS spectra at the Sn K-edge. The 1Pt1Sn/SiO_2 catalysts reduced at 773 K, 1073 K and 1273 K exhibited almost identical EXAFS oscillations. A peak at around 0.16 nm assignable to Sn–O linkage was observed in the FTs of their EXAFS oscillations (Figure 11(B)), suggesting the formation

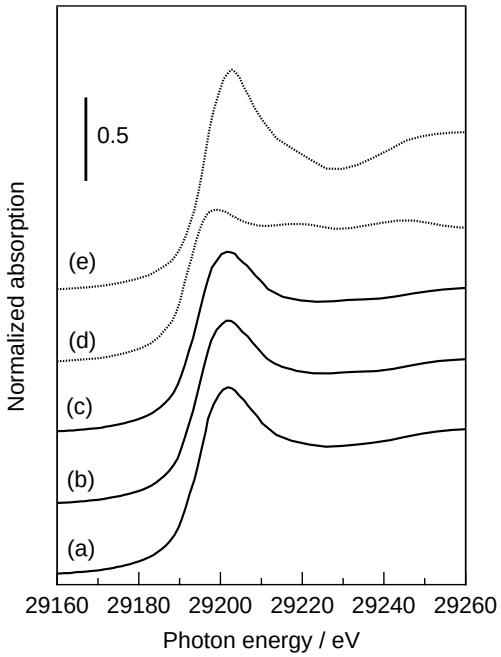

Figure 10 Sn K-edge XANES spectra of 1Pt1Sn/SiO_2 reduced at 773 K, 1073 K, and 1273 K and references: (a) reduced at 773 K, (b) reduced at 1073 K, (c) reduced at 1273 K, (d) Sn foil, (e) SnO_2.

of Sn oxides (SnO or SnO_2). The weak peaks around 0.2–0.3 nm in the FTs of the EXAFS oscillations of the 1Pt1Sn/SiO_2 catalysts suggests the contribution of Sn–Pt linkage as a result of the formation of Pt-Sn alloy phase. Indeed, the EXAFS data for 1Pt1Sn/SiO_2_1073K was well fitted by assuming two shells (Sn–O and Sn–Pt linkages). The Sn–O bond distance (0.203 nm) estimated by curve-fitting analysis was similar to the crystallographic value for SnO_2 ($r_{Sn–O}$ = 0.2052 nm) and smaller than that of SnO ($r_{Sn–O}$ = 0.2153 nm) (data not shown). The number of O atoms surrounding Sn atoms in 1Pt1Sn/SiO_2_1073K was 4.1, which is smaller than that of SnO_2 (N_O = 6), probably owing to amorphous SnO_2 phases and nanoparticles different from bulk SnO_2. These results indicate that Pt-Sn alloy particles were present alongside highly dispersed SnO_2 on the 1Pt1Sn/SiO_2 catalysts.

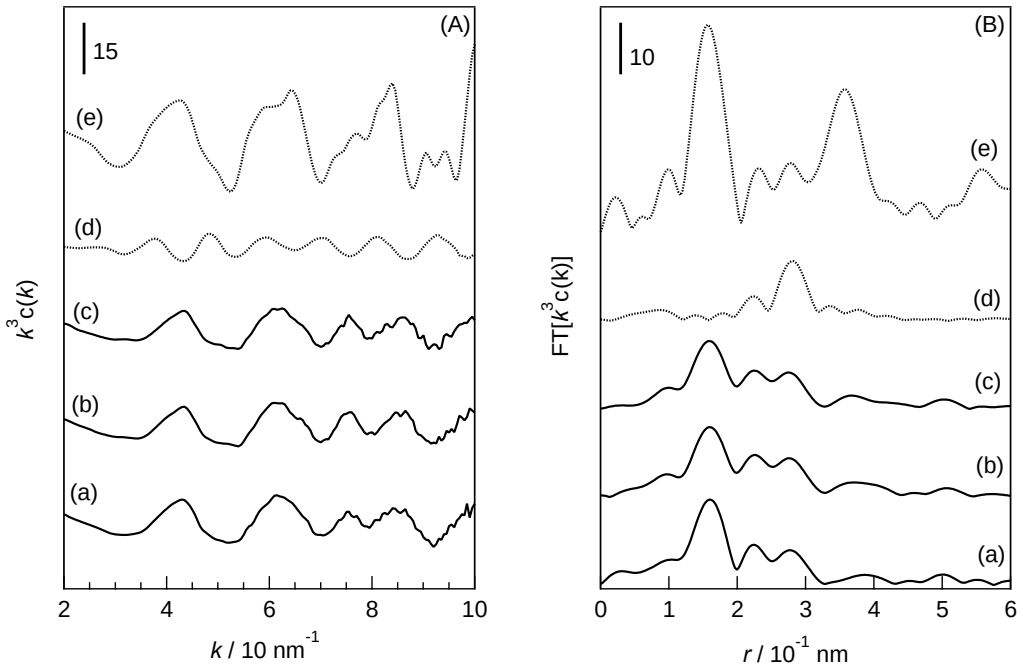

Figure 11 k^3-weighted EXAFS oscillation at Sn K-edge (A) and their Fourier transforms (B) of 1Pt1Sn/SiO_2 reduced at 773 K, 1073 K, and 1273 K and references: (a) reduced at 773 K, (b) reduced at 1073 K, (c) reduced at 1273 K, (d) Sn foil, (e) SnO_2.

Figure 12 shows Sn K-edge XANES spectra for Pt-Sn/SiO_2 catalysts with different Sn/Pt ratio reduced at 1073 K. The catalysts exhibited similar edge position, which was higher than that of Sn foil but lower than that of SnO_2. The intensity decreased with increasing Sn/Pt ratio. These results suggest that a mixture of Sn^0 and Sn cations (Sn^{II} and Sn^{IV}) was present on these Pt-Sn/SiO_2 catalysts and that the extent of alloying increased with the Sn/Pt ratio.

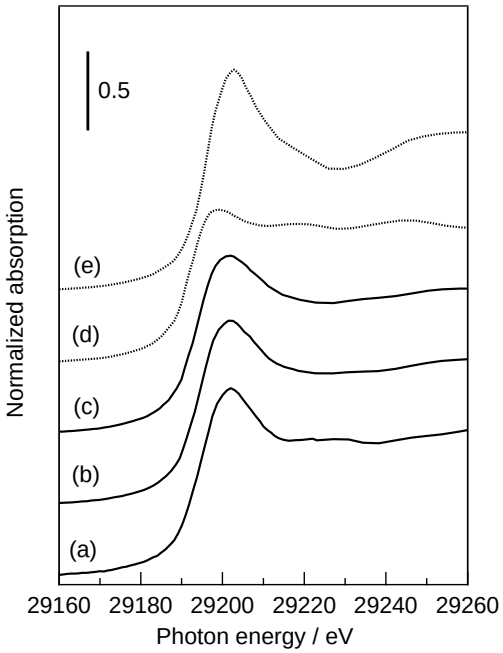

Figure 12 Sn K-edge XANES spectra of Pt-Sn/SiO_2 reduced at 1073 K and references: (a) 3Pt1Sn/SiO_2, (b) 1Pt1Sn/SiO_2, (c) 1Pt3Sn/SiO_2, (d) Sn foil, (e) SnO_2.

Figure 13(A) shows k^3-weighted EXAFS spectra at the Sn K-edge for Pt-Sn/SiO_2 catalysts with different Pt/Sn ratios reduced at 1073 K. First of all, the peak assignable to Sn–O linkage around 0.16 nm was observed in the EXAFS oscillation FTs of the Pt-Sn/SiO_2 catalysts regardless of Sn/Pt ratio (Figure 11(B)). Moreover, the intensities of the peaks around 0.2–0.3 nm, which implied alloy formation between Pt and Sn, decreased with increasing Sn/Pt ratio. The EXAFS oscillations of the 3Pt1Sn/SiO_2 catalyst were obviously different from those of the 1Pt1Sn/SiO_2 and 1Pt3Sn/SiO_2 catalysts in this range. As mentioned above, the interference of the scattered electrons by Pt and Sn atoms with each other in Pt-Sn catalysts can diminish EXAFS oscillations. Therefore, these results indicated that Pt-Sn alloy particles were present alongside highly dispersed SnO_2 on the Pt-Sn/SiO_2 catalysts, and that the extent of alloying between Pt and Sn increased with the Sn/Pt ratio. Furthermore, based on the

XRD patterns of the Pt-Sn/SiO_2 catalysts, the ratio of PtSn phase to Pt_3Sn phase also caused the observed change in the EXAFS oscillations.

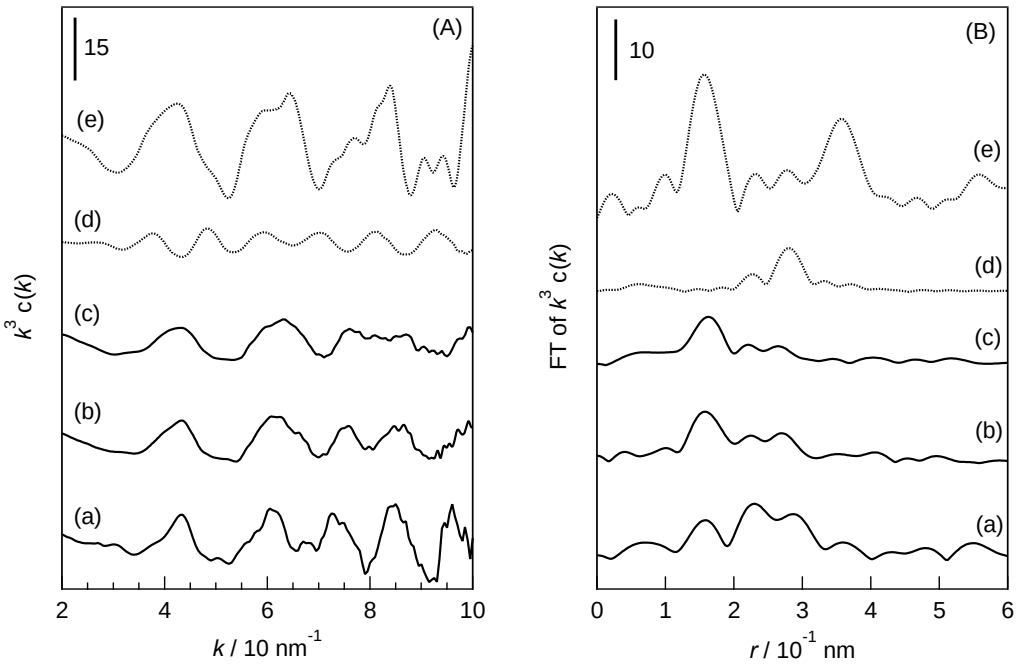

Figure 13 k^3-weighted EXAFS oscillation at Sn K-edge (A) and their Fourier transforms (B) of Pt-Sn/SiO_2 reduced at 1073 K and references: (a) 3Pt1Sn/SiO_2, (b) 1Pt1Sn/SiO_2, (c) 1Pt3Sn/SiO_2, (d) Sn foil, (e) SnO_2.

XPS analysis of Pt-Sn/SiO_2

Figure 14 shows the Pt 4f (A) and Sn 3d (B) XPS spectra of 1Pt1Sn/SiO_2 catalysts reduced at 773 K, 1073 K and 1273 K. The binding energies of the Pt $4f_{7/2}$ and $4f_{5/2}$ peaks were 71.6 and 74.8 eV, respectively, and the position of these peaks did not change with the reduction temperature. Based on these binding energies, the valence of platinum in the 1Pt1Sn/SiO_2 catalysts was assigned to Pt^0. The binding energy of the Sn $3d_{5/2}$ peaks was located at 486.5 eV, higher than the values usually reported for metallic Sn (484.9 eV) and lower than those typically reported for Sn oxides (487.1 eV). This suggests the coexistence of metallic Sn and Sn oxides on the 1Pt1Sn/SiO_2 catalysts

regardless of reduction temperature. Deconvolution of the Sn 3d XPS spectra of the 1Pt1Sn/SiO_2 catalysts revealed that the surface ratios of Sn^0/Sn^{IV} on the catalysts reduced at 773, 1073, and 1273 K were 33/67, 33/67, and 34/66, respectively. This result further confirmed that part of the Sn formed Pt-Sn alloy and part was present as small, highly dispersed SnO_2 particles.

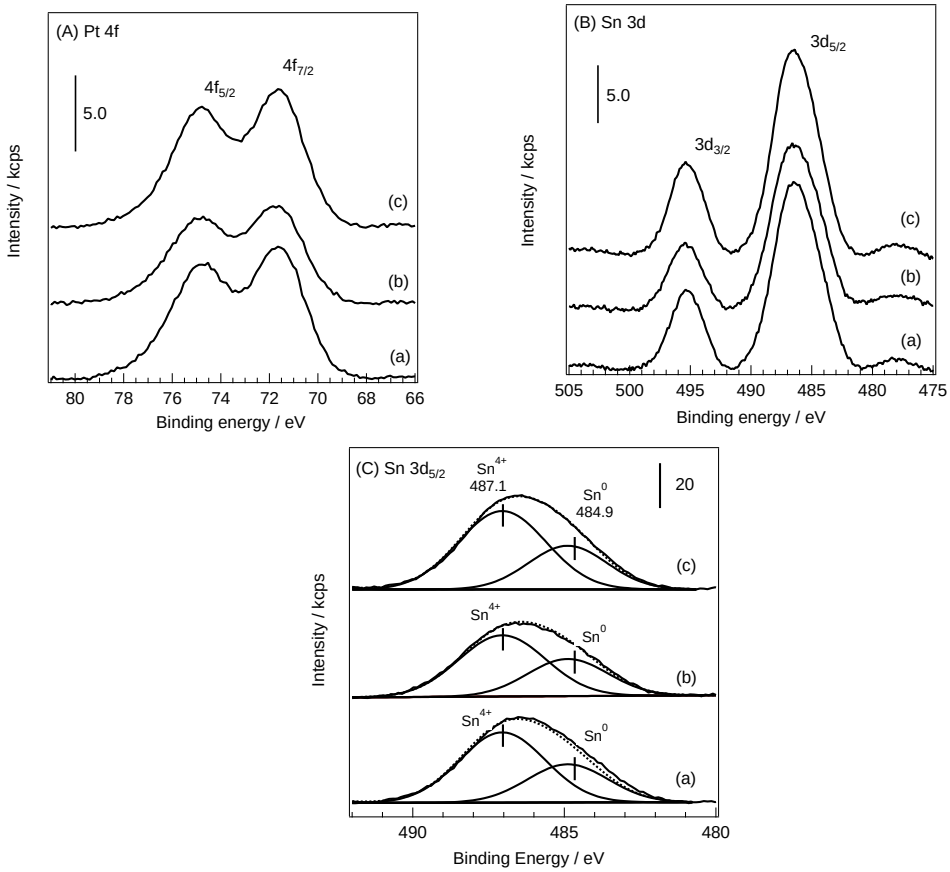

Figure 14 XP spectra of Pt 4f level (A) and Sn 3d level (B), and deconvolution of Sn 3d level (C) for (a) 1Pt1Sn/SiO_2_773K, (b) 1Pt1Sn/SiO_2_1073K, (c) 1Pt1Sn/SiO_2_1273K.

Figure 15 shows the Pt 4f (A) and Sn 3d (B) XP spectra of Pt-Sn/SiO_2 catalysts with various Sn/Pt ratios. The binding energies of the Pt $4f_{7/2}$ and $4f_{5/2}$ peaks were 71.6 and 74.8 eV, respectively, which were assigned to Pt^0. In the case of the Sn 3d region, the intensity of the Sn $3d_{5/2}$ peak increased with Sn/Pt ratio. It is also obvious that the

binding energies of Sn $3d_{5/2}$ peak shifted to higher energy with increasing Sn/Pt ratio, indicating a decrease in the surface Sn^0/Sn^{IV} ratio. The surface ratio of Sn^0/Sn^{IV} on the catalysts with 1/3, 1/1, and 3/1 Sn/Pt ratio was determined to be 53/47, 33/67, and 24/76, respectively, from the deconvolution results. Thus, the fraction of SnO_2 increased with Sn/Pt ratio. This observation is consistent with the Sn K-edge XAFS results discussed above.

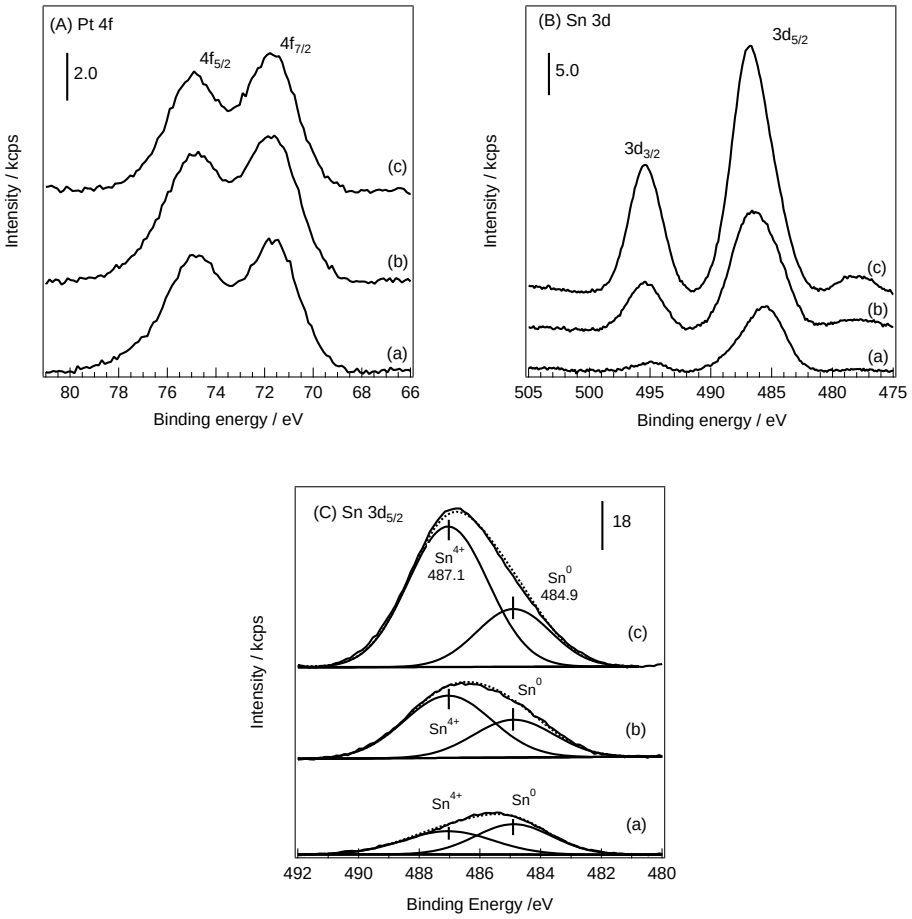

Figure 15 XP spectra of Pt 4f level (A) and Sn 3d level (B), and deconvolution of Sn 3d level (C) for (a) 3Pt1Sn/SiO_2_1073K, (b) 1Pt1Sn/SiO_2_1073K, and (c) 1Pt3Sn/SiO_2_1073 K.

To elucidate the change in surface Sn/Pt ratio with bulk Sn/Pt ratio, the surface Sn/Pt ratios of the Pt-Sn/SiO_2 catalysts were estimated from the areas in the Pt 4f and Sn 3d XPS results. Figure 16 plots the surface Sn/Pt atomic ratio against the bulk Sn/Pt

atomic ratio (nominal Sn/Pt ratio) for Pt-Sn/SiO_2 reduced at 1073 K. The surface Sn/Pt atomic ratios of all of the Pt-Sn/SiO_2 catalysts were found to be much larger than the corresponding bulk Sn/Pt values. This result indicates that surface enrichment with Sn species took place on the surface of the Pt-Sn/SiO_2 catalysts regardless of the initial Sn/Pt ratio. Figure 17 shows the effect of reduction temperature on the surface Sn/Pt ratio of the 1Pt1Sn/SiO_2 catalysts. The surface Sn/Pt ratios were larger than the bulk values for all of the 1Pt1Sn/SiO_2 catalysts, indicating Sn enrichment at the surface even with high reduction temperature. This behavior may be explained by the nature of Sn, which has a lower surface energy than platinum. Similar results have been observed for the Pt-Sn/C prepared by Kim et al[19].

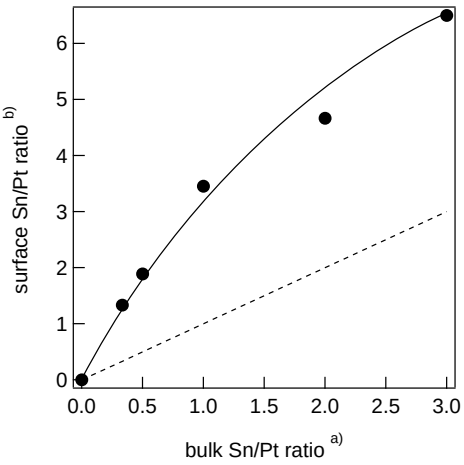

Figure 16　Relationship between bulk Sn/Pt ratio and surface Sn/Pt ratio of Pt-Sn/SiO_2 catalysts reduced at 1073 K. a) bulk Sn/Pt ratio was nominal Sn/Pt ratio, b) Surface Sn/Pt ratio was estimated from the area of XP spectra of Pt 4f level and Sn 3d level.

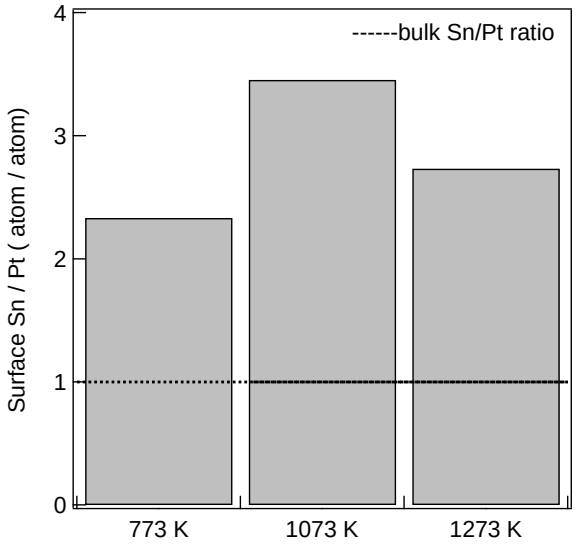

Figure 17 Surface Sn/Pt ratio on 1Pt1Sn/SiO_2 reduced at different temperatures.

Discussion

Based on all of the above characterization results, the effects of the Sn/Pt ratio and reduction temperature on the structure of the series of Pt-Sn/SiO_2 catalysts prepared by direct reduction are represented by Scheme 1. Structural characterization clearly showed that the Pt-Sn/SiO_2 catalysts possessed a Pt-Sn alloy (1–3 nm) core structure with a Sn-rich surface, and that the structure of the Pt-Sn alloy was influenced by the reduction temperature and the Sn/Pt ratio. Moreover, a highly dispersed SnO_2 coexisted with Pt-Sn alloy particles.

At low reduction temperature (773 K), Pt-Sn alloys with low Sn/Pt ratio (Pt_xSn_y alloys ($x/y \geq 3$) with fcc structure, cf. $Pt_{0.84}Sn_{0.16}$) were mainly formed. The surface of the Pt-Sn alloy particles was partially covered with highly dispersed SnO_2, as shown in Scheme 1.The content of Sn in the Pt-Sn alloy (the x/y value) increased with the reduction temperature. As a result, mainly Pt_3Sn alloy particles existed on 1Pt1Sn/SiO_2_1073K, together with a small fraction of PtSn alloy particles. This indicates that higher reduction temperature is suitable for the generation of relatively

Sn-rich Pt-Sn alloys. At high reduction temperature (1273 K), PtSn alloy, the structure of which is hcp, was mainly formed. The low catalytic activity of 1Pt1Sn/SiO_2_1273K suggests that the PtSn phase is not active in the dehydrogenation of propane to propylene, or at least its activity is notably lower than that of Pt_3Sn clusters. Conversely, mainly Pt_3Sn alloy nanoparticles were formed on the 1Pt1Sn/SiO_2_1073K catalyst, which showed the highest activity among the Pt-Sn/SiO_2 catalysts tested. These results are consistent with previous reports, in which superior catalytic performance was assigned to the Pt_3Sn alloy phase over other Pt-Sn alloy phases ($PtSn_4$, $PtSn_2$, Pt_2Sn_3, PtSn, and Pt_3Sn)[4,23] .

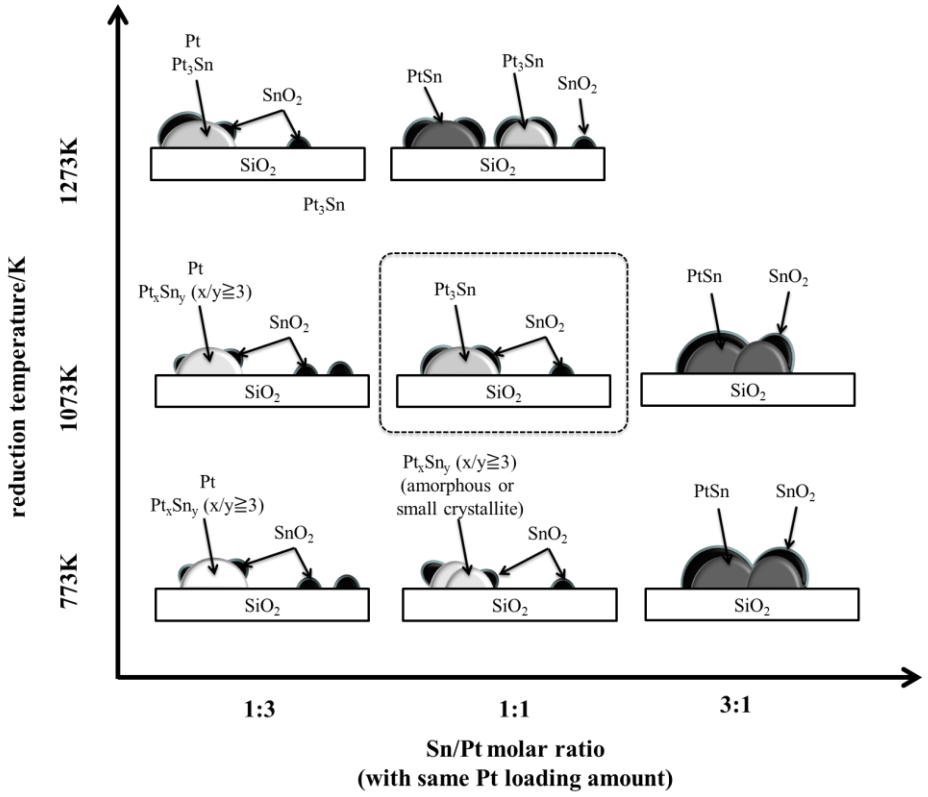

Scheme 1 The effects of Sn/Pt molar ratio and reduction temperature on the structure of Pt-Sn/SiO_2 catalysts.

The Sn/Pt ratio strongly affected the Pt-Sn alloy structure, particle size and the surface Sn/Pt ratio of the Pt-Sn/SiO_2 catalysts. For the Pt-Sn/SiO_2 catalysts reduced at 1073 K, the content of Sn in the Pt_xSn_y alloy increased with nominal Sn/Pt ratio, and a modest increase in particle size was observed on the catalysts when the initial Sn/Pt ratio was in the range of 1/3–2. However, when the initial Sn/Pt ratio was 3, PtSn alloy was mainly observed and the size of the PtSn alloy particles was remarkably increased regardless of the reduction temperature. The CO adsorption and XPS results indicated surface Sn-enrichment. It was found that Sn did not alloy with Pt in the impregnation step of the direct reduction preparation, and that part of the Sn interacted with Pt to form Pt-Sn alloy during the high-temperature reduction. However, the Sn did not completely alloy with Pt even after reduction at 1273 K. The Sn K-edge XAFS spectra showed that non-alloyed Sn was present as Sn oxide (SnO_2), the XPS results suggest that this non-alloyed Sn preferably located on the surface of the Pt-Sn alloy particles. Moreover, non-alloyed Sn was also formed on 3Pt1Sn/SiO_2, the nominal Sn/Pt ratio of which was equal to the stoichiometric proportions of Pt_3Sn alloy, suggesting that surface Sn-enrichment is inevitable on Pt-Sn/SiO_2 catalysts prepared by direct reduction.

Supported bimetallic Pt-Sn alloys have been widely applied to various kinds of reactions such as reforming, refining, and hydrogenation to obtain high activity, selectivity, and to improve the dispersion of the Pt and stability against coke deposition. The role of Sn in Pt-Sn alloy catalysts has been interpreted as modification of the geometric and electronic structures of Pt atoms via Pt-Sn interactions.

In terms of geometry, the XRD and Pt L-edge and Sn K-edge XAFS results indicated that the geometric environment of Pt changed with the addition of Sn to the Pt crystallites (fcc) by forming a solid solution of Pt_xSn_y alloy phase (fcc, $x/y \geq 3$), which

was accompanied by lattice constant expansion. Such elongation of bonding structure may affect catalytic reaction pathways that require specific geometric arrangements of the surface atoms, thus leading to changes in catalytic properties. Using DFT calculations, Alcala et al.[24] reported that surface transition species derived from ethanol on a Pt (111) plane via cleavage of C–C and C–O bonds are sensitive to geometric parameters, i.e., bond lengths and angles. They mentioned that the extended lattice parameter of the Pt may facilitate C–C cleavage, thus improving its catalytic activity for the electro-oxidation of alcohols, and dehydrogenation of alkanes. On the contrary, in our case, the addition of Sn results in the improvement of propane conversion without reducing selectivity and lattic constant expansion by the formation of Pt-Sn alloy. This suggests that the simple geometry effect is not appropriate to explain the positive effect of Sn.

In terms of modification of the electronic structure of the bimetallic Pt-Sn alloy system, the most noticeable change would be the charge transfer from Sn atoms to neighboring Pt atoms. Generally, it has been reported that Pt atoms in Pt-Sn alloys become more electron-rich owing to electron donation from Sn to Pt. The changes observed in the XPS, and Pt L_3 and L_2–edges XANES spectra on the addition of Sn demonstrated the charge transfer from Sn to Pt. This electronic modification of the unfilled *d* band states of Pt atoms may cause a weaker bond between carbon atoms and surface Pt atoms, thereby reducing or preventing strong adsorption of intermediates and products, in other words, catalytic poisoning. The ability of the Pt catalyst to adsorb other molecules such as hydrogen and propylene might be simultaneously diminished. However, this negative effect on the adsorption of molecules coexistent with propane would compromise the beneficial effects of poison-tolerance and inhibition of side

reactions, including cracking, isomerization, and coke formation, during dehydrogenation processes.

Conversely, Rammello-Lopez and co-workers[21] reported an increase in the number of Pt 5d holes due to a *d,s,p* rehybridization process on Pt-Sn/SiO_2 catalysts prepared from platinum ammine complex ($[Pt(NH_3)_4]^{2+}$) and $SnBu_4$ using Pt L_3 and L_2–edges XANES. They concluded that the formation of Pt-Sn bonds leads to an increase in the population of Pt (6s, 6p) and decrease in that of Pt (5d) electrons, resulting in transformation of electrons around Pt into Pt-Sn bonds. Jeon et al.[25] also showed that the 5d electron population of Pt atoms in a Pt-Sn alloy is smaller than that in metallic Pt. Further research and discussion on the electronic state of Pt including 5d holes are necessary, because the electronic state may depend on the mechanism of the incorporation of Sn into the Pt-Sn alloy, which is closely related to the Pt and Sn precursors, catalyst preparation method, and Sn/Pt ratio.

Moreover, on the basis of DFT calculations of Pt-Sn alloy models, Yang et al.[26] found that the *d*-band of Pt was broadened with increasing Sn content, which gave rise to a downshift in the *d*-band center of the Pt-Sn alloy model. Consequently, the bonding strength of propyl and propylene on the Pt-Sn alloy model was lowered. As a result, Pt_3Sn catalyst exhibited a lower energy barrier for propylene desorption and higher activation energy for propylene dehydrogenation with respect to Pt catalyst. Xin and Linic[20] also reported that alloy formation triggers a change in the width of *d*-band localized on Pt, and does not lead to significant charge transfer between the constituent metal elements in the alloys. They demonstrated that the width of local *d*-band is a function of the local geometry and the spatial extent of the valence orbitals of the atoms.

The change in the width of the *d*-band, which is related to its center, probably affects the absorption ability and reactivity of the catalyst.

Usually, Pt-Sn alloy modes having uniform structure are used in DFT calculations. However, the structural characterization in this work has shown that Sn-enrichment took place on the surface of the Pt-Sn alloy nanoparticles, which were partially covered with non-alloyed SnO_2 (highly dispersed SnO_2). Although this indicates that further investigations into the interaction between Pt-Sn alloy nanoparticles and non-alloyed SnO_2 and the catalytic function of non-alloyed SnO_2 in the dehydrogenation of propane are required, until now their existence was still unclear. Miura and co-workers[3e] reported that Pt supported on SnO_2-Al_2O_3 prepared by sol-gel method (a large excess of Sn was present on the catalyst) showed a high catalytic activity for dehydrogenation of n-butane to butadiene. They concluded that highly dispersed Sn oxides on the support surface retarded side reactions, and that the Sn-rich Pt-Sn alloy particles formed on SnO_2-Al_2O_3 support showed high catalytic activity. In the case of 1Pt1Sn/SiO_2_1073K, an excess of SnO_2 may suppress side reactions as well as Pt/SnO_2-Al_2O_3, and the Pt_3Sn alloy nanoparticles showed high catalytic activity. In the future, further investigation is expected to clarify the role of the oxidized Sn on the catalysis.

Conclusion

While Pt-Sn bimetallic catalysts for the dehydrogenation of propane have been widely studied, the nature of their structure and the active site were still unclear. In the present work, a series of SiO_2 supported Pt-Sn bimetallic catalysts were prepared using a direct reduction method and tested for the dehydrogenation of propane. The Sn/Pt

ratio and reduction temperature were found to strongly affect the bulk and surface properties of the obtained Pt-Sn bimetallic catalysts, as well as their catalytic behaviors. Different Pt-Sn alloys were formed with different Sn/Pt ratios and reduction temperatures. Sn was found to incompletely alloy with Pt, and the non-alloyed Sn species existed as the oxidized phase and was preferably located on the catalyst surface. The highest activity for propane dehydrogenation was obtained for the catalysts with Pt_xSn_y ($x/y>3$) and Pt_3Sn alloys, in which Pt became more electron-rich. The structure-reactivity relationship of the Pt-Sn bimetallic catalysts illustrates the importance of increased Pt atom *d* electron population in the dehydrogenation of propane.

References

[1] a Y. Yoshimura, N. Kijima, T. Hayakawa, T. Hayakawa, K. Murata, K. Suzuki, F. Mizukami, K. Matano, T. Konishi, T. Oikawa, M. Saito, T. Shiojima, K. Shiozawa, K. Wakui, G. Sawada, K. Sato, S. Matsuo, N. Yamaoka, Catal. Surv. Jpn. 2000, 4, 157-167; b N. Rahimi, R. Karimzadeh, Appl. Catal. A-Gen. 2011, 398, 1-17.

[2] a V. Rane, A. Rajput, A. Karkamkar, V. R. Choudhary, Applied Energy 2004, 77, 375-382; b B. Weckhuysen, R. Schoonheydt, Catal. Today 1999, 51, 223-232.

[3] a R. D. Cortright, J. A. Dumesic, J. Catal. 1994, 148, 771-778; b O. A. Barias, A. Holmen, E. A. Blekkan, J. Catal. 1996, 158, 1-12; c V. Galvita, G. Siddiqi, P. P. Sun, A. T. Bell, J. Catal. 2010, 271, 209-219; d A. Iglesias-Juez, A. M. Beale, K. Maaijen, T. C. Weng, P. Glatzel, B. M. Weckhuysen, J. Catal. 2010, 276, 268-279; e I. Kikuchi, M. A. Ohshima, H. Kurokawa, H. Miura, J. Jpn. Pet. Inst 2012, 55, 206-213; f J. Llorca, N. Homs, J. L. G. Fierro, J. Sales, P. R. delaPiscina, J. Catal. 1997, 166, 44-52.

[4] C. Kappenstein, M. Guerin, K. Lazar, K. Matusek, Z. Paal, J. Chem. Soc.-Faraday Trans. 1998, 94, 2463-2473.

[5] X. Wang, J. Stoever, V. Zielasek, L. Altmann, K. Thiel, K. Al-Shamery, M. Baumer, H. Borchert, J. Parisi, J. Kolny-Olesiak, Langmuir 2011, 27, 11052-11061.

[6] a M. Boualleg, D. Baudouin, J.-M. Basset, F. Bayard, J. P. Candy, J. C. Jumas, L. Veyre, C. Thieuleux, Chem. Commun. 2010, 46, 4722-4724; b M. Boualleg, J.-M. Basset, J.-P. Candy, V. Caps, J.-C. Jumas, S. Norsic, E. A. Quadrelli, L. Veyre, C. Thieuleux, ChemCatChem 2012, 4, 1729-1732.

[7] L. Deng, T. Shishido, K. Teramura, T. Tanaka, Catal. Today 2014, 232, 33-39.

[8] T. Tanabe, Y. Nagai, T. Hirabayashi, N. Takagi, K. Dohmae, N. Takahashi, S. i. Matsumoto, H. Shinjoh, J. N. Kondo, J. C. Schouten, H. H. Brongersma, Appl. Catal. A-Gen. 2009, 370, 108-113.

[9] C. Ocal, S. Ferrer, J. Chem. Phys. 1986, 84, 6474-6478

[10] P. Meriaudeau, A. Thangaraj, J. F. Dutel, C. Naccache, J. Catal. 1997, 167, 180-186.

[11] X. D. Wang, L. Altmann, J. Stover, V. Zielasek, M. Baumer, K. Al-Shamery, H. Borchert, J. Parisi, J. Kolny-Olesiak, Chem. Mat. 2013, 25, 1400-1407.

[12] Z. F. Liu, G. S. Jackson, B. W. Eichhorn, Angew. Chem.-Int. Edit. 2010, 49, 3173-3176.

[13] M. Ellner, Journal of the Less-Common Metals 1981, 78, 21-32.

[14] P. Durussel, R. Massara, P. Feschotte, J. Alloy. Compd. 1994, 215, 175-179.

[15] I. Harris, M. Norman, A. Bryant, Journal of the Less-Common Metals 1968, 16, 427-440.

[16] F. W. Lytle, J. Catal. 1976, 43, 376-379.

[17] a Y. Uemura, Y. Inada, K. K. Bando, T. Sasaki, N. Kamiuchi, K. Eguchi, A. Yagishita, M. Nomura, M. Tada, Y. Iwasawa, J. Phys. Chem. C 2011, 115, 5823-5833; b Y. Uemura, Y. Inada, K. K. Bando, T. Sasaki, N. Kamiuchi, K. Eguchi, A. Yagishita, M. Nomura, M. Tada, Y. Iwasawa, Phys. Chem. Chem. Phys. 2011, 13, 15833-15844.

[18] R. S. Mulliken, J. Chem. Phys. 1934, 2, 782-793.

[19] J. H. Kim, S. M. Choi, S. H. Nam, M. H. Seo, S. H. Choi, W. B. Kim, Applied Catalysis B: Environmental 2008, 82, 89-102.

[20] a H. L. Xin, N. Schweitzer, E. Nikolla, S. Linic, Journal of Chemical Physics 2010, 132, 111101; b H. L. Xin, A. Holewinski, N. Schweitzer, E. Nikolla, S. Linic, Top. Catal. 2012, 55, 376-390.

[21] J. M. Ramallo-Lopez, G. F. Santori, L. Giovanetti, M. L. Casella, O. A. Ferretti, F. G. Requejo, J. Phys. Chem. B 2003, 107, 11441-11451.

[22] J. S. Charlton, Cordeyha.M, I. R. Harris, Journal of the Less-Common Metals 1970, 20, 105-107.

[23] Z. Paal, A. Wootsch, D. Teschner, K. Lazar, I. E. Sajo, N. Gyorffy, G. Weinberg, A. Knop-Gericke, R. Schlogl, Appl. Catal. A-Gen. 2011, 391, 377-385.

[24] R. Alcala, M. Mavrikakis, J. Dumesic, J. Catal. 2003, 218 178-190.

[25] Y. Jeon, J. Chen, M. Croft, Phys. Rev. B 1994, 50, 6555-6563.

[26] M.-L. Yang, Y.-A. Zhu, C. Fan, Z.-J. Sui, D. Chen, X.-G. Zhou, J. Mol. Catal. A-Chem. 2010, 321, 42-49.

Chapter 4

Behavior of active species on Pt-Sn/SiO_2 catalyst during the dehydrogenation of propane to propylene and the regenerations

Abstract

Pt-Sn/SiO_2 catalyst (Sn/Pt ratio = 1.0) was prepared by direct reduction method and tested for the dehydrogenation of propane to propylene. The behaviors of platinum and tin on Pt-Sn/SiO_2 catalyst during the reactions and subsequent regenerations were investigated by transmission electron microscopy (TEM), X-ray diffraction (XRD), X-ray absorption fine structure (XAFS), X-ray photoelectron spectroscopy (XPS), and thermo-gravimetrical analysis (TG). The mechanisms of catalyst deactivation as well as regeneration were discussed based on the catalytic tests and characterizations. Coke was detected on the reacted Pt-Sn/SiO_2 catalysts and found to preferably locate on the metallic Sn (alloyed Sn) species. The catalytic performances of the reacted catalyst can be recovered with "Reduction" or "Oxidation-Reduction" regeneration process. Both of two methods could eliminate coke formed on Pt-Sn/SiO_2 catalyst, even the efficiency of hydrogen in "Reduction" method was lower than that of oxygen in "Oxidation-Reduction" method by which coke was completely burned off. Besides coke formation, the fraction of surface phases (Pt_3Sn and PtSn phases), their morphologies or detailed atomic arrangements on Pt-Sn/SiO_2 catalyst also changed with the reactions as well as regeneration processes. This tunable Pt-Sn alloy structure led to the catalyst deactivation or the reactivation. Overall, the present work suggests the importance of alloying between Pt and Sn towards the dehydrogenation of propane.

Introduction

The catalytic dehydrogenation of light alkanes [1-11], such as propane, is of great commercial interest due to the growing demand of propene as an important base chemical intermediate. Pt-Sn catalysts have been widely used for alkane dehydrogenation reactions because of their superior activity [1-3, 8, 12-20]. However, the deactivation of Pt-Sn catalysts is still not avoidable and led to the short lifetime of the catalyst. Some previous reports[15, 16] pointed that the deactivation of the catalyst was caused by the blocking of active Pt-Sn sites with coke formation. Bert M. Weckhuysen's group[16] measured the amount of coke deposited on Pt-Sn/Al_2O_3 catalyst was 7.3 % after 6 h of propane dehydrogenation at 590 ℃ using thermo-gravimetrical analysis. Bao Khanh Vu et al. [15] improved the catalytic stability of Pt-Sn/Al_2O_3 using Zn as the support promoter. The deactivated rate and coke formation over Pt-Sn/$ZnAl_2O_4$ were much lower than that over Pt-Sn/Al_2O_3. Moreover, the coke formed on Pt-Sn/$ZnAl_2O_4$ presented better mobility from the active site to the support than Pt-Sn/Al_2O_3.

Even though the coke formation was generally regarded as the main reason for the deactivation of Pt-Sn catalysts in propane dehydrogenation, the deactivation of Pt-Sn catalyst in the dehydrogenation of propane seems not such simple phenomenon. Bert M. Weckhuysen[16] once found that after one regeneration process, Pt-Sn/Al_2O_3 catalyst possesses both different activity and different coke formation in comparison with the initial dehydrogenation cycle, which suggests a modification of the properties of the active sites on Pt-Sn/Al_2O_3 during the regeneration. In fact, the bimetallic catalyst is the complex system and its structure differed with the metals properties, metal(s) support interactions, atmosphere (oxidant, reductive, reaction, etc.), temperature and so

on[21-27]. In 2008, Feng Tao et al.[28, 29] reported the flexible and tunable structure of bimetallic nanoparticle catalysts during catalytic reactions. With XPS, they observed the $Rh_{0.5}Pd_{0.5}$ nanoparticles underwent dramatic and reversible changes in composition and chemical state in response to reaction conditions. The structural changes of Pt-Sn bimetallic catalyst also took place in its regeneration. The regeneration of Pt-Sn bimetallic catalyst typically consists of exposing the coked catalyst to air or oxygen at high temperatures to burn the deposits, followed by a reduction step to return the active catalyst. Uemura. Y.[30, 31] carefully studied this process with *in situ* time-resolved XAFS technique. It was observed that Pt_3Sn alloy nanoparticles on Al_2O_3 transformed into Pt metal and SnO_2 in the oxidation process and the following reduction in H_2 led to the alloying between Pt and SnO_2 and the final formation of Pt_3Sn alloy. Bert M. Weckhuysen[16] also used XAFS technique to unveil a gradual Sn enrichment of the alloy due to multiple dehydrogenation-regeneration cycles.

These previous works encouraged us to systemically investigate Pt-Sn/SiO_2 catalyst during its operation and regeneration. Besides coke formation and possible metal sintering, structure, especially the surface structure of Pt-Sn active sites was also concentrated. Pt-Sn/SiO_2 catalyst during the reaction and regeneration process was characterized using a combined TG-DTA, HADDF-STEM, XRD, XAFS and XPS techniques. Based on these results, the deactivation and regeneration behaviors of Pt-Sn/SiO_2 in the dehydrogenation of propane were expected to be clarified.

Experimental

Catalyst preparation

Silica (JRC-SIO-9, 334 m^2 g^{-1}) was used as support to prepare Pt-Sn catalysts. Prior to impregnation, the SiO_2 support was treated at 773 K for 3h in air. Pt/SiO_2 was

prepared by impregnating SiO_2 support with an adequate volume of aqueous solution of $H_2PtCl_6 \cdot 6H_2O$ (Wako, 99.9 %), stirring at 353 K for 3h, and then drying at 353 K for 20 h. The precipitate was noted as Pt/SiO_2 precursor. A bimetallic $Pt\text{-}Sn/SiO_2$ precursor was prepared by sequential impregnation. The Pt/SiO_2 precursor was added to acetone solution of $SnCl_2 \cdot 2H_2O$ (Wako, 97 %), stirred at 353 K for 3 h, and dried at 353 K for 20h. The molar ratio of Sn to Pt was 1.0, and the Pt loading was 3 wt%.

Dehydrogenation of propane

Prior to the reaction, the catalyst precursor (50 mg) was *in situ* reduced in 20 vol% H_2 diluted with N_2 (total flow rate 50ml min^{-1}) at 1073 K. Finally, the catalyst was cooled to 773 K in N_2 (100 ml min^{-1}). Typically, the reaction was started by introducing a gas mixture of C_3H_8 and N_2 (20/80) to a quartz reactor (i.d. 10 mm) at atmospheric pressure. The total flow rate was 100 ml min^{-1}. A gas mixture of $C_3H_8/H_2/N_2$ (20/5/75) was also used to investigate the effect of H_2 in the feeding gas. The gas hourly space velocity (GHSV) is about 21741 h^{-1}. The composition of gas was analyzed with an on-line gas chromatograph (Shimadzu GC-8A, Japan) equipped with TCD (5A Molecular Sieve column) and methanizer FID (Porapak-Q column) detectors. The amount of coke formed over the $Pt\text{-}Sn/SiO_2$ catalyst after the reaction for 7 h at 773 K was measured by thermo gravimetrical-differential thermal analysis (TG-DTA, Shimadzu DTG-60H, Japan) in air.

Catalyst regeneration processes

(1) Regeneration with Reduction method

After the dehydrogenation of propane proceeds for 7 h at 773 K, the sample was regenerated at 1073 K in the mixture of H_2 (10 ml min^{-1}) and N_2 (40 ml min^{-1}) for 1 h. And then the catalyst was cooled to 773 K in N_2 (100 ml min^{-1}). The reactivated

catalyst with Reduction method was noted as "Pt-Sn/SiO_2 (*R*)".

(2) Regeneration with Oxidation-Reduction method

After the dehydrogenation of propane proceeds for 7 h at 773 K, the sample was regenerated at 773 K in the gas mixture of O_2 (10 ml min^{-1}) and N_2 (40 ml min^{-1}) for 1 h, following the reduction at 1073 K in the mixture of H_2 (10 ml min^{-1}) and N_2 (40 ml min^{-1}) for another 1 h. Finally, the catalyst was cooled to 773 K in N_2 (100 ml min^{-1}). The reactivated catalyst with Calcination-Reduction was noted as "Pt-Sn/SiO_2 (O*R*)".

Characterization

The fresh Pt-Sn/SiO_2 catalyst was characterized after *in situ* reduction in 20 vol% H_2 diluted with N_2.

Brunauer—Emmett—Teller (BET) specific surface area was estimated from N_2 isotherm at 77 K. The N_2 adsorption isotherm measurements were carried out by using a BELSORP 28SA (BEL Japan, Osaka, Japan) at 77 K. The analyzed samples were evacuated at 573 K for 3 h prior to the measurements.

X-ray diffraction (XRD) patterns were obtained using a RINT-TTR III powder X-ray diffractometer (Rigaku, Tokyo, Japan) with Cu Kα radiation (λ = 1.5405 Å, 50 kV, 300 mA). The samples were scanned from 2θ=38° to 46° at the scanning resolution of 0.01°.

High angle annular dark field-Scanning transmission electron microscope (HADDF-STEM) images were obtained using a JEOL JEM-3200FS transmission electron microscope. The samples were prepared by depositing drops of ethanol suspensions containing small amounts of the powders onto carbon-coated copper grids (Okenshoji Co. Ltd.), followed by evaporation of the ethanol in air.

X-ray absorption experiments were carried out at the BL01B1 at SPring-8

(Hyogo, Japan). The ring energy was 8 GeV, and the stored current was 99.5 mA. The Pt L_3-edge (11.56 keV) X-ray absorption spectra were recorded by using a Si (111) monochromator in transmission mode in air at room temperature. Sn K-edge (29.19 keV) X-ray absorption spectra were recorded by using a Si (311) monochromator in fluorescence mode in air at room temperature. The data processing was performed by using the REX2000 Ver.2.5.9 (Rigaku) and FEFF8.40 programs. Pt foil and Sn foil were purchased from Nilaco Corp.. SnO_2 (98%) was purchased from Wako Corp..

X-ray photoelectron spectra (XPS) were acquired using an ULVAC PHI 5500MT. The spectra were measured using Mg Kα radiation (15 kV, 400 W) in a chamber at a base pressure of ~ 10^{-7} Pa. All spectra were calibrated using C1s (284.80 eV) as a reference. Peak fitting was performed for Sn $3d_{5/2}$ using XPSPeak software (UK Surface Analysis Forum). Shirley function was used for background subtraction.

Results

Propane dehydrogenation

Figure 1 (A) shows the results of propane dehydrogenation over Pt-Sn/SiO_2 catalyst in the first run. In the absence of hydrogen in the feeding gas, the propane conversion was 23.7 % at the initial stage, and decreased to 15.5 % after 7 h. The amount of coke on the Pt-Sn/SiO_2 catalyst after 7 h of the reaction was estimated to be ca. 2.8 wt% by TG-DTA, shown in Table 1. This value was smaller than 7.3 wt% on Pt-Sn/Al_2O_3 (after 6 h at 590℃)[16], and 4.9 wt% on Pt-Sn/$ZnAl_2O_4$ (after 4 h at 1 bar and 600℃)[15]. This is probably due to the lower reaction temperature (500℃) and amorphous SiO_2 used in the present study. The acid strength of SiO_2 is weaker than that on Al_2O_3 and $ZnAl_2O_4$, thus leading to the weaker strength of propylene or other

intermediate (the precursors of coke) adsorption on SiO_2 supported catalyst. In the presence of hydrogen, the initial propane conversion was 23.4 %, almost similar to the case without hydrogen. And it was 19.1 % after 7h, suggesting the lower catalyst deactivation rate. Moreover, the amount of coke on the Pt-Sn/SiO_2 catalyst after 7 h reaction with H_2 was estimated to be ca. 0.7 %. These results suggest that hydrogen in the feeding gas improved the stability of Pt-Sn/SiO_2 catalyst by the inhibition of coke formation.

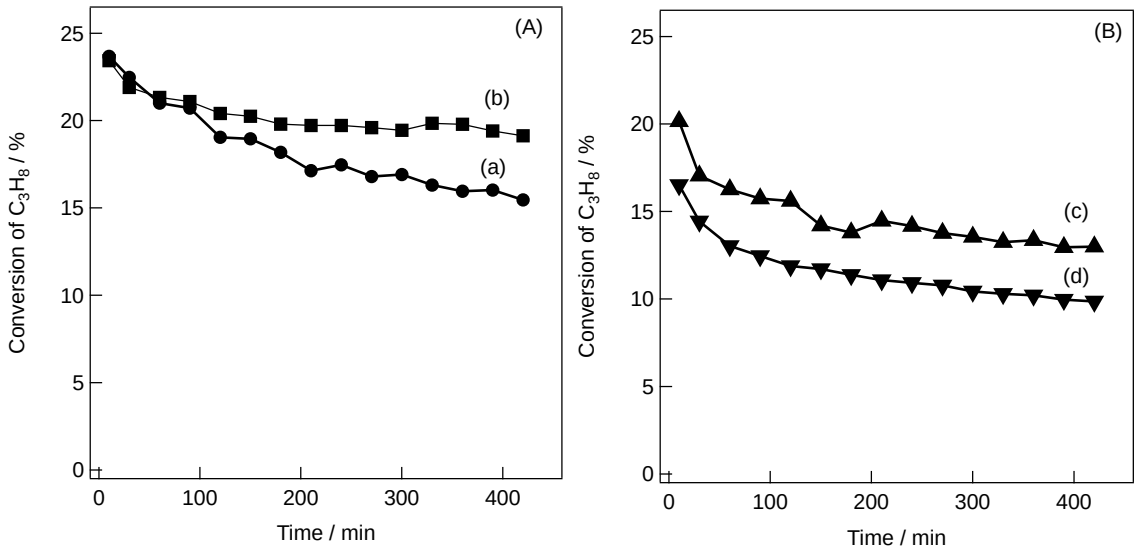

Figure 1 Time-course of propane dehydrogenation over Pt-Sn/SiO_2 catalyst. (A) 1st run, (B) 2nd run (after regeneration): (a) reduced at 1073 K, without H_2, (b) reduced at 1073 K, with H_2, (c) Pt-Sn/SiO_2 (*R*), (d) Pt-Sn/SiO_2 (O*R*), Reaction conditions: catalyst weight, 50 mg; reaction temperature, 773 K; (a), (c), (d) *P* (C_3H_8) = 20.3 kPa; *P* (N_2) = 81.0 kPa; (b) *P* (C_3H_8) = 20.3 kPa; *P* (H_2) = 5.0 kPa; *P* (N_2) = 76.0 kPa.

After 7 h reaction without H_2, the deactivated Pt-Sn/SiO_2 catalyst was regenerated with the treatment with H_2 at 1073 K for 1h (Reduction method, denoted as Pt-Sn/SiO_2 (*R*)) or the treatment with O_2 at 773 K and the subsequent H_2 reduction at 1073 K (Oxidation-Reduction method, denoted as Pt-Sn/SiO_2 (*OR*)). Table 1 showed that both methods effectively eliminated the formed coke on the deactivated Pt-Sn/SiO_2

catalyst. The amount of coke was 0.7 % on Pt-Sn/SiO_2 (*R*) and no coke on Pt-Sn/SiO_2 (*OR*). The catalytic behaviors of the regenerated catalysts (the second reaction run) were shown in Figure 1 (B). With Reduction method, the activity of the deactivated Pt-Sn/SiO_2 catalyst was slightly recovered (16.5 %). In contrast, it was remarkably recovered by the Oxidation-Reduction method. The initial propane conversion of Pt-Sn/SiO_2 (*OR*) is 20.2 %.

The activities of regenerated Pt-Sn/SiO_2 catalysts gradually decreased regardless the regeneration methods in the second run. The propane conversion on Pt-Sn/SiO_2 (*R*) decreased to 9.9 % after 7 h. The conversion on Pt-Sn/SiO_2 (*OR*) decreased from 20.2 % to 13.0 % after 7 h. Different from the first run, the amount of coke formed in the second run is small. It is only 0.1 % on the reacted Pt-Sn/SiO_2 (*R*) and 0.6 % on the reacted Pt-Sn/SiO_2 (*OR*) after 7 h of the reaction.

Table 1 The amount of coke deposited on Pt-Sn/SiO_2 catalysts (measured with TG-DTA).

Catalyst	Coke amount (wt%)
Pt-Sn/SiO_2	0.0
reacted without H_2	2.8
reacted with H_2	0.7
Pt-Sn/SiO_2 (*R*)	0.7
reacted Pt-Sn/SiO_2 (*R*)	0.1
Pt-Sn/SiO_2 (*OR*)	0.0
reacted Pt-Sn/SiO_2 (*OR*)	0.6

XRD patterns of Pt-Sn/SiO_2

Figure 2 shows the XRD patterns of Pt-Sn/SiO_2 catalysts before and after the reactions and the regenerations. The XRD pattern of Pt-Sn/SiO_2 reduced at 1073 K (fresh one) exhibits diffraction peaks due to Pt_3Sn alloy (2θ=39.0° and 45°) (ICSD

105796) and PtSn alloy (2θ=42° and 44°) (ICSD 105796). These peaks are assigned to Pt_3Sn(111) (2θ=38.96°), PtSn(102) (2θ=41.73°), PtSn(110) (2θ=44.08°) and Pt_3Sn(200) (2θ=45.28°), respectively. A small peak appeared around 2θ=39.6°. This peak is assignable to $Pt_{0.94}Sn_{0.06}$ alloy (ICSD 105798). Its crystal structure is face-centered cubic (fcc), similar to Pt metal and Pt_3Sn. The intensity of diffraction peak for Pt_3Sn phase was much stronger than PtSn alloy phase, indicating that the major part of Pt on Pt-Sn/SiO_2 reduced at 1073 K formed Pt_3Sn alloy with fcc arrangement. No diffraction peaks due to Sn compounds such as Sn metal and Sn oxides (SnO and SnO_2) were observed.

The XRD patterns of reacted Pt-Sn/SiO_2 catalysts with and without H_2 ((b) and (c)) were almost similar to that of Pt-Sn/SiO_2 reduced at 1073 K. In the case of Pt-Sn/SiO_2 (*R*), the intensity of diffraction peaks due to PtSn alloy slightly increased, while the intensity of diffraction peaks due to Pt_3Sn alloy was maintained. It indicates that the fraction of PtSn alloy slightly increased during the regeneration with H_2. After the second reaction run, the intensity of diffraction peaks due to Pt_3Sn alloy slightly increased, while those due to PtSn alloy did not change. In the case of Pt-Sn/SiO_2 (*OR*), the intensity of diffraction peaks due to Pt_3Sn was slightly stronger than those of reacted Pt-Sn/SiO_2. On the other hand, the intensity of diffraction peaks due to PtSn alloy was similar to that of reacted Pt-Sn/SiO_2. After the reaction in the second run, the intensity of diffraction peaks due to Pt_3Sn and PtSn alloys slightly increased.

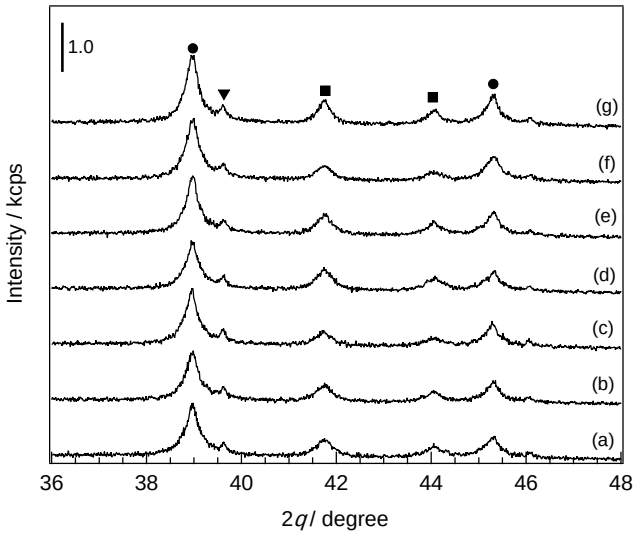

Figure 2 XRD patterns of Pt-Sn/SiO_2 catalyst. (a) reduced at 1073 K, (b) reacted without H_2, (c) reacted with H_2, (d) regenerated by Reduction method (Pt-Sn/SiO_2 (*R*)), (e) regenerated by Oxidation-Reduction method (Pt-Sn/SiO_2 (*OR*)), (f) reacted Pt-Sn/SiO_2 (*R*), and (g) reacted Pt-Sn/SiO_2 (*OR*). ●: Pt_3Sn; ▼: $Pt_{0.94}Sn_{0.06}$; ■: PtSn.

HADDF-STEM images of Pt-Sn/SiO_2

As for metal nanoparticles in heterogeneous catalysis, an increase in the size of metal nanoparticle is referred as sintering[32]. Sintering is often regarded to be important for the loss of catalyst activity because it results into the decrease of number of active site. Fig.3 shows HAADF-STEM images of Pt-Sn/SiO_2 catalysts before and after the dehydrogenation of propane together with the particle size distribution. The average size of Pt-Sn alloy nanoparticle on Pt-Sn/SiO_2 reduced at 1073 K was 1.7 ± 0.7 nm. After propane dehydrogenation, the average particle size of Pt-Sn alloys was 1.2 ± 0.5 nm on reacted catalyst with H_2, 1.2 ± 0.6 nm on reacted catalyst without H_2, indicating that an noticeable sintering of Pt-Sn alloy nanoparticle did not take place during 7 h of reaction regardless of the presence of H_2.

Fig.3 also shows HAADF-STEM images of Pt-Sn/SiO_2(*R*), Pt-Sn/SiO_2(*OR*),

reacted Pt-Sn/SiO_2(*R*) and reacted Pt-Sn/SiO_2(*OR*). Their average particle sizes were similar with each other, implying the slight difference of particle size during the regeneration and the second reaction run.

(a)

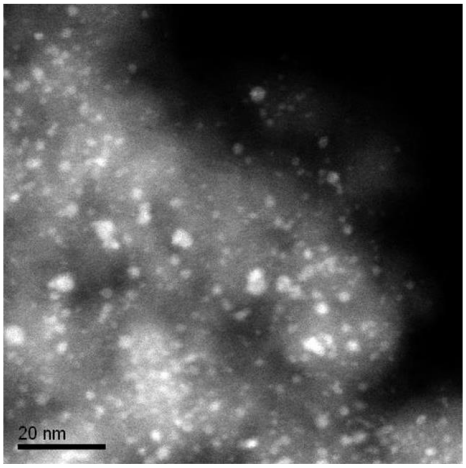

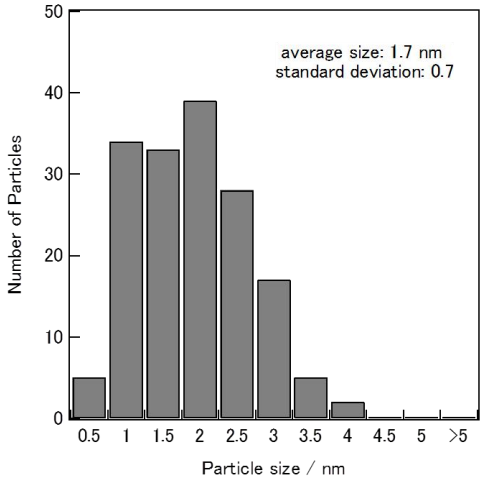

(b)

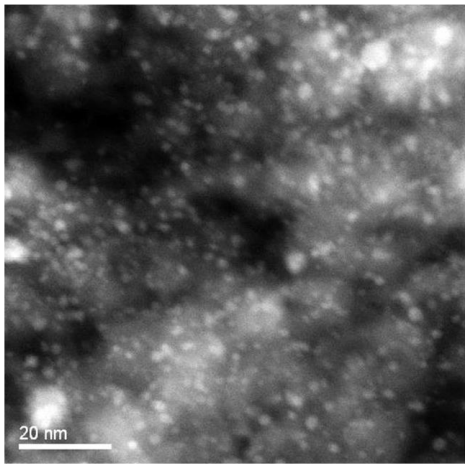

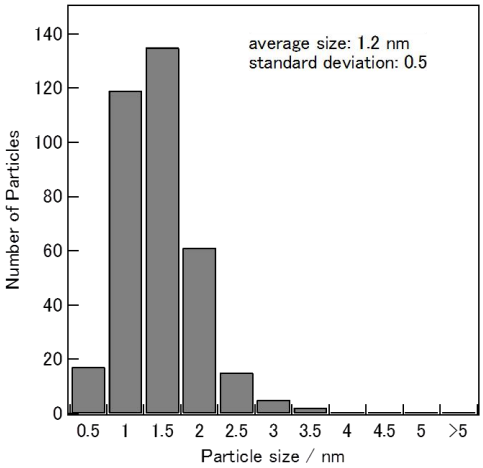

(c)

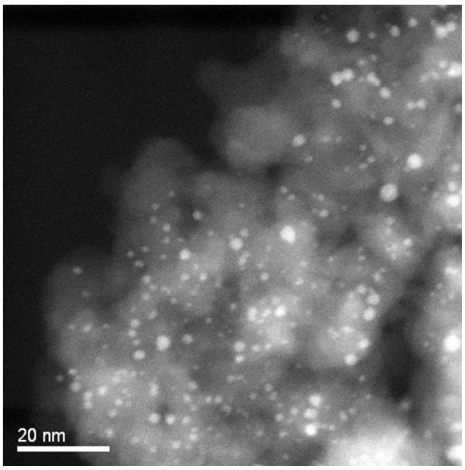

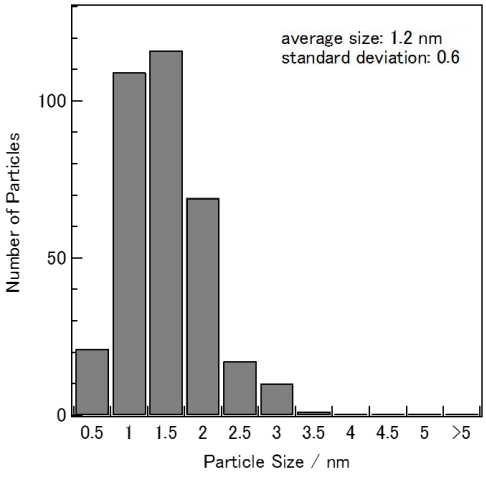

(d)

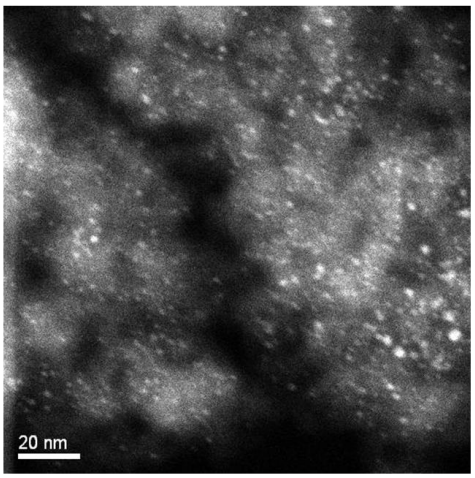
20 nm

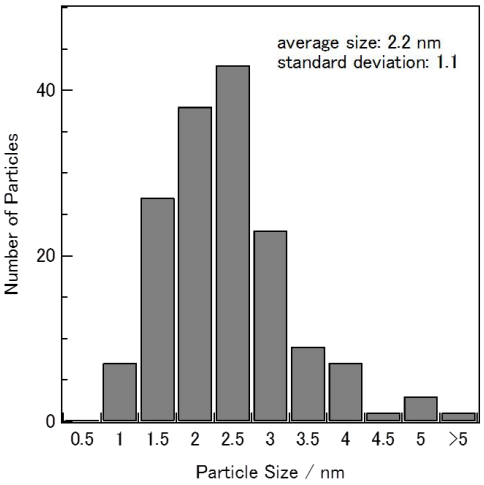
average size: 2.2 nm
standard deviation: 1.1
Number of Particles
0
20
40
0.5 1 1.5 2 2.5 3 3.5 4 4.5 5 >5
Particle Size / nm

(e)

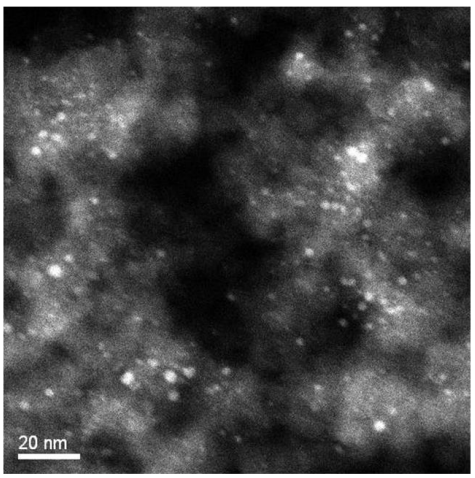
20 nm

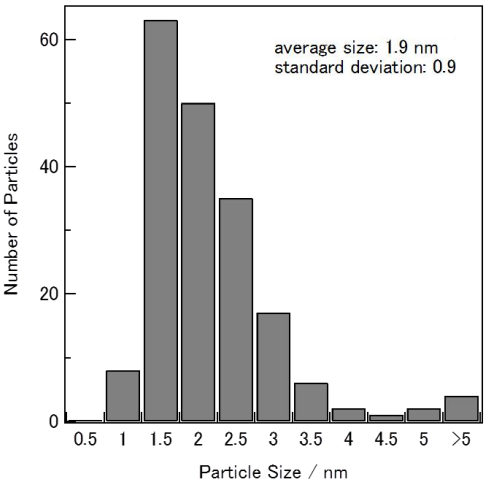
average size: 1.9 nm
standard deviation: 0.9
Number of Particles
0
20
40
60
0.5 1 1.5 2 2.5 3 3.5 4 4.5 5 >5
Particle Size / nm

(f)

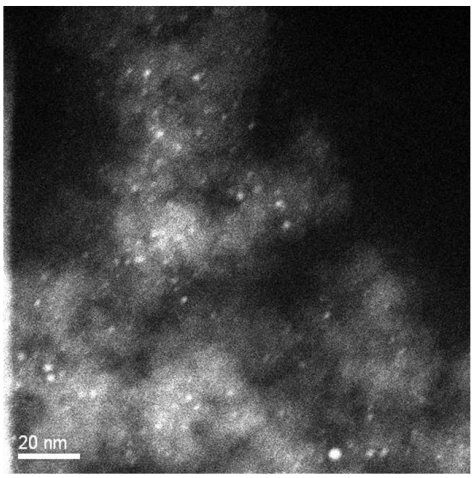
20 nm

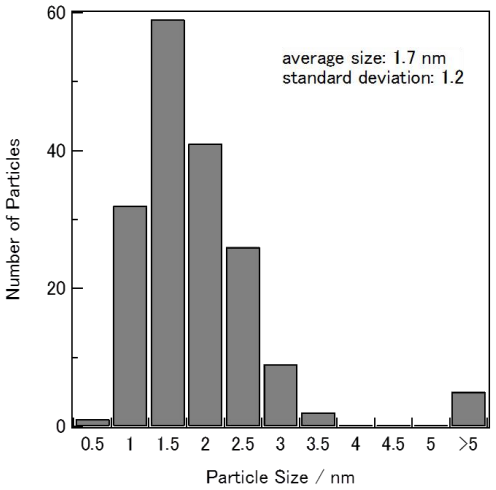
average size: 1.7 nm
standard deviation: 1.2
Number of Particles
0
20
40
60
0.5 1 1.5 2 2.5 3 3.5 4 4.5 5 >5
Particle Size / nm

Figure 3 HAADF-STEM images of (a) Pt-Sn/SiO_2 catalyst reduced at 1073 K (fresh), (b) reacted Pt-Sn/SiO_2 catalyst without H_2, (c) reacted Pt-Sn/SiO_2 catalyst with H_2 as well as their histograms (counting up about 200 bright dots from HAADF-STEM images).

XAFS analysis of Pt-Sn/SiO_2

Pt L_3-edge XAFS

Fig. 4 shows Pt L_3-edge XANES spectra of Pt-Sn/SiO_2 catalysts and Pt foil. The Pt L_3-edge X-ray absorption white lines correspond to the electronic transitions form $2p_{3/2}$ core level states and reflects the final vacant *d* states of both $5d_{3/2}$ and $5d_{5/2}$ levels of platinum. Lytle et al.[33] reported that the intensity of the Pt L_3 X-ray absorption spectra is concerned to the *d*-electron valences and the chemical environment of Pt atoms. The white line intensity at Pt L_3-edge of Pt-Sn/SiO_2 reduced at 1073 K in the present work was slightly less than that of Pt foil. It suggests an electron donation from Sn to Pt in accompanying with alloying between Pt and Sn. Uemura et al.[30] reported a lower white line intensity of Pt-Sn/Al_2O_3 than that of Pt foil. J H. Kim et al.[34] also reported that the intensity of white line was lower in Pt-Sn/C catalysts than that of Pt/C catalyst. They assigned this decrease in the white line intensity to the formation of a Pt-Sn alloy since the *d*-electron density of Pt atom is increased when alloyed with Sn atom that show lower electronegativity than Pt (Pt 2.2, Sn 1.8).

After propane dehydrogenation reactions, as shown in Fig.4 (B), the white line intensities at Pt L_3-edge of Pt-Sn/SiO_2 catalysts were quite similar to Pt-Sn/SiO_2 reduced at 1073 K. The white line intensity of Pt-Sn/SiO_2 (*R*) was almost similar to those of reacted Pt-Sn/SiO_2 and Pt-Sn/SiO_2 (*OR*).

In compare with reacted Pt-Sn/SiO_2 without H_2, as shown in Fig.4(C), the peak positions at Pt L_3-edge of regenerated Pt-Sn/SiO_2 (Pt-Sn/SiO_2 (*R*) and Pt-Sn/SiO_2 (*OR*)) shifted to higher energy region, implying that the fraction of Pt-Sn alloys changed by regeneration treatments.

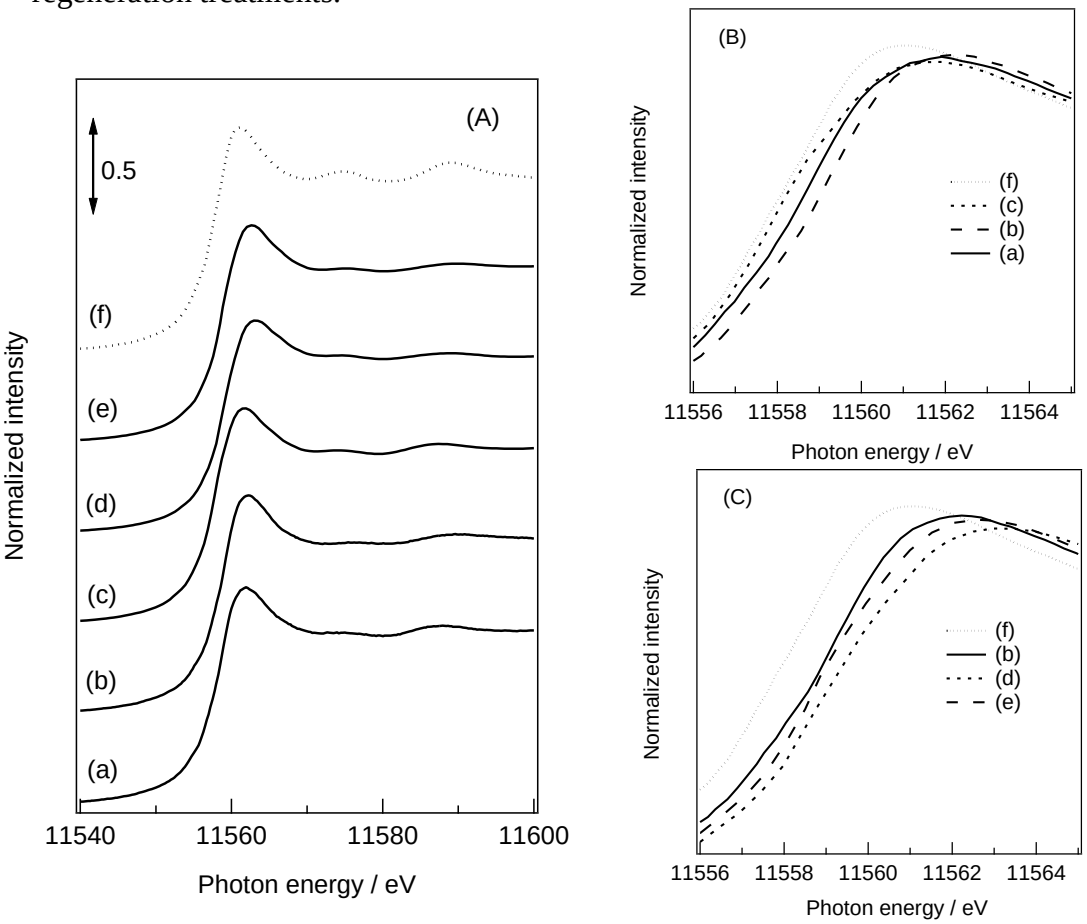

Figure 4 Pt L_3-edge XANES spectra of Pt-Sn/SiO_2 catalyst and Pt foil. (a) reduced at 1073 K, (b) reacted without H_2, (c) reacted with H_2, (d) regenerated by Reduction method (Pt-Sn/SiO_2 (*R*)), (e) regenerated by Oxidation-Reduction method method (Pt-Sn/SiO_2 (*OR*)), (f) Pt foil.

After propane dehydrogenation reactions, as shown in Fig.4 (B), the white line intensities at Pt L_3-edge of Pt-Sn/SiO_2 catalysts were quite similar to Pt-Sn/SiO_2 reduced at 1073 K. The white line intensity of Pt-Sn/SiO_2 (*R*) was almost similar to those of reacted Pt-Sn/SiO_2 and Pt-Sn/SiO_2 (*OR*).

In compare with reacted Pt-Sn/SiO_2 without H_2, as shown in Fig.4(C), the peak positions at Pt L_3-edge of regenerated Pt-Sn/SiO_2 (Pt-Sn/SiO_2 (*R*) and Pt-Sn/SiO_2 (*OR*)) shifted to higher energy region, implying that the fraction of Pt-Sn alloys changed by regeneration treatments.

Fig.5(A) shows k^3-weighted EXAFS oscillation at Pt L_3-edge of Pt-Sn/SiO_2 catalysts and Pt foil. The EXAFS oscillation of reacted Pt-Sn/SiO_2 reduced at 1073 K and reacted Pt-Sn/SiO_2 catalysts ((a), (b), and (c)) exhibited essentially similar features. Their EXAFS oscillations are significantly different from and much weaker than that of Pt foil. A weak and split feature around 0.21-0.28 nm in their Fourier transforms (FTs) (Figure 5(B)) suggests the interference of scattered electrons by Sn and Pt atoms in Pt-Sn alloys[14]. Indeed, the curve-fitting analysis for Pt-Sn/SiO_2 reduced at 1073 K showed the presence of two shells (Pt–Pt and Pt–Sn linkages). The bond distances of Pt–Pt and Pt–Sn were slightly shorter than the crystallographic values (Pt–Pt = 0.283 nm and Pt–Sn = 0.283 nm) in the Pt_3Sn crystal[13]. This is due to the formation of small particles of Pt_3Sn alloy. Both the coexistence of a small fraction of PtSn phase and the interference of Pt and Sn scattering resulted in relatively larger *R*-factors. The EXAFS oscillation and FTs of regenerated Pt-Sn/SiO_2 catalyst are slightly different from those of reduced and reacted Pt-Sn/SiO_2 catalysts. This indicates that the local structure of Pt in regenerated Pt-Sn/SiO_2 is slightly different from those in reduced and reacted Pt-Sn/SiO_2 catalysts. Combined with the XRD patterns, this is probably due to change in the fraction of Pt_3Sn and PtSn phases.

Sn K-edge XANES

Fig. 6 shows Sn K-edge XANES spectra of Pt-Sn/SiO_2 catalyst and reference samples (Sn foil and SnO_2). The intensity of absorption band of Pt-Sn/SiO_2 reduced at

1073 K was higher than that of Sn foil, but lower than that of SnO_2. Its absorption edge position was also higher than that of Sn foil, and lower than that of SnO_2. The intensity of

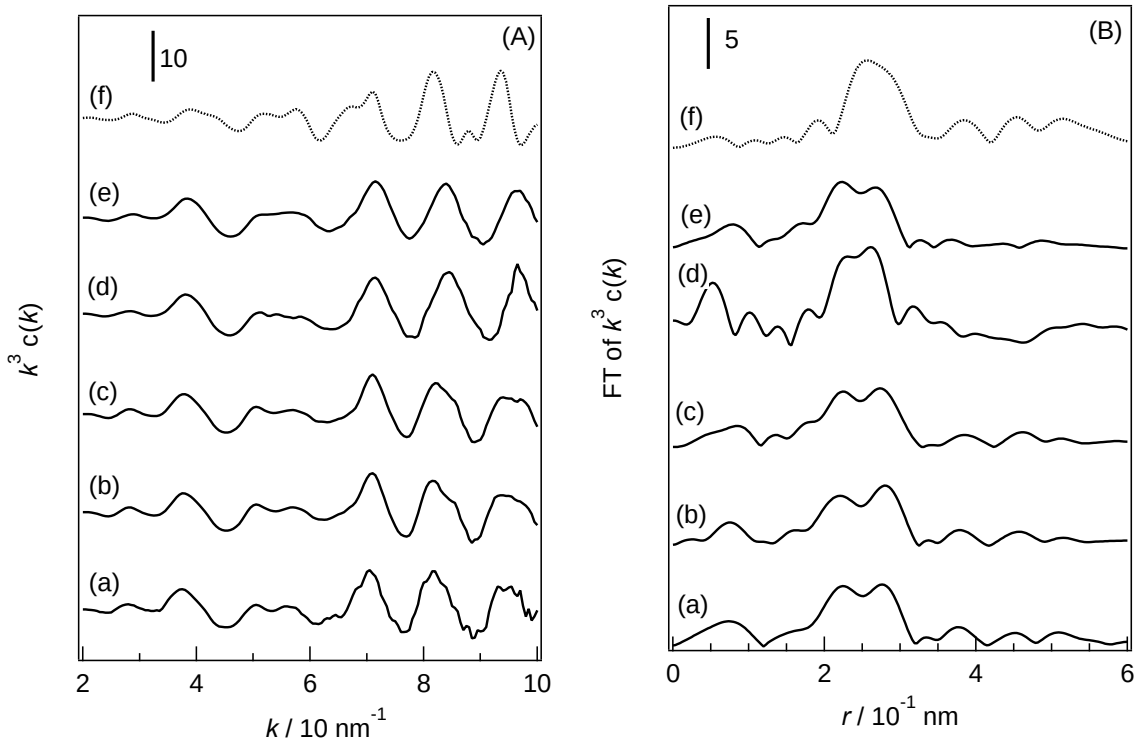

Figure 5 k^3-weighted EXAFS oscillation at Pt L_3-edge (A) and their Fourier transforms (B) of Pt-Sn/SiO_2 and Pt foil: (a) reduced at 1073 K, (b) reacted without H_2, (c) reacted with H_2, (d) regenerated by Reduction method (Pt-Sn/SiO_2 (*R*)), (e) regenerated by Oxidation-Reduction method (Pt-Sn/SiO_2 (*OR*)), (f) Pt foil (x 1/3).

absorption band of reacted Pt-Sn/SiO_2 ((b) and (c)) was almost equal to that of Pt-Sn/SiO_2 reduced at 1073 K. Moreover, the intensity of absorption band of regenerated Pt-Sn/SiO_2 was also similar to that of reacted Pt-Sn/SiO_2 regardless of regeneration method. These results suggest that a mixture of Sn (0) and Sn cations (Sn(II) and Sn(IV)) present on these Pt-Sn/SiO_2 catalysts, as previously reported.

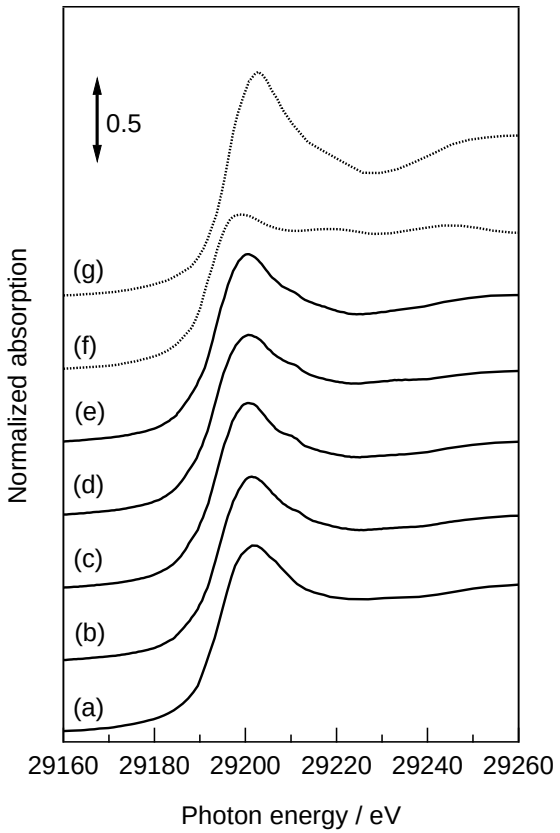

Figure 6 Sn K-edge XANES spectra of Pt-Sn/SiO_2 catalyst and SnO_2. (a) reduced at 1073 K, (b) reacted without H_2, (c) reacted with H_2, (d) regenerated by Reduction method (Pt-Sn/SiO_2 (*R*)), (e) regenerated by Oxidation-Reduction method (Pt-Sn/SiO_2 (*OR*)), (f) Sn foil, (g) SnO_2.

XPS analysis of Pt-Sn/SiO_2

Fig. 7 shows the XP spectra of Pt 4f (A) and Sn 3d (B) regions for Pt-Sn/SiO_2 catalyst after the reaction and regeneration process. In the case of Pt-Sn/SiO_2 catalyst reduced at 1073 K (spectrum (a)), the binding energies of Pt $4f_{7/2}$ and $4f_{5/2}$ peaks were 71.3 and 74.6 eV, which were assignable to Pt^0. After 7 h of the reaction without H_2, the position of the Pt $4f_{7/2}$, $4f_{5/2}$ peak of the catalyst (spectrum (c)) were almost similar to those of Pt-Sn/SiO_2 reduced at 1073 K. However, in the cases of reacted Pt-Sn/SiO_2 catalysts with H_2 (spectrum (b)), its position intensity of the Pt $4f_{7/2}$, $4f_{5/2}$ peak slightly shifted to the higher binding energy. After regenerating the reacted Pt-Sn/SiO_2 catalysts

without H_2, the Pt $4f_{7/2}$, $4f_{5/2}$ peaks (spectrum (d) and (e) again became similar with those of Pt-Sn/SiO_2 catalyst reduced at 1073 K. Moreover, there is no obvious peak shifts over regenerated catalysts in the second reaction run (spectrum (f) and (g)).

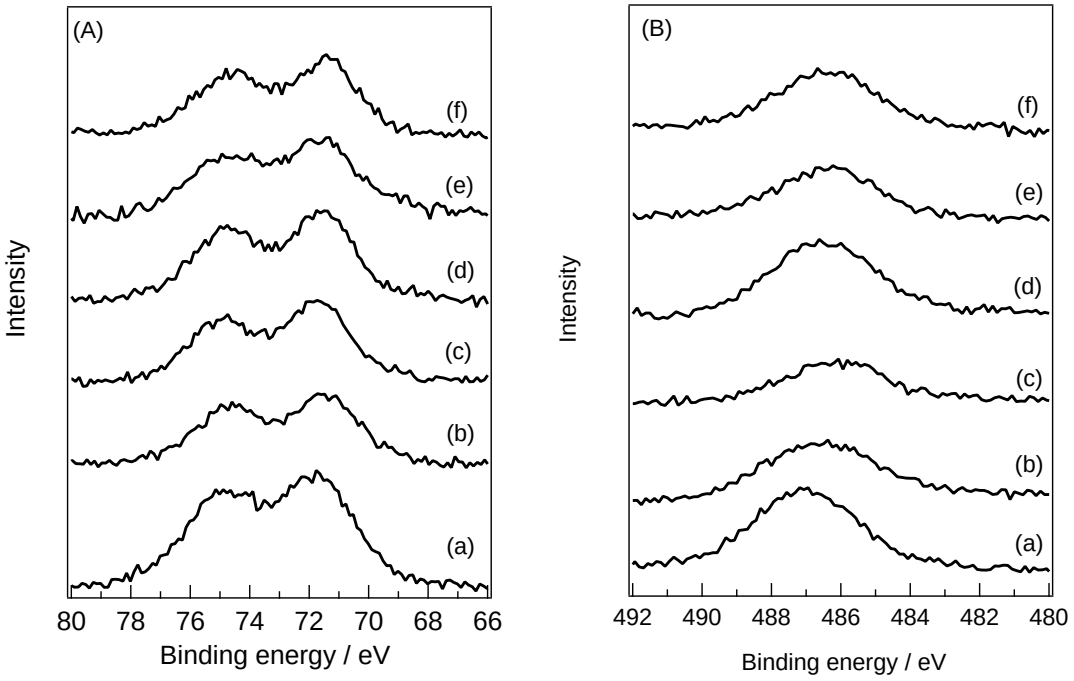

Figure 7 Pt and Sn XPS profiles for reacted and regerated Pt-Sn/SiO_2 catalyst. (A) Pt 4f level and (B) Sn 3d level. (a) reacted without H_2, (b) reacted with H_2, (c) regenerated by Reduction method (Pt-Sn/SiO_2 (*R*)), (d) regenerated by Oxidation-Reduction method (Pt-Sn/SiO_2 (*OR*)), (e) reacted Pt-Sn/SiO_2 (*R*), and (f) reacted Pt-Sn/SiO_2 (*OR*).

As shown in Fig. 7 (B), the binding energy of the Sn $3d_{5/2}$ peak over Pt-Sn/SiO_2 catalyst reduced at 1073 K was located at 486.2 eV. This was higher than the values usually reported for metallic Sn (484.9 eV) and lower than values typically reported for Sn oxides (487.1 eV), suggesting that the coexistence of metallic Sn and Sn oxides on the Pt-Sn/SiO_2 catalyst reduced at 1073 K. Deconvolution of the Sn 3d XPS spectra of Pt-Sn/SiO_2 catalyst reduced at 1073 K (Fig. 8 (A)) revealed that the surface ratios of Sn^0/Sn^{IV} on the catalyst was 33:67. The binding energy of Sn $3d_{5/2}$ peaks on reacted

Pt-Sn/SiO_2 with H_2 (spectrum (b)) at 486.9 eV, reacted Pt-Sn/SiO_2 without H_2 (spectrum (c)) was located at 486.5 eV, higher than that of Pt-Sn/SiO_2 catalyst reduced at 1073 K. A small fraction of metallic Sn was detected on the reacted Pt-Sn/SiO_2 catalysts based on their Sn deconvolution results shown in Figure 8 (B) and (C). This result shows that the surface ratio of Sn^0/Sn^{IV} was remarkably decreased after the dehydrogenation of propane. The subsequent regeneration led the Sn $3d_{5/2}$ peak slightly shift towards lower binding energy on Pt-Sn/SiO_2 (*R*) catalyst and Pt-Sn/SiO_2 (*OR*) catalyst. The obvious peak shift was not observed after the second reaction due to the weak peak intensity.

The intensities of both Pt and Sn XP spectra were highest over Pt-Sn/SiO_2 reduced at 1073 K, and decreased on the reacted catalysts, especially for reacted Pt-Sn/SiO_2 without H_2. This attenuation of Pt and Sn signals may be resulted from the coke deposited on Pt-Sn alloy particles. TG-DAT results suggest that the amount of coke formed on the reacted Pt-Sn/SiO_2 in the presence of H_2 was smaller than that in the absence of H_2. Agreeably, the intensities of Pt and Sn XP spectra signals of the former catalyst were slightly stronger than those of the latter one. Through the regeneration processes, coke was removed from the reacted catalysts. Few cokes remained on Pt-Sn/SiO_2 (*R*), no coke on Pt-Sn/SiO_2 (*DR*) indicated from TG-DTA measurements. However both Pt and Sn XPS signals did not remarkably increase with the elimination of coke. Only the Sn $3d_{5/2}$ peak was observed towards lower degree. It was suggested that the Pt-Sn alloys on the regenerated catalysts were different from the initial ones in the first reaction run. The compositions or morphologies of the Pt-Sn alloys on Pt-Sn/SiO_2 catalyst reduced at 1073 K probably changed with the reaction and also regenerations, thus the regenerated catalysts presented the different surface Pt and Sn XPS signals. After the second reaction run, the reacted Pt-Sn/SiO_2 (*R*) and reacted

Pt-Sn/SiO_2 (*DR*) presented the similar Pt and Sn XPS signals with those of Pt-Sn/SiO_2 (*R*) and Pt-Sn/SiO_2 (*DR*).

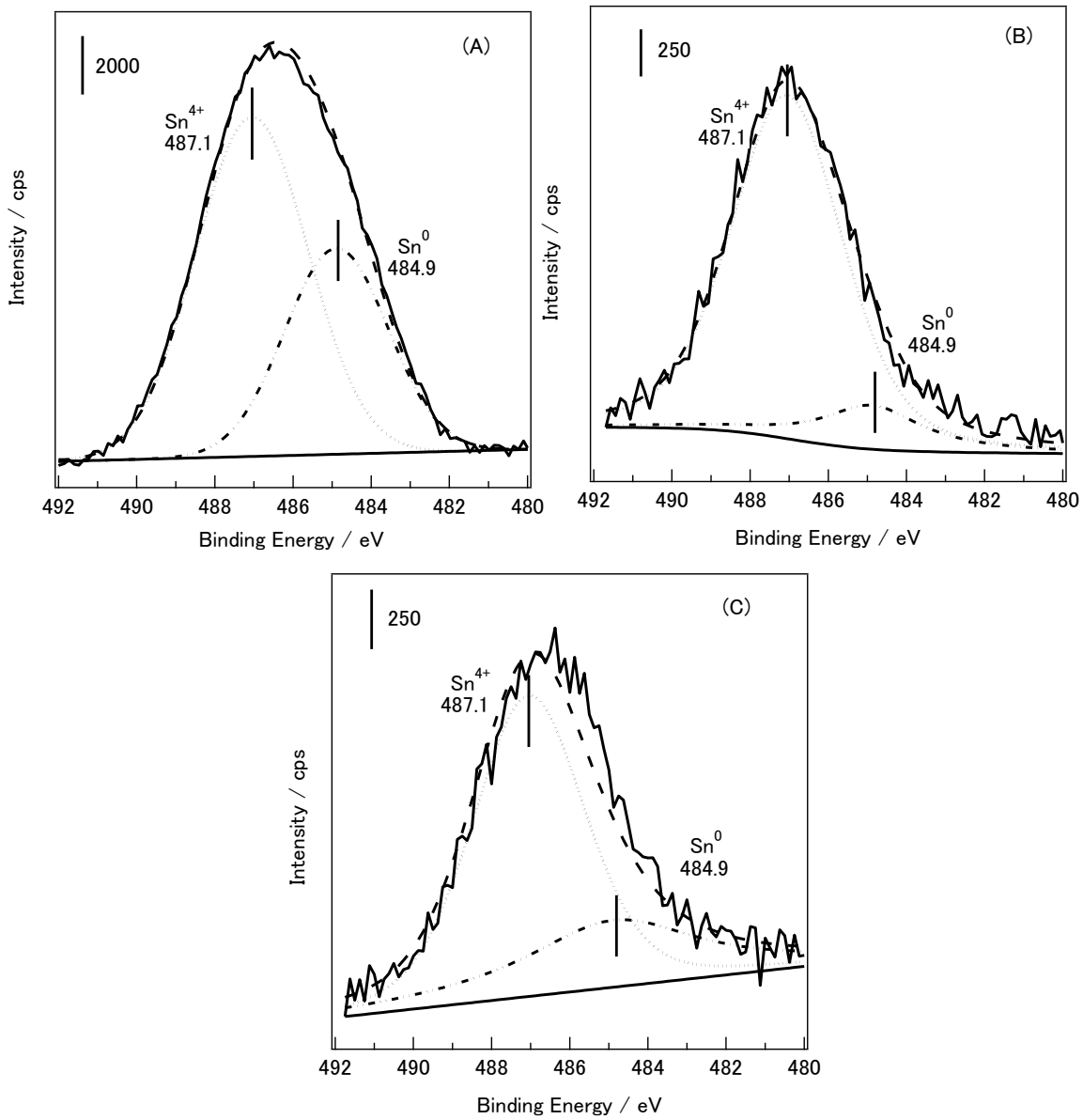

Figure 8 Deconvolution of Sn $3d_{5/2}$ XPS profiles of (A) Pt-Sn/SiO_2 reduced at 1073 K, (B) reacted with H_2 and (C) reacted without H_2.

Discussion

We recently reported that[14] the Pt-Sn/SiO_2 catalyst reduced at 1073 K possessed a Pt-Sn alloy (1–3 nm) core structure with a Sn-rich surface and that a highly

dispersed SnO_2 coexisted with Pt-Sn alloy particles. Based on this model, the characterization results mentioned above together with the discoveries from the other researchers[16, 30, 31], the structure properties of Pt-Sn/SiO_2 catalyst reduced at 1073 K before and after propane dehydrogenation as well as regeneration processes are represented by Scheme 1.

In the first reaction run, much more coke formed in the absence of H_2 in the feeding gas (Table 1) and led to the higher deactivation rate of Pt-Sn/SiO_2 catalyst reduced at 1073 K (Fig. 1). The addition of small amount of H_2 into the feeding gas inhibited coke formation and improved the catalyst stability during 7 h of the reaction. XPS analysis (Fig. 7 and 8) further suggested that the formation of coke on the reacted catalysts' surfaces weakened the XPS signals of both Pt and Sn elements on them, and these coke probably preferably located on the active sites involving Sn(0) based on the shift of Sn $3d_{5/2}$ peak over the reacted catalysts. In the regeneration stages, both "Reduction" and "Oxidation-Reduction" methods eliminated coke formed on reacted Pt-Sn/SiO_2 catalyst without H_2, even though the efficiency of hydrogen in "Reduction" method was lower than that of oxygen in "Oxidation-Reduction" method. Few cokes formed on the reacted Pt-Sn/SiO_2 (*R*) and reacted Pt-Sn/SiO_2 (*DR*).

Beside coke formation, the states of Pt and Sn on Pt-Sn/SiO_2 catalyst also changed with the reaction and regenerations. XRD and XAFS analysis of the reacted catalysts suggested the different fraction of bulk Pt-Sn alloy phases from that of Pt-Sn/SiO_2 catalyst reduced at 1073 K. XPS results show that the electronic states of surface Pt and Sn atoms on the reacted catalyst without H_2, the reacted catalyst with H_2 and Pt-Sn/SiO_2 catalyst reduced at 1073 K (fresh one) were different with each other. More surface Sn oxides were detected on the surface of the reacted catalysts. The states

of surface Pt and Sn atoms also differed with the small amount of H_2 in the feeding gas or not. Virnovskaia, Anastasia[35] once found that the surface state of Pt and Sn in the pure $PtSn_2$ alloy differed with atmosphere (reductive or reaction mixed gas) and temperature with *in situ* XPS investigation. It was shown that when $PtSn_2$ going form reduction to reaction conditions, the amount of reduced Sn decreased to below 10 %. In the dehydrogenation of propane, the reaction conditions are reductive regardless of H_2 feeding due to the production of H_2 in this reaction. Even the bulk Pt-Sn alloys were detected on the fresh and reacted catalyst with H_2 and reacted catalyst without H_2, the surface states of those Pt-Sn alloys differed with the reaction and H_2 in feeding gas reflected from XPS results. There are probably the slight differences on the fraction of Pt-Sn alloy, their morphologies or the detailed surface atomic arrangements on them. Therefore, $(Pt\text{-}Sn)^{0\text{-}4}$ in Scheme 1 were used to denote these different Pt-Sn alloys. As for the regenerated catalysts, the intensities of Pt and Sn XP spectra on Pt-Sn/SiO_2 (*R*) and reacted Pt-Sn/SiO_2 (*DR*) did not recover to the level like the Pt-Sn/SiO_2 catalyst reduced at 1073 K even the coke on were partially or completely eliminated from the surface of the reacted catalysts. Sn XP spectra shifted towards lower binding energy after the regeneration processes. Uemura. Y.[30, 31] also found the phase segregation of Pt-Sn alloys into Pt metal and SnO_2 under the oxidized atmosphere as well as the re-alloying under the H_2 treatment to form Pt-Sn alloys. Combined with the characterization results in the present study, it was implied that there are some differences between the initial Pt-Sn alloys and the ones obtained from regenerations.

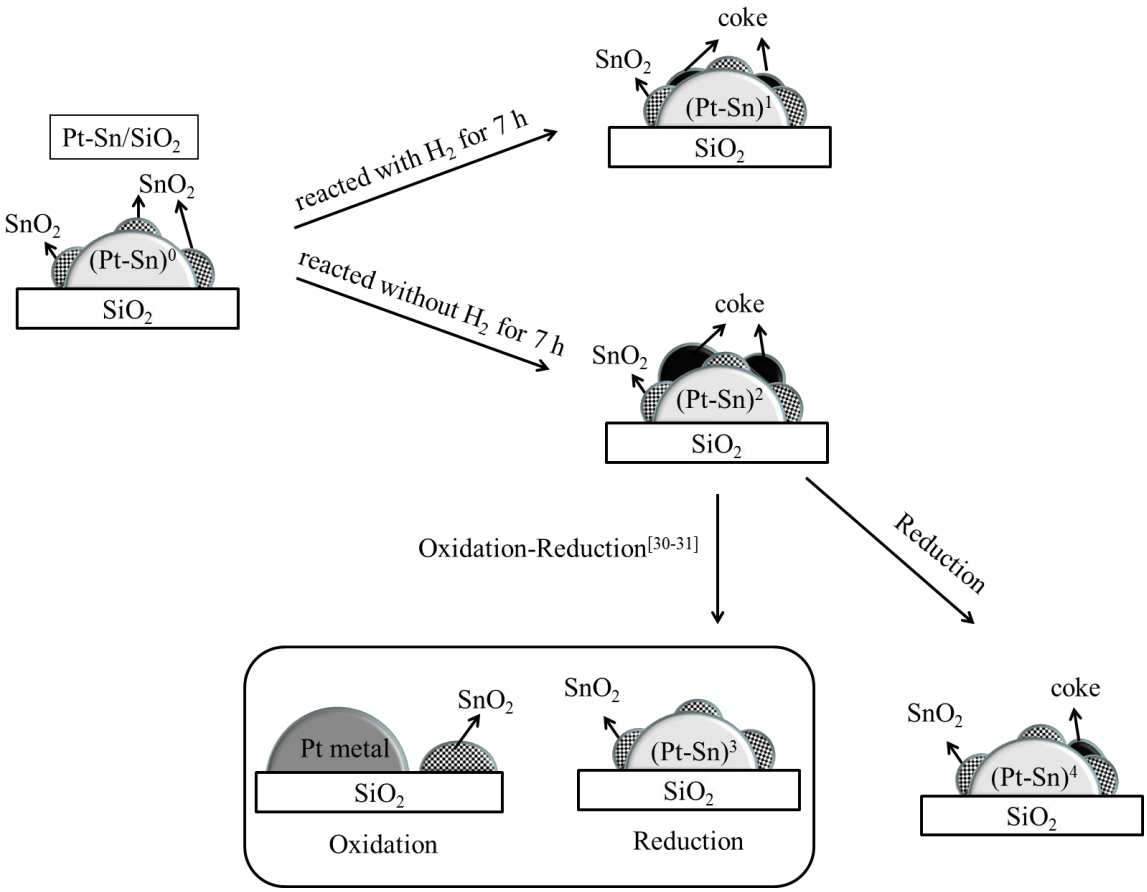

Scheme 1 The models of Pt-Sn/SiO_2 catalyst during the dehydrogenation of propane and regeneration process: $(Pt\text{-}Sn)^{0\text{-}4}$ mean the Pt-Sn alloy particles with the different morphologies and compositions of Pt-Sn alloys(Pt_3Sn and PtSn phases).

Conclusion

The catalytic behaviors and structures of Pt-Sn/SiO_2 catalyst reduced at 1073 K in the dehydrogenation of propane and subsequent regenerations has been investigated by the catalytic tests together with the characterization techniques, including TG-DTA, HAADF-STEM, XRD, XANES-EXAFS and XPS. The main findings can be summarized as follows:

(1) About 2.8 wt% coke deposited on the reacted catalyst throughout 7 h of reaction without H_2. A small amount of H_2 in the feeding gas effectively decreased the coke amount, and improved the catalyst stability. Only 0.7wt% coke formed on the

reacted catalyst in the presence of H_2. The subsequent regeneration, Reduction or Oxidation-Reduction resulted into the partially or completely elimination of the coke deposited on the reacted catalyst without H_2. The trace amount of coke formed during the second reaction run.

(2) Pt dispersion shown form the HAADF-STEM image is stable before and after propane dehydrogenation for 7 h. The particle sizes retained in the range of ca. 1.2 to 1.7 nm, strongly suggesting that particle sintering is not responsible for the observed deactivation in the first reaction run.

(3) It was probably that the composition of surface Pt-Sn alloys or their morphologies redistributed with the reactions and regenerations. H_2 in the feeding reaction gas also affected the surface states of active species on Pt-Sn/SiO_2 catalyst during the reaction. In the regeneration processes, Reduction method partially regenerated the active Pt-Sn alloy phases. With respect to Oxidation-Reduction regeneration, Sn segregated form Pt-Sn alloy during the calcination step, and then alloyed with Pt again under the reduction conditions. This phenomenon leads to the higher recovery of catalytic activity over the deactivated catalyst.

References

[1] R. Cortright and J. Dumesic, Journal of catalysis, 148 (1994) 771.

[2] O. Barias, A. Holmen and E. Blekkan, Journal of catalysis 158 (1996) 1.

[3] J. Llorca, N. Homs, J. Fierro, J. Sales and P. Piscina, Journal of catalysis, 166 (1997) 44.

[4] S. Wang and Z. Zhu, Energy & Fuels, 18 (2004) 1126.

[5] F. Cavani, N. Ballarini and A. Cericola, Catalysis Today, 127 (2007) 113.

[6] H.M.T. Galvis and K.P. De Jong, ACS CATALYSIS, 3 (2013) 2130.

[7] F. Cavani and F. Trifiro, Applied Catalysis A: General, 133 (1995) 219.

[8] R. Buyanov and N. Pakhomov, Kinetics and Catalysis, 42 (2001) 64.

[9] N. Rahimi and R. Karimzadeh, Applied Catalysis A: General, 398 (2011) 1.

[10] Y. Yoshimura, N. Kijima, T. Hayakawa, K. Murata, K. Suzuki, F. Mizukami, K. Matano, T. Konishi, T. Oikawa, M. Saito, T. Shiojima, K. Shiozawa, K. Wakui, G. Sawada, K. Sato, S. Matsuo and N. Yamaoka, Catalysis Surveys from Japan, 4 (2000) 157.

[11] N. Miura, I. Takahara, M. Saito, T. Hattori, K. Ohkuma and M. Ando, Catalysis Today, 45 (1998) 61.

[12] Y. Zhang, Y. Zhou, J. Shi, S. Zhou and X. Sheng, Journal of Molecular Catalysis A: Chemical, 381 (2014) 138.

[13] L. Deng, T. Shishido, K. Teramura and T. Tanaka, Catalysis Today, 232 (2014) 33.

[14] L. Deng, H. Miura, T. Shishido, S. Hosokawa, K. Teramura and T. Tanaka, ChemCatChem, in press (2014).

[15] B.K. Vu, M.B. Song, I.Y. Ahn, Y.-W. Suh, D.J. Suh, W.-l. Kim, H.-L. Koh, Y.G. Choi and E.W. Shin, Applied Catalysis A: General, 400 (2011) 25.

[16] A. Iglesias-Juez, A.M. Beale, K. Maaijen, T.C. Weng, P. Glatzel and B.M. Weckhuysen, Journal of catalysis, 276 (2010) 268.

[17] I. Contreras-Andrade, A. Vazquez-Zavala and T. Viveros, Energy & Fuels, 23 (2009) 3835.

[18] D. Akporiaye, S. Jensen, U. Olsbye, F. Rohr, E. Rytter, M. Ronnekleiv and A. Spjelkavik, Ind. Eng. Chem. Res. , 40 (2001) 4741.

[19] E. Merlen, P. Beccat, J. Bertolini, P. Delichere, N. Zanier and B. Didillon,

Journal of catalysis, 159 (1996) 178.

[20] R. BURCH, Journal of catalysis, 71 (1981) 348.

[21] V. Ponec, Applied Catalysis A: General, 222 (2001) 31.

[22] W. Yu, M.D. Porosoff and J.G. Chen, Chemical Reviews, 112 (2012) 5780.

[23] A.K. Singh and Q. Xu, ChemCatChem, 5 (2013) 652.

[24] S. Zafeiratos, S. Piccinin and D. Teschner, Catalysis Science & Technology, 2 (2012) 1787.

[25] V. Dal Santo, A. Gallo, A. Naldoni, M. Guidotti and R. Psaro, Catalysis Today, 197 (2012) 190.

[26] X. Wang, J. Stoever, V. Zielasek, L. Altmann, K. Thiel, K. Al-Shamery, M. Baumer, H. Borchert, J. Parisi and J. Kolny-Olesiak, Langmuir, 27 (2011) 11052.

[27] J. Ruiz-Martinez, A. Sepulveda-Escribano, J.A. Anderson and F. Rodriguez-Reinoso, Catalysis Today, 123 (2007) 235.

[28] F. Tao, M.E. Grass, Y. Zhang, D.R. Butcher, F. Aksoy, S. Aloni, V. Altoe, S. Alayoglu, J.R. Renzas, C.-K. Tsung, Z. Zhu, Z. Liu, M. Salmeron and G.A. Somorjai, Journal of the american chemical society 132 (2010) 8697.

[29] F. Tao, M.E. Grass, Y. Zhang, D.R. Butcher, J.R. Renzas, Z. Liu, J.Y. Chung, B.S. Mun, M. Salmeron and G.A. Somorjai, Science, 322 (2008) 932.

[30] Y. Uemura, Y. Inada, K.K. Bando, T. Sasaki, N. Kamiuchi, K. Eguchi, A. Yagishita, M. Nomura, M. Tada and Y. Iwasawa, The journal of physical chemistry, 115 (2011) 5823.

[31] Y. Uemura, Y. Inada, K.K. Bando, T. Sasaki, N. Kamiuchi, K. Eguchi, A. Yagishita, M. Nomura, M. Tada and Y. Iwasawa, Phys. Chem. Chem. Phys., 13 (2011) 15833.

[32] T.W. Hansen, A.T. Delariva, S.R. Challa and A.K. Datye, Accounts of chemical research, 46 (2013) 1720.

[33] F. Lytle, Journal of catalysis, 43 (1976) 376.

[34] J.H. Kim, S.M. Choi, S.H. Nam, M.H. Seo, S.H. Choi and W.B. Kim, Applied Catalysis B: Environmental, 82 (2008) 89.

[35] A. Virnovskaia, S. Jorgensen, J. Hafizovic, O. Prytz, E. Kleimenov, M. Havecker, H. Bluhm, A. Knop-Gericke, R. Schlogl and U. Olsbye, Surface Science 601 (2007) 30.

Chapter 5

Dehydrogenation of ethylbenzene over Pt-Sn/SBA-15 and Pt-Sn/SiO_2 catalysts: stability improvement of Pt-Sn alloy catalyst by using SBA-15 as support

Abstract

Amorphous silica and mesoporous silica (SBA-15) supported Pt-Sn alloy catalysts with different Sn/Pt atomic ratios (0.33 and 1.0) were prepared by direct reduction method and applied for the ethylbenzene dehydrogenation to styrene. Pt-Sn/SBA-15 showed higher activity, selectivity to styrene, and stability than Pt-Sn/SiO_2 regardless of Sn/Pt ratio. Structural characterization by X-ray diffraction (XRD), Transmission electron microscope (TEM), and CO adsorption, revealed that highly dispersed and stable Pt-Sn alloy particles (Pt_3Sn, Pt_xSn_y (x/y>3), and PtSn) were formed on SBA-15, resulting in a high activity and stability in the ethylbenzene dehydrogenation. TPO (Temperature-Programmed Oxidation) results clearly indicated that the coke formation was strongly inhibited by addition of Sn, and Sn can drain coke formed on Pt-Sn species into support (drain-off effect).

Introduction

Styrene, an important basic chemical as a raw material for polymers, has been commercially produced by the dehydrogenation of ethylbenzene using a typical Fe-K-Cr oxide-based catalyst in the presence of excess of steam at high temperatures of 873-973 K, just below the temperature where the thermal cracking becomes significant[1-3]. Promotion of iron oxide (hematite; Fe_2O_3) with potassium enhances the reactivity of iron oxide by an order of magnitude and reduces the formation of carbonaceous surface deposits or coke that deactivates the catalysts. Small amounts of other metal oxides like Cr_2O_3 are added as structural promoters to stabilize the catalyst morphology and prevent sintering.

Although the typical Fe-K-Cr catalysts are quite active and selective, these catalysts has some disadvantages such as instability of active Fe^{3+} sites[4], loss and redistribution of potassium promoter[4], and a rapid deactivation due to the coke deposition[5]. Moreover, a large excess of steam necessary to suppress coke formation leads to a huge amount of energy consumption [6]. Therefore, the development of new catalysts possessing high activity, selectivity and stability under environment-friendly conditions is desired.

Moran et al. [7] reported that supported Pt on a synthetic clay was active in the dehydrogenation of ethylbenzene, with a styrene conversion ca. 50 % and high styrene selectivity at low reaction temperatures such as 673 K in the absence of steam. In fact, platinum or modified platinum catalysts have been widely studied in the recent developments about the catalytic dehydrogenations [8-25]. Platinum-Tin alloy catalyst (Pt-Sn), in the form of supported nanoparticles, is one of the most suitable catalysts for the dehydrogenation of ethane[9], propane[15, 20, 21, 23, 24], isobutene and

n-butane[12-14, 17]. Recently, we reported[26, 27] that Pt-Sn/SiO_2 catalysts, on which Pt was dominantly present as Pt_3Sn alloy nanoparticles, exhibited a good catalytic performance for C-H bond activation in the dehydrogenation of propane, and that both Sn/Pt ratio and reduction temperature affected the catalytic performance.

Mesoporous silicate such as M41S, FSM-16, and SBA-15 possesses uniform and well-ordered channels with controllable pore size from 2 to 10 nm, high surface area (ca. 1000 m^2 g^{-1}), small crystallite size of primary particles and complementary textural porosity. Because of these unique characteristics, mesoporous silicate has received much attention in areas of catalysis, chromatography and adsorption [24, 28-35]. SBA-15 has been widely used as a catalyst support [22, 24, 28, 29, 35-37]. Kumar et al. [24] reported the highly dispersed Pt nanoparticles on SBA-15 support showed higher activity in the dehydrogenation of propane. Chen et al.[36] found that highly dispersed Pt nanoparticles confined in the mesochannels of SBA-15 showed higher stability then the conventional supported Pt/SiO_2 catalysts in the catalytic dehydrogenation of methylcyclohexane. The confinement of Pt nanoparticles in the ordered mesochannels of SBA-15 restricted its further growth during the reaction.

In the present study, a series of supported Pt and Pt-Sn bimetallic nanoparticles on SBA-15 were prepared by the direct reduction method [26, 27], and applied for ethylbenzne dehydrogenation to styrene. Transmission electron microscopy (TEM), X-ray diffraction (XRD), CO adsorption, X-ray photoelectron spectroscopy (XPS), and temperature-programmed oxidation (TPO) were used to characterize the bulk and surface states of the Pt-Sn bimetallic catalysts. Comparing with the amorphous silica supported Pt-Sn alloy catalysts, the catalytic behaviors of SBA-15 supported Pt-Sn alloy catalysts were clarified.

Experimental

Catalyst Preparation

SBA-15 was synthesized according to the method reported previously[30]. P123 (10 g) was dissolved in 240 ml of H_2O. The solution was mixed with 22 g of tetraethoxysilane (TEOS). And then 40 ml 36 % HCl was dropped during 30 min. The solution was heated to 308 K and maintained under vigorous stirring for 20 h. Then, the mixture was aged under static conditions at 368 K for 24 h. The white precipitate was recovered by filtration, washed with water to remove impurities until pH = 7, and dried at 353 K for 24 h. SBA-15 was obtained after the calcination in air at 823 K for 6 h.

The SBA-15 and amorphous silica (JRC-SIO-9, 334 m^2 g^{-1}, after calcination at 773 K for 3 h in air) were used as supports to prepare Pt-Sn catalysts. Pt-Sn/SiO_2 or Pt-Sn/SBA-15 precursor was prepared by sequential impregnation method. The support was firstly impregnated with an aqueous solution of $H_2PtCl_6 \cdot 6H_2O$, stirred at 353K for 3h, and dried at 353 K for 20h. The obtained precipitate was added to an acetone solution of $SnCl_2 \cdot 2H_2O$ (Wako, 97%), stirred at 353 K for 3h and dried at 353 K for 20h to yield Pt-Sn/SiO_2 or Pt-Sn/SBA-15 precursor. The Pt content was 3wt. %. The molar ration of Sn to Pt was 1/3 or 1. The obtained catalysts were denoted xPtySn/SiO_2 (or xPtySn/SBA-15), where x and y indicate the molar ratio of Pt to Sn.

The dehydrogenation of ethyl benzene

Dehydrogenation of ethylbenzene was carried out using a fixed-bed flow reactor at atmospheric pressure. A quartz glass tube with an inner diameter of 8 mm was used as a reactor. In the dehydrogenation reactions, typically 0.05 g of catalyst precursor, which has been pelletized to the particles with 25 - 50 mesh, was loaded into the reactor.

Prior to the reaction, the catalyst precursor was *in situ* reduced with 20 vol% H_2 diluted with N_2 (total flow rate 50 ml min^{-1}) at 1073 K for 1 h. Finally, the catalyst was cooled to 773 K in N_2 (100 ml min^{-1}). The reaction was started by introducing a gas mixture of ethylbenzene and N_2 to the reactor. Ethylbenzene (0.059 ml min^{-1}; 0.48 mmol min^{-1}) was fed by pumping (PU-980 intelligent HPLC pump) to vaporizer (433 K) and mixing with the carry gas N_2 in vaporizer. All the lines and valves between the cold trap and the reactor were heated to 393 K to prevent any condensation of ethylbenzene or the dehydrogenation products. The liquid products (styrene, toluene, and benzene) were analyzed with an on-line FID gas chromatograph (Shimadzu GC-14B) equipped with CBP-10 column (025 μm, 30 m). The gaseous products (CO_2, CO, H_2 and CH_4) were analyzed by an on-line TCD gas chromatograph (Shimadzu GC-8A) equipped with a Molecular Sives-5A Column.

Characterization

The Brunauer—Emmett—Teller (BET) specific surface area was estimated from N_2 isotherm obtained using a BELSORP-miniII (BEL Japan, Osaka, Japan) at 77 K. The analyzed samples were evacuated at 573 K for 3 h prior to the measurement.

The amount of CO adsorbed on the catalysts at room temperature was determined by the CO pulse method with an Okura BP-2 instrument (Okura Riken, Japan) interfaced with a TCD. Prior to CO adsorption, the catalyst precursor was *in situ* reduced in 20 vol% H_2 diluted with N_2 (total flow rate 50 mL min^{-1}) at 1073 K for 1 h. 1:1 stoichiometry ratio of Pt:CO was used to estimate the number of accessible Pt atoms on the catalysts' surface.

X-ray diffraction (XRD) patterns were obtained using a RINT-TTR III powder X-ray diffractometer (Rigaku, Tokyo, Japan) with Cu Kα radiation (λ = 1.5405 Å). The

samples were scanned from 2θ=38° to 46° at the scanning scanning resolution of 0.01°.

High angle annular dark field-scanning transmission electron microscope (HADDF-STEM) images were obtained using a JEOL JEM-3200FS transmission electron microscope. The samples were prepared by depositing drops of ethanol suspensions containing small amounts of the powders onto carbon-coated copper grids (Okenshoji Co. Ltd.) followed by evaporation of the ethanol in air.

The temperature programmed oxidation (TPO) analysis of the coke deposited on the catalysts in the dehydrogenation of ethylbenzene was conducted by combustion with air in a Okura BP-2 instrument (Okura Riken, Japan), coupled to a BELMass (BEL Japan, Osaka, Japan) for monitoring the signal corresponding to CO_2. The flow rate of air = 50 ml/min, heating rate=10 K/min.

Results

Catalysts characterization

The conversions of ethylbenzene over both SBA-15 and SiO_2 supported catalysts were shown in Fig. 1(a). The initial conversion of ethylbenzene on Pt/SBA-15 (21.4 %) was much higher than that on Pt/SiO_2 (10.6 %). However, the activity rapidly decreased regardless of support, indicating that monometallic Pt catalyst showed a low stability. Sn improved the activities and stabilities of the supported Pt catalysts. This result is consistent with the previous reports about the promoting effect of Sn in the dehydrogenation of propane[24, 26], butane[13] and isobutane[11]. Moreover, Pt-Sn/SAB-15 showed a higher activity than that of Pt-Sn/SiO_2, suggesting that the support also affects the activity. Among the catalysts tested, 1Pt1Sn/SBA-15 exhibited the highest activity and stability, exhibiting an initial ethylbenzene conversion of 37.0 % and a final one of 33.8 %. In contrast, the ethylbenzene conversion on

1Pt1Sn/SiO_2 gradually decreased from 30.8% to 15.7% during 4 h of the reaction. These results indicate that the activity and stability were improved by using SBA-15 as support.

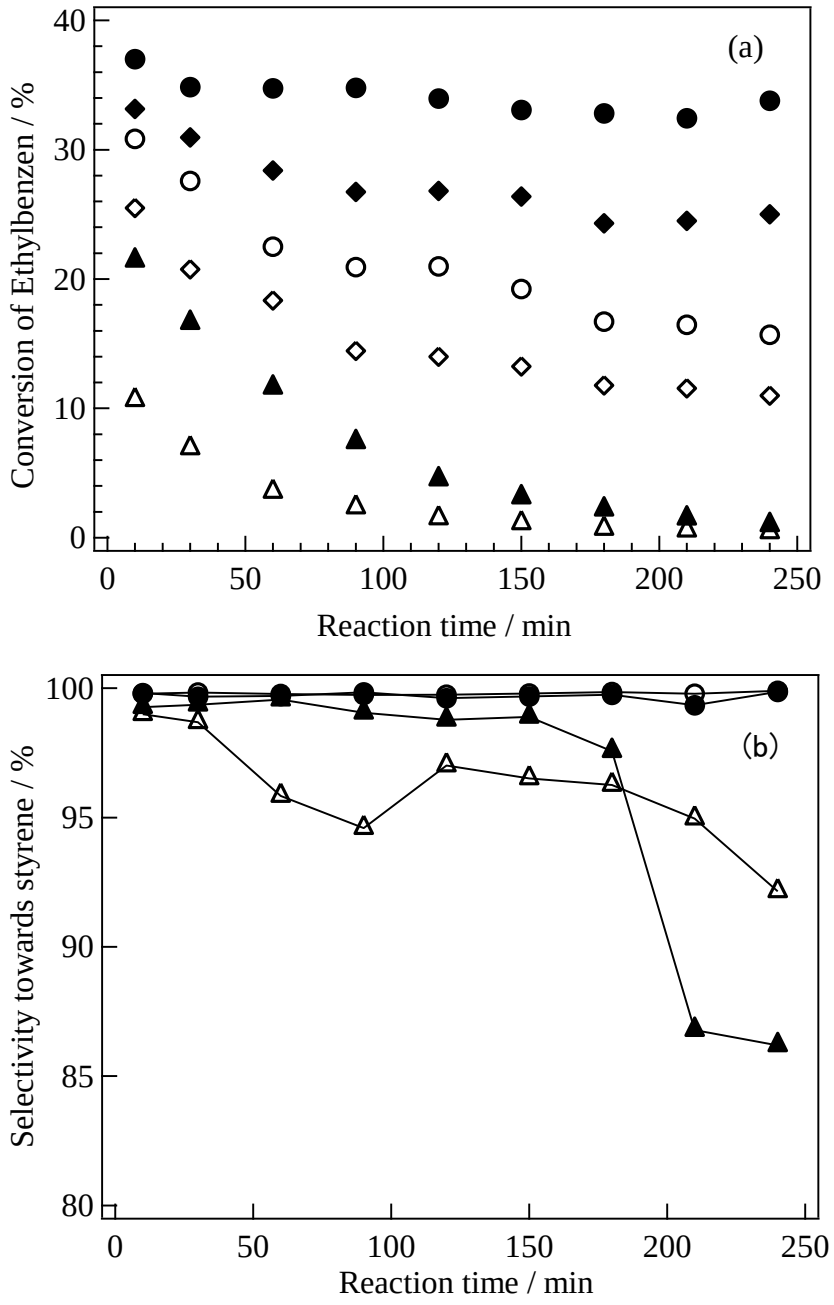

Figure 1 Catalytic activities (a) and selectivities (b) of supported Pt and Pt-Sn catalysts in the dehydrogenation of ethylbenzene. (▲: Pt/SBA-15; ◆: 3Pt1Sn/SBA-15; ●1Pt1Sn/SBA-15; △: Pt/SiO_2; ◇: 3Pt1Sn/ SiO_2; ○1Pt1Sn/ SiO_2.)

It was shown in Fig. 1(b) that the addition of Sn into Pt/Support catalysts effectively improved the selectivity towards styrene. The selectivities over 1Pt1Sn/SBA-15 and 1Pt1Sn/SiO_2 were above 99%. A trace of benzene, ethane, and methane were detected as by-products.

Physical properties of supported Pt and Pt-Sn catalysts

Figure 2 shows the nitrogen adsorption-desorption isotherms of SBA-15, SiO_2, Pt/SBA-15 and Pt-Sn/SBA-15. The physical properties are summarized in Table 1. Pore size distributions (the Barrett-Joyner-Halenda (BJH) plot) were shown in Fig. 3. Pt/SBA-15 and Pt-Sn/SBA-15 presented type IV isotherm N_2 adsorption, high surface areas like SBA-15. Their BJH plots also showed the narrow pore size distribution around diameter of 5.0 nm. These results indicate that the uniform and well-ordered two-dimensional (2D)-hexagonal channels of SBA-15 were still present after the modification with platinum and tin. Indeed, XRD patterns of SBA-15, Pt/SBA-15 and Pt-Sn/SBA-15 showed the characteristic low angle peaks attributed to d_{100}, d_{110}, d_{200} reflections assuming a 2D-hexagonal lattice at the same position (data not shown)[22, 38]. The BET surface area and pore volume of SBA-15 were decreased after the introduction of platinum and tin. In the case of SiO_2, Pt/SiO_2, and Pt-Sn/SiO_2, the BET surface area is ca. 300 m^2 g^{-1}, which is much smaller than SBA-15, Pt/SBA-15 and Pt-Sn/SBA-15.

XRD patterns of supported Pt and Pt-Sn catalysts

Figure 4 shows the XRD patterns of supported Pt and Pt-Sn catalysts. The XRD pattern of Pt/SiO_2 exhibited the diffraction peak at 2θ=39.8°, which is due to Pt metal (111) (ICSD 41525). In contrast, a very weak diffraction peak due to Pt metal was observed in XRD pattern of Pt/SBA-15, suggesting the formation of highly dispersed Pt

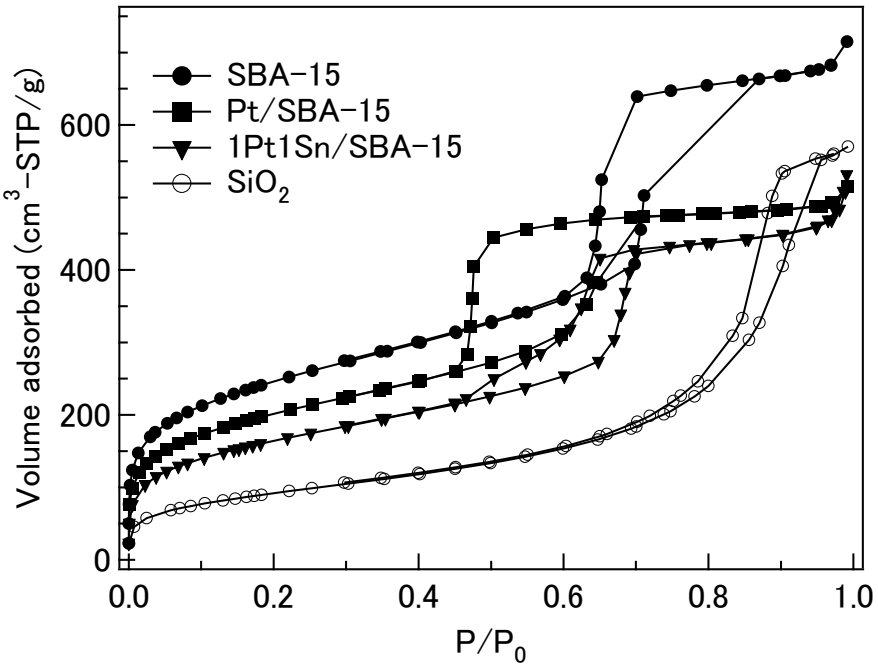

Figure 2 Nitrogen adsorption-desorption isotherms of SiO_2, SBA-15, Pt/SBA-15 and Pt-Sn/SBA-15 catalysts.

Table 1 Physical properties of SBA-15 and SiO_2 supported Pt and Pt-Sn catalysts.

Catalysts[a]	S_{BET}[b] (m^2/g)	D_p[c] (nm)	V_p[d] (cm^3/g)
SBA-15	890	5.0	1.10
Pt/SBA-15	717	4.7	0.84
3Pt1Sn/SBA-15	647	4.8	0.77
1Pt1Sn/SBA-15	598	5.4	0.80
SiO_2	311	10.6	0.82
Pt/SiO_2	340	11.2	0.95
3Pt1Sn/SiO_2	281	10.7	0.76
1Pt1Sn/SiO_2	300	11.5	0.86

a: the catalysts were prepared with direct reduction method (reducing the catalyst precursor at 1073 K in H_2 for 1h).
b: S_{BET} is the BET surface area.
c: D_p is the average pore size with BJH method.
d: V_p is the total pore volume.

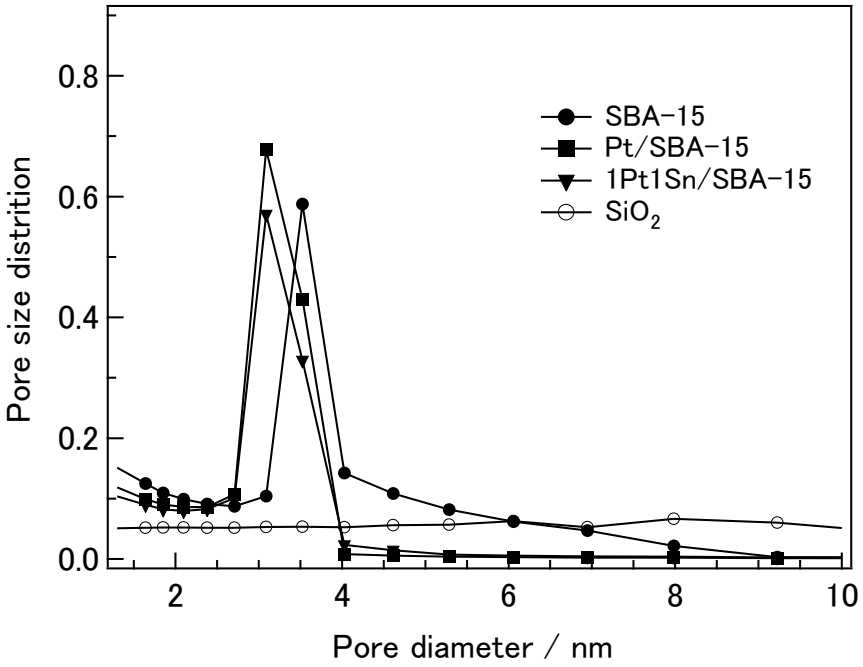

Figure 3 The pore size distributions of SiO_2, SBA-15, Pt/SBA-15 and Pt-Sn/SBA-15 catalysts.

metal particle (< 3 nm). In the case of 3Pt1Sn/SBA-15, a broad peak at 2θ=39.1° was observed. This position is lower than the diffraction peak due to Pt metal (111) (2θ =39.8°) and higher than the diffraction peak due to Pt_3Sn alloy (111) (2θ=39.0°) (ICSD 105796). A shift of the characteristic peak to lower angle by addition of Sn was previously reported on various Pt_xSn_y (x/y>3) alloys such as $Pt_{0.94}Sn_{0.06}$[39], $Pt_{0.93}Sn_{0.07}$[40], $Pt_{0.90}Sn_{0.10}$[41] and $Pt_{0.75}Sn_{0.25}$(Pt_3Sn)[39], accompanying an expansion of lattice constant. A broad full-width at half maximum (FWHM) of the diffraction peak on 3Pt1Sn/SBA-15 suggests the coexistence of various Pt_xSn_y (x/y>3) alloys and Pt_3Sn alloy and/or highly dispersed Pt_xSn_y (x/y≧3) alloy particles. In the case of 3Pt1Sn/SiO_2, a broad diffraction peak at 2θ=39.1° was also observed, while the narrower FWHM than that of Pt/SBA-15 implied that the particle sizes of formed Pt_xSn_y (x/y≧3) alloys on

SiO_2 were larger than those on SBA-15.

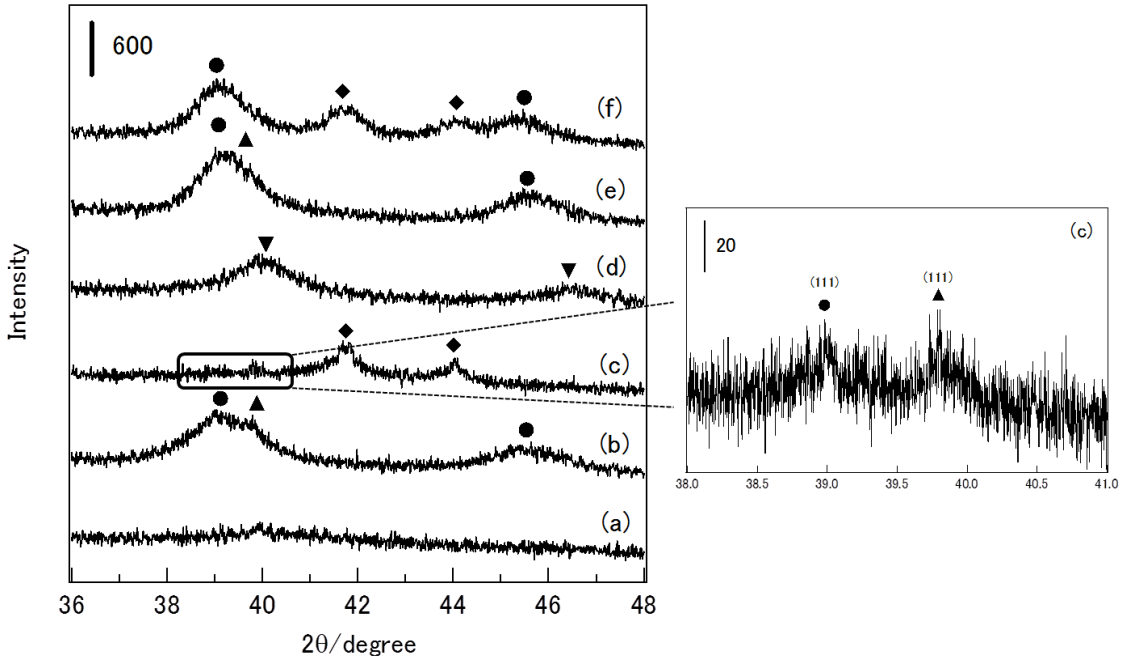

Figure 4 XRD patterns of supported Pt and Pt-Sn catalysts: (a) Pt/SBA-15, (b) 3Pt1Sn/SBA-15, (c) 1Pt1Sn/SBA-15, (d) Pt/SiO_2, (e) $3Pt1Sn/SiO_2$, (f) $1Pt1Sn/SiO_2$. ▼: Pt metal ▲: Pt_xSn_y (x/y>3) ●: Pt_3Sn alloy ◆: PtSn alloy

In the case of 1PtSn1/SBA-15, two diffraction peaks around 42° and 44°, which are assignable to PtSn phase (ICSD 42593), appeared together with very weak diffraction peaks due to Pt_3Sn alloy and Pt metal. Similarly, PtSn alloy was also detected on $1Pt1Sn/SiO_2$ besides Pt_3Sn alloy.

Furthermore, there were no obvious diffraction peaks due to Sn compounds such as Sn metal and Sn oxides (SnO and SnO_2) on all catalysts including SBA-15 and SiO_2 supported 1Pt1Sn catalysts with 1.8 wt% Sn.

Particle size and CO adsorption of supported Pt and Pt-Sn alloy

Fig. 5 shows the HADDF-STEM images together with histograms of white spots

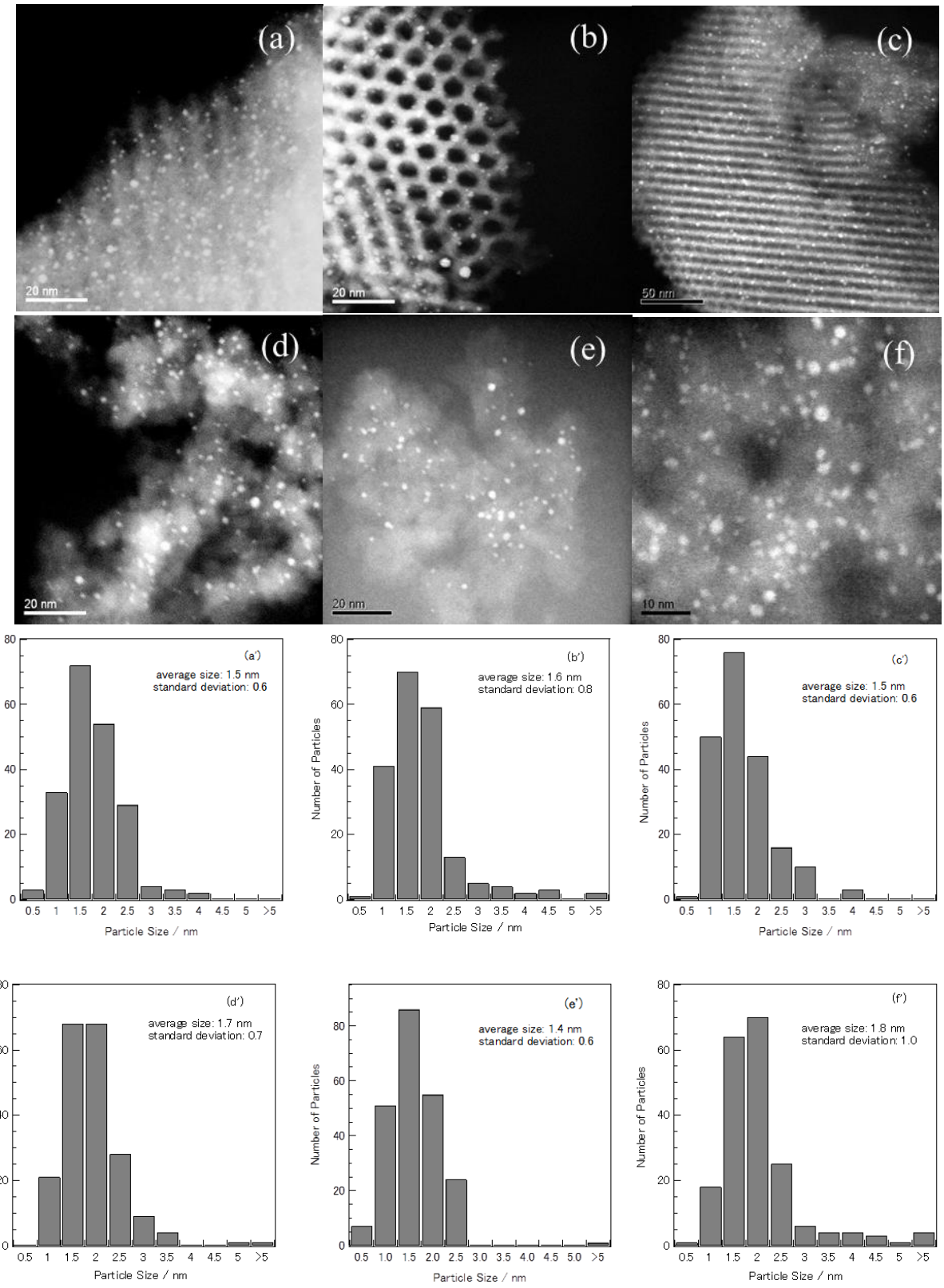
(a)
20 nm
(b)
20 nm
(c)
50 nm
(d)
20 nm
(e)
20 nm
(f)
10 nm
(a')
average size: 1.5 nm
standard deviation: 0.6
(b')
average size: 1.6 nm
standard deviation: 0.8
(c')
average size: 1.5 nm
standard deviation: 0.6
(d')
average size: 1.7 nm
standard deviation: 0.7
(e')
average size: 1.4 nm
standard deviation: 0.6
(f')
average size: 1.8 nm
standard deviation: 1.0
Number of Particles
Particle Size / nm

Figure 5 HAADF-STEM images and corresponding histgrams of SBA-15 and SiO_2 supported Pt or Pt-Sn catalysts: (a) (a') Pt/SBA-15, (b) (b') 3Pt1Sn/SBA-15, (c) (c')1Pt1Sn/SBA-15, (d) (d') Pt/SiO_2, (e) (e')3Pt1Sn /SiO_2, (f) (f')1Pt1Sn /SiO_2.

observed in HADDF-STEM images. White spots were assigned to Pt or Pt-Sn alloy particle. Figure 3(b) and (c) presented the cross and longitudinal sections of SBA-15, respectively. Uniform and well-ordered two-dimensional (2D)-hexagonal channels with a diameter about 6.0 nm of SBA-15 were clearly observed.

Table 2 CO adsorption and average particle size of SBA-15 and SiO_2 supported Pt and Pt-Sn catalysts.

Catalysts	Pt content / wt%	Sn content[a] / wt%	CO adsorption[b] / μmol g^{-1}	Average particle Size[c] / nm
Pt/SBA-15	3.0	-	44.0	1.5±0.6
3Pt1Sn/SBA-15	3.0	0.6	14.8	1.6±0.8
1Pt1Sn/SBA-15	3.0	1.8	13.6	1.5±0.6
Pt/SiO_2	3.0	-	40.3	1.7±0.7
3Pt1Sn/SiO_2	3.0	0.6	26.3	1.4±0.6
1Pt1Sn/SiO_2	3.0	1.8	6.5	1.8±1.0

a: The molar ratio of Sn to Pt is 1/3 or 1.

b: CO adsorption was measured from the CO-pulse experiments.

c: Average particle size was determined from the histogram of ca. 200 bright dots from HAADF-STEM images.

On the Pt/SBA-15 and Pt/SiO_2, small Pt particles whose mean particle size was about 1.5±0.6 and 1.7±0.7 nm were respectively shown in Fig. 5(a) and (d). The amount of adsorbed CO on Pt/SBA-15 (44.0 μmol g^{-1}) was slightly larger than that on Pt/SiO_2 (40.3 μmol g^{-1}) (Table 2). In the cases of Pt-Sn/SBA-15 and Pt-Sn/SiO_2, their average particle sizes ranged from 1.4 ~ 1.8 nm with different Sn/Pt ratios and supports, which were similar with supported Pt monometallic catalysts. However, the amount of adsorbed CO remarkably decreased on the bimetallic catalysts with the addition of Sn. CO is generally regarded to indicate the number of accessible Pt sites on the surface.

These results suggest the formation of Pt-Sn alloy and/or the deposition of Sn species on the surface for Pt-Sn/SBA-15 and Pt-Sn/SiO_2 catalysts. Wang et al.[42] synthesized Pt, PtSn (random alloy) catalyst with colloidal synthesis method. By comparing of PtSn (random alloy) with pure Pt, a clear decrease in the intensity of linearly adsorbed CO on Pt sites was found. The small amount of CO adsorbed on PtSn alloy catalyst was attributed to both geometric and electronic role of alloying between Pt and Sn. Meriaudeau et al. [43] reported that the addition of Sn to Pt reduced the strength of Pt-CO bond by the preferential blocking of higher binding sites of Pt by Sn. The reduction of strength of Pt-CO bond was interpreted as this geometric effect. In contrast, Liu et al [44] reported that the PtSn@Pt core-shell nanoparticle electrocatalysts prepared by potential cycling of PtSn intermetallic nanoparticles in CO-saturated H_2SO_4 solutions exhibited a substantially higher CO-tolerance property to Pt, PtRu alloy, and PtSn alloy catalysts. They proposed that the superior CO-torelance of the PtSn@Pt catalyst was mainly due to the electronic effect of the PtSn core on the Pt shell. The significant decrease in CO adsorbed on supported Pt-Sn catalysts in the present studies indicates that in addition to geometric blocking of CO adsorption due to the dilution of Sn by the formation of Pt-Sn alloys, the electronic role of Sn towards Pt with alloying and the Sn enrichment on surface of Pt-Sn alloys may be also important.

Characterization of the spent catalyst

Figure 6 represents the HADDF-STEM images of the spent 1Pt1Sn/SBA-15 and 1Pt1Sn/SiO_2 catalysts and the histograms of particle size. Highly dispersed Pt-Sn alloy particles were observed on 1Pt1Sn/SBA-15 even after 4 h of ethylbenzene dehydrogenation. The average size of Pt-Sn particles was 1.9 ± 0.7 nm, indicating that the size of Pt-Sn alloy slightly increased during the reaction. In contrast, the average

size of Pt-Sn alloy particles on 1Pt1Sn/SiO_2 remarkably increased from 1.8 to 3.2 nm, and a large size of particles (> 5nm) was also observed. These results clearly indicated that stability of Pt-Sn alloy on SBA-15 is higher than that on amorphous SiO_2.

Figure 7 shows TPO profiles of supported Pt and Pt-Sn catalysts after the ethylbenzene dehydrogenation. A small and broad peak around 390 K was observed on Pt/SiO_2. The addition of Sn to Pt/SiO_2 led to the formation of another larger TPO peak around 520 K. The normalized amounts of coke to converted ethylbenzene on Pt/SiO_2 and Pt-Sn/SiO_2 catalysts were summarized in Table 3. It was found that this value was much larger on Pt/SiO_2 than 1Pt1Sn/SiO_2, indicating that the addition of Sn inhibited

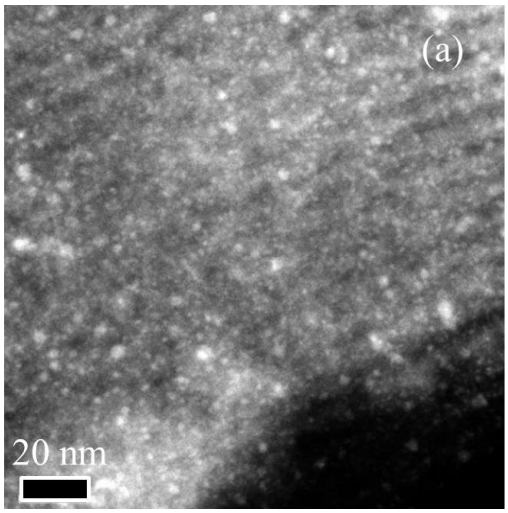

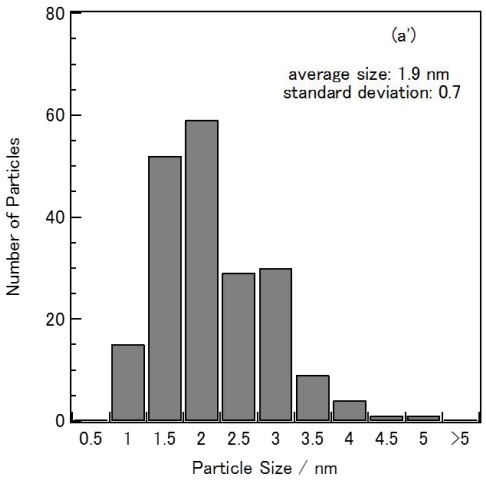

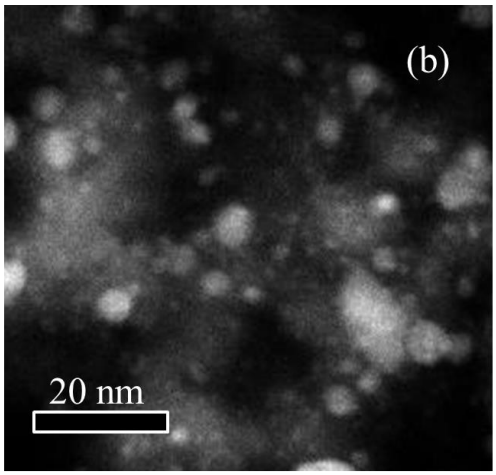

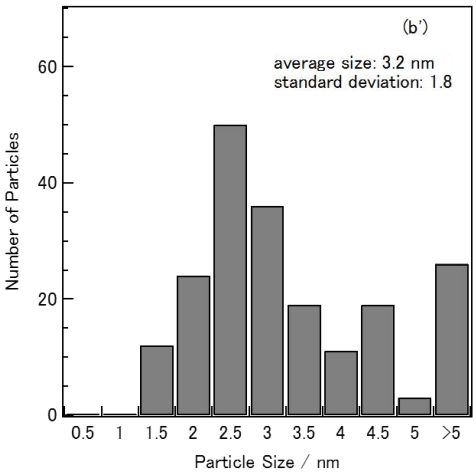

Figure 6 HAADF-STEM images of spent 1Pt1Sn/SBA-15(a) and 1Pt1Sn/SiO_2 (b) and their histograms of the distribution of particle sizes: after ethylbenzene dehydrogenation at 773 K for 4 h.

the coke formation to some extent. In the case of Pt/SBA-15, a large peak around 390 K (α-peak) was observed together with a small shoulder peak around 480 K (β-peak). For 1Pt1Sn/SBA-15, the peak intensity around 400 K (α-peak) decreased and the intense peak around 500 K (β-peak) appeared. Normalized amount of coke to converted ethylbenzne on 1Pt1Sn/SBA-15 was also much smaller than that on Pt/SBA-15, indicating that Sn strongly inhibited the coke formation. The α- and β-peaks were usually assigned to carbon formed on active metal, and carbon located on the surface of the support[23]. TPO profiles clearly showed that the area of α-peak was reduced by the addition of Sn, while that of β-peaks increased. These results indicate that Sn inhibited the formation of coke on active site and can work as the drain of coke into support (drain-off effect). Therefore, although larger amount of coke was deposited on the Pt-Sn/SBA-15 than Pt/SBA-15, Pt-Sn/SiO_2 and Pt/SiO_2, Pt-Sn/SBA-15 exhibited higher catalytic behaviors in the dehydrogenation of ethylbenzene. It seems that the location of coke affects the activity and stability of the catalyst.

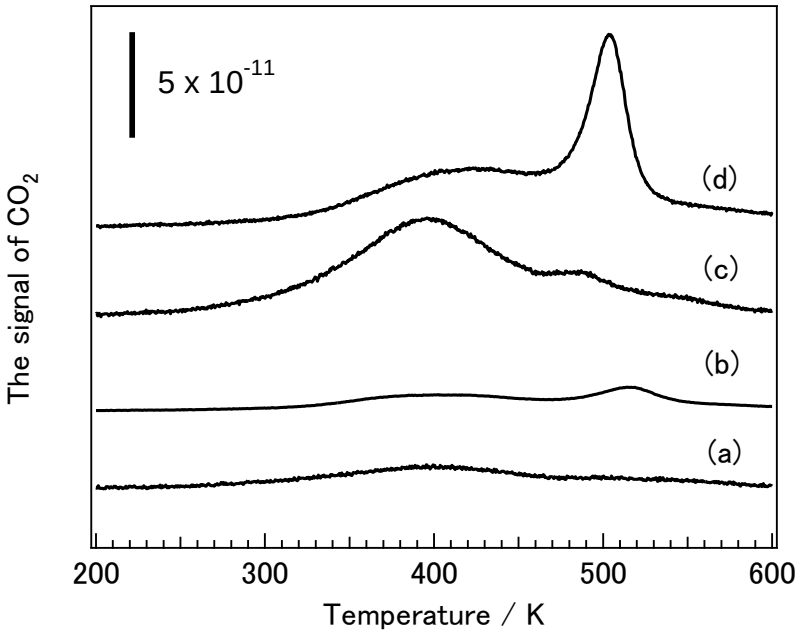

Figure 7 TPO profiles of spent catalysts: (a) Pt/SiO_2, (b) $1Pt1Sn/SiO_2$, (c) Pt/SBA-15, (d) 1Pt1Sn/SBA-15: after ethylbenzene dehydrogenation at 773 K for 4 h.

Table 3 Amount of coke formed on SBA-15 and SiO_2 supported Pt and Pt-Sn catalysts.

Catalysts	Amount of coke[a] / a.u.	Nomarlized coke amount[b] / a.u.
Pt/SBA-15	10.3	1.38
3Pt1Sn/SBA-15	7.3	0.12
1Pt1Sn/SBA-15	12.9	0.12
Pt/SiO_2	2.2	0.79
$1Pt1Sn/SiO_2$	1.9	0.08

a: estimated form area of TPO profile.

b: normalized to total amount of converted ethylbenzne.

Discussion

Pt-Sn/SBA-15 exhibited higher catalytic activity, selectivity as well as higher stability than Pt-Sn/SiO_2. The results of XRD pattern, CO adsorption, and HAADF-STEM images showed that with the direct reduction method, highly dispersed Pt-Sn alloys (Pt_xSn_y (x/y>3), Pt_3Sn and PtSn) particles formed on Pt-Sn/SBA-15. Recently, we reported that 1Pt1Sn/SiO_2, composed of Pt_3Sn alloy with a small fraction of PtSn alloy, exhibited a high activity in propane dehydrogenation, and part of the Pt-Sn alloy surface was covered with highly dispersed SnO_2. Moreover, we found that Pt_3Sn and Pt_xSn_y (x/y>3) alloys work as active species in propane dehydrogenation, but PtSn alloy particles exhibited a low activity [26, 27]. The structural characterization results of 1Pt1Sn/SBA-15 in the present work were consistent with those of 1Pt1Sn/SiO_2. Thus the high catalytic activity of 1Pt1Sn/SBA-15 suggest that Pt_3Sn and Pt_xSn_y (x/y>3) alloys also show a high activity in the dehydrogenation of ethylbenzene.

HAADF-STEM images of the spent catalysts demonstrate that SBA-15 effectively inhibited the sintering of the Pt-Sn alloy particles as compared to SiO_2. The similar role of the support with the mesoporous structure against a sintering of active sits has been reported. Gonzalo et al. [45] found that under relevant reactive conditions, confinement of the Cu particles in cage-like silica pores from SBA-16 notably enhanced catalyst stability by limiting Cu particle growth as compared to catalysts deposited in SiO_2-gel host materials with 3D and highly interconnected though unconstrained porosity. Takenaka et al. [46] also found that the carbon nanotube-supported Pd catalysts covered with silica layers were highly durable for the oxygen reduction reaction. The silica layer having porous structure prevented the diffusion of dissolved Pd species from the Pd metal out of the layers.

The characterization of the spent catalyst by TPO measurements revealed that the amount of coke deposition over 1Pt1Sn/SBA-15 was larger than those on Pt/SBA-15, Pt-Sn/SiO_2 and Pt/SiO_2. Despite a largest amount of coke formed, 1Pt1Sn/SBA-15 showed higher stability than 1Pt1Sn/SiO_2 and Pt/SBA-15. The change in TPO profiles suggests that the location of coke was changed by the addition of Sn to Pt because of a 'drain-off' effect of Sn. It appears that the drain-off effect keeps the Pt-Sn active sites clean by removing the coke precursors from the vicinity of active sites to the support. Lieske et al. [47] firstly proposed the drain-off effect. Recently, Khanh et al. [21] also reported the different coke mobility behaviors of Pt-Sn/Al_2O_3 and Pt-Sn/$ZnAl_2O_4$. The transport of the coke from metallic sites to the support became easier than that on Pt-Sn/Al_2O_3 catalyst. Moreover, the normalized coke amount to converted ethylbenzene remarkably reduced by the addition of Sn, indicating that the selectivity to coke formation is also reduced by the addition of Sn.

Conclusion

Pt-Sn/SBA-15 prepared by direct reduction method exhibited higher catalytic activity, higher catalytic selectivity towards styrene as well as higher stability than Pt-Sn/SiO_2 in the ethylbenzene dehydrogenation. The results of XRD pattern, CO adsorption, and HAADF-STEM images showed that with the direct reduction method, highly dispersed Pt-Sn alloys (Pt_xSn_y (x/y>3), Pt_3Sn and PtSn) particles formed on Pt-Sn/SBA-15. Pt-Sn alloy particles on SBA-15 showed higher stability during the reaction than those on amorphous SiO_2 due to the unique textural properties of SBA-15. The characterization of the spent catalyst by TPO measurements revealed that a larger amount of coke was formed on 1Pt1Sn/SBA-15 than those on Pt/SBA-15. However, the normalized coke amount to converted ethylbenzene remarkably reduced by the addition

of Sn. Moreover, Sn drained coke formed from the active Pt-Sn sites to the support (drain-off effect), kept Pt-Sn alloy sites clean, thus 1Pt1Sn/SBA-15 showed higher stability than Pt/SBA-15 and 1Pt1Sn/SiO_2.

References

[1] F.T. Cavani, F, Applied Catalysis A: General, 133 (1995) 219.

[2] E. Lee, Catalysis Reviews-Science and Engineering, 8 (1973) 285.

[3] B.B. Tope, R.J. Balasamy, A. Khurshid, L.A. Atanda, H. Yahiro, T. Shishido, K. Takehira and S.S. Al-Khattaf, Applied Catalysis A: General, 407 (2011) 118.

[4] B. Herzog and H. Rase, Industrial & Engineering Chemistry Product Research and Development, 23 (1984) 187.

[5] G. Meima and P. Menon, Applied Catalysis A: General, 212 (2001) 239.

[6] N. Mimura, I. Takahara, M. Saito, T. Hattori, K. Ohkuma and M. Ando., Catalysis Today, 45 (1998) 61.

[7] C. Moran, E. Gonzalez, J. Sanchez, R. Solano, G. Carruyo and A. Moronta, Journal of Colloid and Interface Science, 315 (2007) 164.

[8] B.V. Vora, Topics in Catalysis, 55 (2012) 1297.

[9] V. Galvita, G. Siddiqi, P. Sun and A.T. Bell, Journal of Catalysis, 271 (2010) 209.

[10] O. Barias, A. Holmen and E. Blekkan, Journal of Catalysis, 158 (1996) 1.

[11] R. Cortright and J. Dumesic, Journal of Catalysis, 148 (1994) 771.

[12] S. Kobayashi, S. Kaneko, M.-a. Ohshima, H. Kurokawa and H. Miura, Applied Catalysis A: General, 417 (2012) 306.

[13] I. Kikuchi, M.-a. Ohshima, H. Kurokawa and H. Miura, Journal of Japan Petroleum Institute, 55 (2012) 206.

[14] S.A. Bocanegra, S.R. de Miguel, I. Borbath, M.J. L.; and O.A. Scelza, Journal of molecular catalysis. A, Chemical, 301 (2009) 52.

[15] B. Linyang, Z. Yuming, Z. Yiwei, L. Hui and M. Tang, Catalysis Letter, 129 (2009) 449.

[16] A.D. Ballarini, C.G. Ricci, S.R. de Miguel and O. A. Scelza, Catalysis today, 133 (2008) 28.

[17] A.D. Ballarini, P. Zgolicz, I.M.J. Vilella, S.R. De Miguel, A.A. Castro and O.A. Scelza, Applied catalysis. A, General, 381 (2010) 83.

[18] S.A. Bocanegra, A.A. Castro, O.A. Scelza and S.R. De Miguel, Applied catalysis. A, General, 333 (2007) 49.

[19] S.R. De Miguel, S.A. Bocanegra, I.M.J. Vilella, A. Guerrero-Ruiz and O.A. Scelza, Catalysis letters, 119 (2007) 5.

[20] A. Iglesias-Juez, A.M. Beale, K. Maaijen, T. Chien Weng, G. Pieter and W.B. M., Journal of Catalysis, 276 (2010) 268.

[21] B.K. Vu, M.B. Song, I.Y. Ahn, Y.-W. Suh, D.J. Suh, W.-l. Kim, H.-L. Koh, Y.G. Choi and E.W. Shin, Applied Catalysis A: General, 400 (2011) 25.

[22] J. Bassil, A. AlBarazi, P. Da Costa and B. Maya, Catalysis Today, 176 (2011) 36.

[23] M. Xue, Y. Zhou, Y. Zhang, X. Liu, Y. Duan and X. Sheng, Journal of Natural Gas Chemistry, 21 (2012) 324.

[24] M.S. Kumar, D. Chen, A. Holmen and I.C. Walmslev, Catalysis today, 142 (2009) 17.

[25] Z. Paal, A. Wootsch, D. Teschner, K. Lazar, I.E. Sajo, N. Gyorffy, G. Weinbery, A. Knop-Gericke and R. Schlogl, Applied Catalysis A: General, 391 (2011)

377.

[26] L. Deng, T. Shishido, K. Teramure and T. Tananka, Catalysis Today, 232 (2013) 33.

[27] L. Deng, H. Miura, T. Shishido, S. Hosokawa, K. Teramura and T. Tanaka, ChemCatChem, in press (2014).

[28] R. Huirache-Acuna, R. Nava, C.L. Peza-Ledesma, J. Lara-Romero, G. Alonso-Nunez, B. Pawelec and E.M. Rivera-Munoz, Materials, 6 (2013) 4139.

[29] L. Zexiang, J. Shengfu, L. Hui and L. Chengyue, Chinese Journal of Chemical Engineering, 16 (2008) 740.

[30] D. Zhao, J. Feng, Q. Huo, N. Melosh, G.H. Fredrickson, B.F. Chmelka and G.D. Stucky, Science, 279 (1998) 548.

[31] F. Hoffmann, M. Cornelius, J. Morell and M. Froba, Angewandte Chemie-International Edition 45 (2006) 3216.

[32] A. Stein, Advanced Materials, 15 (2003) 763.

[33] A. Stein, B. Melde and R. Schroden, Advanced Materials, 12 (2000) 1403.

[34] H. Hata, S. Saeki, T. Kimura, Y. Sugahara and K. Kuroda, Chemistry of materials, 11 (1999) 1110.

[35] A. Taguchi and F. Schuth, Microporous and mesoporous materials, 77 (2005) 1.

[36] A. Chen, W. Zhang, X. Li, D. Tan, X. Han and X. Bao, Catalysis letters, 119 (2007) 159.

[37] M.S. Kumar, D. Chen, J.C. Walmsley and A. Holmen, Catalysis Communications, 9 (2008) 747.

[38] S. O'Brien, R. Francis, A. Fogg, D. O'Hare, N. Okazaki and K. Kuroda,

Chemistry of materials, 11 (1999) 1822.

[39] M. Ellner, Journal of the Less-Common Metals, 78 (1981) 21.

[40] P. Durussel and R.M.e.P. Feschotte, Journal of Alloys and Compounds, 215 (1994) 175.

[41] I.R. Harris, M. Norman and A.W. Bryant, Journal of the Less-Common Metals, 16 (1968) 427.

[42] X. Wang, L. Altmann, J. Stoever, V. Zielasek, M. Baumer, K. Al-Shamery, H. Borchert, J. Parisi and J. Kolny-Olesiak, Chemistry of Materials, 25 (2013) 1400.

[43] P. Meriaudeau, A. Thangaraj, J. Dutel and N. C., Journal of Catalysis, 167 (1997) 180.

[44] Z. Liu, G.S. Jackson and B.W. Eichhorn, Angewandte Chemie (International ed.), 49 (2010) 3173.

[45] G. Prieto, M. Shakeri, K.P. de Jong and P.E. De Jong, ACS NANO, 8 (2014) 2522.

[46] S. Takenaka, N. Susuki, H. Miyamoto, E. Tanabe, H. Matsune and M. Kishida, Journal of Catalysis, 279 (2011) 381.

[47] H. Lieske, A. Sarkany and J. Volter, Applied Catalysis, 30 (1987) 69.

Chapter 6

Effect of reduction temperature on the catalytic performance of Pt/SiO_2 catalysts for propane dehydrogenation: Metal-Support interaction between Pt and SiO_2

Abstract

Pt/SiO_2 catalysts were prepared with the direct reduction method (impregnation-reduction) at different temperature. With increasing reduction temperature, the interaction between Pt and SiO_2 became stronger and stronger. When Pt/SiO_2 catalyst was reduced at 773 K, Pt metal particles were highly dispersed on SiO_2 and the interaction between them was weak. After reducing at 1073 K, Pt metal in Pt/SiO_2 catalyst became electron-richer, implying the strong interaction between Pt and SiO_2. CO adsorption on it also decreased even the Pt particle size almost unchanged. As for Pt/SiO_2 catalyst reduced at 1273 K, Pt metal size retained small (ca. 3.2nm), but no CO adsorbed on it. Its HR-TEM image presented SiO_2 layer covered with Pt metal, confirming the strongest interaction between metal and the support. The catalytic tests in the dehydrogenation of propane showed that Pt/SiO_2 catalyst reduced at 1073 K exhibited the highest activity with 21% propane conversion and 94% propylene selectivity, while Pt/SiO_2 catalysts reduced at 773 K and 1273 K were inactive. These results suggested that the accessible interface between Pt and SiO_2 reduced at 1073 K may be the active site for propane dehydrogenation.

Introduction

Metal supported on the support represents an important class of materials widely applied in heterogeneous catalysis. During the past forty years considerable attention has been given to the effect of metal-support interaction on the chemisorptive and catalytic properties of the metal phase. Perhaps the most famous instance is the so-called strong metal support interaction (SMSI) that occurs between Pt metal and TiO_2 support [1]. In this system, the SMSI effect was induced by reducing the Pt/TiO_2 in H_2 at temperatures above 773 K, and dramatically reduced the catalyst's capacity to adsorb H_2 and CO. This interaction also could modify the activity and selectivity of Pt metal in different reactions [2-10]. For example, Vannice, MA [9] found that the turnover frequency (TOF) value for CO hydrogenation to CH_4 on Pt/TiO_2 catalysts (with SMSI effect) were 100 fold higher than the TOF on Pt/SiO_2 (without SMSI effect). He further reported [10] that SMSI effects induced in Pt/TiO_2 not only enhance specific activity but also markedly shift selectivity in the vapor-phase hydrogenation of a group of aldehydes and ketones which contain unsaturated C=C bonds. The hydrogenation of the carbonyl bond is favored.

A series of explanations for this distinctive behavior has been reported. An electronic effect of support TiO_2 to the Pt particles has been proposed using X-ray photoelectron spectroscopy (XPS). The electrons were found to transfer from the reduced Ti centers to the Pt particles [11]. The formation of a Pt-Ti alloy was possible. Pesty, F [12] further demonstrated the encapsulation of the Pt islands by a reduced Ti^{n+} species ($1 \leqq n \leqq 3$) with SMSI effects using low energy ion scattering (LEIS) and XPS.

Therefore, a reducible oxide support such as TiO_2, CeO_2[13], Nb_2O_5[14] was generally regards as a necessary component in a SMSI system. However, there is now

the increasing evidences for similar phenomena involving silica which was generally regards as the inert support [15, 16]. For example, Lamber, R [15] observed Pt_3Si alloy on platinum with SiO_2 substrates when they were thermally treated in hydrogen at 840 K. During our experiments, the interaction between Pt and SiO_2 has also been found when they were treated in H_2 at high temperature (ca. 1073 K). And it showed high activity in propane dehydrogenation, which was not observed on the catalysts reduced at low tempertatures, for example, 773 K. Therefore, the present work will present more evidences of this metal-support interaction. The observations can elucidate the mechanism of strong metal-support interactions in the Pt/SiO_2 system, and will be also helpful for understanding SMSI phenomenon and its role on C-H bond activation in the dehydrogenation of propane.

Experimental

Catalyst Preparation

Silica (JRC-SIO-9, 334 m^2 g^{-1}) was used as support for the preparation of the Pt/SiO_2 catalysts. Prior to impregnation, the SiO_2 support was treated at 773 K for 3h in air. Pt/SiO_2 was prepared by impregnating the SiO_2 support with an adequate volume of aqueous $H_2PtCl_6 \cdot 6H_2O$ (3wt% Pt), stirring at 353 K for 3h, and then drying at 353 K for 20 h. The precipitate was noted as Pt/SiO_2 precursor. Prior to catalytic experiments, the catalyst precursor was reduced *in situ* in 20 vol% H_2 diluted with N_2 (total flow rate 50 ml min^{-1}) at temperatures ranged from 773K to 1273K. Finally, the catalyst was cooled to 773 K in N_2 (100 ml min^{-1}). The obtained catalysts were denoted as Pt/SiO_2_x K, where x indicates the reduction temperature.

Dehydrogenation of propane

Propane dehydrogenation was carried out by in a quartz reactor (i.d. 10 mm) at

atmospheric pressure with 20 vol. % of propane diluted with N_2 at 773 K. Total flow rate was 100 ml min^{-1}. The catalyst precursor (50 mg) was placed between glass-wool. The composition of gas was analyzed with an on-line gas chromatographs (Shimadzu GC-8A, Japan) equipped with a TCD (5A Molecular Sives column) and methanizer FID (Porapak-Q column) detectors.

Characterization

All characterization was carried out on catalysts after *in situ* reduction in H_2 atmosphere. Brunauer—Emmett—Teller (BET) specific surface areas were estimated from N_2 isotherms obtained using a BELSORP 28SA (BEL Japan, Osaka, Japan) at 77 K. The analyzed samples were evacuated at 573 K for 3 h prior to the measurements.

The amount of adsorbed CO on the catalysts at room temperature was determined by the CO pulse method with an Okura BP-2 instrument (Okura Riken, Japan) interfaced with a TCD.

X-ray diffraction (XRD) patterns were obtained using a MultiFlex DR powder X-ray diffractometer (Rigaku, Tokyo, Japan) with Cu Kα radiation (χ = 1.5405 Å). The samples were scanned from 2θ=38° to 46° at the scanning resolution of 0.01°.

Transmission electron microscope (TEM) images were obtained using a JEOL JEM-3200FS transmission electron microscope. The samples were prepared by depositing drops of ethanol suspensions containing small amounts of the powders onto a carbon-coated copper grid (Okenshoji Co. Ltd.), followed by evaporation of the ethanol in air.

X-ray absorption experiments were carried out at the BL01B1 at SPring-8 (Hyogo, Japan). The ring energy was 8 GeV, and the stored current was 99.5 mA. The Pt L_3 and L_2-edge (11.56 and 13.27 keV) X-ray absorption spectra were recorded in air

at room temperature using a Si(111) monochromator in transmission mode. The data processing was performed using the REX2000 Ver.2.5.9 (Rigaku) and FEFF8.40 programs.

X-ray photoelectron spectra (XPS) were acquired using an ULVAC PHI 5500MT. The spectra were measured using Mg Kα radiation (15 kV, 400 W) in a chamber with the base pressure of ~ 10^{-7} Pa.

The temperature programmed oxidation (TPO) analysis of the coke deposited on the catalysts in the dehydrogenation of propane was conducted by combustion with air in a Okura BP-2 instrument (Okura Riken, Japan), coupled to a BELmass (BEL JAPAN, INC) for monitoring the signal corresponding to CO_2.

Results

Surface area, Pt species and dispersion

Table 1 summarizes the BET specific surface area of Pt/SiO_2 catalysts reduced at 773 K, 1073 K and 1273 K. The BET surface area of Pt/SiO_2_773K (ca. 340 m^2 g^{-1}) was the largest one among all samples. Pt/SiO_2_1073K exhibited the similar surface area (ca. 320 m^2 g^{-1}). In contrast, BET surface area was drastically decreased with the reduction at 1273 K. The BET surface area of Pt/SiO_2_1273K was about 217 m^2 g^{-1}.

Table 1 the surface areas of the catalysts.

Catalyst	surface area / m^2 g^{-1}
SiO_2	325
Pt/SiO_2_773K	340
Pt/SiO_2_1073K	320
Pt/SiO_2_1273K	217

Figure 1 shows the XRD patterns of the catalysts. The X-ray diffraction peaks of Pt metal (111) (2θ = 39.8°) and (200) (2θ = 46.3°) (ICSD 41525) were observed on all

catalysts. The full-width at half maximum (FWHM) of this diffraction peak became slightly narrower with reduction temperature, implying that the particle size of Pt crystal slightly increased under the higher temperature.

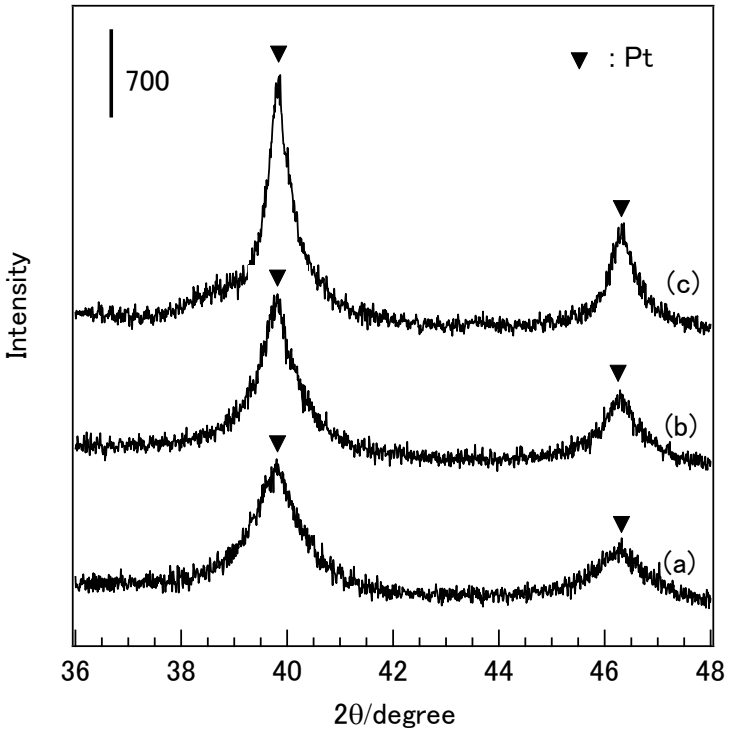

Figure 1 XRD patterns of Pt/SiO_2 reduced at (a) 773 K, (b) 1073 K, (c) 1273 K. ▼: Pt metal.

The TEM images of the catalysts, shown in Figure 2, displayed the high dispersion of Pt on SiO_2. The average particle size of Pt particle is ca. 2.4 nm on Pt/SiO_2_773K, 2.2 nm on Pt/SiO_2_1073K and 3.2 nm on Pt/SiO_2_1273K. The average particle size of Pt particle slight increased when the catalyst was reduced at 1273 K. This result is compatible with the slightly grow up of Pt crystal suggested from their XRD patterns. Overall, Pt metal particles retained small size even after the high-temperature reduction. The aggregation, which often takes place after the high-temperature reduction, did not appear on Pt/SiO_2 catalysts involved in the present

work.

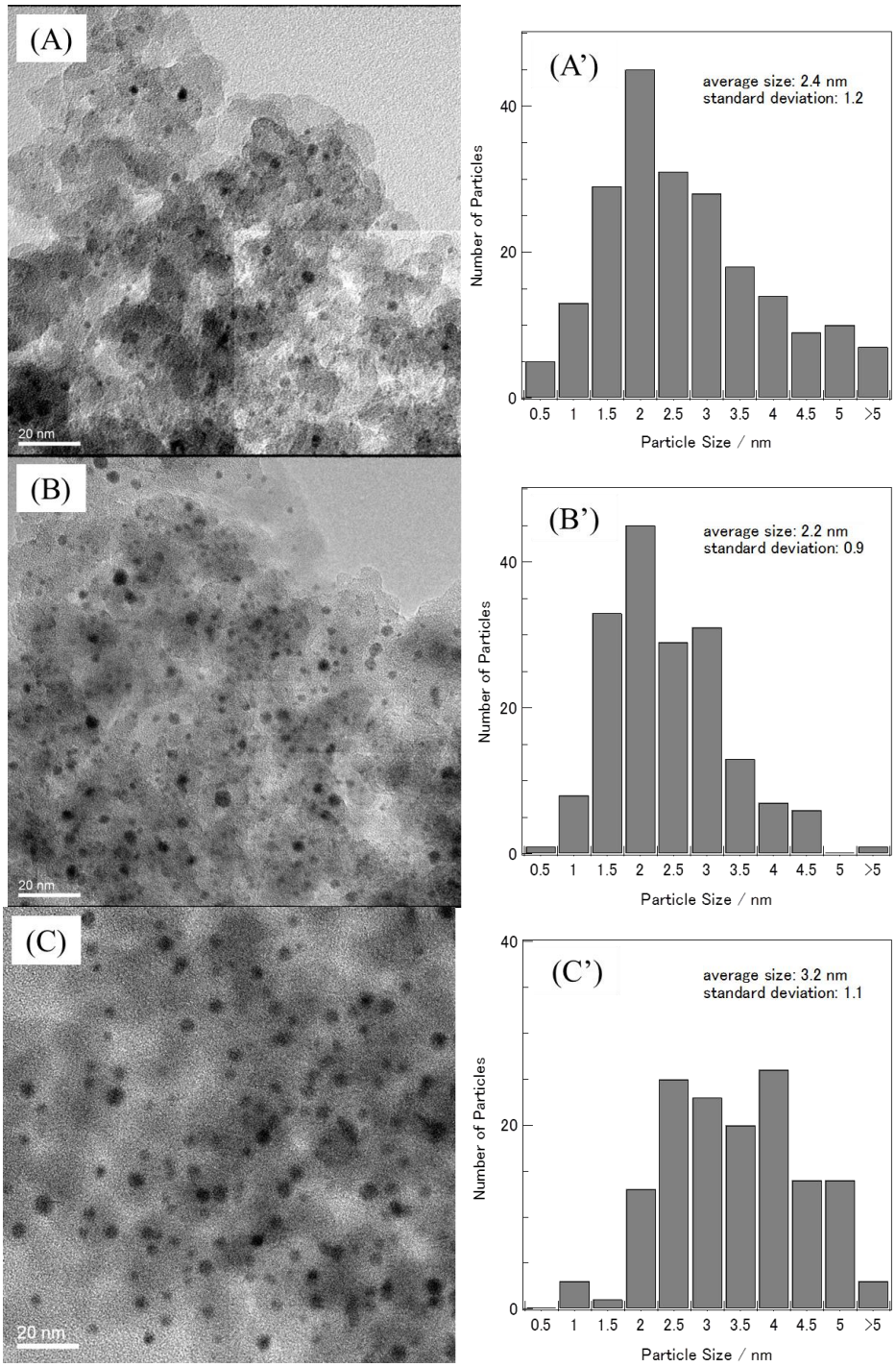

Figure 2 TEM images of Pt/SiO_2 reduced at (A) 773 K, (B) 1073 K, (C) 1273 K as well as their corresponding histograms.

Catalytic activity of Pt/SiO_2 catalysts

Figure 3 shows the effect of reduction temperature on the catalytic activity of Pt/SiO_2 catalysts in propane dehydrogenation. The initial conversion of propane firstly increased and then decreased with reduction temperature. Pt/SiO_2_1073K showed the highest activity, exhibiting a propane conversion of 21.3% and selectivity toward propylene of 94.4%. A trace amount of methane and ethane were detected as by-products. The catalyst reduced at 773 K or 1273 K showed a quite low activity.

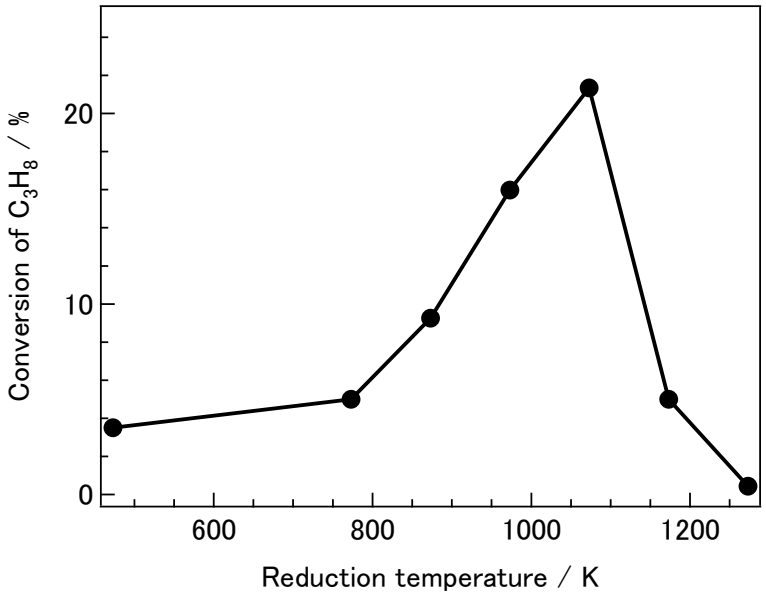

Figure 3 The effect of reduction temperature on the initial conversion of propane over Pt/SiO_2 catalysts.

Figure 4 displays the catalytic performances of Pt/SiO_2_1073K during the reaction time (3h). The activity was found to slightly decrease with reaction time. Selectivity towards propylene was 94% and stable during 3 h of reaction. Selectivity shown here was calculated with respect to the sum of C1 to C3 hydrocarbons detected with GC. This method does not exactly match the propane at the inlet of the reactor because the coke formed on the surface of the catalyst will escapes the GC analysis. Thus TPO experiment was carried out on the spent catalyst Pt/SiO_2_1073K after 3 h of

reaction. It was found that at least two kinds of coke were formed on the spent catalyst, seen in Fig. S1. The gradual activity decrease of the catalyst may be related to the coke formation and its blockage on the active sites of Pt/SiO_2_1073K.

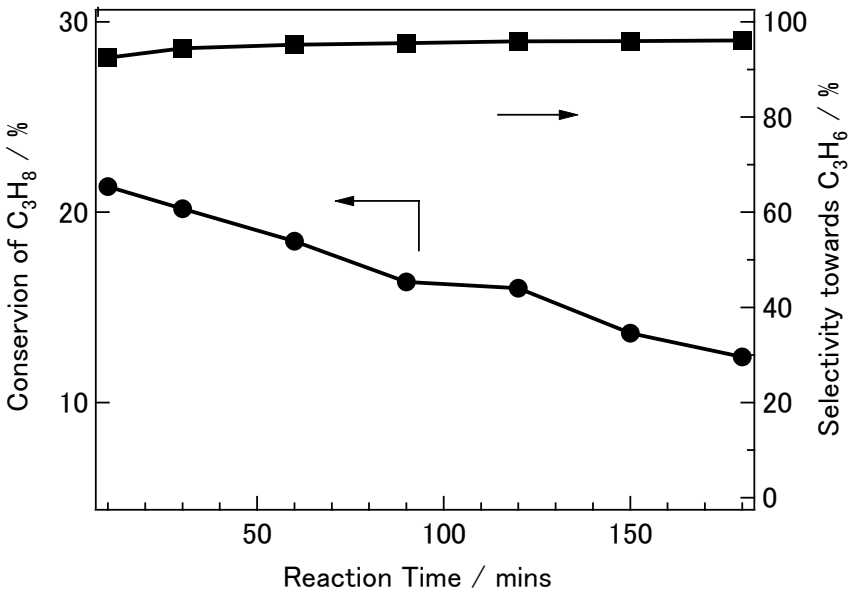

Figure 4 The effect of reduction temperature on the conversion of propane and selectivity towards propylene over Pt/SiO_2_1073K.

XANES and EXAFS analysis of the catalysts

Figure 5 shows the Pt L_3 and L_2-edge XANES spectra of Pt/SiO_2 catalysts reduced at 773 K, 1073 K and 1273 K, and those of Pt foil as the reference sample. The white line intensities at Pt L_3 and L_2-edges of all catalysts were almost equal to that of Pt foil, indicating the properties of metallic Pt on all catalysts. The white lines of Pt/SiO_2_773K and Pt foil were observed at 11561.0 eV and 11562.0 eV respectively. The white line intensity for Pt/SiO_2_773K was slightly higher than that of Pt foil. These differences may be caused by the difference of Pt particle size between Pt/SiO_2_773K and Pt foil. Pt atoms in Pt/SiO_2_773K were in the nano-size Pt particles (ca. 2.4 nm), while Pt foil is the bulk metal. Gallezot et al[17] studied Pt L_3-edge spectra in various

catalyst samples as a function of crystallize size. From evaluation of the area under the normalized L_3 X-ray absorption edge spectrum, they concluded that the electronic properties of Pt particles change with size.

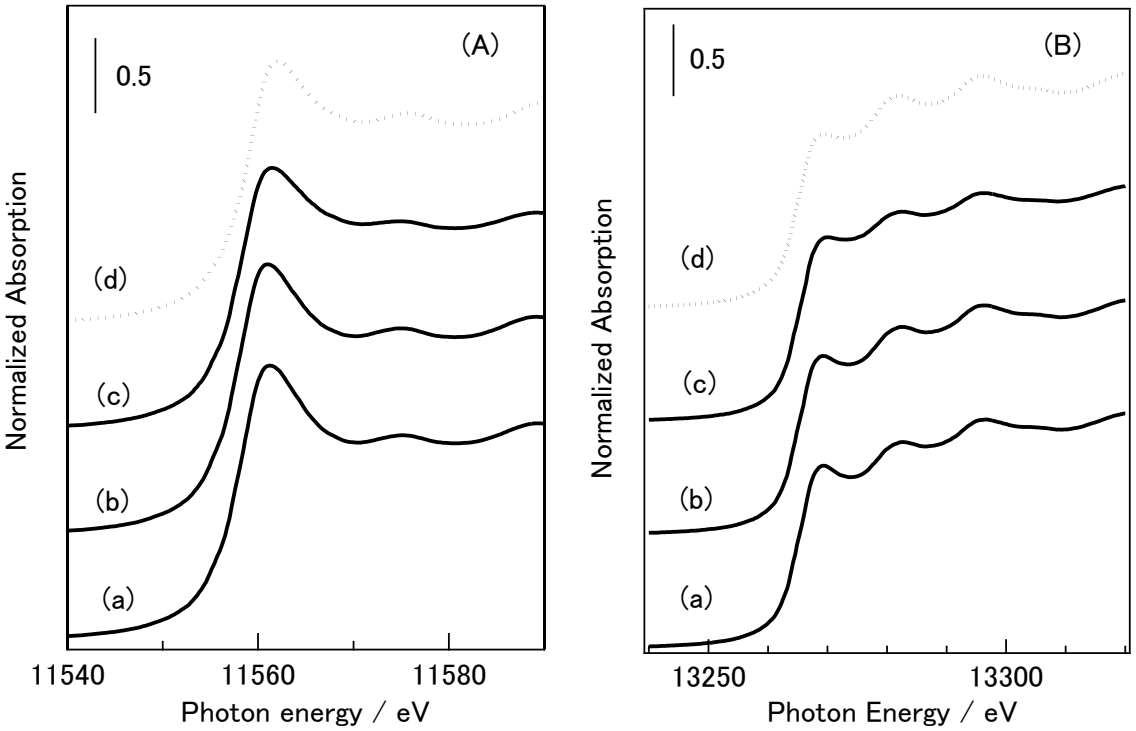

Figure 5 Pt L_3 and L_2-edge XANES spectra of Pt/SiO_2 catalysts reduced at different temperatures and Pt foil: (A) L_3-edge, (B) L_2-edge, (a) Pt/SiO_2_773 K, (b) Pt/SiO_2_1073 K, (c) Pt/SiO_2_1273 K, (d) Pt foil.

The Pt L_3 and L_2-edge X-ray absorption white lines correspond to electronic transitions from $2p_{3/2}$ and $2p_{1/2}$ core level states and directly reflect the electronic states of the vacant *d* orbitals of platinum. The L_3 edge reflects the final vacant *d* states of both $5d_{3/2}$ and $5d_{5/2}$ levels, and the L_2 edge reflects that of only the $5d_{3/2}$ level. Lytle et al.[18] reported that the intensity of the peak at the L_3 X-ray absorption edge is proportional to the d-electron vacancies. Based on these reports, our measurements over Pt/SiO_2 catalysts and Pt foil suggested that Pt atoms in nano-size particles were more

electron-deficient than those in bulk Pt foil.

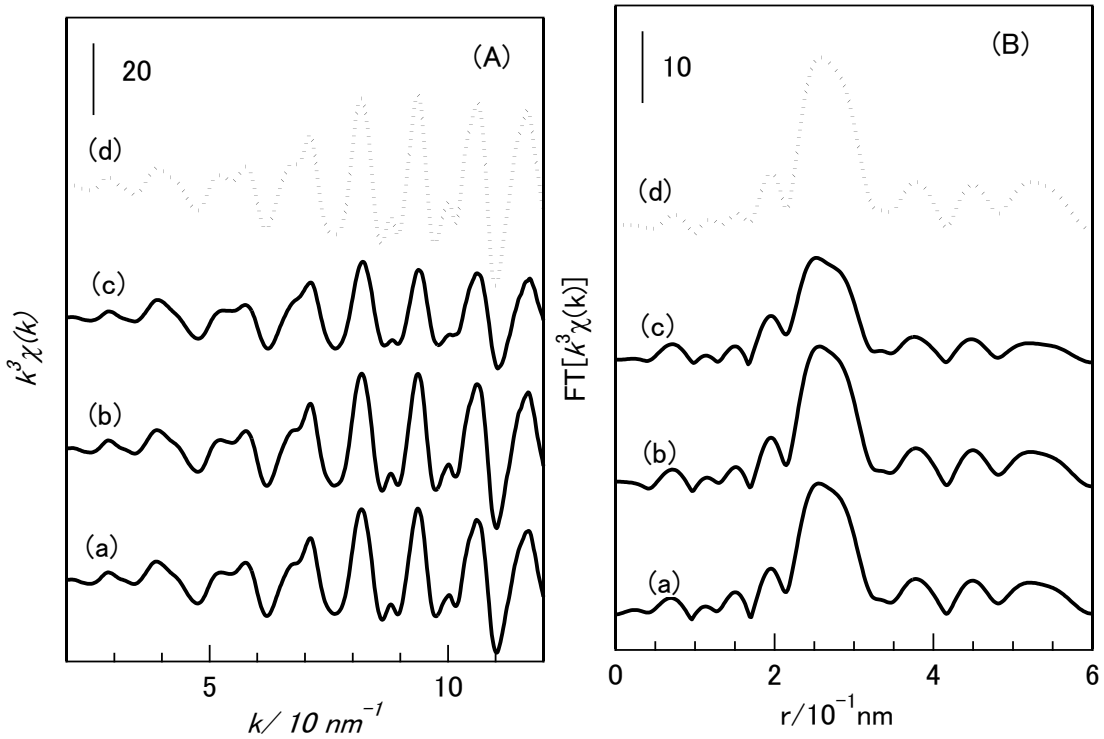

Figure 6 k^3-weighted EXAFS oscillation at Pt L_3-edge (A) and their Fourier transforms (B) of Pt/SiO_2 catalysts reduced at different temperatures and Pt foil: (a) Pt/SiO_2_773 K, (b) Pt/SiO_2_1073 K, (c) Pt/SiO_2_1273 K, (d) Pt foil.

When the reduction temperature increased to 1073 K and 1273 K, the position of white line at both Pt L_3 and L_2-edges almost unchanged, while the white line intensities on Pt/SiO_2_1073K and Pt/SiO_2_1273K decreased. This observation suggested the opposite effect of reduction temperature to the particle size on the electronic state of Pt on Pt/SiO_2 catalysts. The lower intensity of the white lines observed in the Pt/SiO_2 catalysts reduced at higher temperatures suggests much electron-richer of Pt on these catalysts. Lamber, R[15] detected Pt_3Si between Pt and SiO_2 substrate at the high reduction temperature. Similarly, alloying between Pt and Si probably took place on Pt/SiO_2_1073K and Pt/SiO_2_1273K catalysts. The lower electronegativity of Si than Pt

(Pt 2.3, Si 1.9)[19] resulted into the electron donation from Si to Pt in Pt-Si alloys. Thus the *d*-electron density of platinum atoms is increased, and the white line intensities for Pt/SiO_2_1073K and Pt/SiO_2_1273K catalysts decreased.

Figure 6(A) shows the k^3-weighted EXAFS oscillations at the Pt L_3-edge of Pt/SiO_2 catalysts reduced at 773 K, 1073 K, 1273 K, and Pt foil. The EXAFS oscillations of Pt/SiO_2_773K and Pt/SiO_2_1073K exhibited essentially similar features with that of Pt foil. In the Fourier transforms (FTs) of the EXAFS spectra of Pt/SiO_2 catalysts shown in Figure 6(B), Pt–Pt linkage (around 0.26 nm) was observed, indicating that the supported Pt species was reduced to the metallic state after reduction at 773 K and 1073 K. The EXAFS oscillations of Pt/SiO_2_1273K were slightly different and weaker than those of the Pt foil and Pt/SiO_2 reduced at 773 K, suggesting the different environment of Pt atom in Pt/SiO_2_1273K.

CO adsorption and XPS analysis

CO adsorption is a very frequently used method for the characterization of Pt-based catalysts. It can be used to quantify the active surface area of supported Pt catalysts, determine the metal dispersion[20] and also study the interaction between Pt and the support or other promoters[21]. It is the drastic decrease of CO adsorption on Pt/TiO_2 system that opened the finds about SMSI effects between the metal and the support. It has been generally regarded as the important feature of SMSI effect. The amount of adsorbed CO on the Pt/SiO_2 catalysts in this work was summarized in Table 2. About 54.9 μmol g^{-1} CO was adsorbed on Pt/SiO_2_773K, 40.3 μmol g^{-1} on Pt/SiO_2_1073K. In contrast, no CO was found to adsorb on Pt/SiO_2_1273K even the dispersion of Pt particles was almost unchanged. This drastic decrease in CO adsorption for Pt/SiO_2_1273K implied the strong interaction between Pt and SiO_2.

Table 2 amount of CO adsorbed on the catalysts at room temperature.

Catalyst	CO adsorption / μmol g^{-1}
Pt/SiO_2_773 K	54.9
Pt/SiO_2_1073 K	40.3
Pt/SiO_2_1273 K	n.d.

The surface properties of Pt/SiO_2 catalysts were further estimated using XPS. Figure 7 shows their Pt 4f XP spectra. The binding energies of the Pt $4f_{7/2}$ and $4f_{5/2}$ peaks were 71.5 and 74.8 eV, respectively. Based on these binding energies, the valence of platinum in the Pt/SiO_2 catalysts was assigned to Pt^0. Being agreeable with the CO adsorption behaviors, the intensity of Pt 4f peaks of Pt/SiO_2_1273K drastically decreased. It means that there was much less Pt elements on the catalyst surface when it was reduced at high temperature as 1273 K.

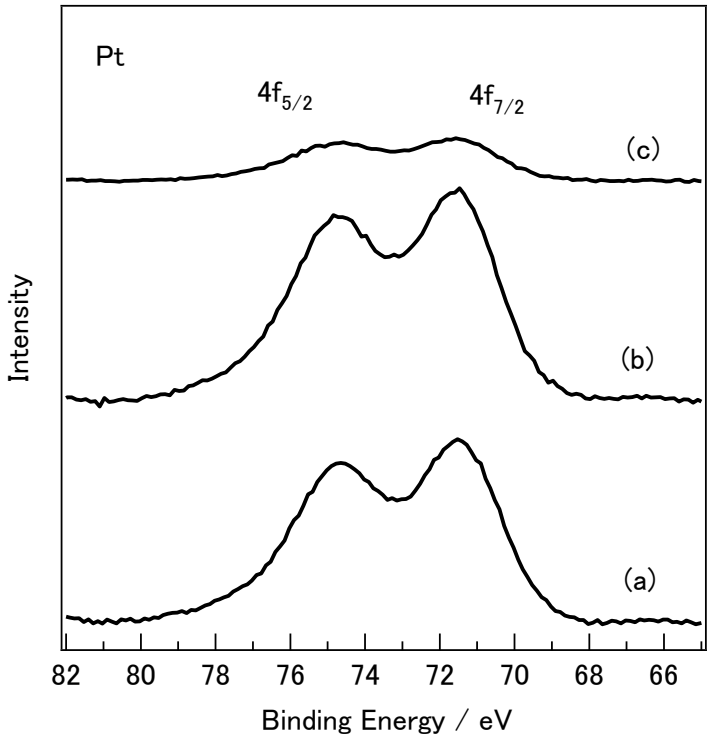

Figure 7 XPS profiles of Pt level for (a) Pt/SiO_2_773K, (b) Pt/SiO_2_1073K, (c) Pt/SiO_2_1273K.

HR-TEM images of the catalysts

In order to further study the detailed mechanism of Pt-SiO_2 interaction in Pt/SiO_2 catalysts reduced at different temperature, the structural changes in the interface between platinum and silicon were further investigated by High-resolution transmission electron microscopy (HR-TEM) observation. The results were shown in Fig. 8.

After direct reducing Pt/SiO_2 at 773 K for 1 h in H_2, well-crystallized Pt particles were observed on SiO_2 support as shown in Fig. 8(A). The interface between Pt and SiO_2 was characterized by necking and large contact angle. This suggests the weak interaction between Pt and SiO_2. As for Pt/SiO_2 catalyst reduced at higher temperature, 1073 K, the hemispherical Pt particles have been discovered as represented in Fig. 8(B). It is noted that the lattice array of Pt particles was matching with that of SiO_2 support. This interface morphology suggests the chemical interaction between platinum and SiO_2 at 1073 K. Pt-Si alloys were also probable to form. However, the similar lattice parameters of Pt metal and Pt_3Si alloy, shown in Table S1and S2, led to the difficulty in the attribution of the observed crystal to Pt metal or Pt-Si alloy. Anyway, the close deposition of Pt on SiO_2 support was clear on Pt/SiO_2_1073K, and it should be related to its active catalytic property in the dehydrogenation of propane. Fig.8(C) shows the HR-TEM image of Pt/SiO_2 reduced at 1273 K. A peculiar structure of Pt deposits appeared. A SiO_2 layer with ca. 1 nm thickness was observed to cover Pt metal core. This structural property in the interface between Pt and SiO_2 confirmed that at high reduction temperature (ca. 1273 K) the strong chemical interaction between them occurred. The encapsulated structure, which is often used to explain the SMSI effects in other Pt-support systems, is also favored to explain the interaction between Pt and SiO_2 at high reduction temperature.

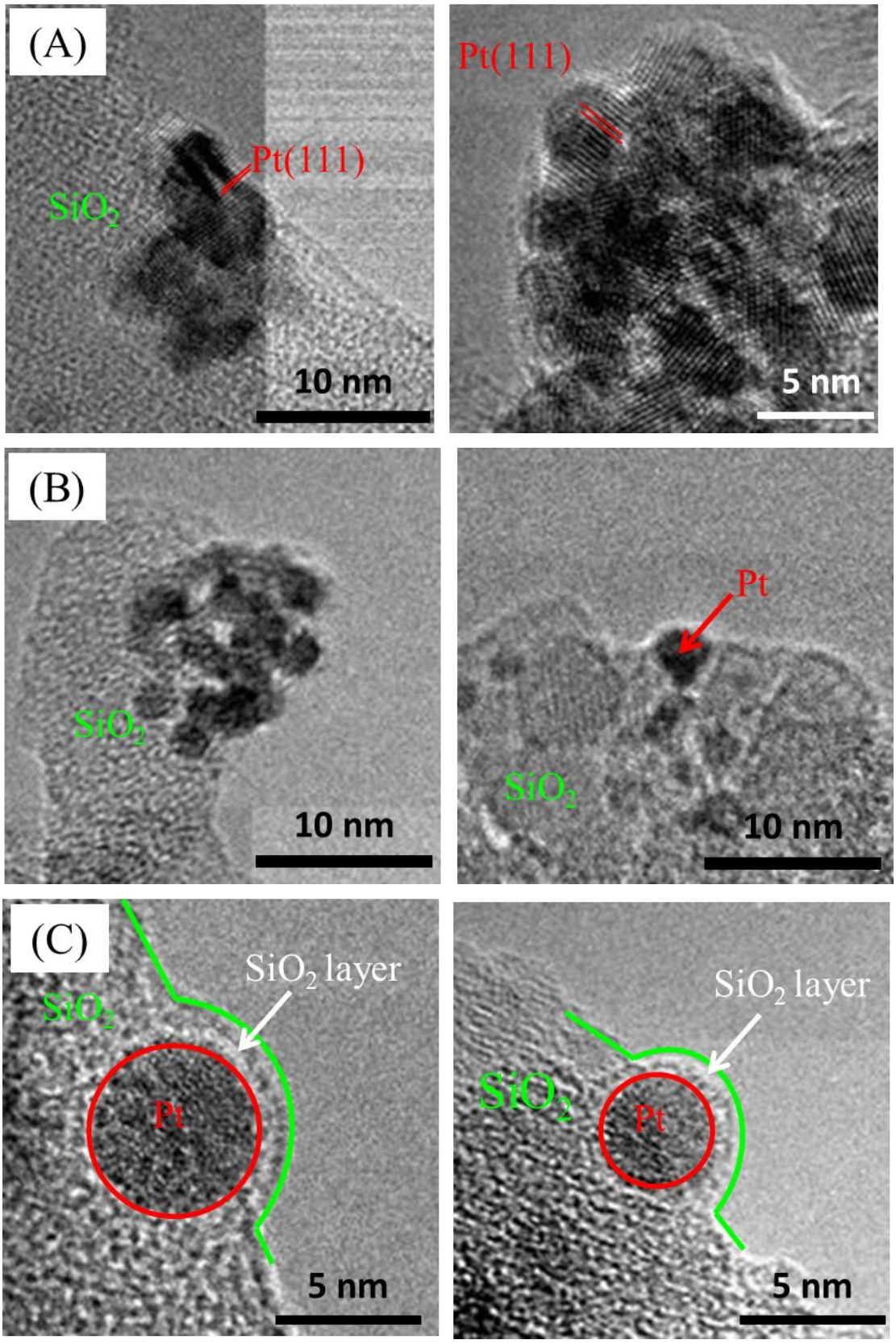

Figure 8 HRTEM images of Pt/SiO_2 reduced at (A) 773 K, (B) 1073 K, (C) 1273 K.

Discussion

Based on all of the above characterization results, the effect of reduction temperature on the structure of the Pt/SiO_2 catalysts prepared by direct reduction method is represented by Scheme 1. Structural characterization clearly showed that the strong interaction can take place in the system of Pt and SiO_2, which is generally thought to show no SMSI effects. Moreover, this interaction was strongly influenced by the reduction temperature.

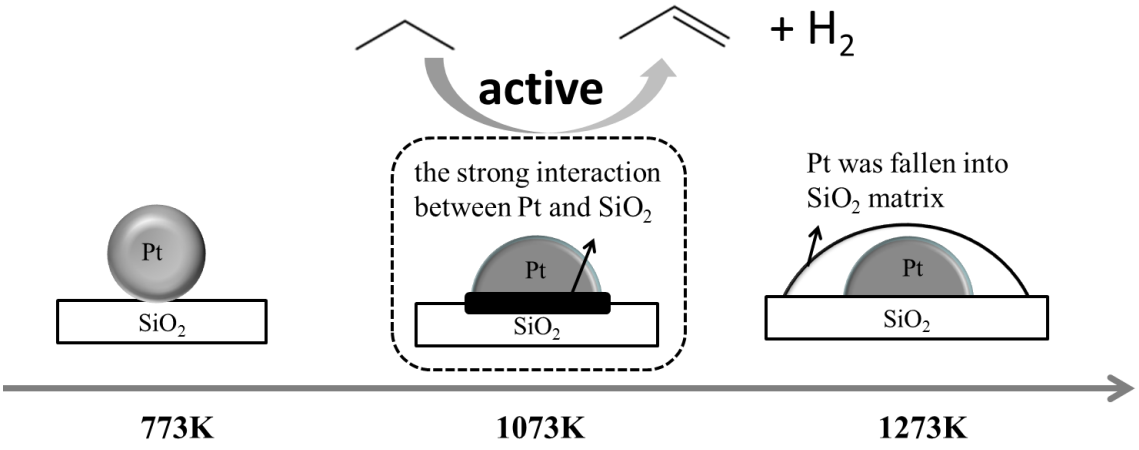

Scheme 1 the effect of reduction temperature on the structure of Pt/SiO_2 catalysts.

At low reduction temperature (773 K), there is no or less interaction between Pt and SiO_2. XRD, XAFS and XPS presented the Pt metallic feature of Pt on Pt/SiO_2_773K. The lattice of Pt (111) was observed in HR-TEM images. TEM observations and CO adsorption measurement suggested the highly dispersion of the Pt metal, its average particle size is small as 2.4 nm, and the amount of CO adsorbed was the largest among all catalysts tested (ca. 54.9 μmol g^{-1}). Based on the amount of CO adsorption, the calculated average particle size of Pt was about 4.2 nm assuming that one CO molecule adsorbed on one Pt atom. In the catalytic dehydrogenation of propane, Pt/SiO_2_773K exhibited the low conversion of propane (ca. 5%).

When reduction temperature increased to 1073 K, the strong interaction between Pt and SiO_2 appeared. Pt/SiO_2_1073K showed the high activity with ca. 21 % conversion of propane. The CO adsorbed on it decreased to 40.3 μmol g^{-1}, even though Pt metal on it did not grow up from the TEM observation. The average particle size of Pt was about 2.2 nm. XRD and XPS characterization on it present the similar results with that of Pt/SiO_2_773K. But the close location of Pt on SiO_2 on Pt/SiO_2_1073K with hemispherical Pt particles from HR-TEM images suggested the interaction between platinum and SiO_2 at 1073 K. This interaction led Pt in Pt/SiO_2_1073K became electron-richer than that in Pt/SiO_2_773K based on the comparison of their Pt L_3 and L_2 XAFS spectra. These Pt atoms with more electrons may be related to the high activity of Pt/SiO_2_1073K for the propane dehydrogenation.

Indeed, the central of catalysis is the redistribution of chemical bonds and charges as the reaction proceeds. The electronic structure of the catalyst for the certain reaction influences chemical bonding of adsorbates and activates the relevant bond cleavage [22]. As for the dehydrogenation of propane, the Pt-Sn alloy catalyst is the main and most important one, on which C-H bond cleavage fluently proceeds to produce propylene [23, 24]. Similar with our results from Pt-SiO_2 system, it was generally accepted that Pt atoms in the Pt-Sn alloy have a 5d electron population larger than that of the atoms in metallic Pt, probed by X-ray absorption measurements in many previous reports [24-26]. Using density functional theory calculations, Yang. Ming-Lei et al. [27] also found the electronic states of Pt (d-band, d-band center) changed with alloying with Sn, consequently lowering the bonding strength of propyl and propylene on the alloyed surfaces. Nykanen, L. et al. [28,29] investigated the adsorption of propane, propene, and C and H atoms on Pt and Pt-Sn alloy surfaces. They pointed out

that alloying Pt (111) with Sn leads to weaker propene adsorption, which has a positive effect on the activity and selectivity toward propylene production. The good catalytic performance over Pt/SiO_2_1073K in the present work may be attributed to the similar mechanism because of the similar electron-richer Pt atoms in the interface between Pt and SiO_2. Pt-Si alloys were probably formed and thus improved the propylene production.

At high reduction temperature (1273 K), even though small Pt metal particles with 3.2 nm average size were found on Pt/SiO_2_1273K from XRD and TEM observation, its local or detailed structure totally differed with that of Pt/SiO_2_773K and Pt/SiO_2_1073K. No CO was detected to absorb on it, and the intensity of Pt XP spectra was very week, implying the small amount of accessible Pt atoms on its surface. Observing it using HR-TEM, a clear SiO_2 layer (the thickness is about 1 nm) was found on the surface of Pt metal particles. This layer inhibited the detection of surface Pt atoms, also blocked C-H bond activation in propane over Pt surface. Therefore, Pt/SiO_2_1273K showed no activity with the strongest interaction between Pt and SiO_2.

Conclusion

Pt or modified Pt catalyst has been widely studied in the dehydrogenation of propane. However, the nature of its structure and the active site are still unclear. In the present work, SiO_2 supported Pt catalysts were prepared with the direct reduction method at different temperatures. Even the catalysts reduced at low temperatures were inactive, Pt/SiO_2_1073K showed the high catalytic activity in the dehydrogenation of propane. The strong Pt-SiO_2 interaction on Pt/SiO_2_1073K was found based on CO adsorption, XAFS analysis and HR-TEM observation. Pt in it became electron-richer because of the chemical interaction between Pt and SiO_2. The interface between them

was considered as the active site, and is related to the admirable catalytic performance of Pt/SiO_2_1073K.

References:

[1] S. Tauster and S. Fung, Journal of catalysis, 55 (1978) 29.

[2] K. Kunimori, S. Matsui and T. Uchijima, Chemistry Letters, (1985) 359.

[3] M. Bonne, P. Samoila, T. Ekou, C. Especel, F. Epron, P. Marecot, S. Royer and D. Duprez, Catalysis Communications, 12 (2010) 86.

[4] A. Dandekar and M. Vannice, Journal of catalysis, 183 (1999) 344.

[5] A. Huidobro, A. Sepulveda-Escribano and E. Rodriguez-Reinoso, Journal of catalysis, 212 (2002) 94.

[6] A.S. Ivanova, E.M. Slavinskaya, R.V. Gulyaev, V.I. Zaikovskii, O.A. Stonkus, I.G. Danilova, L.M. Plyasova, I.A. Polukhina and A.I. Boronin, Applied Catalysis B: Environmental, 97 (2010) 57.

[7] L.F. Liotta, A. Longo, A. Macaluso, A. Martorana, G. Pantaleo, A.M. Venezia and G. Deganello, Applied Catalysis B: Environmental, 48 (2004) 133.

[8] S. Golunski, H. Hatcher, R. Rajaram and T.J. Truex, Applied Catalysis B: Environmental, 5 (1995) 367.

[9] M. Vannice and C. Twu, Journal of Catalysis, 82 (1983) 213.

[10] M. Vannice, Topics in Catalysis, 4 (1997) 241.

[11] S. Fung, Journal of catalysis, 76 (1982) 225.

[12] F. Pesty, H. Steinruch and T. Madey, Surface Science 339 (1995) 83.

[13] D. Mullins and K. Zhang, Surface Science, 513 (2002) 163.

[14] T. Uchijima, Catalysis Today, 28 (1996) 105.

[15] R. Lamber and N. Jaeger, Journal of Applied Physics, 70 (1991) 457.

[16] B. Tsui and M. Chen, Solid-State Electronics, 36 (1993) 583.

[17] P. Gallezot, R. Weber, R. Dallabetta and M. Boudart, Z. Natureforsch. A, 34 (1979) 40.

[18] F. Lytle, Journal of catalysis, 43 (1976) 376.

[19] R.S. Mulliken, Journal of Chemical Physics, 2 (1934) 782.

[20] T. Tanabe, Y. Nagai, T. Hirabayashi, N. Takagi, K. Dohmae, N. Takahashi, S. Matsumoto, H. Shinjoh, J.N. Kondo, J.C. Schouten and H.H. Brongersma, Applied Catalysis A: General, 370 (2009) 108.

[21] C.F. Ocal, S, The Journal of Chemical Physics, 84 (1986) 6474.

[22] S. Kaya, D. Friebel, H. Ogasawara, T. Anniyev and A. Nilsson, Journal of Electron Spectroscopy and Related Phenomena, 190 (2013) 113.

[23] O. Barias, A. Holmen and E. Blekkan, Journal of Catalysis, 158 (1996) 1.

[24] D. L., S. T., T. K. and T. T., Catalysis Today, 232 (2014) 33.

[25] Y. Uemura, Y. Inada, K.K. Bando, T. Sasaki, N. Kamiuchi, K. Eguchi, A. Yagishita, M. Nomura, M. Tada and Y. Iwasawa, Phys. Chem. Chem. Phys., 13 (2011) 15833.

[26] Y. Uemura, Y. Inada, K.K. Bando, T. Sasaki, N. Kamiuchi, K. Eguchi, A. Yagishita, M. Nomura, M. Tada and Y. Iwasawa, The Journal of Physical Chemistry 115 (2011) 5823.

[27] M.-L. Yang, Y.-A. Zhu, X.-G. Zhou, Z.-J. Sui and D. Chen, ACS Catalysis, 2 (2012) 1247.

[28] L. Nykanen and K. Honkala, The Journal of Physical Chemistry 115 (2011) 9578.

[29] L. Nykanen and K. Honkala, ACS Catalysis, 3 (2013) 3026.

Summary

In this thesis, the active structures of supported Pt or Pt-Sn alloy catalysts for the catalytic dehydrogenation of alkanes were comprehensively and accurately elucidated. The general conclusion of this thesis is as follows:

Chapter 1 shows that the interaction between Pt and Sn differed with varying the pretreatment atmosphere over Pt-Sn/SiO_2. Large Pt metal particles formed together with amorphous SnO_2 on Pt-Sn/SiO_2 treated with oxidized pretreatment atmosphere (O_2), which showed no catalytic activity. After the pretreatment in the inert atmosphere (N_2), Pt metal was highly dispersed with a strong Pt-SnO_x ($x<2$) interaction. This interaction became stronger with the treatment temperature and introduced high catalytic activity in propane dehydrogenation. The highest catalytic activity of Pt-Sn/SiO_2 was observed when the catalyst precursor was pretreated in the reductive atmosphere (H_2) which leads to the alloy formation between Pt and Sn. The Pt_3Sn phase was dominant over Pt-Sn/SiO_2 reduced in H_2 atmosphere at 1073 K.

Chapter 2 describes different Pt-Sn alloy formed on SiO_2 when Pt-Sn/SiO_2 catalyst was prepared with different reduction method. Direct reduction (*DR*) caused that Pt_3Sn alloy nanoparticle was mainly formed on Pt-Sn/SiO_2 (*DR*) catalyst, which showed the highest activity. Calcination-reduction (*CR*) method led to PtSn alloy formation. However, this catalyst was not active in propane dehydrogenation.

Chapter 3 further investigated the effects of Sn/Pt ratio and reduction temperature over Pt-Sn/SiO_2 catalysts for the dehydrogenation of propane when they were prepared by direct reduction method. Among the catalysts prepared, 1Pt1Sn/SiO_2_1073K (Sn/Pt ratio=1, reduced at 1073 K), composed of highly dispersed Pt_3Sn alloy particles

decorated with SnO_2 exhibited the highest activity. When the Sn/Pt ratio was larger than 1 and/or the reduction temperature was 1273 K, PtSn alloy was mainly observed, and the Pt-Sn/SiO_2 catalysts showed low activity.

Chapter 4 deals with the behavior of active species on Pt-Sn/SiO_2 catalyst during the dehydrogenation of propane to propylene and regenerations. It was found that besides coke formation, the surface of active species restructured during the reaction and regeneration processes. The surface Sn(Ⅳ)/Sn(0) obviously increased after the reaction. H_2 in the feeding gas increased the stability of Pt-Sn/SiO_2. The regeneration (firstly calcination in air followed reduction in H_2) effectively recovered the activity of the deactivated catalyst trough the re-alloy between Pt and SnO_2.

Chapter 5 compared the catalytic behaviors of Pt-Sn/SiO_2 and Pt-Sn/SBA-15 in the dehydrogenation of ethylbenzene. It was found that the higher surface area and special textural properties of SBA-15 improved catalytic activity, selectivity and stability. Pt-Sn alloy particles were highly dispersed and stable over SBA-15 during the reaction time. Furthermore, the presence of Sn also produced a 'drain-off' effect to keep the Pt-Sn active sites clean by removing the coke precursors to the support SBA-15.

Chapter 6 reported that the strong interaction between Pt and SiO_2 originated from the reduction pretreatment at high temperature (≧1073 K). Pt atoms became electron-richer, and CO adsorption on it also decreased even the Pt particle size almost unchanged compared with Pt/SiO_2 catalyst reduced at lower temperature. A clear SiO_2 layer (ca. 1 nm) covered with small Pt metal size (ca. 3.2nm) was even observed under HR-TEM on Pt/SiO_2 catalyst reduced at 1273 K, and no CO adsorbed on it. Pt/SiO_2 catalyst reduced at 1073 K exhibited activity in the dehydrogenation of propane, suggesting the importance of medium interaction between Pt and SiO_2 for propane

dehydrogenation.

In summary, the interaction between Pt and Sn (or SiO_2) was found to closely relate to the catalytic performance of Pt(-Sn)/SiO_2 catalyst for the dehydrogenation of alkanes (propane or ethylbenzene). As described in this thesis, the different extent of interaction between them caused by the different preparation conditions, introduced the formation of various kinds of alloy such as Pt_xSn_y (x/y>3), Pt_3Sn and PtSn formed. Pt_3Sn alloy showed the highest activity. However, PtSn alloy is not highly active. It was suggested that atomic arrangements of Pt and Sn in Pt-Sn alloy also contribute to the catalytic behaviors of Pt-Sn/SiO_2 catalysts. The following studies on deactivation and regeneration of Pt-Sn/SiO_2 catalysts in the dehydrogenation of propane also implied the structural transformation of the active species during reaction and regenerations. The structure of Pt-Sn alloy particles also can be stabilized using SBA-15 as the support, which has the special textual properties. These new findings elucidated the details about different interaction between Pt and Sn, thus will contribute to the development of academic research on alloy catalysts as well as the application of alloy catalysts in heterogeneous catalysis.

Appendix

Study of formation process of metal nanoparticles on metal oxides by *in-situ* XAFS technique

Abstract

The formation process of platinum nanoparticles (PtNPs) on metal oxide (SiO_2) was investigated by various characterization techniques, especially, *in situ* time-resolved Pt-L_3 edge XAFS (QXAFS and DXAFS) combined with Q-Mass spectroscopy. A series of XAFS spectra was analyzed to evaluate the change in local structure, electronic state, and dispersion of PtNPs during their formation and growth process.

Introduction

The Metal nanoparticles (NPs) are getting much more attention than ever in both fields of fundamental science and engineering. Metal NPs have several unique properties or applications, such as surface plasmon resonance, magnetism, imaging, or catalysis [1]. Various researchers focus their efforts on controlling NP size and/or shape. Their formation mechanisms in solution are also vigorously investigated, but still under discussion. Recently, we proposed the formation process of AuNPs in the presence of the equimolar of dodecanethiol to $HAuCl_4$ using *in situ* millisecond time-resolved QXAFS measurement [2]. We also investigated the formation process of RhNPs from rhodium trichloride trihydrate ($RhCl_3$ $3H_2O$) in ethylene glycol with polyvinylpyrrolidone (PVP) at elevated temperature [3]. A combination of *in situ* time-resolved XAFS and ICP-MS techniques reveals that the formation process is a first-order reaction, which indicates that RhNPs with the uniform size appear consecutively and these Rh NPs do not aggregate with each other.

On the other hand, it is well known that metal nanoparticles (NPs) on metal oxide (solid surface) are effective in various catalytic reactions. The interaction between metal oxide surface and metal NPs is considered to have played an important effect controlling shape (morphology), dispersion (size) and catalytic activity of metal NP. Although the states (local environment and electronic strcuture) of metal NPs on various metal oxides have been studied by using XAFS technique, the detailed mechanism about the formation of metal NPs on metal oxides surface remains unclear. In the present study, we have tried to investigate the dynamic formation process of PtNPs on metal oxide surface (SiO_2). For this purpose, we applied *in-situ* time resolved XAFS (Quick XAFS and Energy-dispersive XAFS (DXAFS)) combined with Q-mass.

Experimental

Platinum was loaded on SiO_2 (homemade, 622 m^2 g^{-1}) by an impregnation with an aqueous solution of $Pt(NH_3)_4(NO_3)_2$ at 353 K. The impregnated sample was dried at 353 K in the air. The content of platinum was 2 wt.%.

Pt L_3-edge XAFS data (QXAFS) were collected at a facility of the BL01B1 station of SPring-8 of Japan Synchrotron Radiation Research Institute (8 GeV, 100 mA), Hyogo, Japan. The spectrum was recorded in a transmittance mode at room temperature, using a Si (111) two-crystal monochromator. The photon energy was calibrated by Pt foil. The wafer of the sample diluted with BN was mounted in an *in-situ* flow cell. DXAFS measurements were recorded at BL28B2 beam line and the spectra were collected using a bent Si(111) polychromator and a position sensitive CCD detector at room temperature. The data acquisition consisted from 100 spectra with a time resolution of 55 ms (5.5 s/spectrum). The exhaust gases during XAFS measurements were analyzed by Q-mass spectrometer (Pfeiffer Omni star). The data reduction was performed by the REX2000 Ver.2.5.9 program (Rigaku) and FEFF8.40.

Results and Discussion

Formation process of Pt NPs on SiO_2 in He

Figure 1 shows a series of in situ time-resolved Pt L_3-edge XANES spectra (QXAFS) of 2.0 wt% Pt/SiO_2 in He flow with increasing treatment temperature and the reference spectra of Pt foil. Figure 2 shows the change in the white line intensity around 11565 eV and Q-mass spectra against the temperature. The intensity of white line slightly increased from 460 to 500 K, then remarkably decreased. The intensity of white line at 700 K is almost similar to that of Pt foil, indicating the reduction of Pt cation

species to Pt^0 during the He treatment. The shift of X-ray absorption edge energy (E_0) to lower energy region also indicates a reduction of Pt^{2+} cation to Pt^0 species. Q-mass spectra clearly indicate that the formation of H_2O (18), N_2 (28) around 520 K as shown in Fig.2. NH_3 (m/e=16), NO (30), and N_2O (44) were also observed (data not shown). The formation of these species was observed up to 560 K. These results indicate that the decomposition of ligands in $Pt(NH_3)_4(NO_3)_2$ took place above 460 K and the ligands was completely decomposed up to 560 K.

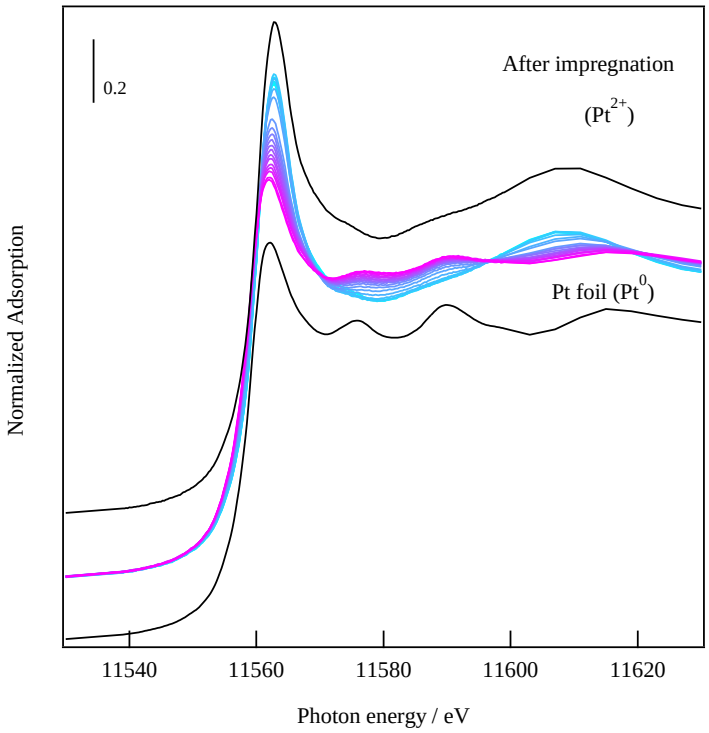

Figure 1 XANES spectra of Pt/SiO_2 under He.

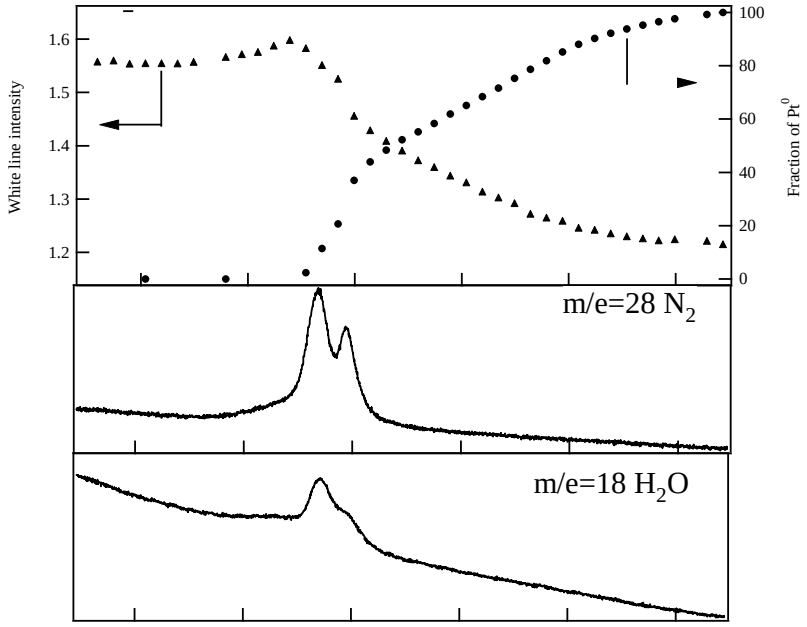

Figure 2 the change of white line intensity and Q-mass spectra

Figure 3 show k^3-weighted EXAFS spectra and their Fourier transforms (FTs) of Pt/SiO_2 sample treated with He and Pt foil. The oscillation of EXAFS spectrum of Pt/SiO_2 remarkably changed above 520K. The peaks at 1.8 Å, appearing at lower treatment temperature can be assigned to the contribution of the Pt-N (or Pt-O, *vide infra*) shell. The second shell due to Pt-Pt was observed above 542 K, although the intensity of Pt-Pt shell (2.5-3.0 Å) was weak due to thermal vibration of a lattice of Pt. This suggests that highly dispersed Pt cation species as a monomer is present on Pt/SiO_2 and that a part of Pt cation species was reduced to Pt^0 to form PtNPs. The change in the coordination number (CN) of Pt-N (or Pt-O) and Pt-Pt shell was shown in Fig. 4.

Above 520 K, the CN of Pt-N decreased with the increase in temperature and reached at ca. 2 even after the complete decomposition of ligands in $Pt(NH_3)_4(NO_3)_2$ (> 560 K). Based on Q-mass spectra, above 560 K, no nitrogen was present on Pt/SiO_2. This suggests that the formation of Pt-O bond (oxygen was lattice oxygen of SiO_2 support; Pt-O-Si bond) proceeds simultaneously with the decomposition of ligands in

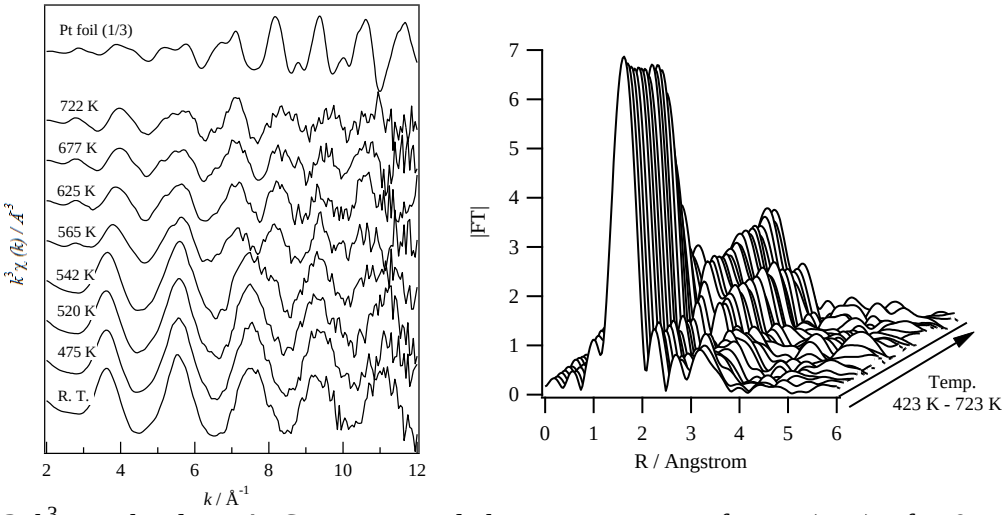

Figure 3 k^3-weighted EXAFS spectra and their Fourier transforms (FTs) of 2.0 wt% Pt/SiO_2 (in H_2, RT to 773K).

$Pt(NH_3)_4(NO_3)_2$. On the other hand, the CN of Pt-Pt bond rapidly increased at 540 K and then linearly increased with the temperature. This increasing in CN of Pt-Pt bonds suggests the growth of Pt NPs during He treatment at a high temperature. However, based on TEM images, the average particle size of PtNPs on Pt/SiO_2 treated with He at 623 K was almost similar to that treated at 723 K (1.7 ± 0.4 nm at 623 K and 1.7 ± 0.6 nm at 723 K), indicating that the growth of Pt NPs did not proceed in He (at least, up to 723 K).

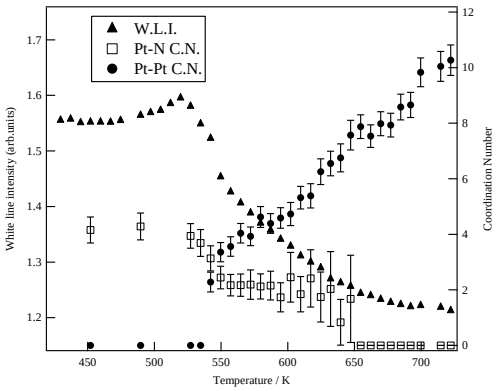

Figure 4 The change in the white line intensity and the coordination number (CN) of Pt-N (or Pt-O) and Pt-Pt shell of 2.0 wt% Pt/SiO_2 (in He, RT to 773 K).

All Pt L_3-edge XANES spectra were analyzed with the linear combination fitting

of XANES spectra of the initial state (Pt^{2+}; before heating) and Pt foil. The fraction of Pt^0 estimated from the coefficient of the linear combination fitting increased with temperature (Fig.5). Moreover, the average CN of Pt-Pt of PtNPs, estimated from the degree of fraction of Pt^0 (= the degree of reduction of platinum species), was almost constant up to 773 K, suggesting that the particle size of PtNPs was independent on temperature, in other words, PtNPs with a uniform size appear consecutively and do not aggregate with each other with increasing threat temperature.

Based on these results, the formation process of PtNPs on SiO_2 under He flow was proposed as follows. First, platinum precursor was decomposed. Then, the formation of intermediate species, which have Pt-O bond (CN of Pt-O is 2; Si-O-Pt-O-Si), takes place. Next, the intermediate species were reduced to form Pt^0 nuclear. Finally, the Pt^0 nuclear aggregated to form PtNPs having uniform particle size.

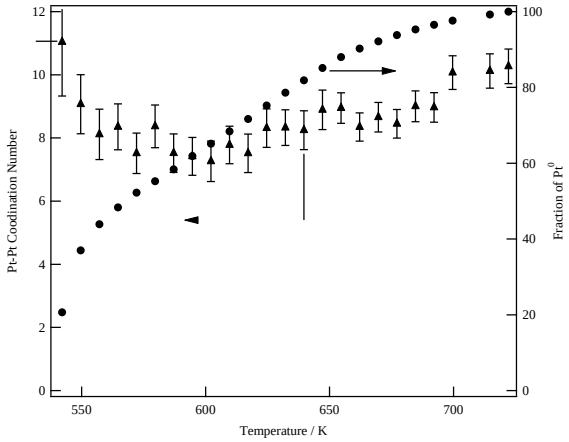

Figure 5 Fraction of Pt^0 and the average coordination number (CN) of Pt-Pt bond in Pt NPs. Fraction of Pt^0 was estimated from the linear combination fitting of XANES spectra of the initial state (Pt^{2+}; before heating) and Pt foil. The average CN of Pt-Pt bond: the CN of Pt-Pt bond x fraction of Pt^0/100.

Formation process of Pt NPs on SiO_2 in H_2

The change in the white line intensity of Pt L_3-edge XANES spectra of Pt/SiO_2 and Q-mass spectra against the temperature in H_2 flow was measured (data not shown). The intensity of white line rapidly decreased from 420 K, which is about 40 K lower than in He. The formation of H_2O was also observed around 420 K. In order to reveal the initial formation process of Pt NPs on SiO_2 in H2, DXAFS technique was applied. Figure 6 shows the time course of the intensity of white line, the CNs of Pt-Pt and Pt-N (or Pt-O) shells, and Q-Mass spectra about 473 K in H_2 flow. After the introduction of H_2, the intensity of the white line immediately decreased within 40 s. In response to changes in the intensity of white line, the CN of Pt-Pt bond increased while the CN of Pt-N decreased. In this stage, no formation of NH_3 was observed, although a quite small amount of N_2 and N_2O were formed. These results suggest that the following processes take place at the initial stage of the formation of PtNPs on SiO_2 in H_2; 1) $Pt(NH_3)_4(NO_3)_2$ react with silanols groups ($Pt(NH_3)_4(NO_3)_2 + 2SiOH \rightarrow Pt(NH_3)_4(OSi)_2 + 2HNO_3$), 2) a part of precursor ($Pt(NH_3)_4(OSi)_2$) was decomposed to form PtNPs, and the formed NH_3 react with HNO_3 ($Pt(NH_3)_4(OSi)_2 + 2HNO_3 + H_2 \rightarrow Pt^0 + 4NH_4NO_3 + 2SiOH$), 3) a rest of precursor ($Pt(NH_3)_4(OSi)_2$) and NH_4NO_3 were decomposed to form PtO and N_2 (O_2 and H_2O), respectively ($Pt(NH_3)_4(OSi)_2 \rightarrow PtO + 4NH_3 + Si\text{-}O\text{-}Si$, $NH_4NO_3 \rightarrow 2N_2 + 4H_2O + O_2$).

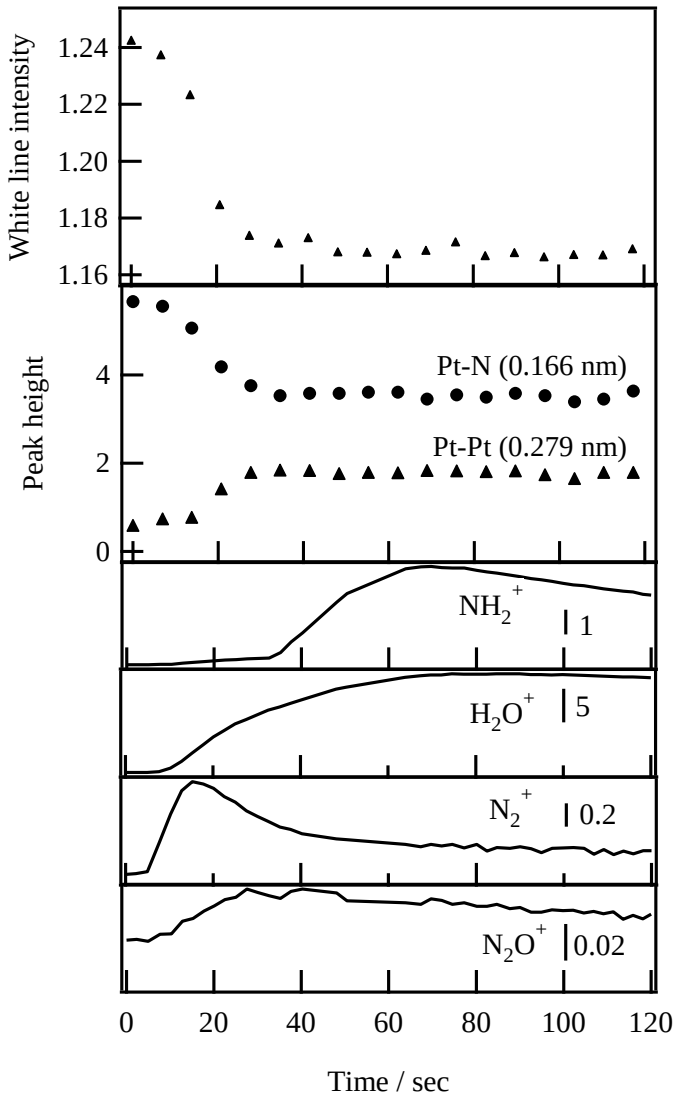

Figure 6 Intensity of white line of Pt L_3-edge XANES (DXAFS), the CN of Pt-Pt and Pt-N shells, and Q-Mass spectra. (at 473 K, in 20 vol.% H_2/He)

Conclusion

A combination of *in situ* time-resolved XAFS and Q-Mass techniques reveals the formation process of PtNPs on SiO_2 in He and H_2. The reduction much more easily proceeds in the case of H_2. Under the He atmosphere, PtNPs with a uniform particle size formed through the reduction of intermediate species (Si-O-Pt-O-Si). While in the case

of H_2, one part of PtNPs formed by the direct decomposition of $Pt(NH_3)_4(OSi)_2$, and another part of PtNPs formed form the reduction of PtO.

References

[1] Yan, N.; Xiao, C.; Kou, Y.; *Coord. Chem. Rev.*, 2010, 254, 1179.

[2] Ohyama, J; Teramura, K.; Higuchi, Y.; Shishido, T.; Hitomi, Y.; Kato, K.; Tanida, H.; Uruga, T.; Tanaka, T., *ChemPhysChem*, 2011, 12, 127.

[3] Asakura, H. ;Teramura, K.; Shishido, T.; Tanaka, T.; Yan, N.; , Xiao, C.; Yao, S. ; Kou, Y., *Phys. Chem. Chem. Phys.*, 2012, 14, 2983.

List of Publications

Chapter 1

Effect of pretreatment atmosphere on the activity of Pt-Sn/SiO_2 for dehydrogenation of propane

Lidan Deng, Tetsuya Shishido, Kentaro Teramura, Tsunehiro Tanaka

In preparation

Chapter 2

Effect of reduction method on the activity of Pt-Sn/SiO_2 for dehydrogenation of propane

Lidan Deng, Tetsuya Shishido, Kentaro Teramura, Tsunehiro Tanaka

Catalysis Today, 232 ***(2014)****, 33-39*

Chapter 3

Dehydrogenation of propane over Pt-Sn/SiO_2 catalysts prepared by direct reduction method: Effects of Sn/Pt ratio and reduction temperature

Lidan Deng, Hiroki Miura, Tetsuya Shishido, Saburo Hosokawa, Kentaro Teramura and Tsunehiro Tanaka

ChemCatChem, in press

Chapter 4

Behavior of active species on Pt-Sn/SiO_2 catalyst during the dehydrogenation of propane to propylene and the regenerations

Lidan Deng, Hiroki Miura, Tetsuya Shishido, Saburo Hosokawa, Kentaro Teramura and Tsunehiro Tanaka

Submitted to Applied Catalysis A: General

Chapter 5

Dehydrogenation of ethylbenzene over Pt-Sn/SBA-15 and Pt-Sn/SiO_2 catalysts prepared by direct reduction method: Stability improvement of Pt-Sn alloy catalyst by using SBA-15 as support

Lidan Deng, Hiroki Miura, Tetsuya Shishido, Saburo Hosokawa, Kentaro Teramura and Tsunehiro Tanaka

in revision Applied Catalysis A: General

Chapter 6

Effect of reduction temperature on the catalytic performance of Pt/SiO_2 catalysts for propane dehydrogenation: Metal-support interaction between Pt and SiO_2

Lidan Deng, Tetsuya Shishido, Kentaro Teramura, Tsunehiro Tanaka

To be submitted

Appendix

Study of formation process of metal nanoparticles on metal oxides by *in-situ* XAFS technique

Shishido, T.; Nasu, H.; Deng, L.; Teramura K. and Tanaka, T.

Journal of Physics Conference Series, *430* ***(2013)***.